PhD Thesis

Development of Inhibitors for Immunosuppressive Indoleamine 2,3-dioxygenase 1 Enzyme

A dissertation submitted to the
Indian Institute of Technology Guwahati
as partial fulfilment for the Degree of
Doctor of Philosophy in Chemistry

By
Niku Moni Das

Department of Chemistry
Indian Institute of Technology Guwahati
Guwahati 781039, Assam, India

To

My Beloved Family

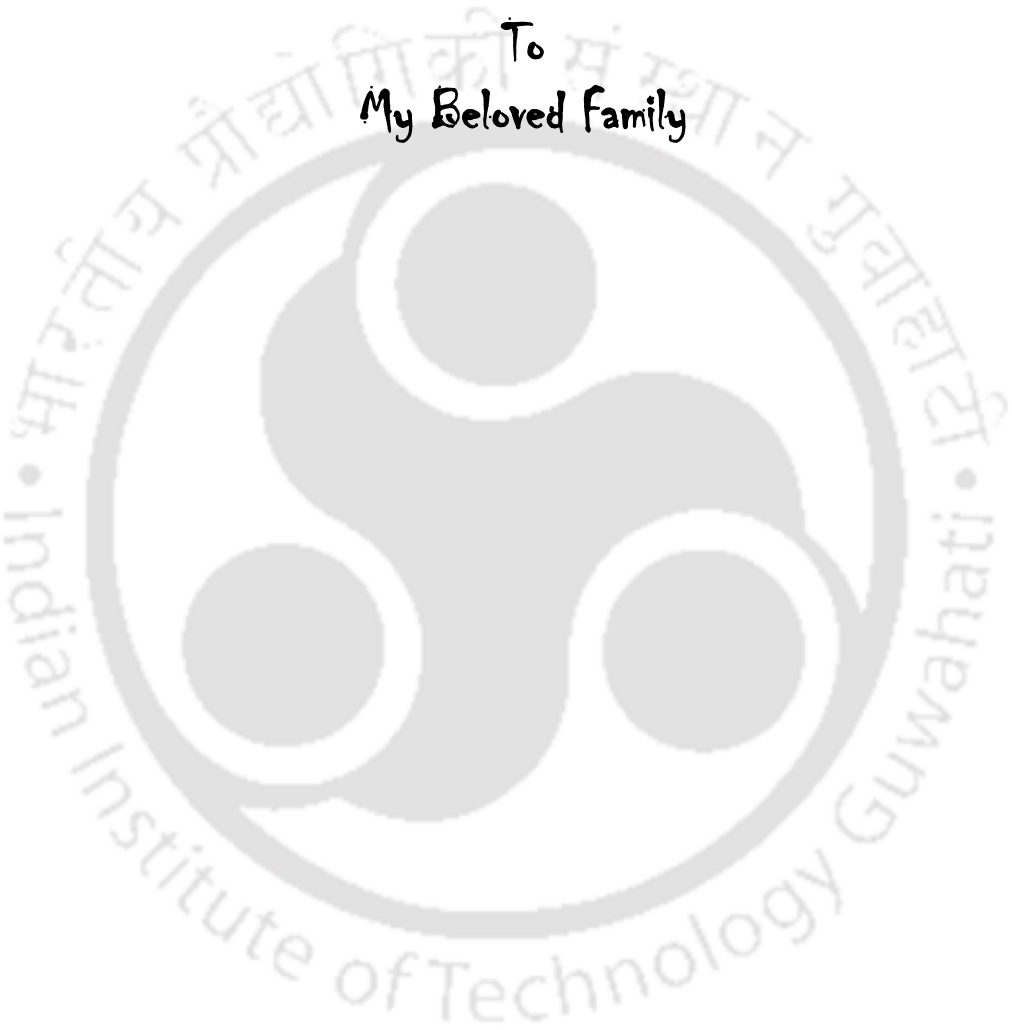

Declaration

10th Dec, 2025

I hereby declare that the thesis entitled **"Development of Inhibitors for Immunosuppressive Indoleamine 2,3-dioxygenase 1 Enzyme"** is compilation of research work which was carried out by me under the supervision of Prof. Debasis Manna, Department of Chemistry, Indian Institute of Technology Guwahati. This thesis has been submitted by me to the Department of Chemistry, Indian Institute of Technology Guwahati, for the award of the degree of Doctor of Philosophy. In keeping with the general practice of reporting scientific observations, due acknowledgements have been made wherever the work described is based on the findings of other investigators.

I further declare that this work has not been submitted anywhere else for any degree, diploma, associateship or membership etc. of any Institute or University to the best of my knowledge.

Niku Moni Das
Candidate
Department of Chemistry
IIT Guwahati, Guwahati-781039
Assam, India

भारतीय प्रौद्योगिकी संस्थान गुवाहाटी
Indian Institute of Technology Guwahati

Prof. Debasis Manna
Department of Chemistry
Phone: +91-0361-258-2325
Fax: +91-0361-258-2349
E-mail: dmanna@iitg.ac.in

10th Dec,2025

To whom it may concern

This is to certify that the thesis entitled **"Development of Inhibitors for Immunosuppressive Indoleamine 2,3-dioxygenase 1 Enzyme"** being submitted by Ms. Niku Moni Das (Roll No. 206122119) for the award of PhD degree in Chemistry to the Indian Institute of Technology Guwahati, is genuinely her own research work which was carried out by her. The information and data reported by her are completely her original findings. She has meticulously carried out the investigations and also followed the guidelines of my laboratory. Neither this thesis nor any part of it has been submitted for the award of any degree/diploma to anywhere before.

Prof. Debasis Manna
Thesis Supervisor
Department of Chemistry
IIT Guwahati, Guwahati-781039
Assam, India

Contents

Acknowledgements

This dissertation is a consequence of endless support and encouragement by numerous well-wishers'. I would like to acknowledge each of them for helping me to reach the milestone in my life.

Prior to all, I would like to convey my sincere gratefulness to my supervising guide, Prof. Debasis Manna who introduced me to the splendid world of Science. His consistent guidance, encouragement and scholarly inputs has enriched me a lot for shining in science. I am truly honoured and blessed to have been a part of his research group. Apart from research, his thoughts and ideas about life paved the way to me a better person in future. Thank you, Sir for being my Mentor.

My sincere and heartfelt thanks to my collaborators, Dr. Horacio Pérez-Sánchez (Dept. of Computer Engineering, University of Catolica San Antonio de Murcia, Spain), Prof. Sachin Kumar (Dept. of BSBE, IIT Guwahati, India), Prof. Siddhartha Shankar Ghosh (Dept. of BSBE, IIT Guwahati, India), and Dr. Debdas Dhabal (Dept. of Chemistry, IIT Guwahati, India) for their constructive support in my research.

I would also like to thank my doctoral committee members Prof. Anil Kumar Saikia, Prof. Manabendra Sarma, and Dr. Animesh Das for their valuable suggestions and consistent evaluation of my research works.

I would like to express my gratitude to all the faculty and staff members of Department of Chemistry for their continuous support. Also, I am immensely thankful to Department of Chemistry, Centre for Environment and CIF (IIT Guwahati) for allowing me to use the sophisticated instrument facility. A special mention in this note of acknowledgement will certainly be of UGC for providing me the scholarship.

I would also like to acknowledge all my past and present lab members including Dr. Nirmalya Pradhan, Dr. Nasim Akhtar, Dr. Oindrila Biswas, Dr. Subhasis Dey, Dr. Sribash Das, Dr. Anjali Patel, Ms. Priyanka Mazumder, Dr. Gunanka Hazarika, Mr. Biswa Mohan Prusty, Ms. Soumya Srimayee, Mr. Mrinal Kanti Kar, Ms. Rama Karn, Mr. Rahul Kumar, Ms. Suravi Chauhan, Mr. Joydip Pal, Mr. Pritam Kumar Mohanta, Mr. Yousuf Sk, Mr. Soumajit Saha, Ms. Ritama Mukherjee for providing me a healthy and friendly atmosphere in the lab.

I extend my sincere thanks to all of my friends for their constant support and encouragement.

Last but not the least, my Ph. D. endeavours would not have been accomplished without acknowledging my loving family and parents, Ms. Sewali Das and Mr. Pradip Das and my sister, Ms Disha Das. Their endless love, continuous support and blessings boost me up to cross the hurdles of my career.

Thank you all for being a memorable part of my life.

Ms. Niku Moni Das

Abstract

This thesis titled as "***Development of Inhibitors for Immunosuppressive Indoleamine 2,3-dioxygenase 1 Enzyme***" focused on developing small molecule for robust and selective inhibition of IDO1. We have explored the therapeutic potential of our synthesised inhibitors for the immunotherapeutic treatment of various diseases, especially cancer. We also induced photopharmacology by synthesizing stimuli sensitive prodrugs. The entire work is arranged into four chapters as mentioned below.

Chapter 1 introduces the Immunosuppressive Indoleamine 2,3-dioxygenase 1 enzyme and its enzymatic role. It also deals with different types of reported IDO1 inhibitors.

Chapter 2 elaborates on how dichloroquinoline-based IDO1 inhibitors target both apo-IDO1 and free heme, thereby demonstrating the dual-action nature of these inhibitors for IDO1 activity.

Chapter 3 primarily focuses on tryptamine-based azole derivatives linked to a photo-sensitive linker, forming a prodrug. This prodrug releases the drug on photoirradiation, showing potent inhibition.

Chapter 4 corroborates how a spiropyran (inactive form) in presence of both external stimuli (light) as well as internal stimuli (pH) converts to merocyanine (active form), hence inhibiting apo-IDO1 as well as binding to free heme. Thereby, inhibiting the tryptophan metabolism through dual mechanism.

List of Abbreviation

ADME	Absorption, distribution, metabolism, excretion
S_a	Active site
K_d	Binding affinity
Bin1	Bridging Integrator-1
CRT	Calreticulin
CD	Circular dichroism
CD80	Cluster of differentiation 80
Cys	Cysteine
CYP	Cytochromes P_{450}
CTL	Cytotoxic T lymphocytes
CTLA-4	Cytotoxic T-lymphocyte-associated protein 4
DAMPs	Damage-associated molecular patterns
DCs	Dendritic cells
$CDCl_3$	Deuterated chloroform
DCM	Dichloromethane
DIAD	Diisopropyl azodicarboxylate
DMF	Dimethylformamide
DMAB	Dimethylaminobenzaldehyde
DMSO	Dimethyl sulfoxide
K_D	Dissociation constant
Dox	Doxorubicin
DMEM	Dulbecco's Modified Eagle Medium
ESI-MS	Electrospray ionization-*mass spectrometry*
λ_{em}	Emission wavelength
EtOAc	Ethyl acetate
EtOH	Ethanol
EDTA	Ethylenediaminetetraacetic acid
λ_{ex}	Excitation wavelength
FBS	Fetal Bovine Serum
GCN2	General control nonderepressible 2
GAPDH	Glyceraldehyde 3-phosphate dehydrogenase

Gly	Glycine
GSH	Glutathione
EC_{50}	Half maximal effective concentration
IC_{50}	Half maximal inhibitory concentration
HPLC	High performance liquid chromatography
HRMS	High-resolution mass spectrometry
His	Histidine
HSA	Human serum albumin
HCl	Hydrochloric acid
H_2O_2	Hydrogen peroxide
HOBt	Hydroxybenzotriazole
ICD	Immunogenic cell death
IDO1	Indoleamine 2,3-dioxygenase 1
K_i	*Inhibitor* constant
S_i	Inhibitory substrate binding site
IFN-γ	Interferon gamma
IL6	Interleukin 6
IP	Isoelectric point
Ile	Isoleucine
IPTG	Isopropyl β-D-1-thiogalactopyranoside
JAK	Janus kinases
Leu	Leucine
LB	Luria-Bertani media
$MgCl_2$	Magnesium chloride
mTORC	Mammalian target of rapamycin
MALDI-TOF	Matrix assisted laser desorption ionization-time of flight
T_m	Melting temperature
mRNA	Messenger Ribonucleic acid
MeOH	Methanol
K_m	Michaelis constant
MD	Molecular dynamic
NAs	Nano-aggregates
NK	Natural killer cells

CHES	N-Cyclohexyl-2-aminoethanesulfonic acid
EDC.HCl	*N*-Ethyl-N′-(3-dimethylaminopropyl)carbodiimide hydrochloride
NFK	*N*-Formylkynurenin
DIPEA	*N,N*-Diisopropylethylamine
NF-κB	Nuclear factor kappa B
N_2	Nitrogen
NMR	Nuclear magnetic resonance
OD	Optical density
O_2	Oxygen
PD-L1	Programmed death-ligand 1
Phe	Phenylalanine
PBS	Phosphate-buffered saline
H_3PO_4	Phosphoric acid
PDT	Photodynamic therapy
KCl	Potassium chloride
KOH	Potassium hydroxide
KPB	Potassium phosphate buffer
PD-1	Programmed cell death protein 1
PI	Propidium iodide
PGE2	Prostaglandin E_2
PDB	Protein Data Bank
PpIX	Protoporphyrin IX
ROS	Reactive oxygen species
RBC	Red blood cells
Treg	Regulatory T cells
RU	Response units
RPM	Revolutions per minute
Ser	Serine
STAT	Signal transducer and activator of transcription
NaCl	Sodium chloride
$Na_2S_2O_4$	Sodium dithionite
SDS	Sodium dodecyl sulfate
SDS-PAGE	Sodium dodecyl sulphate–polyacrylamide gel electrophoresis

NaH	Sodium hydride
Na_2SO_4	Sodium sulfate
SARs	Structure-activity relationship
SPR	Surface plasmon resonance
THF	Tetrahydrofuran
TMS	Tetramethylsilane
TLC	Thin layer chromatography
tRNA	Transfer ribonucleic acid
TGF-β	Transforming growth factor beta
TCA	Trichloroacetic acid
TES	Triethylsilane
Tris	Tris(hydroxymethyl)aminomethane
TFA	Trifluoroacetic acid
TCEP	Tris(2-carboxyethyl)phosphine
Tyr	Tyrosine
Trp	Tryptophan
TDO	Tryptophan 2,3-dioxygenase
TNF-α	Tumor necrosis factor alpha
TDLNs	Tumor-draining lymph nodes
Th	T helper cell
Thr	Threonine
K_{cat}	Turnover number
UV-Vis	Ultraviolet–visible
UGT	Uridine 5'-diphospho-glucuronosyltransferase
H_2O	Water
DPH	1,6-diphenyl-1,3,5-hexatriene
HBTU	(2-(1H-benzotriazol-1-yl)-1,1,3,3-tetramethyluronium hexafluorophosphate
MTT	3-(4,5-dimethylthiazol-2-yl)-2,5-diphenyl tetrazolium bromide
MOPS	3-(*N*-morpholino)propanesulfonic acid
HEPES	4-(2-hydroxyethyl)-1-piperazineethanesulfonic acid

For symbols/units

α	Alpha
Å	Angstrom
atm	Atmosphere
β	Beta
C	Celsius
J	Coupling constant
°	Degree
δ	Delta
Hz	Hertz
K	Kelvin
MHz	Megahertz
m	Meta
µg	Micro gram
µM	Micro mole
mL	Millilitre
mV	Mili Volt
min	Minute
nM	Nano mole
o	Ortho
p	Para
ppm	Parts per million
%	Percent
π	Pi
ps	Pico second
s	Second

Chapter 1

Introduction of IDO1 and Its Inhibitor Towards Immunotherapy

Disruption of host immune signaling contributes to high mortality in many diseases, including cancer.[1] Immunotherapy offers an effective approach by inducing immunogenic cell death (ICD), but tumors often develop immunosuppressive mechanisms that counteract this effect. Immune checkpoint inhibitors, such as PD-1 and CTLA-4 antibodies, have shown promise; however, their clinical responses remain limited by the tumor microenvironment.[2] Moreover, the overexpression of indoleamine 2,3-dioxygenase 1 (IDO1) enzyme depletes tryptophan in tumor tissues, thereby activating pathways that suppress the proliferation of cytotoxic T cells.[3] As a result, IDO1 has emerged as a key immunomodulator and a focus of modern cancer immunotherapy research.

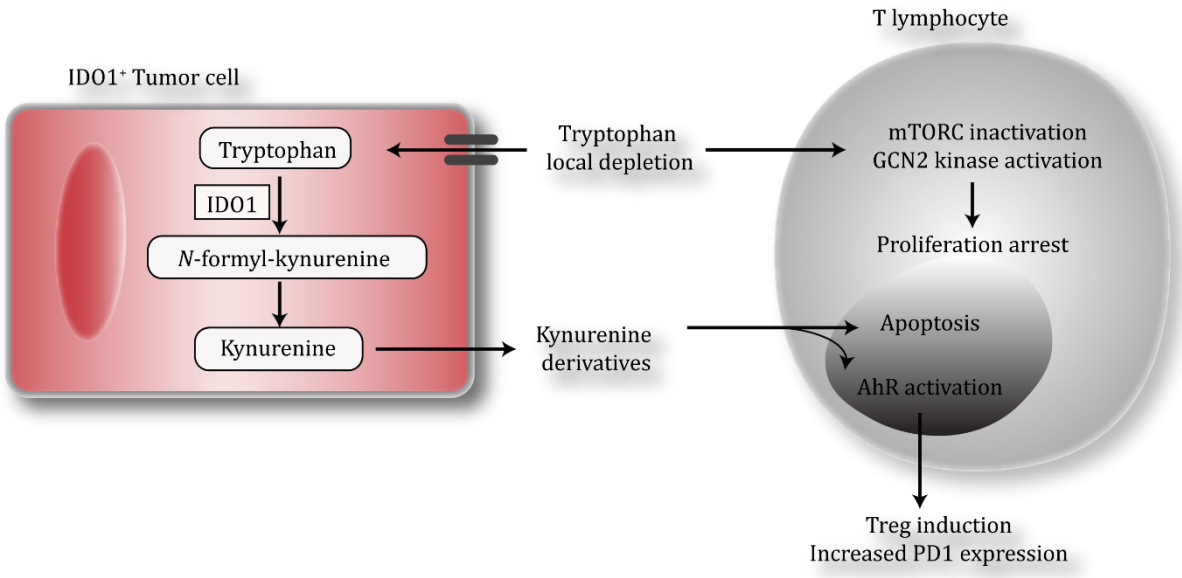

Fig. 1.1. Proposed mechanisms by which IDO1-mediated tryptophan degradation inhibits local T cell responses in tumors.

Several IDO1 inhibitors with different structural entities have been identified, enriching IDO1 as a potential immunotherapeutic target. Diverse structural classes, including *N*-hydroxyamidine, tryptophan, imidathiazole, imidazole, triazole, and several others, were reported as potent IDO1 inhibitors.[4] There are several modes of binding the inhibitors in the IDO1 active pocket.

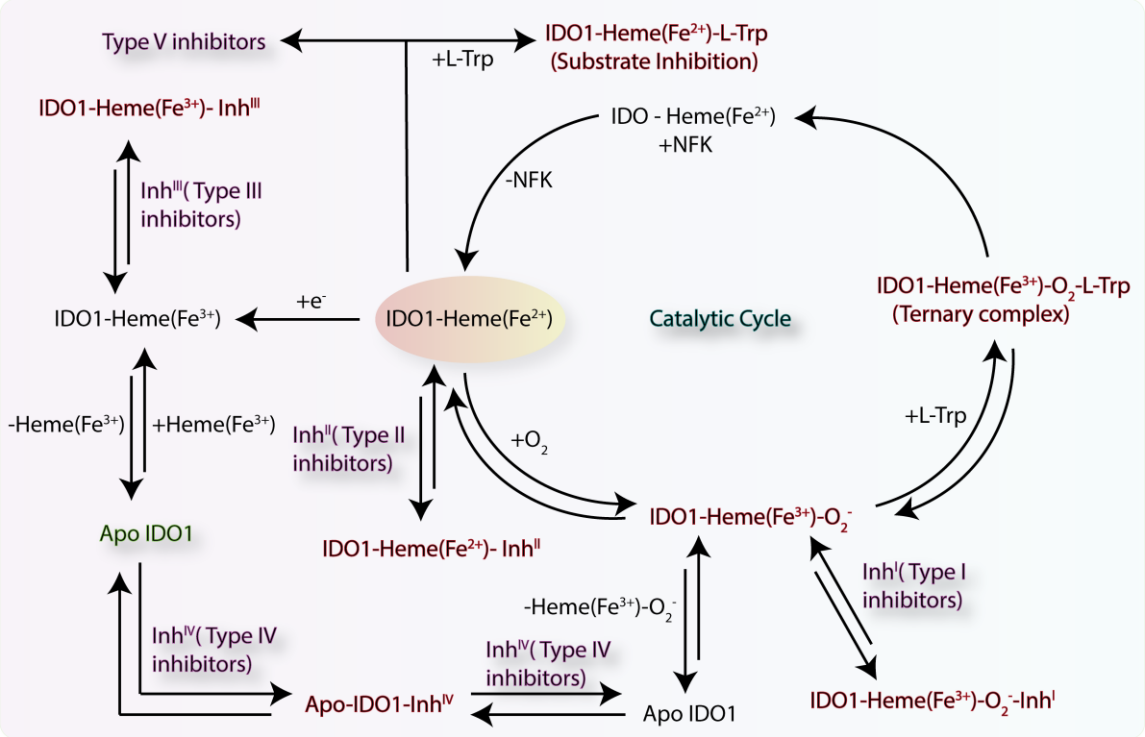

Scheme 1.2. IDO1 ligand binding, redox equilibria, and catalytic cycle (colour box). Five different inhibitor types are defined based on their preferential binding to oxygen-bound holo-IDO1 (type I, Inh^{I}), ferrous holo-IDO1 (type II, Inh^{II}), ferric holo-IDO1 (type III, Inh^{III}), apo-IDO1 (type IV, Inh^{IV}) and catalytic pathway inhibitor (type V, Inh^{V}). Apo-IDO1 is formed primarily by dissociation of free ferric or oxygen-bound ferric heme. L-Trp recruitment before oxygen binding leads to an unproductive complex (substrate inhibition).

In consideration of the binding mode of the inhibitors, they are also classified into a few categories.[5] However, the disappointing Phase 3 trial (ECHO-301) of epacadostat, a selective IDO1 inhibitor, in combination with pembrolizumab, has created uncertainty regarding IDO1 inhibition as an immunotherapeutic treatment for several diseases involving IDO1. Despite resuming the clinical trials of IDO1 inhibitors in combination with immune checkpoint inhibitors, there remains scope for the development of new inhibitors or more convenient strategies to investigate the mechanism of IDO1 inhibition and achieve various clinical benefits.[6,7] There is several evidence supporting the supplementary advantages of dual immunotherapy and chemotherapeutic drugs to the antitumor alerts.[4, 8] A handful of antineoplastic agents, such as (Dox) doxorubicin and oxaliplatin, trigger calreticulin (CRT) exposure on the surface of dying tumor cells, promoting immunogenic cell death (ICD). This process enhances the ability of dendritic

cells (DCs) to recognize and attack cancer cells.[9] Hence, it leads to the strengthening of the antitumor immune response. However, these chemotherapeutic drugs have various side effects and suboptimal tumor targeting, thereby limiting their clinical trials. Recently, chemotherapy in combination with IDO1 inhibitors has shown great potential in various clinical trials. Advanced nano-delivery systems based on amphiphilic materials have emerged as a promising approach for target-specific delivery of therapeutic agents.[10] These nanocarriers help overcome the challenges associated with chemotherapy, particularly in eliciting effective anti-immunosuppressive responses.[10, 11]

Aim of the Thesis

In this thesis, we have focused on development of small molecule for robust and selective IDO1 inhibition. Additionally, we have explored the therapeutic potential of our synthesised inhibitors for the immunotherapeutic treatment in cancer. The entire work is arranged into four chapters as given below. In Chapter 1, we discussed about IDO1 and its inhibitors. **Chapter 2** focused on the mode of evaluation of dichloroquinolines in IDO1 inhibition by showing a dual mode of inhibitory action, binding both apo IDO1 and free heme. **Chapter 3** mainly deals how photopharmacology, where the synthesized tryptamine derivatives are photocaged installing a photosensitive linker, releasing the drug on photoirradiation. **Chapter 4** elaborates how spiropyran derivatives behaves as photoswitchable as well as pH responsive inhibitors, targeting both apo-IDO1 and free heme for the inhibition process.

Chapter 2

Evaluation of mode of Indoleamine 2,3-dioxygenase 1 Inhibition by 4,7-dichloroquinolines.

Currently, different IDO1 inhibitors (such as epacadostat and NLG-919), in combination with immune checkpoint inhibitors, are being explored for the possible treatment of different types of cancer.[12, 13] However, the unfortunate failure of the ECHO-301 phase III clinical trial of epacadostat/keytruda combination against metastatic melanoma came as a complete shock to immunotherapy-related research on cancer.[14] Hence, the reinvestigation of the IDO1 inhibition mechanism has become obligatory to accomplish the clinical benefit.

Linrodostat (BMS-986205), developed by Bristol-Myers Squibb, is an orally available IDO1 (apo-IDO1) inhibitor that restores and induces the proliferation and activation of immune cells and reduces the proliferation of T_{reg}.[15] Consequent growth of

IDO1-expressing tumor cells are getting diminished. Currently, linrodostat is in Phase-III clinical trials for the treatment of muscle-invasive bladder and other cancers.[16] However, the optimized synthesis required more than 12 steps to produce linrodostat, which could limit its large-scale production and enhance production cost.[17] We hypothesized that developing small molecules that could have similar apo-IDO1-mediated inhibitory activity and can be synthesized in fewer steps would benefit IDO1-mediated drug-discovery studies. Hence, inspired by the success linrodostat as an IDO1 inhibitor, we developed synthetically simpler analogs of 4,7-dichloroquinoline (DCQ) (Scheme 2.2).

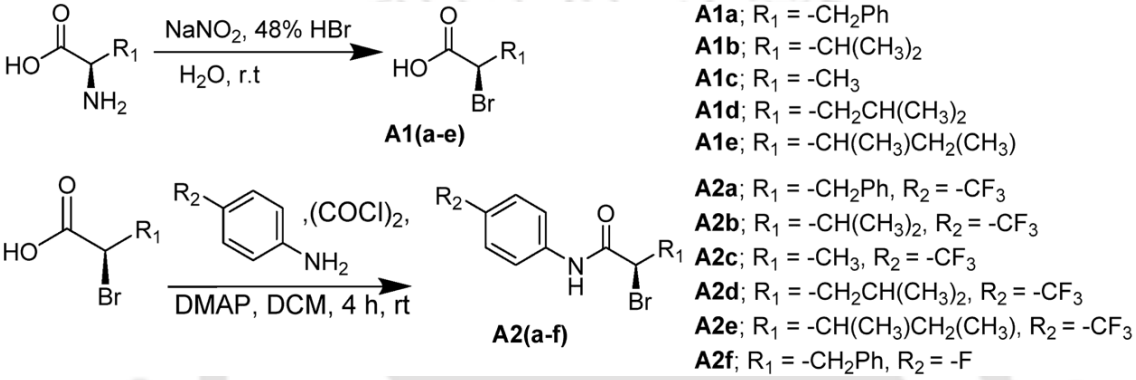

Scheme 2.1. Synthesis of amino acid derivatives.

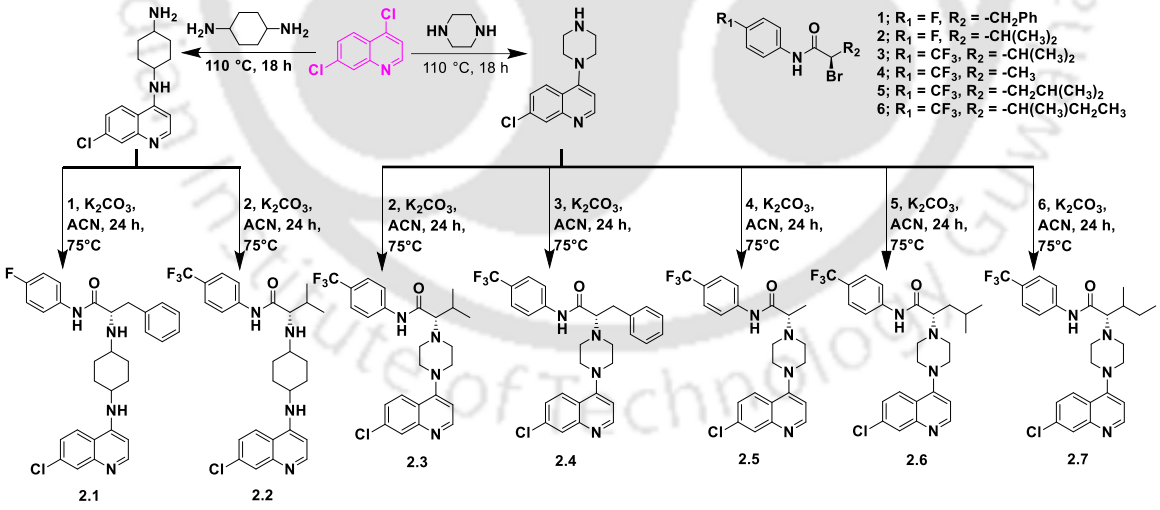

Scheme 2.2. Synthetic routes to DCQ derivatives.

Derivatization of the DCQ moiety enhanced the IDO1 inhibitory activity against both purified enzyme and the cellular environment, without significant cytotoxicity, leading to the identification of piperazine-containing DCQ derivative **2.4** as a potent IDO1 inhibitor with an IC_{50} of 94 ± 4 nM.

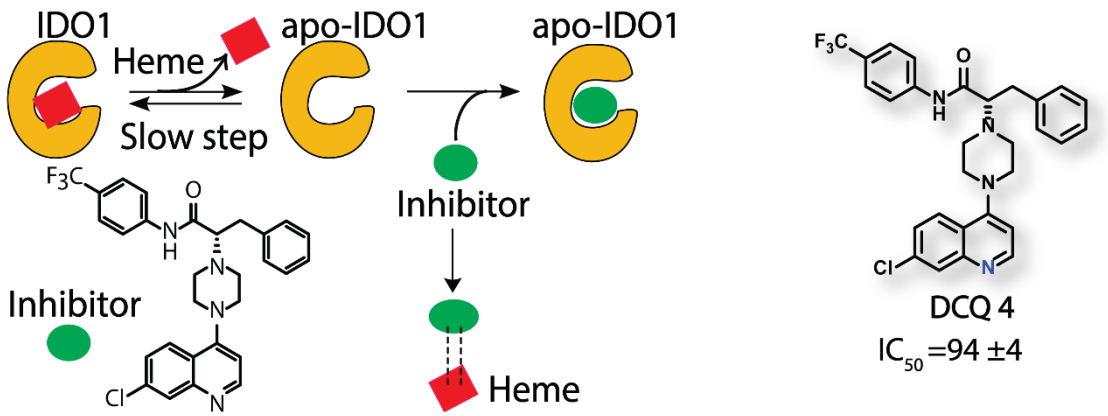

Fig. 2.1. Graphical representation of apo- IDO1 inhibition and free heme binding.

A series of biophysical studies, including UV-Vis spectroscopy of the Soret band (Fig.2.2 A), time and temperature dependent study (Fig. 2.2 A, B), SPR study (Fig. 2.3 A), docking (Fig. 2.3 B, C), as well as protoporphyrin IX binding studies, suggested that the IDO1 inhibitory activity of potent compound could be due to its direct binding to apo-IDO1 protein and formation of **2.4**-heme complex. This simple strategy of developing apo-IDO1-targeting molecules with DCQ, piperazine, and amino acid moieties as potent IDO1 inhibitors could be helpful in combating immune-related diseases.

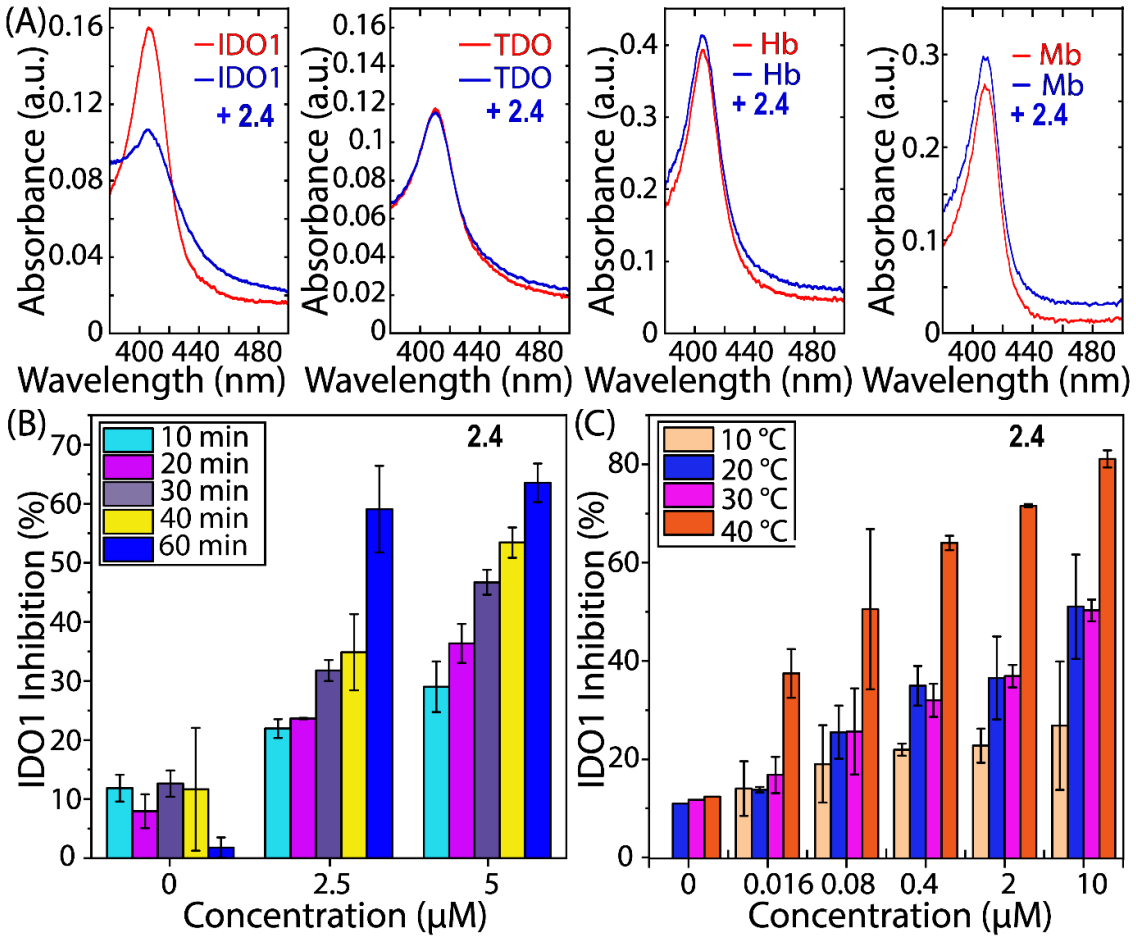

Fig. 2.2. Absorption spectra of the ferric-IDO1 enzyme, ferric-TDO enzyme, hemoglobin, and myoglobin (200 nM) in the absence and presence of the compounds (5 μM) in 100 mM phosphate buffer at pH 6.5 after 60 min of incubation at 37 °C (A). Incubation time was varied to measure the IDO1 (200 nM) activity in the absence and presence of different concentrations of **2.4** (B). Temperature-dependent (C) IDO1 (200 nM) activity in the absence and presence of different concentrations of **2.4** with 60 min of incubation time (C). All of these measurements were performed without preincubating the enzyme with the compound.

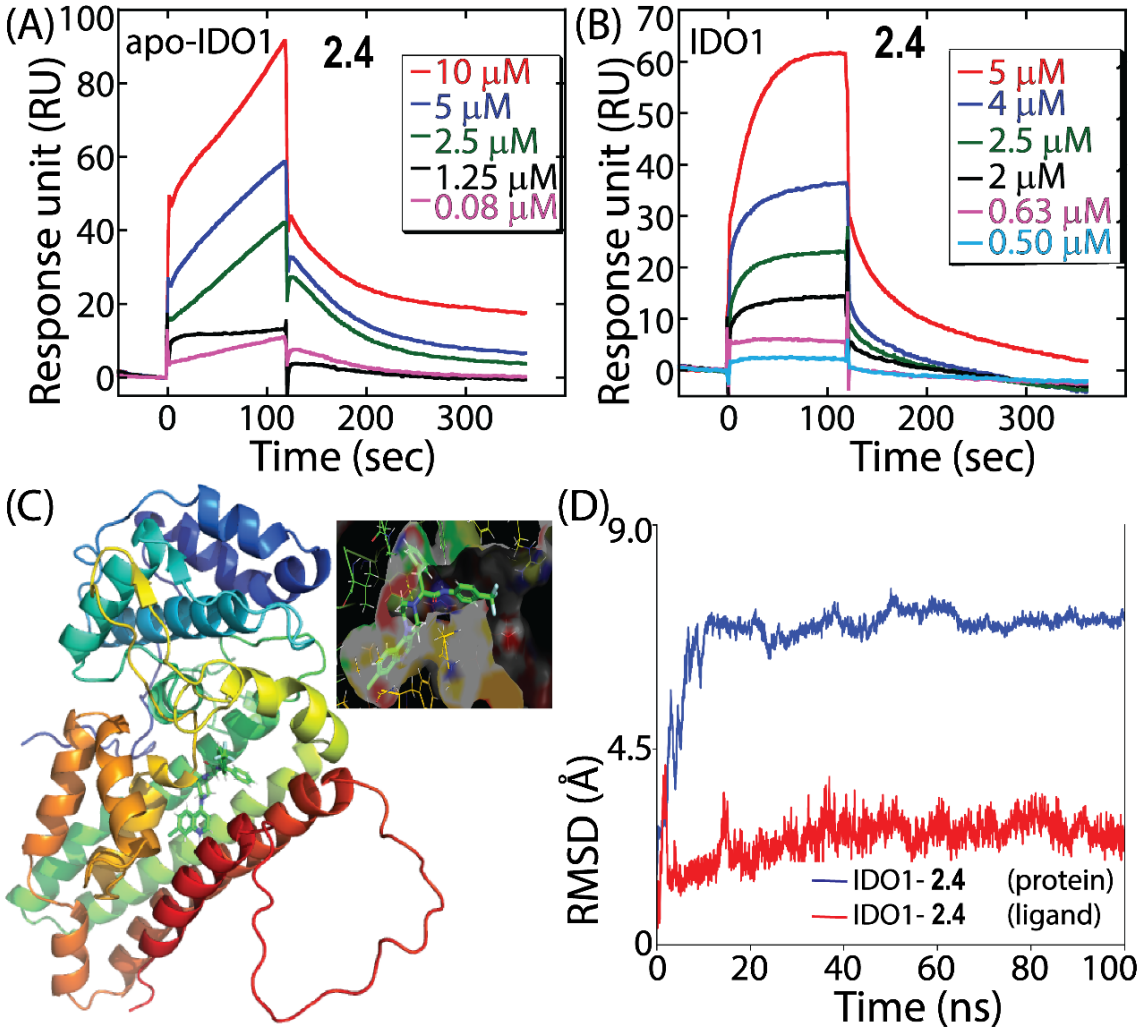

Fig. 2.3. Real-time concentration-dependent binding measurements of the compound, **2.4** with IDO1 enzyme (A) and apo-IDO1 protein by SPR analyses (B). Probable mode of interaction of **2.4** with the apo-IDO1 (PDB ID: 6MQ6) (C). The root-mean-square deviations (RMSD) for protein (apo-IDO1 protein bound to **2.4**; blue) and ligand (**2.4** bound to apo-IDO1; red) (D)

Chapter 3

Photoresponsive prodrug for regulated inhibition of indoleamine 2,3-dioxygenase 1 enzyme

In the second chapter, we have developed apo-IDO1 inhibitors that exhibit dual inhibitory action; however, they lack target-specific action and temporal control over drug release. Therefore, in this chapter, we focused on developing target-specific drug delivery with the temporal release of the drug from the prodrug on photoirradiation.[18] Recently, the role of indole-based IDO1 inhibitors in cancer

and Alzheimer's disease has inspired us to develop thiourea derivatives of 1-methyltryptamine.[19] The novelty of our compound design lies in the development of thiourea derivatives of 2-azole-substituted 1-methyltryptamine, aimed at achieving selective inhibition of the immunosuppressive enzyme, IDO1 (Scheme 3.1).

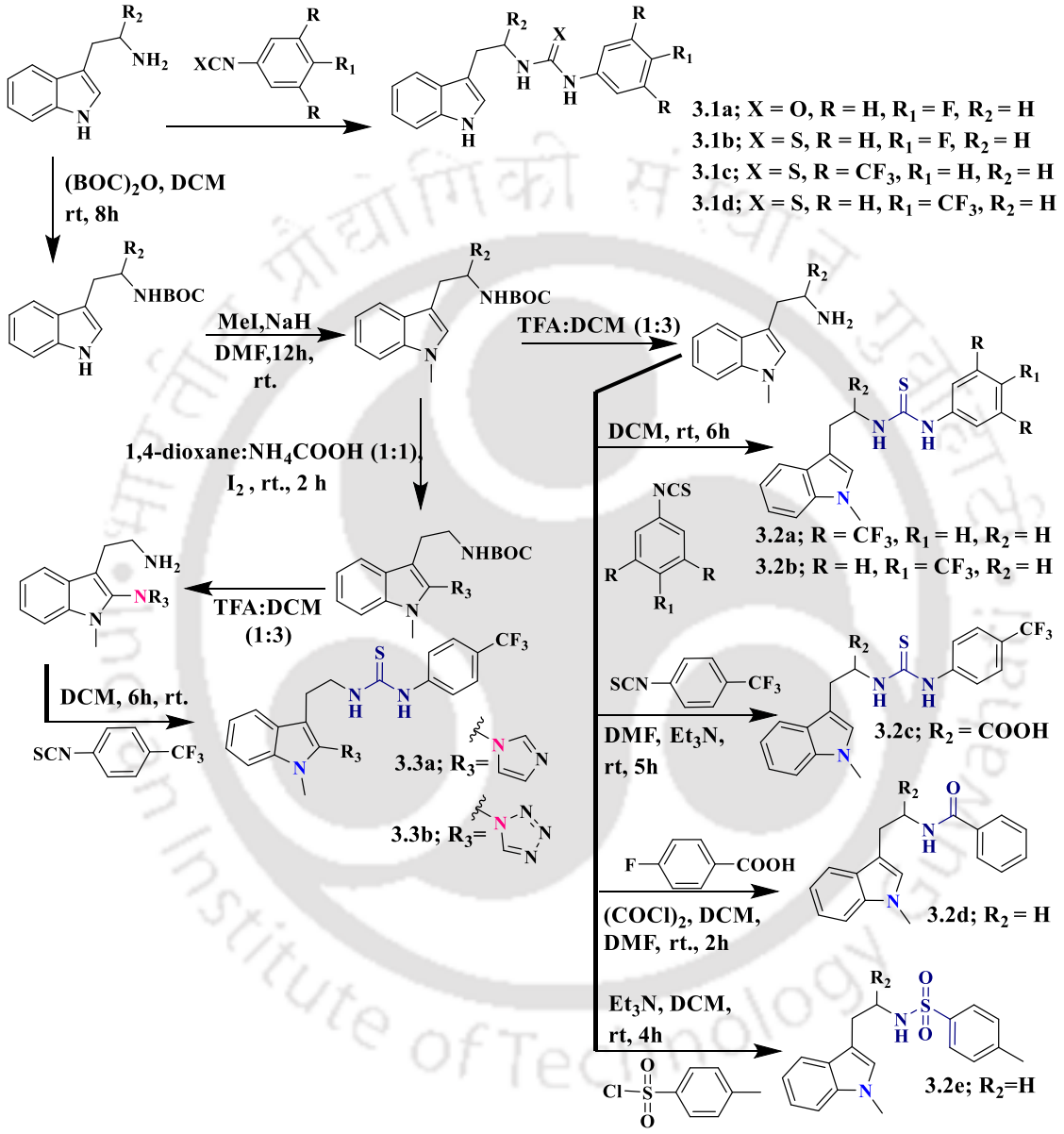

Scheme 3.1. Synthetic routes to various indole derivatives from tryptamine and tryptophan.

From subsequent biochemical studies, it has been confirmed that the potent tryptamine derivative **3.3a** exhibits moderate inhibitory activity against the purified IDO1 enzyme. The potent compound showed strong IDO1 inhibition activity with an IC_{50} value of 120 nM. The most potent compound **3.3a** binds specifically to the active site of IDO1,

interacting with the heme group and surrounding residues, as supported by UV-vis spectroscopy, docking, and molecular dynamics simulations. The compound **3.3a** exhibited strong inhibitory activity with minimal cytotoxicity and high selectivity over related enzymes, such as tryptophan 2,3-dioxygenase.[20]

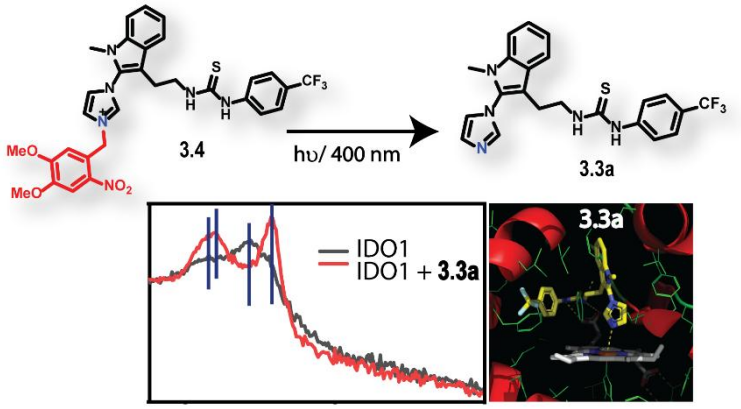

Fig. 3.1. Schematic diagram representing the photocleavable prodrug generating drug on exposure to 400 nm light.

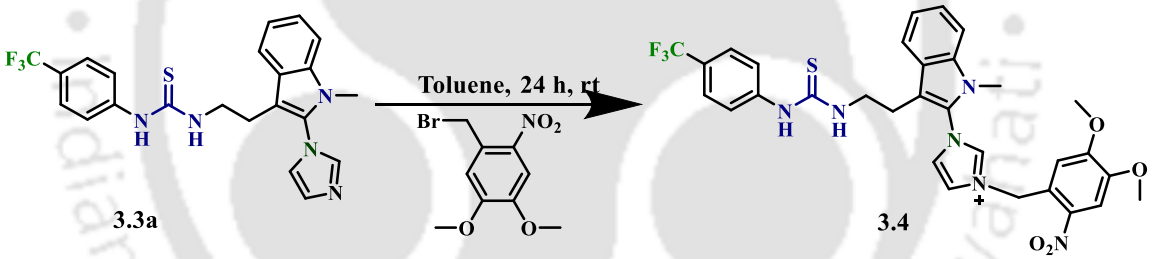

Scheme 3.2. Synthetic pathway of a prodrug from a drug linking a photo-sensitive linker.

Furthermore, a photoresponsive prodrug system has been developed that can regenerate the active, potent IDO1 inhibitor upon exposure to light. This photocaged prodrug exhibits negligible IDO1 inhibition activity under similar experimental conditions as the drug. The photocaged prodrug showed successful regeneration of the active IDO1 inhibitor at visible light irradiation of 400nm light, providing a spatiotemporal control over the drug activation, used to improve the therapeutic efficacy of IDO1 inhibitors (Fig. 3.2)

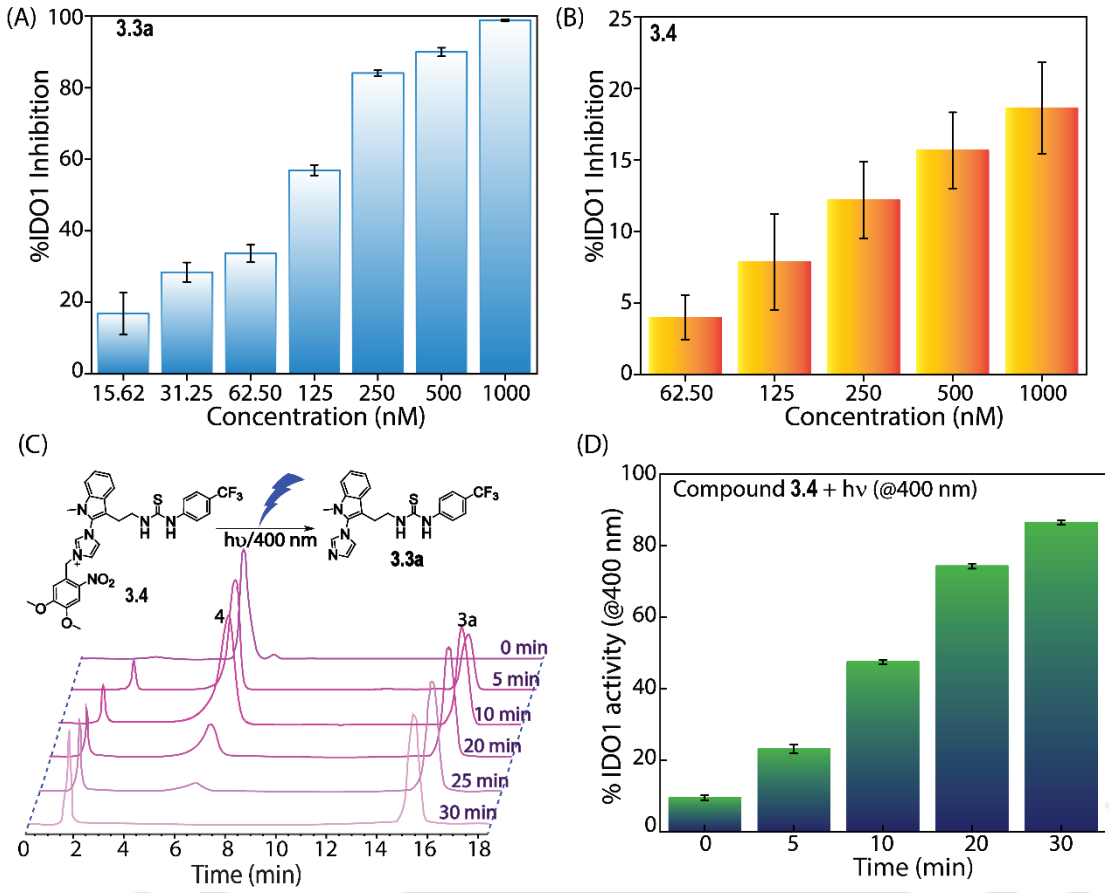

Fig. 3.2. Variation of %IDO1 inhibition in the presence of different concentrations for compound **3.3a** (A) and compound **3.4** (B) in the presence of IDO1 enzyme (650 nM), (C) Photoinduced (λ_{ex} = 400 nm) regeneration of the potent compound **3.3a** from the prodrug **3.4** was analysed by HPLC analysis. (D) IDO1 activity assay of prodrug **3.4** at different time intervals after photoinduction (400 nm).

Chapter 4

Photoswitchable Inhibitors: Temporally Regulated Inhibition of IDO1 Enzyme Using Photoactive Merocyanine Derivatives.

In last chapter, we synthesized a photoresponsive prodrug which release drug on photo irradiation cleaving the photosensitive linker.[21] This linker, if used in excess, can act as a toxic byproduct, leading to other side effects. Therefore, in this chapter, we propose the use of photoswitchable compounds as a promising approach to addressing the challenges of targeted IDO1 inhibition, allowing for temporal control and potentially enhancing therapeutic benefits while minimizing systemic side effects.[22] Spiropyrans are known to undergo reversible isomerization when exposed to light and pH, transitioning between ring-closed spiropyran (SP) and ring-opened merocyanine (MC) form, which

makes them useful in applications such as chemical sensors, drug delivery systems, and smart materials[23, 24] (Fig. 4.1)

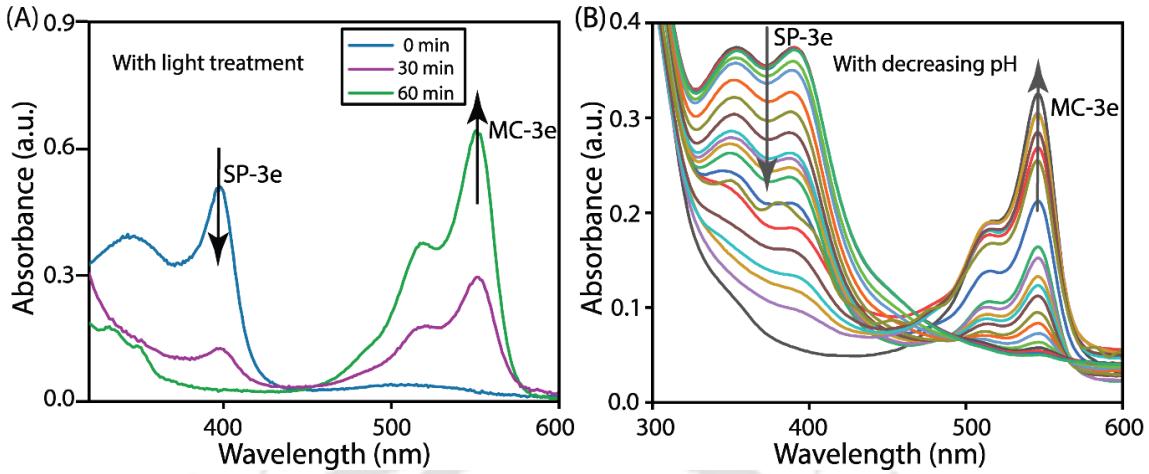

Fig. 4.1. Conversion of spiropyran to merocyanine in the presence of light (A) and pH (B).

We hypothesize that the appropriately substituted MC form could selectively bind and inhibit IDO1 in the targeted tissues, only after photoirradiation. This strategy could allow us to control the formation of the active inhibitor in a spatiotemporal manner and regulate IDO1 activity in the targeted cells and tissues.[25, 26] We synthesized a series of spiropyran derivatives (Scheme 4.1) and identified **4.3e** as a potent and stimuli-responsive inhibitor of IDO1.

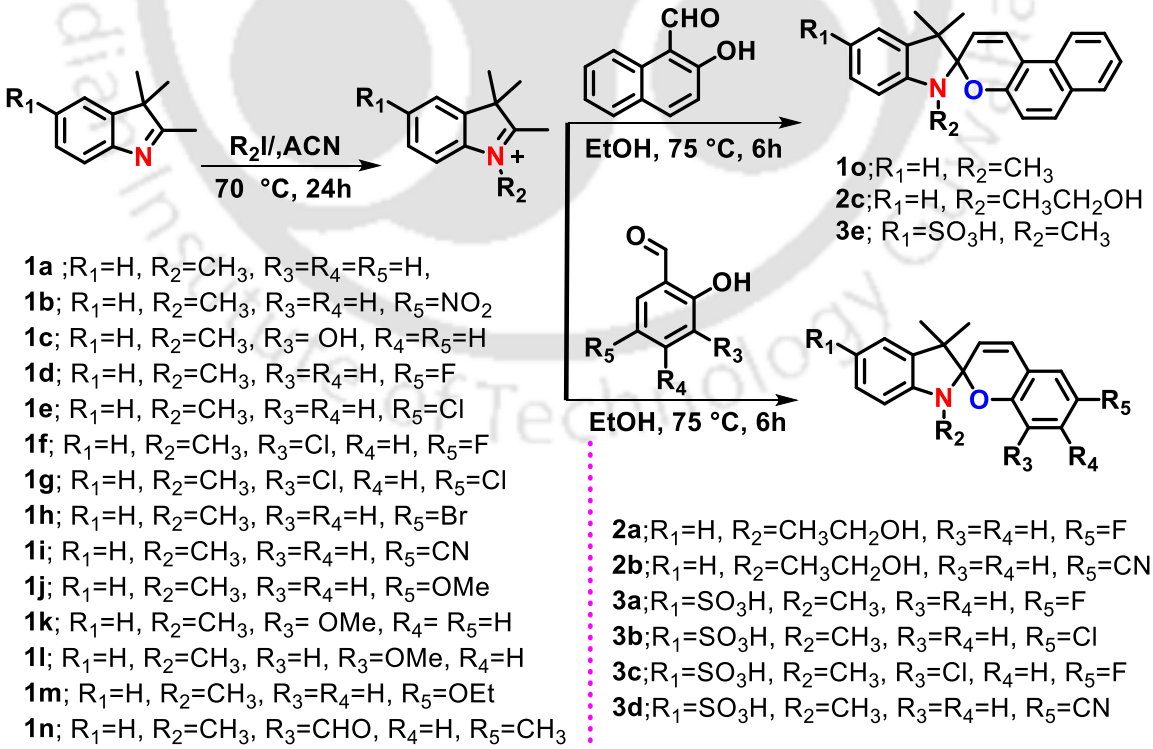

Scheme 4.1. Synthetic routes to spiropyran derivatives from 2,3,3-trimethyl-3*H*-indole.

Upon exposure to light or acidic pH, **4.3e** undergoes conversion to photoactive **4.3e-MC** isoform, which exhibits strong IDO1 inhibitory activity in comparison to that of the photoinactive **4.3e-SP** isoform (Fig. 4A, B, E, F). By facilitating the release of heme from holo-IDO1 and transforming it into the apo form, the **4.3e-MC** exhibits the ability to bind both apo-IDO1 protein and free hemin (Fig. 4.2 C, D)

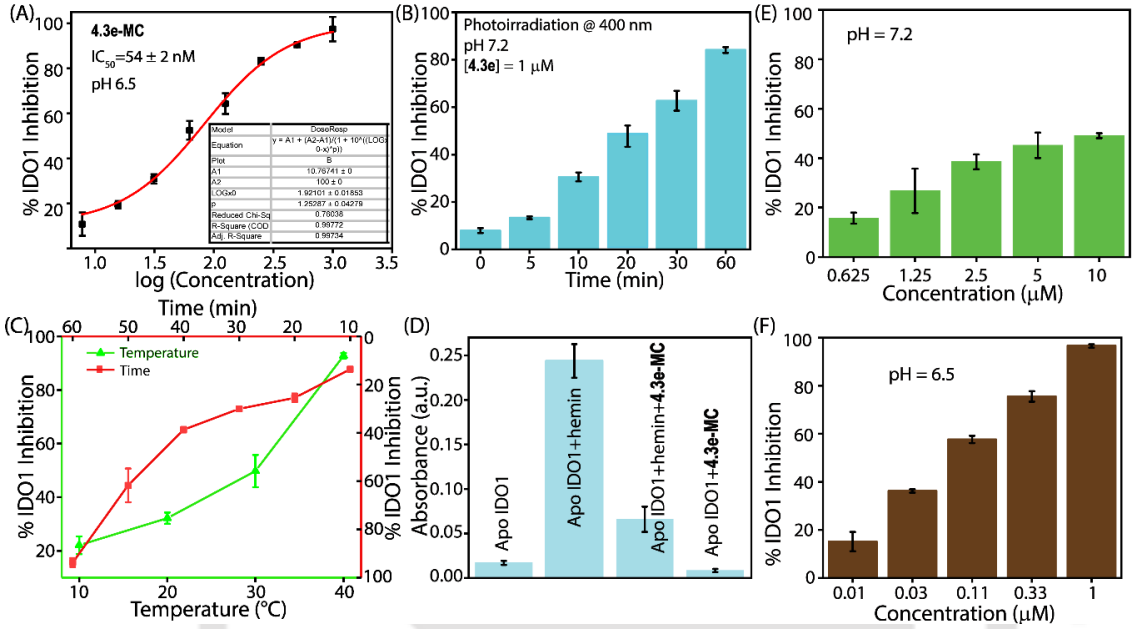

Fig. 4.2. Inhibitory activities of IDO1 at different concentrations of **4.3e-MC** at pH 6.5 (A), after photoirradiation of **4.3e** with 400 nm light at different time intervals (B), IDO1 inhibitory activities at different temperatures and time intervals with **4.3e-MC** at pH 6.5 (C), The activity of apo-IDO1 in the absence and presence of the compound and/or hemin (D), IDO1 inhibitory activities at different pH in presence of **4.3e** (10 and 1µM) (E, F).

From the cellular assay, we can also confirm that **4.3e-MC** binds to apo-IDO1 as well as to free heme, thereby preventing the free heme from reinserting into apo-IDO1 and regaining its enzyme activity (Fig. 4.3C). The confocal microscopic images revealed distinct red fluorescent puncta in treated HeLa cells, confirming internalization of **4.3e-MC**, while untreated control cells showed no fluorescence (Fig. 4.3D).

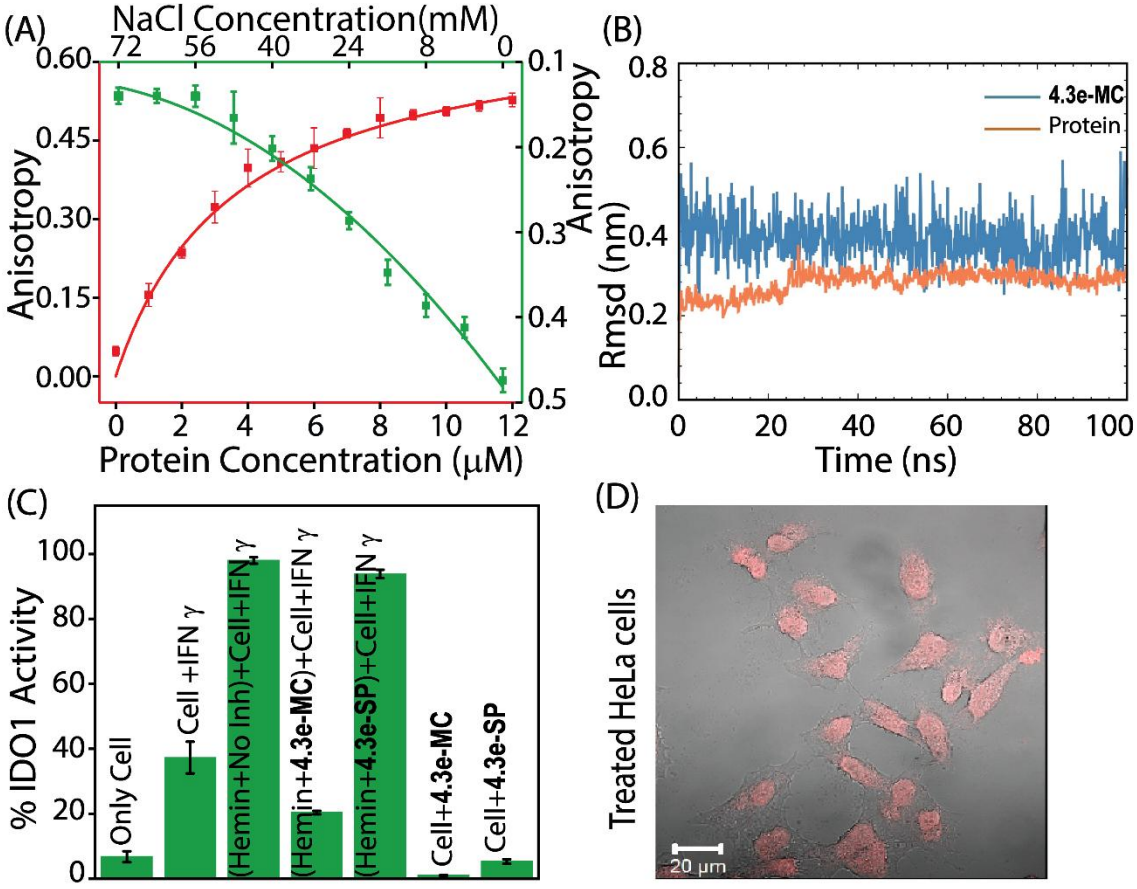

Fig. 4.3. Steady-state fluorescence anisotropy measurements of **4.3e-MC** (500 nM) in the presence of various concentrations of apo-IDO1 protein (0-12 μM) and in the absence and presence of different concentrations of NaCl (0-75 mM) (A), The variation in RMSD obtained for apo IDO1 (orange) and **4.3e-MC** (blue) (B), IDO1 inhibition activity in cells with and without IFN-γ treatment in the presence and absence of the isoforms of **4.3e** (C)**,** Confocal microscopic image of **4.3e-MC**-treated HeLa cells (D).

These findings highlight a novel strategy for temporal regulation of IDO1 activity by utilizing light and pH as the external stimuli. Compared to traditional IDO1 inhibitors, this photoresponsive approach offers significant potential for the development of spatiotemporally regulated therapies for cancer, Alzheimer's disease, and other pathological conditions, enabling greater specificity and safety.

Conclusion

In this thesis, we have successfully described the role of IDO1 in the immunosuppression process associated with various life-threatening diseases. Moreover, the importance of IDO1 inhibition has been described in **Chapter 1**. The linrodostat mimic

dichloroquinoline derivatives (in **Chapter 2**) show moderate apo-IDO1 inhibitory activity by releasing the heme from the holo-IDO1 pocket and also binding with the free heme, preventing it from reinserting inside the apo-IDO1 pocket. Though dichloroquinoline showed moderate inhibition of apo-IDO1 and also binds to heme, it lacks target-specific drug release; hence, the tryptamine-based azole derivatives linked to a photo-sensitive linker (In **Chapter 3**) act as a prodrug, and when 400 nm light is applied, they release the tryptamine-based azole derivative, exhibiting decent IDO1 inhibition. In **Chapter 4**, the spiropyran derivatives, when converted to merocyanine derivatives in the presence of light or pH, act as an apo-IDO1 inhibitor by releasing heme and binding to the apo-IDO1 pocket. The spiropyran derivatives also bind to the free heme. These photoswitch derivatives enable us to explore a dual-stimuli-responsive IDO1 inhibitor, demonstrating temporal and target-specific drug release.

Future prospects

Future research on IDO1 inhibition should prioritize the exploration of non-enzymatic pathways, as these remain underexplored, which can reveal new mechanisms for therapeutic intervention. The development of IDO1 inhibitors with covalent linkers can enable irreversible inhibition and may have the potential to lead more durable and effective suppression of the enzyme activity. Additionally, combining IDO1 inhibition with fluorescent labelling techniques can offers an innovative approach for real-time visualization and precise monitoring of inhibitor binding and enzyme dynamics. Thereby, it can enhance mechanistic understanding and therapeutic targeting. These integrated strategies hold promise for advance designing of next-generation IDO1 inhibitors with diagnostic capabilities and improved efficacy in cancer immunotherapy and other disease contexts.

References

1. Goyal, N.; Sridhar, J.; Do, C.; Bratton, M.; Shaik, S.; Jiang, Q.; Foroozesh, M., Identification of CYP 2A6 inhibitors in an effort to mitigate the harmful effects of the phytochemical nicotine. *J. cancer metastatis treat.* **2021,** *7*, 18.

2. Catanzaro, E.; Beltrán-Visiedo, M.; Galluzzi, L.; Krysko, D. V., Immunogenicity of cell death and cancer immunotherapy with immune checkpoint inhibitors. *Cell Mol Immunol.* **2025,** *22* (1), 24-39.

3. Tufail, M.; Jiang, C.-H.; Li, N., Immune evasion in cancer: mechanisms and cutting-edge therapeutic approaches. *Signal transduct. target. ther.* **2025,** *10* (1), 227.

4. Wang, X.-X.; Sun, S.-Y.; Dong, Q.-Q.; Wu, X.-X.; Tang, W.; Xing, Y.-Q., Recent advances in the discovery of indoleamine 2, 3-dioxygenase 1 (IDO1) inhibitors. *Medchemcomm.* **2019,** *10* (10), 1740-1754.

5. Röhrig, U. F.; Reynaud, A.; Majjigapu, S. R.; Vogel, P.; Pojer, F.; Zoete, V. J. J. o. m. c., Inhibition mechanisms of indoleamine 2, 3-dioxygenase 1 (IDO1). *J. Med. Chem.* **2019,** *62* (19), 8784-8795.

6. Davis, A. A.; Patel, V. G. J. J. f. i. o. c., The role of PD-L1 expression as a predictive biomarker: an analysis of all US Food and Drug Administration (FDA) approvals of immune checkpoint inhibitors. *J. Immunother. Cancer* **2019,** *7* (1), 1-8.

7. Komiya, T.; Huang, C. H., Updates in the clinical development of epacadostat and other indoleamine 2, 3-dioxygenase 1 inhibitors (IDO1) for human cancers. *Front Oncol.* **2018,** *8*, 423.

8. Gao, M.; Yu, W.; Xi, Z.; Zhang, Z.; Fan, X.; Wang, X., Recent Update on the Discovery of Indoleamine-2, 3-Dioxygenase 1 Inhibitors Targeting Cancer Immunotherapy. *Eur. J. Med. Chem.* **2025**, 118017.

9. Zou, Y.; Chen, J.; Qu, Y.; Luo, X.; Wang, W.; Zheng, X., Evolution of nMOFs in photodynamic therapy: from porphyrins to chlorins and bacteriochlorins for better efficacy. *Front. pharmacol.* **2025,** *16*, 1533040.

10. Hu, J.; Arvejeh, P. M.; Bone, S.; Hett, E.; Marincola, F. M.; Roh, K.-H., Nanocarriers for cutting-edge cancer immunotherapies. *J. Transl. Med.* **2025,** *23* (1), 447.

11. Peng, S.; Xiao, F.; Chen, M.; Gao, H., Tumor-microenvironment-responsive nanomedicine for enhanced cancer immunotherapy. *Adv. Sci.* **2022,** *9* (1), 2103836.

12. Yue, E. W.; Sparks, R.; Polam, P.; Modi, D.; Douty, B.; Wayland, B.; Glass, B.; Takvorian, A.; Glenn, J.; Zhu, W., INCB24360 (Epacadostat), a highly potent and selective indoleamine-2, 3-dioxygenase 1 (IDO1) inhibitor for immuno-oncology. *ACS Med. Chem. Lett.* **2017,** *8* (5), 486-491.

13. Kumar, S.; Jaipuri, F. A.; Waldo, J. P.; Potturi, H.; Marcinowicz, A.; Adams, J.; Van Allen, C.; Zhuang, H.; Vahanian, N.; Link Jr, C., Discovery of indoximod prodrugs and characterization of clinical candidate NLG802. *Eur. J. Med. Chem.* **2020,** *198*, 112373.

14. Labadie, B. W.; Bao, R.; Luke, J. J., Reimagining IDO pathway inhibition in cancer immunotherapy via downstream focus on the tryptophan–kynurenine–aryl hydrocarbon axis. *Clin. Cancer Res.* **2019,** *25* (5), 1462-1471.

15. Shore, N. D.; Redorta, J. P.; Robert, G.; Hutson, T. E.; Cesari, R.; Hariharan, S.; Faba, Ó. R.; Briganti, A.; Steinberg, G. D. In *Non-muscle-invasive bladder cancer: An overview of potential new treatment options*, Urol Oncol, Elsevier: 2021; pp 642-663.

16. Balog, A.; Lin, T.-a.; Maley, D.; Gullo-Brown, J.; Kandoussi, E. H.; Zeng, J.; Hunt, J. T., Preclinical characterization of linrodostat mesylate, a novel, potent, and selective oral indoleamine 2, 3-dioxygenase 1 inhibitor. *Mol. Cancer Ther.* **2021,** *20* (3), 467-476.

17. Fraunhoffer, K. J.; DelMonte, A. J.; Beutner, G. L.; Bultman, M. S.; Camacho, K.; Cohen, B.; Dixon, D. D.; Fan, Y.; Fanfair, D.; Freitag, A. J., Rapid development of a commercial process for linrodostat, an indoleamine 2, 3-dioxygenase (IDO) inhibitor. *Org. Process Res. Dev.* **2019,** *23* (11), 2482-2498.

18. Tang, K.; Wu, Y.-H.; Song, Y.; Yu, B., Indoleamine 2, 3-dioxygenase 1 (IDO1) inhibitors in clinical trials for cancer immunotherapy. *J Hematol Oncol.* **2021,** *14* (1), 68.

19. Minhas, P. S.; Jones, J. R.; Latif-Hernandez, A.; Sugiura, Y.; Durairaj, A. S.; Wang, Q.; Mhatre, S. D.; Uenaka, T.; Crapser, J.; Conley, T., Restoring hippocampal glucose metabolism rescues cognition across Alzheimer's disease pathologies. *Science* **2024,** *385* (6711), eabm6131.

20. Pradhan, N.; Akhtar, N.; Nath, B.; Peña-García, J.; Gupta, A.; Pérez-Sánchez, H.; Kumar, S.; Manna, D., Inhibition of immunosuppressive indoleamine 2, 3-dioxygenase by targeting the heme and apo-form. *Chem Commun* **2021,** *57* (3), 395-398.

21. Das, N. M.; Prusty, B. M.; Sahoo, A.; Mazumder, P.; Chauhan, S.; Hazarika, G.; Kumar, S.; Dhabal, D.; Manna, D., Photoresponsive prodrug for regulated inhibition of indoleamine 2, 3-dioxygenase 1 enzyme activity. *RSC Med. Chem.* **2025**.

22. Jiang, K.; Wang, Q.; Chen, X.-L.; Wang, X.; Gu, X.; Feng, S.; Wu, J.; Shang, H.; Ba, X.; Zhang, Y., Nanodelivery optimization of IDO1 inhibitors in tumor immunotherapy: challenges and strategies. *Int. J. Nanomed.* **2024**, 8847-8882.

23. Fleming, C. L.; Li, S.; Grøtli, M.; Andréasson, J., Shining new light on the spiropyran photoswitch: a photocage decides between cis–trans or spiro-merocyanine isomerization. *J. Am. Chem. Soc.* **2018,** *140* (43), 14069-14072.

24. Rad, J. K.; Balzade, Z.; Mahdavian, A. R., Spiropyran-based advanced photoswitchable materials: A fascinating pathway to the future stimuli-responsive devices. *J. Photochem. Photobiol. C.* **2022,** *51*, 100487.

25. Reifarth, M.; Bekir, M.; Bapolisi, A. M.; Titov, E.; Nußhardt, F.; Nowaczyk, J.; Grigoriev, D.; Sharma, A.; Saalfrank, P.; Santer, S., A dual pH-and light-responsive

spiropyran-based surfactant: Investigations on its switching behavior and remote control over emulsion stability. *Angew. Chem., Int. Ed.* **2022,** *61* (21), e202114687.
26. Li, L.; Yang, W.-W.; Xu, D.-G., Stimuli-responsive nanoscale drug delivery systems for cancer therapy. *J. Drug Target.* **2019,** *27* (4), 423-433.

CHAPTER 1

Introduction of IDO1 and Its Inhibitor Towards Immunotherapy

1.1. Introduction

Immunotherapy has emerged as one of the most promising and potentially effective strategies to fight against cancer. The ability to modulate host immune signaling is an innovation that offers new hope in combating high-mortality diseases such as cancer. Immunotherapy is now recognized as one of the most important strategies of cancer treatment alongside chemotherapy, surgery, targeted therapies, and radiation, opening a new frontier in cancer care.[1] By mobilizing the immune cells of the body to selectively target and remove cancer cells, the limitations of conventional treatments are addressed by immunotherapy and offers a more precise and adaptive therapeutic approach. Immunotherapy exercises the anti-cancer effects to induce immunogenic cell death (ICD) and stimulates a sustained immune response against tumor antigens.[2] However, tumors have evolved several immune evasion strategies that weaken the effectiveness of ICD. For instance, the interaction between immune control compounds like PD-L1 or CD80 present on tumor cells and CTLA-4 or PD-1 present on T cells facilitates tumor persistence as well as suppression of the immune system. Monoclonal antibodies, like inhibitors for immune checkpoint compounds that target PD-1 and CTLA-4, have shown promising results to reactivate anti-tumor immunity.[3] Still, clinical outcomes remain suboptimal in many cases due to the limitation in immune cell infiltration and resistance mechanisms inside the tumor microenvironment. For overcoming these challenges, complementary therapeutic strategies are required for enhancing immunotherapy potency.[4] One such approach involves targeting metabolic enzymes contributing to the immune suppression induced by the tumor. Indoleamine 2,3-dioxygenase 1 and tryptophan 2,3-dioxygenase, also known as IDO1 and TDO, respectively, are mostly overexpressed in tumor tissues and tumor-draining lymph nodes (TDLNs), playing an important role in this process. The degradation of L-tryptophan, which is an essential amino acid for T cell proliferation, is catabolized by both of these enzymes. The resulting tryptophan degradation activates downstream signaling pathways, suppressing cytotoxic T lymphocyte (CTL) activity and hence promoting an immunosuppressive microenvironment.[5] Among these two enzymes, IDO1 has emerged as a particularly influential immune modulator in cancer. It involves promoting immune tolerance, making it a focal point of immunotherapy for cancer treatment research nowadays.

In cancer, IDO1 is utilized by tumors to deplete tryptophan and create an immunosuppressive microenvironment. These depletion leads to the production of kynurenine, expanding regulatory T cells and suppressing anti-tumour immunity. Additionally, in neurodegenerative diseases like Alzheimer's and Parkinson's disease, IDO1 is overexpressed in the brain and this enhanced the tryptophan catabolism. This triggered the generation of neurotoxic kynurenine metabolites that induces synaptic dysfunction, neuronal death as well as neuroinflammation. This kynurenine activation pathway contributes to cognitive decline and disease advancement in Alzheimer's disease by weaking the astrocyte support functions for neurons. It is also connected to depression and dementia related to inflammation.[6] Furthermore, in cardiovascular disease, endothelial cell-specific induces IDO1 expression, which then generates kynurenine by tryptophan metabolism, worsening the cardiac outcomes. Through reactive oxygen production, it induces cardiomyocyte apoptosis.[7] Moreover, in autoimmune diseases, the immune system is balanced by IDO1, controlling immune cells called dendritic cells (DCs). In normal conditions, $IDO1^{+}$ dendrite cells prohibit immune exaggeration by preventing the attack towards T cells and supports regulatory T cells, protecting the body from attacking itself. As soon as IDO1 depletes, the control over immune system is lost, that results in an excessive immune response noticed in autoimmune diseases. In infectious diseases, though the tryptophan depletion limits the pathogen replication but it also promotes immune tolerance. It reduces inflammation with the drawback of suppressing the immune system.[8] Additionally, IDO1 is also involved in chronic infections and liver diseases, pregnancy, organ transplant rejections and other infection like pneumonia, HIV.[9]

A wide range of IDO1 inhibitors with different structures, such as N-hydroxyamidines, imidazothiazoles, tryptophan analogs, triazoles, and imidazoles, have been developed to inhibit the enzymatic function of IDO1. These compounds bind to the active site effectively, disrupting the activity of IDO1 through various mechanisms.[10] However, by the disappointing results of the Phase III ECHO-301 trial, the attention for IDO1 as a therapeutic target was restrained, where the selective IDO1 inhibitor epacadostat in combination with the PD-1 inhibitor pembrolizumab was tested.[11] The trial failed to show improved clinical outcomes and raised questions about the therapeutic viability of IDO1 inhibition. In spite of this setback, clinical interest in IDO1 continued with new combination trials and concepts. This demonstrates the necessity to reassess the strategies targeting IDO1 and develop next-generation inhibitors that can more effectively synergize with immune checkpoint blockade.[12, 13]

1.2. Cellular Signaling Pathways Regulating IDO1 Expression

Recent studies have illustrated that due to the overexpression of the enzyme IDO1, the tumor microenvironment is significantly immunosuppressive.[14-16] IDO1 is present in low amounts across various adult human tissues in normal physiological conditions. However, in many cancers, IDO1 expression becomes dysregulated and is highly upregulated in stromal components, immune cells, and tumor cells. This irregular overexpression of IDO1 is caused by several dysregulated signaling series, mostly by the interferon-gamma (IFN-γ) signaling axis.[17, 18] During inflammatory responses, immune cells release various pro-inflammatory mediators such as IFN-γ, tumor necrosis factor-alpha (TNF-α), transforming growth factor-beta (TGF-β), prostaglandin E2 (PGE2), as well as damage-associated molecular patterns (DAMPs). While IFN-γ typically plays a protective anti-tumor role but it also paradoxically activates the JAK–STAT signaling pathway in certain contexts and leads to the enhancement of IDO1 transcription.[16, 19] Moreover, kynurenine metabolites, which are the subsequent products of IDO1 activity, can further initiate the aryl hydrocarbon receptor (AhR) in immune cells, triggering the immune suppression.[19] This activation induces the production of IL-6 and PGE2, and these in turn can reinforce IDO1 expression via continued JAK–STAT signaling. IDO1 upregulation is also contributed by the immune checkpoint interactions such as PD-1/PD-L1 and CTLA-4/CD80. These interactions stimulate the NF-κB pathway in both tumor and immune cells, enhancing immunosuppressive signaling. TGF-β further promotes IDO1 expression, specifically in $CD80^{+}$ dendritic cells.[20, 21] Additionally, cyclooxygenase-2 (COX-2) and PGE2 can activate phosphoinositide 3-kinase (PI3K) and protein kinase C (PKC) pathways, which also contribute to IDO1 overexpression in the tumor microenvironment. RAS and KIT signaling, along with other oncogenic pathways, have been implicated in modulating IDO1 levels. One such regulatory mechanism includes the suppression of gene Bin1, a tumor suppressor, whose downregulation is associated with increasing IDO1 expression.[22-24]

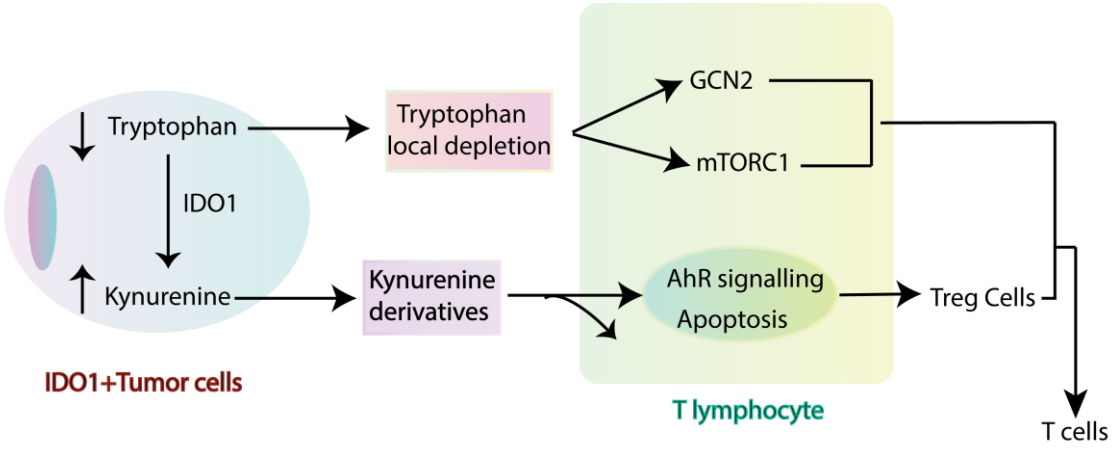

Fig. 1.1. Mechanisms of L-Trp degradation by IDO1, inhibiting local T cell responses in the tumor microenvironment.

1.3. IDO1-Mediated Tryptophan Metabolism Promotes Tumor Immune Escape and Inflammation

IDO1 plays a diverse and crucial role in cancer progression by modulating both immune suppression and promoting tumor inflammation within the tumor microenvironment.[25] The expression of IDO1 is often upregulated in stromal cells, antigen-presenting cells, and tumor cells as a result of various signaling pathways, which include NF-κB and Jak/STAT, as well as inflammatory mediators like IFNγ. The immunosuppressive function of IDO1 is primarily driven by its enzymatic activity of local tryptophan (Trp) depletion, which leads to the accumulation of immunomodulatory metabolites such as kynurenine, 3-hydroxykynurenine, and quinolinic acid.[26, 27] The GCN2 kinase pathway is activated by this Trp depletion in T cells which results in cell cycle arrest, anergy, or apoptosis, while suppressing mTORC signaling and further inducing T cell autophagy and anergy, and promotes regulatory T cell (Treg) differentiation.[28-30] Kynurenine along with its metabolites act as ligands for the aryl hydrocarbon receptor (AhR) which modulates the function of various immune cells and enhances the production of immunosuppressive cytokines such as IL-10 and IL-6 and further reinforced the immune tolerance and supports Treg expansion.[31, 32] Beyond immune evasion, IDO1 acts as a critical modifier of the inflammatory milieu, particularly by influencing neovascularization and supporting tumor growth and metastasis. Experimental models indicate that IDO1 does not directly lead to inflammation or tumor initiation but it rather alters the metabolic character of inflammation and makes it more conducive to tumor development.[32, 33] For example, in skin and lung cancer models,

genetic deletion of IDO1 leads to reduced tumor outgrowth and impaired neovascularization, effects that are closely linked to decreased levels of the pro-inflammatory cytokine IL-6.[33] IDO1 serves as a regulatory node at the interface between IFNγ and IL-6 and shiftes the inflammatory environment from an anti-tumorigenic and IFNγ-dominated state which restricts new blood vessel formation towards a tumor-promoting, IL-6-rich state, sustaining neovascularization and tumor progression. This function distinguishes IDO1 from classical pro-angiogenic factors like VEGF, as IDO1, instead of directly promoting new vessel formation, primarily maintains established neovasculature by limiting vessel regression[18, 33] Moreover, IDO1 has been involved in promoting tumor cell survival through the induction of a dormancy program. In response to IFNγ, expression of IDO1 along with AhR in tumor-repopulating cells can inhibit pro-apoptotic STAT1 signaling and upregulate cell cycle inhibitors such as p27, which can divert cells from apoptosis to a dormant and survival state. This dormancy mechanism enables tumor cells to evade immune-mediated destruction and may contribute to resistance against therapy and tumor relapse.[18]

1.4. Targeting Enzymatic Activity of IDO1 as well as Non-Canonical Signaling in Preclinical Therapeutic Strategies

IDO1, being a pivotal enzyme in cancer immunology, acts as both a metabolic and signaling checkpoint, enabling tumors to evade immune surveillance. IDO1 catalyzes the degradation of tryptophan into kynurenines, immunosuppressive metabolites. This process has several extreme effects on the tumor microenvironment (TME). Firstly, depletion of local tryptophan activates stress-response pathways in neighboring T cells, markedly increasing the GCN2 and mTOR kinases, which lead to T cell cycle arrest, impaired effector function, and anergy. Secondly, accumulation of kynurenine and its downstream metabolites directly inhibit effector T cell proliferation and induces apoptosis as well as encourages the differentiation of naive $CD4^+$ T cells into immunosuppressive regulatory T cells (Tregs) via activation of the aryl hydrocarbon receptor (AhR). Furthermore, the activity of IDO1 supports the development of tolerogenic dendritic cells and myeloid-derived suppressor cells. Hence, further dampening anti-tumor immunity.[34, 35] Along with its well-characterized enzymatic functions, IDO1 also exerts non-enzymatic, signaling-based immunosuppressive effects. The protein exists in two forms: holo-IDO1 (with heme, catalytically active) and apo-IDO1 (heme-free, catalytically inactive). The apo-form can act as a signaling molecule that interacts with SH2-domain-containing proteins such as SHP-2, PI3K, and SOCS3 through its immunoreceptor tyrosine-based inhibitory motifs

(ITIMs). These interactions can further advances a tolerogenic phenotype in dendritic cells and support tumorigenic signaling pathways, independent of tryptophan metabolism.[36] This plasticity complicates therapeutic targeting, as it inhibits only the enzymatic activity, leaving the non-enzymatic, pro-tumorigenic signaling functions intact or even enhanced, as observed with some inhibitors like epacadostat. Observing its primary role in immune evasion, IDO1 has been targeted by various therapeutic strategies. Small-molecule inhibitors such as epacadostat, indoximod, and BMS-986205 have been developed to block or inhibit its enzymatic activity. Despite of it in clinical trials, including the high-profile ECHO-301 phase III trial of epacadostat with pembrolizumab, failed to show significant benefit, likely due to the robustness of non-enzymatic IDO1 functions and insufficient patient stratification.[11] More recent approaches include IDO1-targeted vaccines, which stimulate cytotoxic T cells specific for IDO1, thereby directly killing IDO1-expressing tumor and immunosuppressive cells. For example, a vaccine targeting IDO/PD-L1 epitopes has been demonstrated to attract T cells into tumors, inducing a type 1 helper T cell (TH1) inflammatory response and synergizing with PD-1 blockade, converting the TME from immunosuppressive to immune-permissive.[37] Combination therapies have shown the most promising results, particularly in tumors resistant to single-agent immunotherapy. For instance, in microsatellite-stable colorectal cancer, which is typically unresponsive to PD-1 inhibitors, combining IDO1 inhibition with PD-1 blockade significantly reduced tumor growth and increased infiltration of pro-inflammatory macrophages and $CD8^+$ T cells. This was associated with the upregulation of the JAK2-STAT3-IL6 pathway, which promotes a shift toward a more inflammatory and immunogenic TME.[38, 39]

Moreover, preclinical models have demonstrated that combining IDO1 inhibitors with chemotherapeutic agents like cyclophosphamide yields synergistic anti-tumor effects that lead to substantial tumor necrosis and reduced IDO1 expression in the TME. Despite these advances, the challenge remains to fully neutralize the enzymatic and non-enzymatic functions of IDO1.[40] Current pharmacologic approaches are insufficient as they predominantly target the metabolic activity of the enzyme and leave the signaling functions unaddressed. Future directions include the development of dual-function inhibitors or combination regimens that can simultaneously block both arms of IDO1-mediated immunosuppression as well as the use of biomarkers such as IDO1 expression levels and tryptophan/kynurenine ratios for better selection of patients who are likely to benefit from IDO1-targeted therapies.[33]

1.5. Enzymatic Degradation of L-Tryptophan by IDO1

The catabolism of L-tryptophan (L-Trp) with IDO1 via the kynurenine pathway is a primary process in immune regulation and cancer biology, acting as the primary enzyme catalyzing the initial and rate-limiting step.[26, 40] IDO1, a heme-containing enzyme, is expressed in a wide variety of tissues and is mostly upregulated in response to inflammatory signals such as interferon-gamma, especially in dendritic cells and tumor microenvironments. The main function of IDO1 is to convert L-Trp into N-formylkynurenine (NFK), which is then further metabolized into kynurenine (Kyn) and a series of downstream metabolites that include anthranilic acid, 3-hydroxykynurenine, quinolinic acid, kynurenic acid, and ultimately nicotinamide adenine dinucleotide (NAD+), which is a critical coenzyme in cellular metabolism. With IDO1 and its homologs IDO2 and TDO acting as the key regulatory enzymes in peripheral tissues and the liver, respectively, this pathway accounts for almost 95% of L-Trp depletion in the body.[35]

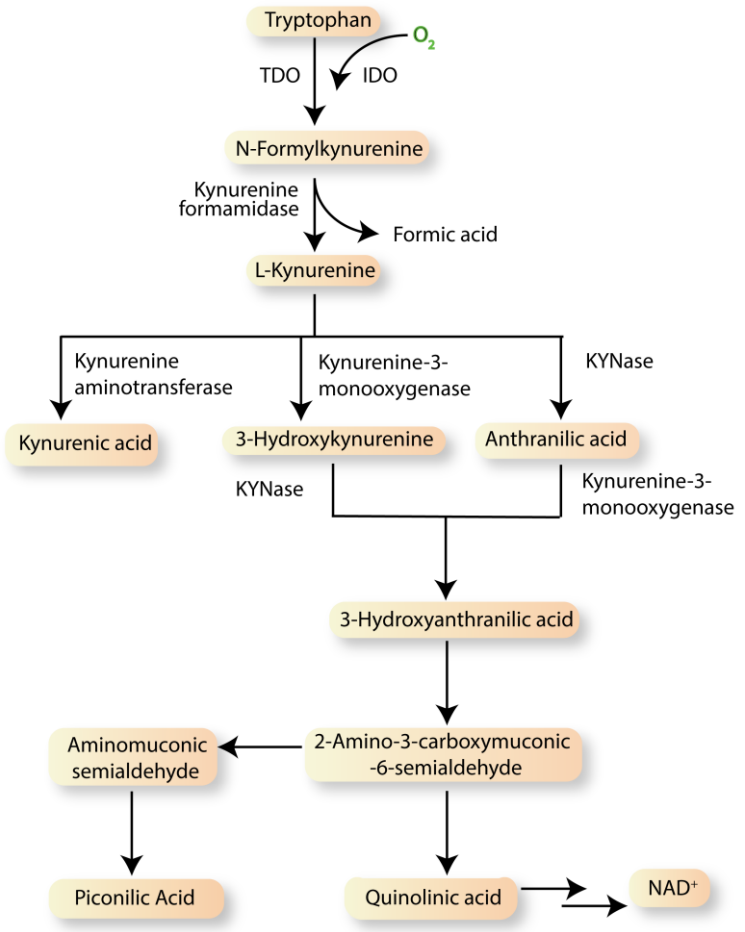

Fig. 1.2. Schematic diagram representing the depletion of L-Trp by IDO1, IDO2, and TDO via kynurenine pathways.

The catabolism of L-Trp by IDO1 begins with L-Trp and molecular oxygen binding to the ferrous (Fe^{2+}) heme center of the enzyme, which forms a ternary complex. This complex undergoes a two-step ferryl-based oxidation. Firstly, the enzyme catalyzes the inclusion of the two atoms of molecular oxygen in the indole ring of L-Trp, generating a ferric-superoxide intermediate. Subsequently, a highly reactive ferryl (Fe^{4+}=O) species and a Trp-epoxide intermediate are formed, finally recombining to produce N-formylkynurenine, leaving the enzyme in an inactive ferric (Fe^{3+}) state. For the continuation of catalysis, the enzyme then reduced back to its active ferrous form. Primarily, the redox state of its heme cofactor regulates the catalytic activity of IDO1. When tryptophan levels are low, IDO1 can accumulate in the inactive ferric state or even lose its heme group and become catalytically inactive (apo-IDO1). This flexible regulation allows cells to modulate IDO1 activity, resulting in metabolic and immunological signals.[41, 42]

From a clinical perspective, the results of IDO1-mediated L-Trp catabolism are profound. The degradation of local tryptophan in the microenvironment activates the general control nonderepressible 2 (GCN2) kinase pathway in T cells, which leads to cell cycle arrest, anergy, and impaired effector function. In parallel, the accumulation of kynurenine and its derivatives act as endogenous ligands for the aryl hydrocarbon receptor (AhR), promotes the differentiation and expansion of regulatory T cells (Tregs), and suppresses immune responses.

For maintaining tolerance for maternal-fetal during pregnancy and for resolving inflammation, these immunosuppressive effects are crucial, but they are also hijacked by tumors to evade immune surveillance, making IDO1 a major target in immunotherapy for cancer. Along with the enzymatic activity, IDO1 has non-enzymatic signaling functions, particularly in dendritic cells, where it can revise immune responses toward long-term tolerance through SHP1/SHP2 and noncanonical NF-κB pathways.[43] Overall, IDO1-mediated L-Trp catabolism is a highly regulated and multifaceted process that not only governs amino acid metabolism but also manages immune responses in disease and health. Its main role in immune suppression, especially in the tumor microenvironment, has driven the development of IDO1 inhibitors as potential cancer therapeutics, although the complexity of its regulation and dual functions present significant challenges for clinical translation.[9, 44]

The architecture of the active site of IDO1 is fundamental to its catalytic efficiency and substrate specificity in L-tryptophan (Trp) catabolism. The catalytic site of IDO1 is

built around a prosthetic heme group (Heme-Porphyrin IX), centrally positioned within a large domain that forms the catalytic cleft. This active site features two primary substrate-binding regions, one is the S_a site, subdivided into a partially hydrophobic pocket A and hydrophilic pocket B on the distal side of the heme, and the unique S_i site on the proximal side. Trp binds primarily at the S_a site, forming a hydrogen bond with the ammonium group and the 7-propionate group of the heme, anchoring the substrate for catalysis. The carboxylate group of Trp establishes a hydrogen bond with Arg231 in pocket B, while the indoleamine moiety is stabilized by a hydrogen bond to Ser167 via a bridging water molecule and hydrophobic interactions with residues in pocket A.[45]

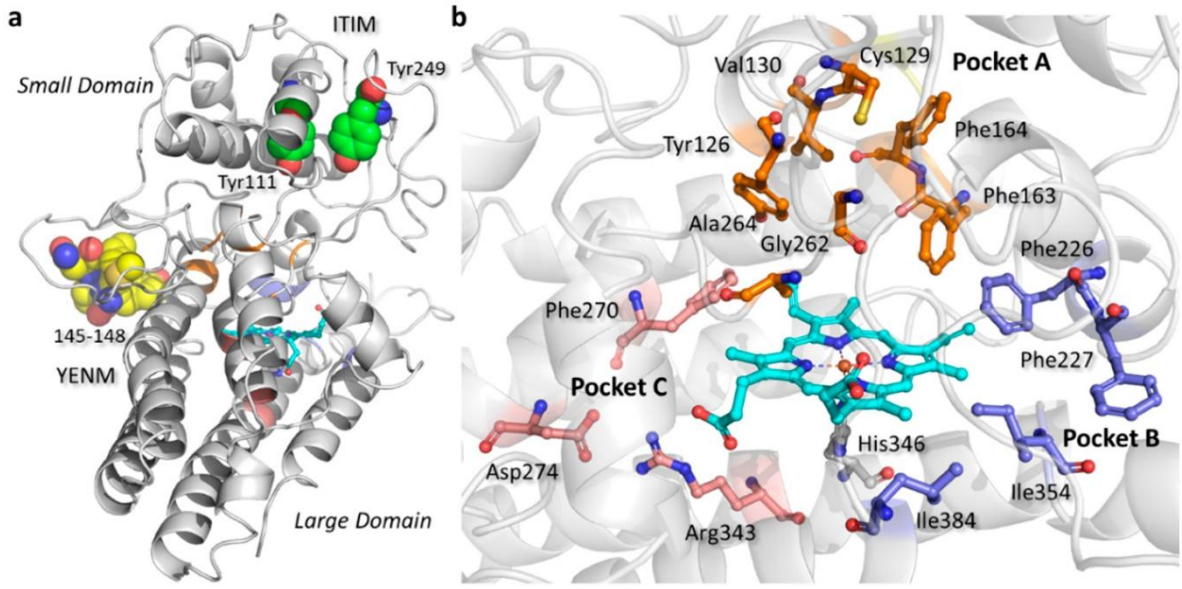

Fig. 1.3. Binding Sites of IDO1 enzyme and the key residues of the binding sites. Reproduced from ref.45 with permission from the Springer Nature.

Crystallographic studies have revealed that the Trp occupying the S_i site can induce conformational changes in the S_a site and disrupt the recombination of the ferryl intermediate with the Trp-epoxide during catalysis. Furthermore, binding of Trp at the S_i site, prompting the movement of Phe270, acts as a gatekeeper residue to block the water tunnel and thereby interfere with O_2 delivery to the S_a site, an essential step for efficient enzyme turnover. The heme cofactor itself is dynamic and can reversibly associate with the protein, where its binding and redox state (ferrous or ferric) critically influence enzyme activity and substrate processing. The main residues for substrate recognition, positioning, and the catalytic process, which are Ser167, Arg231, and Phe270, are known to be crucial. The interaction between these residues, the heme group, and the structural flexibility of

the active site, including the JK loop, checks the substrate access, ensures the precise orchestration of Trp binding, oxygen activation, and product formation in IDO1-mediated catabolism. This detailed understanding of the active site elucidates the molecular basis of IDO1 function and also informs the rational design of selective inhibitors for therapeutic intervention in cancer and immune-related diseases.[45]

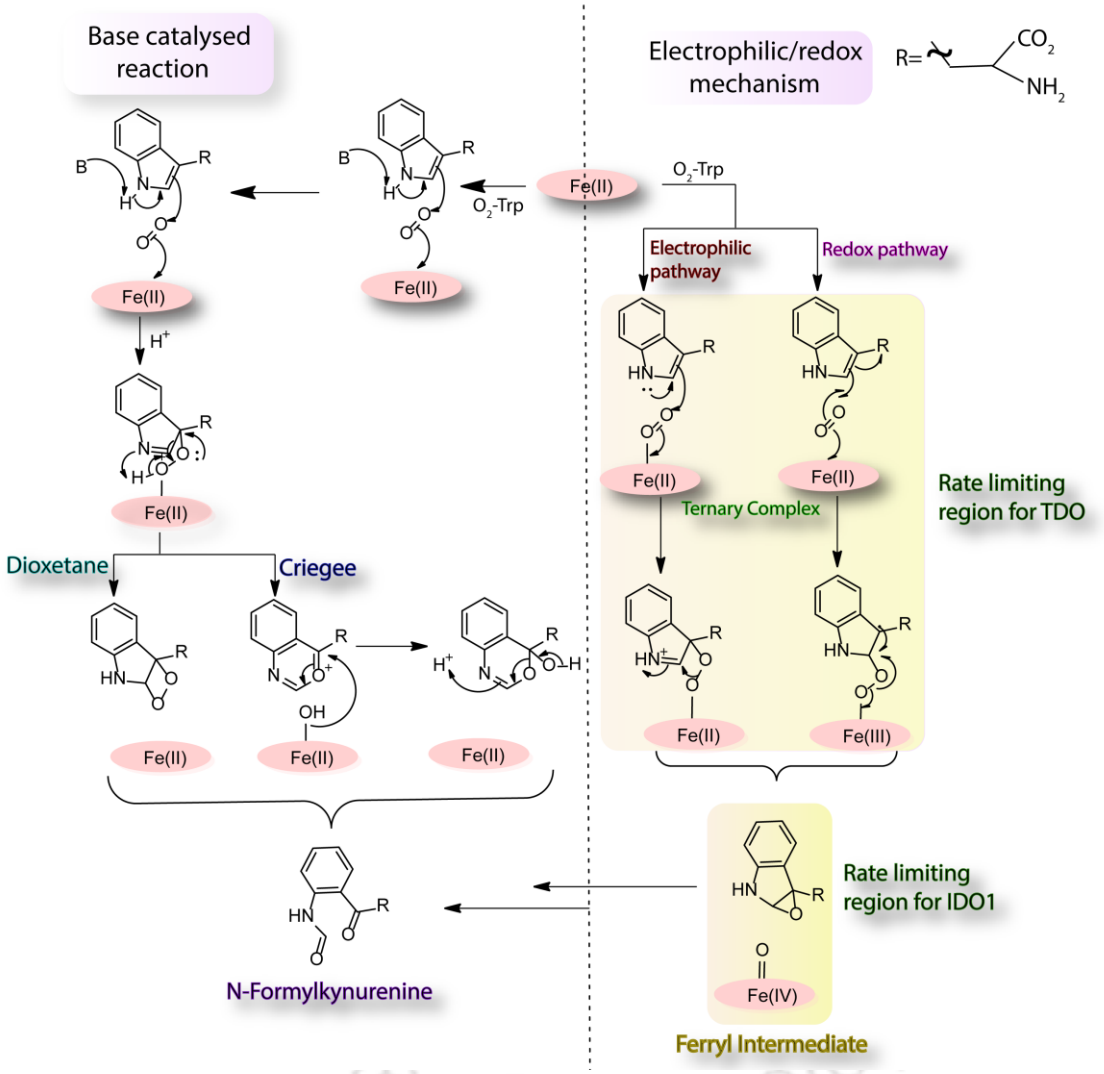

Fig. 1.4. Catabolism of L-Trp by IDO1 enzyme.

1.6. The role of the plasticity of the IDO1 enzyme pocket in inhibitor design.

The plasticity of the IDO1 enzyme pocket plays a crucial role in designing the potent inhibitors. Based on the research, it has been found that the active site of IDO1 has conformational and structural flexibility, particularly, the JK loop region. Depending on the structure of the ligand it can transit between open or close configuration, making room for various structurally different ligands inside the IDO1 pocket, by arranging the key residues and sub pockets in the active site.[46]

The IDO1 pocket is divided into two main regions, pocket A and pocket B. The pocket A region of IDO1 is hydrophobic in nature and it interacts directly with the heme iron. In Pocket B larger molecules can be accommodate as it is spacious and flexible, ensuring the inhibitors can utilize the interacting sites and conformation providing higher potency, selectivity and specific inhibition. The ligands, for accommodating the active site and stabilising the closed JK loop, has to mimic the natural substrate with same polarity. Although, in the substrate (L-Trp) bound structures (PDB IDs 5wmu, 5wmv, 6e35, and 6e46)[47, 48] JK loop is resolved and is always in close conformation but in case of most of the apo-IDO1 structures, it remains unresolved and hence probably in open conformation except for PDB ID 6e43,[47] where the loop is resolved and shows a close conformation. This structural flexibility and adaptability of IDO1 highlights the natural multitasking role of the enzyme and other biological roles beyond tryptophan metabolism. Furthermore, the plasticity of the active site of IDO1 allows a large range of binding modes, promoting the exploration of different interaction sites within the enzyme. For instance, in pocket A hydrophobic interaction combined with the hydrogen bond or van der Waals bond in the pocket B and the JK loop can be optimized for maximizing the potency and selectivity. Therefore, this plasticity of the IDO1 enzyme assists in developing robust, effective and selective inhibitors, enabling a fine-tuning of molecular interactions and dynamics crucial for therapeutic applications. [46]

1.7. Classification of mechanism-based IDO1 inhibitors

The mechanism of tryptophan catabolism by IDO1 is sophistically dependent on redox conditions and the presence of oxygen (O_2). It is crucial to understand how inhibitors interact with the IDO1 active site for elucidating their inhibitory mechanisms. Based on their modes of binding and interaction of the enzyme with its active site and cofactors, IDO1 inhibitors are classified into several different categories. The first category is known as type I inhibitors that function by directly competing with the natural substrate L-tryptophan for accessing the active site of the enzyme. These inhibitors do not bind directly to the heme iron at the catalytic center, but they block the entry of the substrate and prevent the enzyme from catalyzing the oxidative opening of tryptophan. This mode of inhibition is strictly competitive with respect to L-Trp. On the other hand, type II inhibitors exhibit a different mechanism by competing with molecular oxygen to bind with the ferrous (Fe^{2+}) form of the heme group within the active site. These inhibitors effectively block the function of the enzyme by occupying the site that would otherwise be used by oxygen, thus halting the oxidation process required for Trp catabolism, as oxygen binding is

essential for the catalytic activity of IDO1. Type III inhibitors are characterized by their ability to bind to the inactive, oxidized ferric (Fe^{3+}) form of the heme group. They prevent the reduction of the heme iron back to its catalytically active ferrous form by stabilizing this inactive state, resulting in the enzyme remaining in its inactive state, unable to participate in Trp metabolism.[49] The fourth category, type IV inhibitors, involves competition with the heme cofactor itself. These inhibitors preferentially bind to the apo form of IDO1, which lacks the heme group, disrupting the normal incorporation of heme into the enzyme and This process is both time- and temperature-dependent. This leads to a reduction in the amount of catalytically active holo-IDO1 with time and thereby diminishing the activity of the enzyme. Finally, type V inhibitors operate a redox-based mechanism, exerting their inhibitory effect. These inhibitors encourage the reduction of the active ferrous heme to the inactive ferric state rather than binding directly to the active site or the heme group, and hence shift the redox balance in this way; they effectively inactivate the enzyme without directly occupying the substrate or cofactor binding sites.[46]

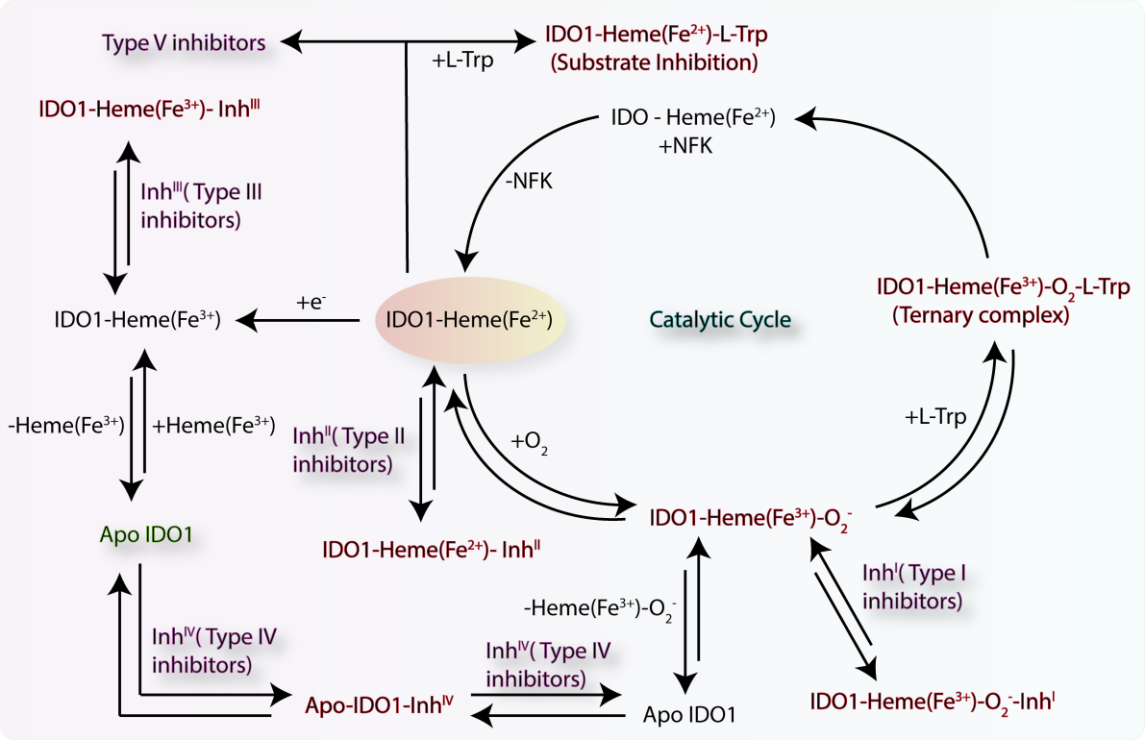

Fig. 1.5. Schematic diagram representing the catalytic cycle, redox equilibrium, and ligand binding with IDO1 enzyme. Reproduced from ref.49 with permission from the American Chemical Society.

1.8. Classifying IDO1 Inhibitors: Binding Mechanisms and Experimental Characterization

In regard to the complexity of inhibition kinetics and the dynamic redox states of the heme cofactor, accurate classification of IDO1 inhibitors requires rigorous experimental scrutiny. Traditional methods rely on N-formylkynurenine (NFK) production kinetics and often yield ambiguous results for inhibitors targeting inactive ferric IDO1 or exhibiting substrate inhibition at high concentrations. These limitations complicate mechanistic assessment, along with the necessity for complementary techniques like optical absorbance spectroscopy. The heme group in IDO1 exhibits a distinct spectral trademark sensitive to oxidation and spin states. That is, ferrous (Fe^{2+}) IDO1 displays a high-spin Soret peak at ~428 nm, while ferric (Fe^{3+}) IDO1 shows peaks at ~405 nm (high-spin) or lower wavelengths (low-spin). The electronic environment of heme iron is altered by inhibitor binding, manifesting as shifts or depletion in the Soret band (~400 nm) and α/β bands (500–600 nm). However, conventional spectroscopy under inert atmospheres (for example, N_2) lacks physiological relevance due to the absence of oxygen (O_2), which is a critical substrate in the catalytic cycle.

Recent O_2-dependent absorbance kinetics simulate catabolic conditions, enabling direct observation of inhibitor interactions with ferrous/ferric IDO1 during catalysis and providing unambiguous mechanistic insights.[50] For instance, L-1-methyl-tryptophan (L-1MT) exhibits competitive inhibition with L-Trp and shows non-competitive behavior with O_2. Despite this kinetic profile, spectroscopic analysis reveals no shift in Soret peak in ferric (405 nm), ferrous (428 nm), or ferrous-oxy (411 nm) IDO1, indicating there is no direct heme-iron coordination. This absence of spectral perturbation, combined with weak binding to IDO1, confirms L-1MT as a type I inhibitor that competes with L-Trp that does not engage with the heme cofactor. Similarly, the stereoisomer D-1MT (indoximod) and PF-06840003 demonstrate analogous spectral behavior, with no wavelength shifts in ferric (405 nm) or ferrous (427 nm) IDO1 under N_2, but depletion of Soret peaks. This depletion suggests altered active-site polarity upon binding rather than direct heme interaction. As a result, both compounds are definitively classified as type I inhibitors.[51] These findings highlight the necessity of integrated kinetic and spectroscopic approaches for resolving inhibition mechanisms

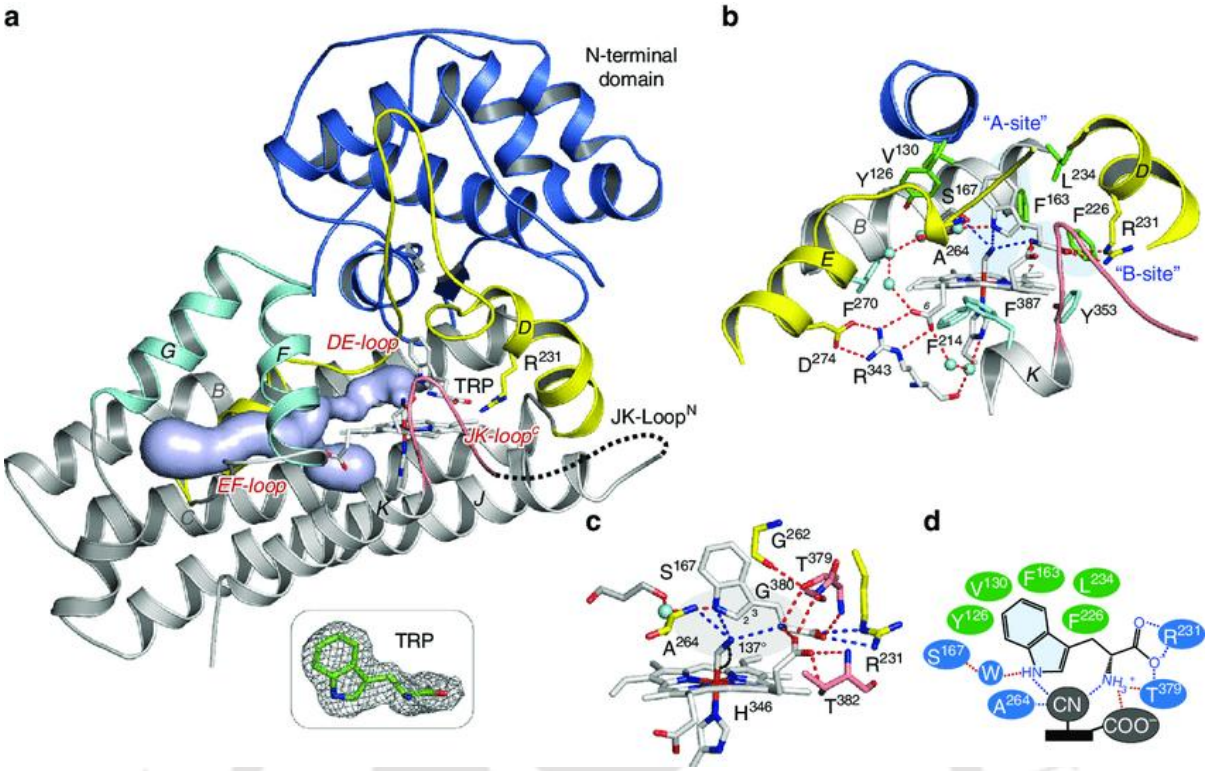

Fig. 1.6. Crystal structure of the hIDO1-CN-Trp complex (a), Active site of IDO1, S_a. (b, c). The Trp, via various hydrophobic and polar interactions, interacts with the protein matrix, as well as the heme (d).[45] Reproduced from ref.45 with permission from the Springer Nature.

While type I inhibitors exploit substrate competition, other classes target distinct vulnerabilities. For instance, type II inhibitors (such as epacadostat) compete with O_2 for ferrous heme binding, whereas in type III, inactive ferric heme is stabilized, and type IV (like linrodostat) displaces heme from IDO1 to form apo-IDO1. Type IV inhibitors were first characterized in 2018, demonstrating time- and temperature-dependent inhibition due to heme dissociation.[41] Such subtlety highlights how advanced spectroscopic methods are indispensable for elucidating true inhibition modes and guiding therapeutic design, particularly under O_2-replete conditions.

The hydroxyamidine chemotype has become a keystone in the development of potent IDO1 inhibitors, standing out as a particularly well-studied representative of this class. These inhibitors are particularly known for their unique mechanism of action compared to other classes of IDO1 inhibitors. Incyte-5l has shown IDO1 inhibition activity through a competitive mechanism in regard to both L-tryptophan and D-tryptophan, a natural and a synthetic substrate of the enzyme, respectively. This competitive inhibition

suggests that Incyte-5l binds directly within the active site of IDO1, effectively blocking substrate access and thereby impeding the catalytic function of the enzyme. The binding characteristics and mechanistic details of IDO1 inhibition of Incyte-5l have been thoroughly explored using UV-Visible spectroscopy, a powerful technique for probing the electronic environment of heme-containing proteins. The heme group in IDO1 is responsible for its catalytic activity, exhibiting distinct spectral features depending on its oxidation state. When Incyte-5l binds with the ferric (Fe^{3+}) form of the Soret peak associated with the heme group, it shifts from its typical position to 412 nm. Similarly, when Incyte-5l interacts with the ferrous (Fe^{2+}) form of the enzyme, the Soret peak has been observed at 419 nm. These shifts indicate that Incyte-5l directly interacts with the heme iron in both redox states by altering its electronic structure.[52, 53] A particularly revealing experiment involves the addition of a reducing agent to the ferric IDO1-Incyte-5l complex, where over the course of time, the Soret peak shifted from 411 nm to 419 nm, revealing that Incyte-5l not only binds to the ferric form but has a higher affinity for the catalytically relevant ferrous form of the enzyme. This preferential binding to ferrous heme is critical because the ferrous state is needed for oxygen binding and then catalysis of the tryptophan degradation pathway. By stabilizing the ferrous heme in a form that cannot bind oxygen, Incyte-5l effectively shuts down the activity of the enzyme at a fundamental level.

Epacadostat (INCB024360), another hydroxyamidine-based inhibitor developed as a derivative of Incyte-5l, exhibits nearly identical spectroscopic behavior. Epacadostat, when bound to IDO1, induces the same Soret peak maxima at 412 nm for the ferric complex and 419 nm for the ferrous complex, which confirms that it shares the same binding mode and mechanism of action as Incyte-5l.[52] As their inhibitory mechanism are very comparable, both compounds are classified as type II IDO1 inhibitors. Type II inhibitors are defined by their ability to specifically target the ferrous heme within the IDO1 active site, forming a stable inhibitor-heme complex that blocks the binding of oxygen. This is a crucial distinction, as oxygen binding is the first step in the tryptophan catabolism pathway, and its inhibition halts the entire catabolic process. These findings are significant for the development of a drug where IDO1 activity is often upregulated for suppression of immune responses and promoting tumor survival. By precisely targeting the active and catalytically essential form of IDO1, hydroxyamidine-based type II inhibitors like Incyte-5l and epacadostat offer a rational and effective strategy for modulating immune function. Their mode of action is validated through both kinetic

studies and sophisticated spectroscopic analyses, providing a blueprint for next-generation inhibitors of IDO1 with improved potency, selectivity, and therapeutic potential. This mechanistic clarity enhances our understanding of enzyme inhibition and also guides the optimization of inhibitor scaffolds for clinical application.[52, 53]

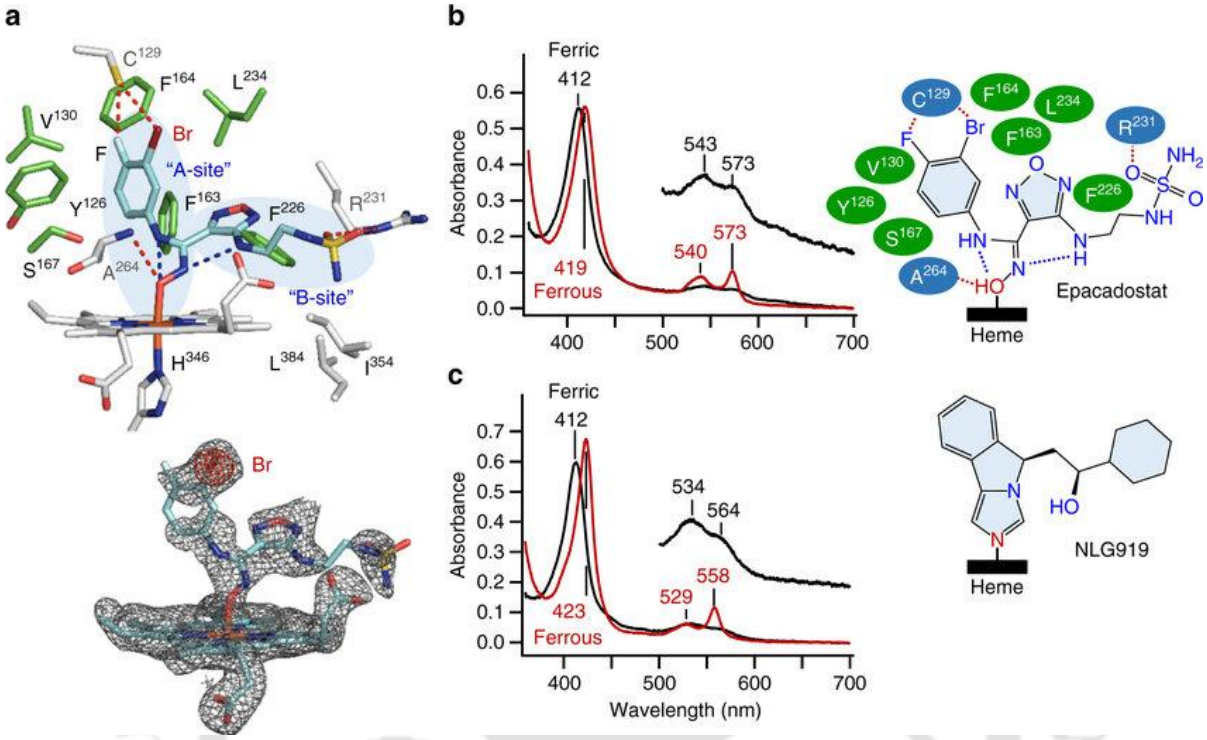

Fig. 1.7. Epacadostat and spectral markers for O and N-based inhibitors binding to the crystal structure of the hIDO1-epacadostat complex (a). Absorption spectra of hIDO1 with epacadostat (b) and NLG919 (c). Reproduced from ref.45 with permission from the Springer Nature.

Imidazole-based inhibitors have played a pivotal role in uncovering the structural mechanisms behind the inhibition of IDO1. The first known co-crystal structure of IDO1 with a small molecule inhibitor was 4PI, an imidazole-based compound (PDB: 2D0T). In this structure, the imidazole moiety of 4PI coordinates directly with the heme group of the enzyme, anchoring the inhibitor within the active site. The phenyl group of 4PI settles into a hydrophobic region, known as "pocket A" of IDO1, stabilized by aromatic stacking interactions with the residues of the protein. Notably, a buffer molecule, CHES, is also present in the active site and forms salt bridges with both the propionate group of heme and the Arg231 residue, providing additional stability to the complex.[54]

Additional efforts based on the 4PI scaffold led to the development of a more advanced imidazole-based inhibitor known as NLG919, containing an imidazoleisoindole

core allied with a hydroxyl group and a cyclohexyl substituent. The co-crystal structure demonstrates that the imidazole nitrogen of NLG919 (PDB: 5EK3) binds to the heme iron in a manner similar to 4PI. The rest of the molecule fits snugly into "pocket A," making multiple hydrophobic contacts with neighboring protein residues. The cyclohexyl group extends into an adjacent region towards "pocket B," involving hydrophobic residues such as Phe226, Ile354, and Leu384.[55] Additionally, the hydroxyl group on NLG919 forms an intramolecular hydrogen bond with the isoindole nitrogen, enabaling it to participate in hydrogen bonding with the heme 7-propionate and Ala264, thus stabilizing a unique inhibitor conformation and strengthening its interaction with the enzyme. These findings highlight the importance of the imidazole scaffold and have been instrumental in the rational design and optimization of potent and selective IDO1 inhibitors. GDC-0919 (navoximod) is an advanced analog of NLG919, designed with strategic structural modifications, including a hydroxyl group attached to the cyclohexane moiety and a fluorine atom at the C_6 position of the imidazoisoindole core. These changes enhance its binding efficiency and potency as an IDO1 inhibitor. According to the co-crystal structure of navoximod complexed with IDO1 (PDB: 6O3I), the overall binding mode is quite similar to that observed with NLG919. However, the additional hydroxyl group on the cyclohexane ring forms a hydrogen bond with Ser235, while the presence of the C_6-fluorine enables a notable interaction with Gly262, adding to the stability of the inhibitor in the binding pocket.[56, 57]

MMG-0358, a well-known inhibitor, consisting of a triazole ring and a substituted phenyl group.[49] Structural analysis of its complex with IDO1 (PDB: 6R63) reveals that MMG-0358 coordinates the ferric heme within the active pocket of the enzyme. The substituted phenyl group fits neatly into pocket A, where its chlorine substituent is closely associated with Leu234, Cys129, and Gly262. The hydroxy group on MMG-0358 forms a hydrogen bond with Ser167. The compound is also found to occupy the so-called S_i site of IDO1. Notably, the triazole ring exists partly in its deprotonated state, and quantum mechanical calculations suggest that this form exhibits even stronger binding to IDO1 compared to the neutral state. Both imidazole and triazole-based inhibitors exploit their nitrogen atoms for direct coordination to the heme iron at the active site. The strong hydrogen bonding network and optimal positioning of these nitrogen atoms contribute to vigorous enzyme inhibition. Furthermore, the hard nature of imidazole and triazole ligands provides a strong affinity for the ferric ion in the heme, consistent with a type III inhibition

mechanism. These observations highlight the importance of carefully designed heterocyclic scaffolds in achieving potent and selective inhibition of IDO1.[49]

Vertex-AT is an IDO1 inhibitor featuring a 4-amino-substituted triazole core and a chloro-substituted phenyl ring.[58] Structural data (PDB: 6F0A) shows that the triazole moiety directly coordinates to the heme iron, similar to other triazole-based inhibitors like MMG-0358. The chlorophenyl group occupies the hydrophobic pocket A, and the 4-amino group forms a hydrogen bond with Ser167. The ammonium and carboxylate group of L-Trp mediates a salt-bridge interactions among the triazole, heme propionate, Arg231, and Thr379. Notably, the nitrogen of triazole prefers binding to ferric heme (type III inhibition), but the influence of the buffer can facilitate interaction with ferrous heme as well (type II inhibition). Thus, Vertex-AT shows dual type II and III inhibition mechanisms due to its versatile triazole scaffold and dynamic binding environment.[58]

BMS-986205, also known as linrodostat, is composed of phenyl propenamide, cyclohexane, and quinoline scaffolds and is also known as suicide inhibitor.[59] It exhibits a unique mechanism of inhibiting IDO1 by targeting the apo form of the enzyme. The co-crystal structure of BMS-986205 bound to heme-deficient IDO1 (PDB: 6MQ6) reveals that the quinoline moiety extends into the S_i pocket of the enzyme, establishing hydrogen bonding with His343 and π-stacking interactions with Phe270. Meanwhile, the propenamide forms additional hydrogen bonds with Ser167 and His346 residues, whereas the phenyl and propenamide groups occupy the S_a pocket. Significantly, the cyclohexane group occupies the position normally held by the heme, effectively mimicking its placement within the binding cavity. Mechanistic studies have explained that inhibition of BMS-986205 relies on a distinct binding trajectory responsible for its specific affinity for apo-IDO1. Initially, BMS-986205 associates with the enzyme in a solvent-exposed surface binding mode that induces conformational changes in the active site, facilitating heme release (as observed in structure PDB: 6DPQ). This initial interaction is driven predominantly by the hydrophobic characteristics of the quinoline and the elongated cyclohexane substituent, which help to destabilize the heme-occupied conformation. Subsequently, the cyclohexane moiety undergoes a conformational transition, shifting from a kinked (PDB: 6DPR) to a bent form (PDB: 6MQ6) that stabilizes the heme-deficient enzyme-inhibitor complex and impedes re-association of the heme group. Overall, BMS-986205 is an example of a type IV inhibition mechanism, promoting heme dissociation and targeting the apo enzyme form. This dual-pocket binding, along with conformational modulation of the active site, underscores the unique strategy by which

BMS-986205 achieves irreversible inhibition of IDO1 by preventing heme to come back to the protein.[59]

In brief, Type I inhibitors act as substrate mimics occupying the active site. Type II inhibitors preferentially bind the ferrous (Fe^{2+}) form of IDO1, whereas Type III inhibitors coordinate directly to the ferric (Fe^{3+}) heme iron. Type IV inhibitors are elongated hydrophobic molecules that target solvent-exposed pockets on apo-IDO1, promoting heme dissociation and stabilizing the heme-free enzyme. Lastly, type V inhibitors consist of redox-active quinone derivatives that modulate IDO1 activity through redox cycling, affecting the electronic environment of the enzyme. Together, these classifications highlight diverse strategies exploiting the metal state of IDO1 and structural conformations to achieve selective inhibition.

1.9. Efficacy of IDO1 Inhibitors

The first identified IDO1 inhibitors were L-tryptophan (L-Trp) and related indole compounds were among, with 1-methyl-D/L-tryptophan (1MT) being mostly studied. IDO1 inhibition activity of 1MT is moderate with K_i = 34 μM, but only the L-isomer (L-1MT) binds to the active site of IDO1 for direct inhibition. Interestingly, the D-isomer (D-1MT) does not directly inhibit the enzyme but triggers strong anticancer effects by restoring T-cell function that is suppressed in tumors. D-1MT also reactivates the mTORC1 metabolic pathway under L-Trp depletion, leading to immune cell function and adding to its antitumor activity. High-throughput screening discovered PF-06840003 as a highly selective IDO1 inhibitor with low micromolar or submicromolar IC_{50} values, particularly the R-enantiomer showing strong potency. PF-06840003 is active in cells, has a long half-life, and crosses the blood-brain barrier, enabling trials for brain cancers. Incyte-5l, with a potency of IC_{50} = 67 nM, has poor oral bioavailability, which halted its clinical development. Epacadostat is a clinical lead with very high potency and good bioavailability, and it shows antitumor effects preclinically but failed to improve survival when combined with pembrolizumab in melanoma trials. Other inhibitors like 4PI, NLG0919, navoximod, MMG0358, Vertex-AT, and BMS-986205 vary in potency and mechanism. Notably, BMS-986205 shows nanomolar potency in cells. Naphthoquinone derivatives, such as menadione and β-lapachone, inhibit IDO1 enzymatically and can also induce tumor cytotoxicity through redox cycling via the enzyme NQO1.[46, 60] The IDO1 inhibitors can be classified by binding mechanism into five types. Type IV inhibitors targeting apo-IDO1 show picomolar inhibition, Type II hydroxyamidines have low nanomolar IC_{50}s, Type III inhibitors show 100 nM IC_{50}s, and Type I inhibitors that mimic

substrates generally have weaker micromolar potency. Type V acts via redox mechanisms, causing cytotoxicity rather than direct inhibition. IDO1 exists mostly as apo-IDO1 (~85%) in cells, with the rest as heme-bound forms. Catalytic activity relies on ferrous-heme generated by cellular reductase systems. Apo-IDO1, being the more promising target for effective inhibition, shows differential potency against the IDO1 forms. The mTORC1 pathway interacts with IDO1 activity. Tryptophan depletion catalyzes suppression of mTORC1 signaling, which leads to immune suppression. D-1MT can reactivate mTORC1 activity and support immune cell function even though it cannot inhibit tryptophan degradation. This interaction impacts tumor immune evasion and influences the effectiveness of therapies targeting these pathways. These findings highlight mTOR and IDO1 as linked targets in cancer immunotherapy.

Collectively, the efficacy of IDO1 inhibitors depends not only on direct enzyme inhibition but also on favorable cellular activity, pharmacokinetics, and interaction with metabolic pathways such as mTORC1 to modulate immune responses for antitumor effects. This comprehensive understanding leads to the development of next-generation drugs for IDO1 inhibition with better clinical prospects.[61-63]

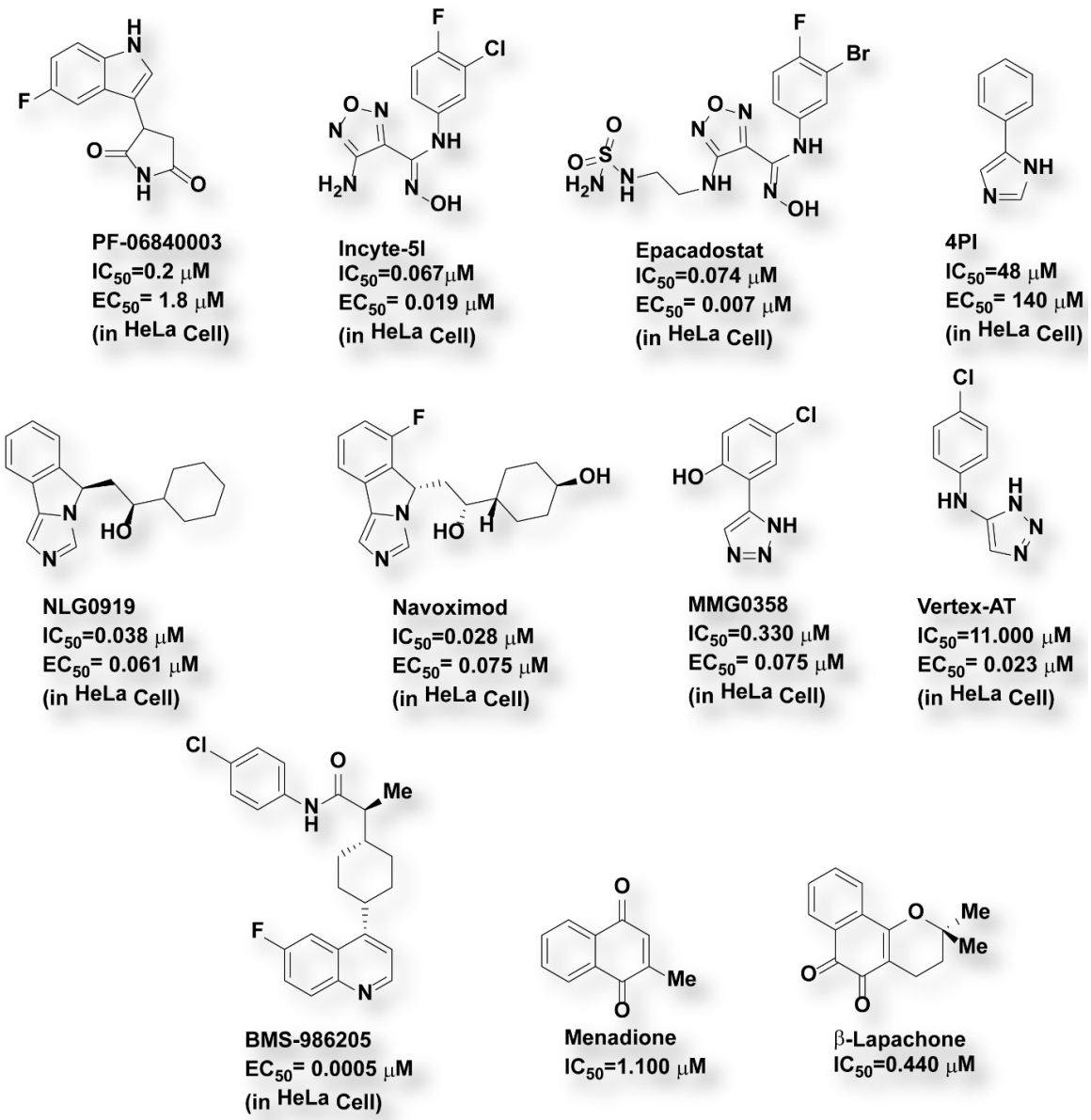

Fig. 1.8. Potent IDO1 inhibitors along with their inhibitory potency**.**

1.10. Characterization of Off-Target Pharmacological Effects of Reported IDO1 Inhibitors

The aryl hydrocarbon receptor (AhR) is a helix-loop-helix transcription factor that binds various xenobiotic ligands, undergoes nuclear translocation, and subsequently regulates the expression of numerous target genes. The IDO1-mediated kynurenine pathway generates L-Trp metabolites, including kynurenine itself, serving as endogenous agonists of AhR, and establishing a regulatory axis between these two proteins. Notably, AhR can directly associate with the promoter region of the IDO1 gene and facilitates its transcription, forming a positive regulatory AhR-IDO1 feedback loop.[61] High-affinity, naturally occurring AhR agonists include the L-Trp mimetic compounds 6-

formylindolo[3,2-b] carbazole (FICZ) and 2-(1'H-indole-3'-carbonyl)-thiazole-4-carboxylic acid methyl ester (ITE), as well as indole-3-carbinol (I3C).[62] I3C enhances IDO1 expression, partly through upregulation of immune modulatory mediators such as prostaglandin E2 (PGE2) and interleukin-6 (IL-6).[63] Activation of the AhR also promotes immunosuppressive mechanisms in the tumor microenvironment, which includes the differentiation of regulatory T cells (Tregs) and regulatory dendritic cells through IL-10 signaling pathways. Overall, L-Trp-mimetic xenobiotics featuring polycyclic, planar molecular scaffolds are well-suited for high-affinity interaction with AhR and can elicit pronounced AhR-mediated immunoregulatory and immune tolerance effects.[64]

Recent studies have shown that many IDO1 inhibitors are in clinical development, like indoximod, also function as AhR agonists. Indoximod markedly increased AhR-driven luciferase activity by 19.6-fold in human Hep-G2 cells, which indicates strong AhR activation. Similarly, epacadostat and navoximod, following metabolic conversion by UGT and CYP enzymes, have enhanced AhR-mediated luciferase activity by 1.2-fold and 1.3-fold, respectively, in the same cell line. These findings suggest that IDO1 inhibitors with L-Trp-like or planar, polycyclic scaffolds can act as AhR agonists, potentially diminishing their therapeutic efficacy by activating immunosuppressive pathways.[65]

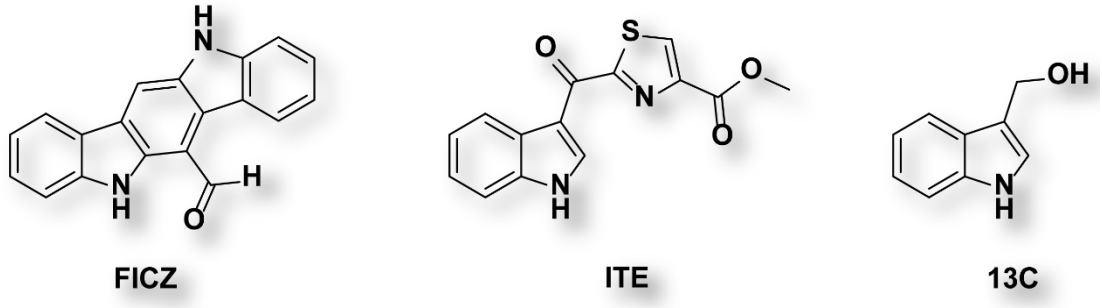

Fig. 1.9. Reported structure of the AHR-activated molecule.

1.11. Compounds Targeting Both IDO1 as well as TDO Pathways

Several small-molecule compounds with different chemical scaffolds have been developed and characterized as potential inhibitors of the IDO1 enzyme, aiming to modulate immune responses in the tumor microenvironment. Despite initial success, the clinical efficacy of selective IDO1 inhibition, such as in the widely publicized phase 3 ECHO-301 trial, where epacadostat in combination with the PD-1 checkpoint inhibitor pembrolizumab, fell short of expectations. This outcome raised questions about whether targeting IDO1 alone for effective cancer immunotherapy is sufficient. Consequently, the scientific and clinical communities have shifted focus towards combination strategies,

integrating IDO1 inhibitors with other immune checkpoint agents, and have called for a thorough understanding of the mechanisms incorporated in IDO1 inhibition to maximize its therapeutic benefit.[66]

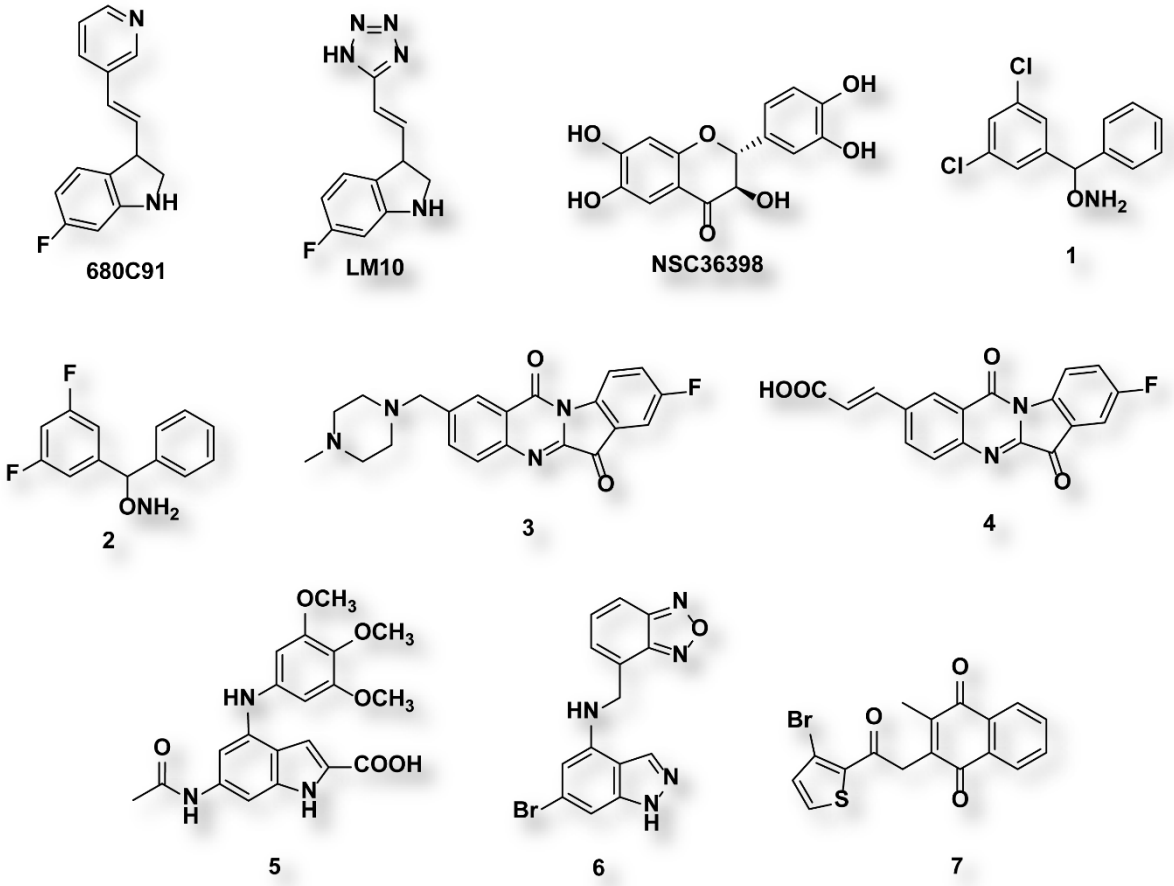

Fig. 1.10. Structure of reported dual IDO1 and TDO inhibitors.

Moreover, the roles of other related enzymes, TDO and IDO2, have come into sharper focus. Though TDO and IDO2 were thought to function primarily in hepatic tryptophan metabolism, however, recent research has revealed that TDO is not only confined to the liver, but it is also expressed in various tumor cells, promoting the establishment of immune tolerance and supporting tumor progression by sustaining local kynurenine production, which suppresses immune activity. Comprehensive cellular and animal studies now support the notion that TDO is a critical, tumor-associated player in tryptophan catabolism. As a result, attention has shifted towards the development of dual inhibitors that can simultaneously target both IDO1 as well as TDO. Such an approach is increasingly recognized as essential for effectively disrupting the kynurenine pathway, overcoming mechanisms of immune escape, and broadening the impact of immunotherapeutic interventions in cancer. This dual inhibition strategy holds the promise

of achieving more robust and clinically relevant anti-tumor immune responses than IDO1 inhibition alone.[67] The active site of both IDO1 and TDO plays a pivotal role in the catalytic function during L-Trp metabolism. Even though there are distinct differences in the overall structures of the two enzymes, their active sites are remarkably similar, each featuring a prosthetic heme group and a S_a site composed of both hydrophobic (pocket A) and hydrophilic (pocket B) regions on the distal side of the heme group. L-Trp binds at the S_a site in both enzymes, but IDO1 possesses an additional substrate-binding region known as the Si site, which is located on the proximal side of the heme group, whereas it is absent in TDO. The exact binding interactions of L-Trp with the two enzymes varied. In IDO1, the indoleamine ring of L-Trp binds to Ser167, forming a hydrogen bond via a bridging water molecule. Whereas, in TDO, the same moiety engaged in a direct hydrogen bond with His76. When L-Trp occupies the S_i site in IDO1, it induces a conformational change in the S_a site. Further, L-Trp binding in the S_i site facilitates the repositioning of the Phe270 residue, effectively blocking the water tunnel and eventually disrupting the delivery of molecular oxygen to the S_a site during enzyme turnover. This regulatory mechanism is unique to IDO1. The active pocket of TDO is more structurally rigid, leading to high substrate-specific properties. This characteristic leads to a comparatively limited variety of small-molecule inhibitors for TDO inhibition. From these structural and mechanistic aspects, it can be concluded that both enzymes overlap but still have their own unique features to influence inhibitor design and the broader regulation of tryptophan catabolism in different biological contexts.[68]

Numerous indole derivatives, including 68OC91, LM10, and NSC36398, have demonstrated selective inhibitory activity against TDO.[69, 70] However, due to the limited availability of bioisosteres that effectively mimic the substrate L-Trp, the development of TDO inhibitors has been relatively underexplored. Recent research into L-Trp-induced immunosuppression has highlighted the potential clinical advantage of designing dual inhibitors that target both IDO1 and TDO enzymes. Although only a few dual inhibitors have been reported in the literature, cell-based inhibition studies on diaryl hydroxylamine compounds (**1** and **2**) indicate that many of these molecules act as PAN inhibitors, affecting multiple enzymes.[71] Additionally, N-benzyl and aryl-substituted tryptanthrin derivatives (**3**) have been shown to directly interact with IDO1, IDO2, and TDO, which leads to significant T cell proliferation and inhibition of L-Trp catabolism via the kynurenine pathway. Furthermore, a cinnamic acid derivative of tryptanthrin (**4**) has demonstrated potent inhibitory effects against IDO1 and TDO enzymatic activities.[72] Moreover, a series

of indole-2-carboxylic acid derivatives was synthesized and evaluated for their inhibitory effects on both enzymes. Structure-activity relationship (SAR) investigations highlighted a 6-acetamido-indole-2-carboxylic acid derivative **5** as a potent dual inhibitor, showing low micromolar IC_{50} values against both IDO1 and TDO. This compound also promoted T cell proliferation and effectively suppressed tumor growth in the B16F10 melanoma mouse model, demonstrating promising immunomodulatory and antitumor potential.[73] Researchers have also explored 1H-indazole derivatives, especially 4,6-substituted variants, as dual enzyme inhibitors. The benzo-oxadiazole–substituted 1H-indazole derivative **6** exhibited strong inhibition of both purified IDO1 and TDO in enzymatic assays, as well as under cellular conditions. Notably, **6** remarkably reduced IDO1 protein expression in interferon-γ-stimulated HeLa cells, demonstrating substantial tumor-suppressive activity in the CT26 xenograft model. Additionally, recent advances have recognized quinone scaffolds as promising candidates for designing dual IDO1/TDO inhibitors. Computational techniques, such as 3D-shape similarity and pharmacophore-based in silico screening, have identified quinone derivatives with high dual-inhibitory potential.[74] Some of these compounds displayed strong, low nanomolar inhibitory activity against both enzymes in biochemical assays, reinforcing the viability of this scaffold for future development.[73, 74]

Cellular assays have shown that the quinone derivative **7** is capable of inhibiting both IDO1 and TDO enzyme activities. However, the mechanism by which the redox-active quinone moiety exerts its inhibitory effects still has some uncertainty, as this aspect has not been thoroughly elucidated.[75] In parallel, the compound CMG017 has demonstrated potent suppression of kynurenine production in various human and murine cancer cell lines, seemingly outperforming inhibitors that selectively target either IDO1 or TDO alone. In mouse models bearing tumors, CMG017 significantly reduced kynurenine concentrations in both tumors and plasma and effectively inhibited tumor growth without causing much notable toxicity. Additionally, administration of CMG017 was associated with increased infiltration of $CD8^+$ effector T cells into tumors and considerable changes in the expression of immune-related genes within the tumor microenvironment. Combination therapies, CMG017 along with immune checkpoint inhibitors such as anti-PD-1 or anti-CTLA-4 antibodies, led to more pronounced tumor regression and improved long-term survival rates. Nevertheless, detailed structural information regarding CMG017 has not been made publicly available. It is worth noting that several dual IDO1/TDO inhibitors have recently advanced into clinical trials, considering the growing interest in

this therapeutic strategy for cancer treatment.[76] Navoximod in combination with the PD-L1 inhibitor atezolizumab is being evaluated in a phase I clinical trial for the treatment of solid tumors. Early findings involving this combination in patients with advanced cancers demonstrated favorable safety, tolerability, and pharmacokinetic profiles.[77] Although, navoximod is classified as a dual inhibitor targeting both IDO1 and TDO, it displays 20-fold greater selectivity for IDO1 compared to TDO. In 2019, clinical evaluation began for SHR-9146 (with structure not publicly disclosed), another dual IDO1/TDO inhibitor.[78] Ongoing investigations are assessing SHR-9146 in combination with the PD-1 inhibitor SHR-1210 and/or the VEGFR inhibitor Apatinib for treating advanced or metastatic solid tumors.[79] In parallel, the compound DN1406131 (structure also undisclosed), which functions as a dual IDO1/TDO inhibitor, is currently in clinical trials. In contrast, the clinical program for M4112 (structure undisclosed), a dual IDO1/TDO inhibitor, was recently discontinued due to inadequate pharmacodynamic outcomes.[80] Overall, dual inhibitors targeting both IDO1 and TDO incorporate several natural product-derived scaffolds, such as tryptanthrin, quinone, and bioisosteres of L-tryptophan, like indole and indazole derivatives. Moreover, certain heterocyclic fused aromatic compounds have demonstrated dual inhibitory effects in both enzymatic and cellular assays. The strategy of simultaneously inhibiting IDO1 and TDO is anticipated to offer a more comprehensive blockade of the kynurenine pathway, a benefit increasingly supported by the initiation of related clinical trials focused on kynurenine-driven immunosuppression. Therefore, it is crucial to develop new, potent, and selective dual inhibitors for effective counteraction of kynurenine-mediated immune suppression involved in cancer and other diseases.

1.12. Selectivity of the design of Inhibitors

The unsatisfactory outcome of the phase III clinical trial investigating epacadostat combined with pembrolizumab (KEYTRUDA®) redirected the trajectory of IDO1-based therapeutic strategies. Since then, research has increasingly emphasized approaches aimed at augmenting the potency of IDO1 blockade, particularly through multimodal therapies that integrate chemotherapy or photodynamic therapy (PDT).[81] A collective research work has explored the use of advanced nanoscale carriers capable of co-delivering IDO1 inhibitors together with cytotoxic agents, or of incorporating stimuli-responsive molecular scaffolds to achieve superior synergistic effects.

Among these strategies, bio-responsive injectable hydrogels have surfaced as a promising platform. For example, thermosensitive peptide-polymer hydrogels have been engineered to enable the sustained and localized release of programmed cell death protein-

1 (PD-1) antibodies along with the IDO pathway modulator 1-methyl-D-tryptophan (D-1MT).[82] Incorporation of methionine moieties within the hydrogel matrix provides reactive oxygen species (ROS)-sensitive functionalities regulates the release kinetics of the encapsulated agents and also actively scavenge intratumoral ROS, thereby alleviating oxidative stress-driven immunosuppression.[83] By leveraging both controlled release and microenvironment modulation, these intelligent hydrogel systems markedly amplify antitumor responses when compared with administration of free drug formulations. Such synergistic biomaterial-assisted delivery strategies represent a promising direction to overcome the limitations of earlier IDO1-based therapies and advance next-generation cancer immunotherapy. Drug delivery systems target IDO1 and are strategically engineered using tumor-homing peptide conjugation and stimuli-responsive nanocarriers [84]

One notable design involves arginyl-glycyl-aspartic acid (RGD) peptide-modified IDO1 nanoinhibitors, which leverage the RGD motif for receptor-mediated accumulation at tumor sites. With dual responsive characteristics, these nanostructures are designed, like pH-triggered dissociation of the polypeptide backbone in the acidic tumor microenvironment or a combination of esterase-catalyzed cleavage of the drug carrier linkages. This stimulus-triggered responsiveness ensures localized drug liberation, and it leads to enhanced suppression of intratumoral IDO1 activity and improved therapeutic benefit in *in vivo* models.[85]

Another progressive approach employs a nanoscale metal-organic framework (nMOF), based on chlorin, that combines the photodynamic properties of chlorin with the controlled release of encapsulated IDO1 inhibitors. Upon light activation, the nMOF generates cytotoxic reactive oxygen species while simultaneously liberating the inhibitor in a spatially confined manner, thereby restricting toxicity to surrounding healthy tissues.[86] Similarly, glutathione-responsive nanoplatforms utilizing porphyrin-conjugated phospholipids have been developed for achieving synergistic photodynamic therapy (PDT) effects. The elevated glutathione concentrations within tumor cells selectively trigger structural disassembly and promote precise and effective drug activation in such systems. A glutathione-responsive liposomal formulation based on porphyrin–phospholipid conjugates was developed for the co-delivery of IDO1 inhibitors, where the elevated glutathione concentration in the tumor microenvironment cleaves the redox-sensitive linkages of the liposome and releases the encapsulated drug locally. This platform extended systemic drug circulation, improving selective accumulation within

tumors, which translated into enhanced antitumor efficacy of the payload. Certain chemotherapeutic compounds have been shown to augment immune responses by inducing immunogenic cell death (ICD). Based on this principle, a cationic nanocarrier system was engineered to co-deliver IDO1-targeting siRNA together with oxaliplatin, an ICD-inducing chemotherapeutic. This dual-delivery platform enabled efficient deposition of both cargos in tumor tissues and tumor-draining lymph nodes, thereby modulating immune processes such as dendritic cell maturation and regulatory T cell activity, and producing synergistic antitumor effects.[86] Another reported strategy employed poly(vinyl alcohol) (PVA)-based nanogels for the co-delivery of NLG919, a small-molecule IDO1 inhibitor along with docetaxel.[87] These nanogels were functionalized with folic acid to selectively target tumors via folate receptor recognition, and incorporated acid-degradable linkages to enable rapid release of the therapeutic agents under the acidic conditions, which is a characteristic of the tumor microenvironment. In addition, a chemo-immunotherapeutic design was developed to co-deliver doxorubicin, an ICD-inducing agent, together with indoximod.[87] In this formulation, phospholipid-conjugated dual-prodrugs underwent self-assembly into liposomal nanostructures and ensured effective tumor-targeted release of both the chemotherapeutic and the IDO1 pathway modulator. Building on the development of stimuli-responsive nanocarriers for IDO1 inhibition, photo-responsive delivery systems have recently earned significant attention due to their capacity for precise spatiotemporal control over drug release. By integrating photosensitive components, such as porphyrin-based photosensitizers, into nanocarriers, these platforms enable activation upon targeted light irradiation specifically at tumor sites. This light-mediated release mechanism allows for localized liberation of IDO1 inhibitors and also facilitates combination therapeutic effects through photodynamic or photothermal actions. Such dual-function nanoplatforms improve intratumoral drug accumulation and pharmacokinetics while minimizing systemic exposure and off-target toxicity. The remotely controlled drug delivery ability with external light represents a crucial approach for enhancing the safety and efficacy profile of IDO1-targeted cancer treatments within the broader landscape of responsive nanotherapeutics.[87, 88]

1.13. Summary

IDO1 has surfaced as a crucial enzyme in cancer immunology for its primary role in modulating immune tolerance in the tumor microenvironment. By tryptophan depletion via the kynurenine pathway, IDO1 inhibits effector T-cell function and encourages regulatory T-cell activity and thereby facilitates tumor immune escape.[89] This

immunoregulatory mechanism operates synergistically with immune checkpoint pathways that include CTLA-4 and PD-1/PD-L1, placing IDO1 as an attractive immunotherapeutic target.

Despite developing several classes of IDO1 inhibitors, only limited compounds have successfully advanced to clinical trials. The variability of enzymatic and cell-based screening platforms has complicated the identification of selective inhibitors. The most notable example is the phase III ECHO-301/KEYNOTE-252 trial, where epacadostat, in combination with pembrolizumab, failed to demonstrate improved clinical outcomes, thus raising doubts over the therapeutic value of IDO1 inhibition as immunotherapy.[7] To overcome new strategies have focused on dual IDO1/TDO inhibition, showing promising preclinical outcomes with stronger suppression of tumor immune escape. Combination therapies that include IDO1 blockade together with radiotherapy, chemotherapy, or immune-checkpoint inhibitors are being actively explored as potentially more effective approaches.[90] Furthermore, nanocarrier-based delivery platforms have shown improved tumor targeting and enhanced efficacy of IDO1 inhibitors in preclinical models.[91] Nevertheless, significant challenges still remain unchanged, such as the widespread induction of IDO1 in non-hepatic tissues and its multifactorial regulation across tumor, immune, and stromal compartments, complicating targeted therapeutic development.[92] To overcome these barriers, integrated therapeutic strategies that enhance tumor specificity, efficacy, and durability of immune responses are required. Ultimately, defining the multi-dimensional role of IDO1 will be a critical step toward advancing cancer immunotherapy and addressing the limitations observed in recent clinical trials. Also, exploring controlled delivery of these inhibitors can lead to more efficacy and less toxicity in clinical trials.

1.14. Research gap

IDO1, being a crucial immunoregulatory enzyme, is a critical target for immune evasion. Although lots of efforts has been put forward for the discovery of potent and efficient IDO1 inhibitors still considerable research gaps exist to achieve immune modulation that are effective under pathological and physiological state. The inhibitors developed till date includes canonical tryptophan-binding antagonists, displays moderate potency, and only few exhibiting effective results in vivo conditions. Moreover, after the failure of Phase III clinical trial of epacadostat, indicated the limitations of targeting only the active, heme-bound (holo) form of IDO1, suggesting to emphasize on exploring the mechanistic innovation in designing inhibitors.[7]

In 2018, a new and promising strategy emerged, where the inactive, heme-free also known as apo, form of IDO1 is directly targeted.[47] Apo-IDO1 inhibitors, like linrodostat, releases the heme or stabilizing the apo-IDO1 state oxidatively.[53] It induces more tenacious and in some cases, irreversible enzyme inhibition in comparison to classical competitive inhibitors. Recent research demonstrated that in cancer cells, apo- IDO1 is predominant and hence making apo-IDO1 inhibition a suitable route for improving pharmacodynamic control. Despite, numerous chemotypes have displayed potent apo-IDO1 inhibition, nevertheless, groundbreaking approaches exploiting heme competition or stabilization are growing therapeutic possibilities. Simultaneously, the conceptual growth of stimuli-responsive IDO1 inhibitor has gained attraction as it leads to overcome the limitations of spatial, temporal, and toxicity that cannot be controlled in systemic therapies. Most of the current research are exploring photo-responsive drug systems by utilizing UV light activation to deliver "on-demand" enzyme inhibition but it results in poor tissue penetration, phototoxicity, and limited physiological application. This, in combination with, lack of real-time monitoring and insufficient non-invasive activation modalities, affects the vivo applications. Recently, innovative research is turning toward external stimuli employing visible or near-infrared (NIR) light, as it can penetrate tissues with higher efficacy, more specificity and lower cytotoxicity, providing spatiotemporal control of drug delivery or its activation. In addition, internal stimuli, such as pH differential found in tumor microenvironments are being explored for developing pH-sensitive IDO1 inhibitors and nanocarriers and this development can ensure selective activation in cancer cells and spare the healthy cells. Multifunctional nanomaterials and smart drug delivery systems are being advanced for enhancing tissue penetration, reducing toxicity in healthy cells, and also for active monitoring of therapeutic action, therefore offering approaches to overcome the difficulties experienced with earlier strategies

Overall, these research directions, apo-form inhibition, externally and internally stimuli responsive delivery inhibitors, and precise stimulation modalities, highlighted underlying research gaps in this field. Henceforth, the accomplishing NIR or visible light-activated, as well as pH-sensitive, IDO1 inhibitors can reshape and help us to achieve spatiotemporal control over drug delivery, hence maximizing its therapeutic benefit and minimizes adverse effects. This innovation is expected to significantly improve the results in immunotherapeutic strategies where immune regulation via IDO1 is crucial.

1.15. Objective of research work

Based on the comprehensive literature, IDO1 serves an important role in suppression of the immune system in tumour cells as well as other diseases, by catabolising tryptophan and generating kynurenine metabolites which act as immunosuppressive metabolites. These studies encouraged the investigation of IDO1 inhibition techniques. Inhibiting the enzyme can restraint immune suppression which can enhance tumor infiltration by immune cells. This can also boost the outcomes of the treatments when combined with immunotherapy, chemotherapy or other known therapies. Recent findings also featured the participation of IDO1 in other immunoregulatory conditions, for instance, Alzheimer's, suggesting it can be a promising therapeutic target for various diseases that are caused by pathological immune suppression.

In this thesis, we focused on designing and synthesizing small molecules for robust and selective inhibition of IDO1. The entire thesis is arranged into three chapters. In **chapter 2**, we have focused on how the substrate, linradostat, mimics DCQ derivative inhibitors targeting both apo IDO1 as well as free heme for the inhibition process. **Chapter 3** mainly deals with selective drug delivery with a photo-responsive linker linked to the tryptamine derivative IDO1 inhibitors. **Chapter 4** corroborates how a dual stimuli-responsive spiropyran inhibitor selectively binds with apo IDO1 as well as free heme, inhibiting the IDO1 activity.

1.16. References

1. Goyal, N.; Sridhar, J.; Do, C.; Bratton, M.; Shaik, S.; Jiang, Q.; Foroozesh, M., Identification of CYP 2A6 inhibitors in an effort to mitigate the harmful effects of the phytochemical nicotine. *J. cancer metastatis treat.* **2021,** *7*, 18.

2. Catanzaro, E.; Beltrán-Visiedo, M.; Galluzzi, L.; Krysko, D. V., Immunogenicity of cell death and cancer immunotherapy with immune checkpoint inhibitors. *Cell Mol Immunol.* **2025,** *22* (1), 24-39.

3. Tufail, M.; Jiang, C.-H.; Li, N., Immune evasion in cancer: mechanisms and cutting-edge therapeutic approaches. *Signal transduct. target. ther.* **2025,** *10* (1), 227.

4. Yu, J.; Kong, X.; Feng, Y., Tumor microenvironment-driven resistance to immunotherapy in non-small cell lung cancer: strategies for Cold-to-Hot tumor transformation. *Cancer Drug Resist.* **2025,** *8*, 21.

5. Fujiwara, Y.; Kato, S.; Nesline, M. K.; Conroy, J. M.; DePietro, P.; Pabla, S.; Kurzrock, R., Indoleamine 2, 3-dioxygenase (IDO) inhibitors and cancer immunotherapy. *Cancer Treat. Rev.* **2022,** *110*, 102461.

6. Duan, Z.; Shi, L.; He, Z. N. T.; Kuang, C.; Han, T.; Yang, Q., The protective effect of IDO1 inhibition in Aβ-Treated neurons and APP/PS1 mice. *Am. J. Alzheimers Dis. Other Demen.* **2023,** *38*, 15333175231214861.

7. Long, G. V.; Dummer, R.; Hamid, O.; Gajewski, T. F.; Caglevic, C.; Dalle, S.; Arance, A.; Carlino, M. S.; Grob, J.-J.; Kim, T. M., Epacadostat plus pembrolizumab versus placebo plus pembrolizumab in patients with unresectable or metastatic melanoma (ECHO-301/KEYNOTE-252): a phase 3, randomised, double-blind study. *Lancet Oncol.* **2019,** *20* (8), 1083-1097.

8. Pallotta, M. T.; Rossini, S.; Suvieri, C.; Coletti, A.; Orabona, C.; Macchiarulo, A.; Volpi, C.; Grohmann, U. J. T. F. j., Indoleamine 2, 3-dioxygenase 1 (IDO1): an up-to-date overview of an eclectic immunoregulatory enzyme. *FEBS J.* **2022,** *289* (20), 6099-6118.

9. Hornyák, L.; Dobos, N.; Koncz, G.; Karányi, Z.; Páll, D.; Szabó, Z.; Halmos, G.; Székvölgyi, L., The role of indoleamine-2, 3-dioxygenase in cancer development, diagnostics, and therapy. *Front. immunol.* **2018,** *9*, 151.

10. Labadie, B. W.; Bao, R.; Luke, J. J., Reimagining IDO pathway inhibition in cancer immunotherapy via downstream focus on the tryptophan–kynurenine–aryl hydrocarbon axis. *Clin. Cancer Res.* **2019,** *25* (5), 1462-1471.

11. Komiya, T.; Huang, C. H., Updates in the clinical development of epacadostat and other indoleamine 2, 3-dioxygenase 1 inhibitors (IDO1) for human cancers. *Front Oncol.* **2018,** *8*, 423.

12. Wang, X.-X.; Sun, S.-Y.; Dong, Q.-Q.; Wu, X.-X.; Tang, W.; Xing, Y.-Q., Recent advances in the discovery of indoleamine 2, 3-dioxygenase 1 (IDO1) inhibitors. *Medchemcomm.* **2019,** *10* (10), 1740-1754.

13. Gao, M.; Yu, W.; Xi, Z.; Zhang, Z.; Fan, X.; Wang, X., Recent Update on the Discovery of Indoleamine-2, 3-Dioxygenase 1 Inhibitors Targeting Cancer Immunotherapy. *Eur. J. Med. Chem.* **2025**, 118017.

14. Prendergast, G. C.; Smith, C.; Thomas, S.; Mandik-Nayak, L.; Laury-Kleintop, L.; Metz, R.; Muller, A. J., Indoleamine 2, 3-dioxygenase pathways of pathogenic inflammation and immune escape in cancer. *Cancer Immunol. Res.* **2014,** *63* (7), 721-735.

15. Munn, D. H.; Mellor, A. L., IDO in the tumor microenvironment: inflammation, counter-regulation, and tolerance. *Trends Immunol.* **2016,** *37* (3), 193-207.

16. Metz, R.; Rust, S.; DuHadaway, J. B.; Mautino, M. R.; Munn, D. H.; Vahanian, N. N.; Link, C. J.; Prendergast, G. C., IDO inhibits a tryptophan sufficiency signal that

stimulates mTOR: A novel IDO effector pathway targeted by D-1-methyl-tryptophan. *Oncoimmunology* **2012,** *1* (9), 1460-1468.

17. Munn, D. H.; Sharma, M. D.; Baban, B.; Harding, H. P.; Zhang, Y.; Ron, D.; Mellor, A. L., GCN2 kinase in T cells mediates proliferative arrest and anergy induction in response to indoleamine 2, 3-dioxygenase. *Immunity* **2005,** *22* (5), 633-642.

18. Smith, C.; Chang, M. Y.; Parker, K. H.; Beury, D. W.; DuHadaway, J. B.; Flick, H. E.; Boulden, J.; Sutanto-Ward, E.; Soler, A. P.; Laury-Kleintop, L. D., IDO is a nodal pathogenic driver of lung cancer and metastasis development. *Cancer Discov.* **2012,** *2* (8), 722-735.

19. Pallotta, M. T.; Orabona, C.; Volpi, C.; Vacca, C.; Belladonna, M. L.; Bianchi, R.; Servillo, G.; Brunacci, C.; Calvitti, M.; Bicciato, S., Indoleamine 2, 3-dioxygenase is a signaling protein in long-term tolerance by dendritic cells. *Nat. Immunol.s* **2011,** *12* (9), 870-878.

20. Kang, I.; Theodoropoulos, G.; Wangpaichitr, M., Targeting the kynurenine pathway: another therapeutic opportunity in the metabolic crosstalk between cancer and immune cells. *Front. Oncol.* **2025,** *14*, 1524651.

21. Bruner, J. T.; Cozis, J. D.; Marrah, A. J.; Mayberry, T. G.; Cowan, B. B.; Wakefield, M. R.; Fang, Y., Mechanisms and Clinical Implications of Immune Checkpoint Inhibitors PD-1, CTLA-4, and TIM-3 in Cancer. *Cancer Immunol. Res.* **2024,** *7* (1), 20-29.

22. Muller, A. J.; DuHadaway, J. B.; Donover, P. S.; Sutanto-Ward, E.; Prendergast, G. C., Inhibition of indoleamine 2, 3-dioxygenase, an immunoregulatory target of the cancer suppression gene Bin1, potentiates cancer chemotherapy. *Nat. Med.* **2005,** *11* (3), 312-319.

23. Balachandran, V. P.; Cavnar, M. J.; Zeng, S.; Bamboat, Z. M.; Ocuin, L. M.; Obaid, H.; Sorenson, E. C.; Popow, R.; Ariyan, C.; Rossi, F., Imatinib potentiates antitumor T cell responses in gastrointestinal stromal tumor through the inhibition of Ido. *Nat. Med.* **2011,** *17* (9), 1094-1100.

24. Muller, A. J.; Sharma, M. D.; Chandler, P. R.; DuHadaway, J. B.; Everhart, M. E.; Johnson III, B. A.; Kahler, D. J.; Pihkala, J.; Soler, A. P.; Munn, D. H., Chronic inflammation that facilitates tumor progression creates local immune suppression by inducing indoleamine 2, 3 dioxygenase. *Proc. Natl. Acad. Sci. U.S.A.* **2008,** *105* (44), 17073-17078.

25. Uyttenhove, C.; Pilotte, L.; Théate, I.; Stroobant, V.; Colau, D.; Parmentier, N.; Boon, T.; Van den Eynde, B. J., Evidence for a tumoral immune resistance mechanism

based on tryptophan degradation by indoleamine 2, 3-dioxygenase. *Nat. Med.* **2003,** *9* (10), 1269-1274.

26. Zhao, J.; Bai, X.; Du, J.; Chen, Y.; Guo, X.; Zhang, J.; Gan, J.; Wu, P.; Chen, S.; Zhang, X., Tryptophan metabolism: From physiological functions to key roles and therapeutic targets in cancer. *Oncol. Rep.* **2025,** *54* (1), 86.

27. Tsuji, A.; Ikeda, Y.; Yoshikawa, S.; Taniguchi, K.; Sawamura, H.; Morikawa, S.; Nakashima, M.; Asai, T.; Matsuda, S., The tryptophan and kynurenine pathway involved in the development of immune-related diseases. *Int. J. Mol. Sci.* **2023,** *24* (6), 5742.

28. Wu, H.; Gong, J.; Liu, Y., Indoleamine 2, 3-dioxygenase regulation of immune response. *Mol. Med. Rep.* **2018,** *17* (4), 4867-4873.

29. Fougeray, S.; Mami, I.; Bertho, G.; Beaune, P.; Thervet, E.; Pallet, N., Tryptophan depletion and the kinase GCN2 mediate IFN-γ–Induced Autophagy. *J. Immunol.* **2012,** *189* (6), 2954-2964.

30. Solvay, M.; Holfelder, P.; Klaessens, S.; Pilotte, L.; Stroobant, V.; Lamy, J.; Naulaerts, S.; Spillier, Q.; Frédérick, R.; De Plaen, E., Tryptophan depletion sensitizes the AHR pathway by increasing AHR expression and GCN2/LAT1-mediated kynurenine uptake, and potentiates induction of regulatory T lymphocytes. *JITC* **2023,** *11* (6), e006728.

31. Grishanova, A. Y.; Perepechaeva, M. L., Kynurenic acid/AhR signaling at the junction of inflammation and cardiovascular diseases. *Int. J. Mol. Sci.* **2024,** *25* (13), 6933.

32. Muller, A. J.; Mondal, A.; Dey, S.; Prendergast, G. C., IDO1 and inflammatory neovascularization: bringing new blood to tumor-promoting inflammation. *Front. Oncol.* **2023,** *13*, 1165298.

33. Shen, S.-C.; Dey, S.; DuHadaway, J. B.; Sutanto-Ward, E.; Hampton, M. T.; Kozlov, S. V.; Prendergast, G. C.; Muller, A. J., Neovascular pruning by IDO1 inhibitors can potentiate immunogenic cytotoxicity of ischemia-targeted agents to synergistically enhance anti-PD-1 responsiveness. *JITC* **2025,** *13* (5), e011398.

34. Zhai, L.; Ladomersky, E.; Lenzen, A.; Nguyen, B.; Patel, R.; Lauing, K. L.; Wu, M.; Wainwright, D. A., IDO1 in cancer: a Gemini of immune checkpoints. *Cell Mol Immunol.* **2018,** *15* (5), 447-457.

35. Zhai, L.; Bell, A.; Ladomersky, E.; Lauing, K. L.; Bollu, L.; Sosman, J. A.; Zhang, B.; Wu, J. D.; Miller, S. D.; Meeks, J. J., Immunosuppressive IDO in cancer: mechanisms of action, animal models, and targeting strategies. *Front. Immunol.* **2020,** *11*, 1185.

36. Rossini, S.; Ambrosino, S.; Volpi, C.; Belladonna, M. L.; Pallotta, M. T.; Panfili, E.; Suvieri, C.; Macchiarulo, A.; Mondanelli, G.; Orabona, C., Epacadostat stabilizes the apo-form of IDO1 and signals a pro-tumorigenic pathway in human ovarian cancer cells. *Front. Immunol.* **2024,** *15*, 1346686.

37. Kjeldsen, J. W.; Lorentzen, C. L.; Martinenaite, E.; Ellebaek, E.; Donia, M.; Holmstroem, R. B.; Klausen, T. W.; Madsen, C. O.; Ahmed, S. M.; Weis-Banke, S. E., A phase 1/2 trial of an immune-modulatory vaccine against IDO/PD-L1 in combination with nivolumab in metastatic melanoma. *Nat. Med.* **2021,** *27* (12), 2212-2223.

38. Xu, C.; Cao, K.; Ma, A.; Zheng, M.; Xu, Y.; Tang, L., KLRG1 expression induces functional exhaustion of NK cells in colorectal cancer patients. *Cancer Immunol Immunother* **2025,** *74* (7), 203.

39. Guangzhao, L.; Xin, W.; Miaoqing, W.; Wenjuan, M.; Ranyi, L.; Zhizhong, P.; Rongxin, Z.; Gong, C., IDO1 inhibitor enhances the effectiveness of PD-1 blockade in microsatellite stable colorectal cancer by promoting macrophage pro-inflammatory phenotype polarization. *Cancer Immunol Immunother* **2025,** *74* (2), 71.

40. Zeitler, L.; Murray, P. J., IL4i1 and IDO1: oxidases that control a tryptophan metabolic nexus in cancer. *J. Biol. Chem.* **2023,** *299* (6), 104827.

41. Nelp, M. T.; Kates, P. A.; Hunt, J. T.; Newitt, J. A.; Balog, A.; Maley, D.; Zhu, X.; Abell, L.; Allentoff, A.; Borzilleri, R., Immune-modulating enzyme indoleamine 2, 3-dioxygenase is effectively inhibited by targeting its apo-form. *Proc Natl Acad Sci U S A* **2018,** *115* (13), 3249-3254.

42. Basran, J.; Efimov, I.; Chauhan, N.; Thackray, S. J.; Krupa, J. L.; Eaton, G.; Griffith, G. A.; Mowat, C. G.; Handa, S.; Raven, E. L., The mechanism of formation of N-formylkynurenine by heme dioxygenases. *J. Am. Chem. Soc.* **2011,** *133* (40), 16251-16257.

43. Platten, M.; von Knebel Doeberitz, N.; Oezen, I.; Wick, W.; Ochs, K., Cancer immunotherapy by targeting IDO1/TDO and their downstream effectors. *Front. immunol.* **2015,** *5*, 673.

44. Nguyen, N. T.; Nakahama, T.; Le, D. H.; Van Son, L.; Chu, H. H.; Kishimoto, T., Aryl hydrocarbon receptor and kynurenine: recent advances in autoimmune disease research. *Front. immunol.* **2014,** *5*, 551.

45. Lewis-Ballester, A.; Pham, K. N.; Batabyal, D.; Karkashon, S.; Bonanno, J. B.; Poulos, T. L.; Yeh, S.-R., Structural insights into substrate and inhibitor binding sites in human indoleamine 2, 3-dioxygenase 1. *Nat. Commun.* **2017,** *8* (1), 1693.

46. Röhrig, U. F.; Michielin, O.; Zoete, V., Structure and plasticity of indoleamine 2, 3-dioxygenase 1 (IDO1). *J. Med. Chem.* **2021,** *64* (24), 17690-17705.

47. Davies, C.; Dötsch, L.; Ciulla, M. G.; Hennes, E.; Yoshida, K.; Gasper, R.; Scheel, R.; Sievers, S.; Strohmann, C.; Kumar, K., Identification of a novel pseudo-natural product type IV IDO1 inhibitor chemotype. *Angew. Chem. Int. Ed.* **2022,** *134* (40), e202209374.

48. Pei, Z.; Mendonca, R.; Gazzard, L.; Pastor, R.; Goon, L.; Gustafson, A.; VanderPorten, E.; Hatzivassiliou, G.; Dement, K.; Cass, R., Aminoisoxazoles as potent inhibitors of tryptophan 2, 3-dioxygenase 2 (TDO2). *ACS Med. Chem. Lett.* **2018,** *9* (5), 417-421.

49. Röhrig, U. F.; Reynaud, A.; Majjigapu, S. R.; Vogel, P.; Pojer, F.; Zoete, V., Inhibition mechanisms of indoleamine 2, 3-dioxygenase 1 (IDO1). *J. Med. Chem.* **2019,** *62* (19), 8784-8795.

50. Prendergast, G. C.; Malachowski, W. P.; DuHadaway, J. B.; Muller, A. J., Discovery of IDO1 inhibitors: from bench to bedside. *Cancer Res* **2017,** *77* (24), 6795-6811.

51. Paul, S.; Roy, A.; Deka, S. J.; Panda, S.; Trivedi, V.; Manna, D., Nitrobenzofurazan derivatives of N′-hydroxyamidines as potent inhibitors of indoleamine-2, 3-dioxygenase 1. *Eur. J. Med. Chem.* **2016,** *121*, 364-375.

52. Yue, E. W.; Douty, B.; Wayland, B.; Bower, M.; Liu, X.; Leffet, L.; Wang, Q.; Bowman, K. J.; Hansbury, M. J.; Liu, C., Discovery of potent competitive inhibitors of indoleamine 2, 3-dioxygenase with in vivo pharmacodynamic activity and efficacy in a mouse melanoma model. *J. Med. Chem.* **2009,** *52* (23), 7364-7367.

53. Röhrig, U. F.; Majjigapu, S. R.; Vogel, P.; Zoete, V.; Michielin, O., Challenges in the discovery of indoleamine 2, 3-dioxygenase 1 (IDO1) inhibitors. *J. Med. Chem.* **2015,** *58* (24), 9421-9437.

54. Kumar, S.; Jaller, D.; Patel, B.; LaLonde, J. M.; DuHadaway, J. B.; Malachowski, W. P.; Prendergast, G. C.; Muller, A. J., Structure based development of phenylimidazole-derived inhibitors of indoleamine 2, 3-dioxygenase. *J. Med. Chem.* **2008,** *51* (16), 4968-4977.

55. Peng, Y.-H.; Ueng, S.-H.; Tseng, C.-T.; Hung, M.-S.; Song, J.-S.; Wu, J.-S.; Liao, F.-Y.; Fan, Y.-S.; Wu, M.-H.; Hsiao, W.-C., Important hydrogen bond networks in indoleamine 2, 3-dioxygenase 1 (IDO1) inhibitor design revealed by crystal structures of imidazoleisoindole derivatives with IDO1. *J. Med. Chem.* **2016,** *59* (1), 282-293.

56. Tang, K.; Wu, Y.-H.; Song, Y.; Yu, B., Indoleamine 2, 3-dioxygenase 1 (IDO1) inhibitors in clinical trials for cancer immunotherapy. *J Hematol Oncol.* **2021,** *14* (1), 68.

57. Coletti, A.; Greco, F. A.; Dolciami, D.; Camaioni, E.; Sardella, R.; Pallotta, M. T.; Volpi, C.; Orabona, C.; Grohmann, U.; Macchiarulo, A., Advances in indoleamine 2, 3-dioxygenase 1 medicinal chemistry. *Medchemcomm.* **2017,** *8* (7), 1378-1392.

58. Alexandre, J. A. C.; Swan, M. K.; Latchem, M. J.; Boyall, D.; Pollard, J. R.; Hughes, S. W.; Westcott, J., New 4-amino-1, 2, 3-triazole inhibitors of Indoleamine 2, 3-Dioxygenase form a long-lived complex with the enzyme and display exquisite cellular potency. *ChemBioChem* **2018,** *19* (6), 552-561.

59. Pham, K. N.; Yeh, S.-R., Mapping the binding trajectory of a suicide inhibitor in human indoleamine 2, 3-dioxygenase 1. *J. Am. Chem. Soc.* **2018,** *140* (44), 14538-14541.

60. Jiang, K.; Wang, Q.; Chen, X.-L.; Wang, X.; Gu, X.; Feng, S.; Wu, J.; Shang, H.; Ba, X.; Zhang, Y., Nanodelivery optimization of IDO1 inhibitors in tumor immunotherapy: challenges and strategies. *Int. J. Nanomed.* **2024**, 8847-8882.

61. Pallotta, M. T.; Fallarino, F.; Matino, D.; Macchiarulo, A.; Orabona, C., AhR-mediated, non-genomic modulation of IDO1 function. *Front Immunol.* **2014,** *5*, 497.

62. Smirnova, A.; Wincent, E.; Vikström Bergander, L.; Alsberg, T.; Bergman, J.; Rannug, A.; Rannug, U., Evidence for new light-independent pathways for generation of the endogenous aryl hydrocarbon receptor agonist FICZ. *Chem. Res. Toxicol.* **2016,** *29* (1), 75-86.

63. Hwang, W.-B.; Kim, D.-J.; Oh, G.-S.; Park, J.-H., Aryl hydrocarbon receptor ligands indoxyl 3-sulfate and indole-3-carbinol inhibit FMS-like tyrosine kinase 3 ligand-induced bone marrow-derived plasmacytoid dendritic cell differentiation. *Immune Netw.* **2018,** *18* (5).

64. Griffith, B. D.; Frankel, T. L., The aryl hydrocarbon receptor: impact on the tumor immune microenvironment and modulation as a potential therapy. *Cancers* **2024,** *16* (3), 472.

65. Brincks, E. L.; Adams, J.; Wang, L.; Turner, B.; Marcinowicz, A.; Ke, J.; Essmann, M.; Mautino, L. M.; Van Allen, C.; Kumar, S., Indoximod opposes the immunosuppressive effects mediated by IDO and TDO via modulation of AhR function and activation of mTORC1. *Oncotarget* **2020,** *11* (25), 2438.

66. Li, X.; Meng, H.; Wang, H.; Zhang, Y.; Yu, W., Indoleamine 2, 3-dioxygenase 1 in cancer immunotherapy: from small-molecule inhibition to PROTAC-mediated degradation. *Front. pharmacol.* **2025,** *16*, 1640073.

67. Peng, X.; Zhao, Z.; Liu, L.; Bai, L.; Tong, R.; Yang, H.; Zhong, L.; therapy, Targeting indoleamine dioxygenase and tryptophan dioxygenase in cancer immunotherapy: clinical progress and challenges. *Drug Des Devel Ther.* **2022**, 2639-2657.

68. Dolšak, A.; Gobec, S.; Sova, M., Indoleamine and tryptophan 2, 3-dioxygenases as important future therapeutic targets. *CPT* **2021,** *221*, 107746.

69. Salter, M.; Hazelwood, R.; Pogson, C. I.; Iyer, R.; Madge, D. J., The effects of a novel and selective inhibitor of tryptophan 2, 3-dioxygenase on tryptophan and serotonin metabolism in the rat. *Biochem. Pharmacol.* **1995,** *49* (10), 1435-1442.

70. Pilotte, L.; Larrieu, P.; Stroobant, V.; Colau, D.; Dolušić, E.; Frédérick, R.; De Plaen, E.; Uyttenhove, C.; Wouters, J.; Masereel, B., Reversal of tumoral immune resistance by inhibition of tryptophan 2, 3-dioxygenase. *Proc Natl Acad Sci USA.* **2012,** *109* (7), 2497-2502.

71. Winters, M.; DuHadaway, J. B.; Pham, K. N.; Lewis-Ballester, A.; Badir, S.; Wai, J.; Sheikh, E.; Yeh, S.-R.; Prendergast, G. C.; Muller, A. J., Diaryl hydroxylamines as pan or dual inhibitors of indoleamine 2, 3-dioxygenase-1, indoleamine 2, 3-dioxygenase-2 and tryptophan dioxygenase. *Eur. J. Med. Chem.* **2019,** *162*, 455-464.

72. Zhou, X., Recent advances of tryptanthrin and its derivatives as potential anticancer agents. *RSC med. chem.* **2024,** *15* (4), 1127-1147.

73. Cui, G.; Lai, F.; Wang, X.; Chen, X.; Xu, B., Design, synthesis and biological evaluation of indole-2-carboxylic acid derivatives as IDO1/TDO dual inhibitors. *Eur. J. Med. Chem.* **2020,** *188*, 111985.

74. Sari, S.; Tomek, P.; Leung, E.; Reynisson, J., Discovery and characterisation of dual inhibitors of tryptophan 2, 3-dioxygenase (TDO2) and indoleamine 2, 3-dioxygenase 1 (IDO1) using virtual screening. *Molecules* **2019,** *24* (23), 4346.

75. Tan, Y.; Liu, M.; Li, M.; Chen, Y.; Ren, M., Indoleamine 2, 3-dioxygenase 1 inhibitory compounds from natural sources. *Front. pharmacol.* **2022,** *13*, 1046818.

76. Al-Zoubi, R. M.; Elaarag, M.; Al-Qudimat, A. R.; Al-Hurani, E. A.; Fares, Z. E.; Farhan, A. a.; Al-Zoubi, S. R.; Khan, A.; Agouni, A.; Shkoor, M., IDO and TDO inhibitors in cancer immunotherapy: mechanisms, clinical development, and future directions. *Front. pharmacol.* **2025**.

77. Jung, K. H.; LoRusso, P.; Burris, H.; Gordon, M.; Bang, Y.-J.; Hellmann, M. D.; Cervantes, A.; Ochoa de Olza, M.; Marabelle, A.; Hodi, F. S., Phase I study of the indoleamine 2, 3-dioxygenase 1 (IDO1) inhibitor navoximod (GDC-0919) administered

with PD-L1 inhibitor (atezolizumab) in advanced solid tumors. *Clin Cancer Res* **2019,** *25* (11), 3220-3228.

78. Xiao, M.; Zhong, K.; Guo, L.; Li, W.; Wang, X.; Qiu, Z.; Hang, T., Preclinical PK investigation of a novel IDO1/TDO dual inhibitor—SHR9146 in mouse plasma and tissues by LC-MS/MS. *Front. Oncol.* **2023,** *13*, 1191778.

79. Xu, J.; Zhang, Y.; Jia, R.; Yue, C.; Chang, L.; Liu, R.; Zhang, G.; Zhao, C.; Zhang, Y.; Chen, C., Anti-PD-1 antibody SHR-1210 combined with apatinib for advanced hepatocellular carcinoma, gastric, or esophagogastric junction cancer: an open-label, dose escalation and expansion study. *Clin Cancer Res.* **2019,** *25* (2), 515-523.

80. Naing, A.; Eder, J. P.; Piha-Paul, S. A.; Gimmi, C.; Hussey, E.; Zhang, S.; Hildebrand, V.; Hosagrahara, V.; Habermehl, C.; Moisan, J., Preclinical investigations and a first-in-human phase I trial of M4112, the first dual inhibitor of indoleamine 2, 3-dioxygenase 1 and tryptophan 2, 3-dioxygenase 2, in patients with advanced solid tumors. *JITC* **2020,** *8* (2), e000870.

81. Mitchell, T. C.; Hamid, O.; Smith, D. C.; Bauer, T. M.; Wasser, J. S.; Olszanski, A. J.; Luke, J. J.; Balmanoukian, A. S.; Schmidt, E. V.; Zhao, Y., Epacadostat plus pembrolizumab in patients with advanced solid tumors: phase I results from a multicenter, open-label phase I/II trial (ECHO-202/KEYNOTE-037). *JCO* **2018,** *36* (32), 3223-3230.

82. Qin, X.; He, L.; Feng, C.; Fan, D.; Liang, W.; Wang, Q.; Fang, J., Injectable micelle-incorporated hydrogels for the localized chemo-immunotherapy of breast tumors. *ACS Appl. Mater. Interfaces* **2021,** *13* (39), 46270-46281.

83. Ma, S.; Zhu, W.; Ji, X.; Liu, C.; Chen, N.; Guo, D.; Song, H., Multiplex Methionine Modulating Hydrogel for Cancer Metabolic Therapy. *Adv. Mater.* **2025**, 2420445.

84. Wang, B.; Tang, D.; Cui, J.; Jiang, H.; Yu, J.; Guo, Z., RGD-based self-assembling nanodrugs for improved tumor therapy. *Front Pharmacol.* **2024,** *15*, 1477409.

85. Lu, K.; He, C.; Guo, N.; Chan, C.; Ni, K.; Weichselbaum, R. R.; Lin, W., Chlorin-based nanoscale metal–organic framework systemically rejects colorectal cancers via synergistic photodynamic therapy and checkpoint blockade immunotherapy. *J. Am. Chem. Soc.* **2016,** *138* (38), 12502-12510.

86. Zou, Y.; Chen, J.; Qu, Y.; Luo, X.; Wang, W.; Zheng, X., Evolution of nMOFs in photodynamic therapy: from porphyrins to chlorins and bacteriochlorins for better efficacy. *Front. pharmacol.* **2025,** *16*, 1533040.

87. Hu, J.; Arvejeh, P. M.; Bone, S.; Hett, E.; Marincola, F. M.; Roh, K.-H., Nanocarriers for cutting-edge cancer immunotherapies. *J. Transl. Med.* **2025,** *23* (1), 447.

88. Peng, S.; Xiao, F.; Chen, M.; Gao, H., Tumor-microenvironment-responsive nanomedicine for enhanced cancer immunotherapy. *Adv. Sci.* **2022,** *9* (1), 2103836.

89. Dendrou, C. A.; Petersen, J.; Rossjohn, J.; Fugger, L., HLA variation and disease. *Nat. Rev. Immunol.* **2018,** *18* (5), 325-339.

90. Sabit, H.; Abdel-Ghany, S.; Albrahim, Y.; Wadan, A.-H. S.; Rashwan, S.; Arneth, R.; Arneth, B., Bridging the Gap in Breast Cancer Dormancy: Models, Mechanisms, and Translational Challenges. *Pharmaceuticals (Basel)* **2025,** *18* (7), 961.

91. Zhang, J.; Xiao, C.; Zhang, X.; Lin, Y.; Yang, H.; Zhang, Y. S.; Ding, J., An oxidative stress-responsive electrospun polyester membrane capable of releasing anti-bacterial and anti-inflammatory agents for postoperative anti-adhesion. *J Control Release* **2021,** *335*, 359-368.

92. Renoux, V. M.; Zriwil, A.; Peitzsch, C.; Michaëlsson, J.; Friberg, D.; Soneji, S.; Sitnicka, E., Identification of a human natural killer cell lineage-restricted progenitor in fetal and adult tissues. *Immun.* **2015,** *43* (2), 394-407.

CHAPTER 2

Evaluation of mode of indoleamine 2,3-dioxygenase 1 inhibition by 4,7-dichloroquinolines

2.1. Background and objective of present work

Guided by the findings in previous chapter, in this second chapter, establishing IDO1 as a therapeutic target for diseases is emphasized on. This therapeutic target involves immune suppression. Overexpression of this immunosuppressive enzyme has led to poor clinical outcomes across various malignancies.[1] In multiple cancer cells, blocking of IDO1 activity effectively restrain abnormal tumor growth. Moreover, through IDO1 inhibition, both radiation and chemotherapy efficacy has been enhanced. Inhibitors such as epacadostat, linrodostat, PF-06840003, and prodrugs like NLG802 have been developed and tested.[2-5] However, significant clinical setbacks of the ECHO-301 trial with epacadostat plus pembrolizumab highlighted the need to for new mechanisms of IDO1 inhibition.[6] According to recent study, most IDO1 exists in its heme-free (apo-IDO1) form. This generates excess free heme that may encourage cancer cell survival via oxidative stress and activate other heme proteins. Therefore, targeting apo-IDO1 directly, while reducing free heme toxicity, is now considered a promising strategy.[7]

Inspired by the success of the apo-IDO1 inhibitor, linrodostat, in the clinical trials, herein we report the development of 4,7-dichloroquinoline (DCQ) derivatives in effort to develop an apo-IDO1 inhibitor. The novelty of our design of compounds is the use of amino acids with chiral center and the easy installation of piperazine moiety. We also tried to incorporate a heme binding moiety, 7-chloro-4-aminoquinoline, to these drugs.[8] The biophysical studies revealed that the potent DCQ derivative binds to apo-IDO1 and free heme, inhibiting IDO1 enzyme activity.

2.2. Result and discussion

2.2.1. Synthesis of DCQ derivatives

Linrodostat (BMS-986205), developed by Bristol-Myers Squibb, is an orally available IDO1 (apo-IDO1) inhibitor that restores and induces the proliferation and activation of immune cells and reduces the proliferation of T_{reg}.[9] Consequent growth of IDO1-expressing tumor cells are getting diminished. Currently, linrodostat is in Phase-III clinical trials for the treatment of muscle-invasive bladder and other cancers.[10] However, the optimized synthesis required more than 12 steps to produce linrodostat, which could limit its large-scale production and enhance production cost.[11] We hypothesized that developing small molecules that could have similar apo-IDO1-mediated inhibitory activity and be synthesized in fewer steps would benefit IDO1-mediated drug-discovery studies. In this regard, we designed and synthesized DCQ derivatives in 4 steps

from commercially available DCQ, piperazine, and amino acids with moderate yields. The heme-binding efficacy of the 7-chloro-4-aminoquinoline moiety also prompted us to develop a DCQ-based compound with a hydrophobic moiety suitable to occupy the ligand binding site of the apo-IDO1. To synthesize these DCQ derivatives, first 4,7-dichloroquinoline was reacted with 1,4-diaminocyclohexane or piperazine in the presence of triethylamine to obtain 4-substituted 7-chloroquinoline.[12] Meanwhile, the α-amino group of corresponding amino acid was brominated using 48% HBr and $NaNO_2$ (Scheme 2.1).[13] The brominated product was then coupled with the respective amine using oxalyl chloride.

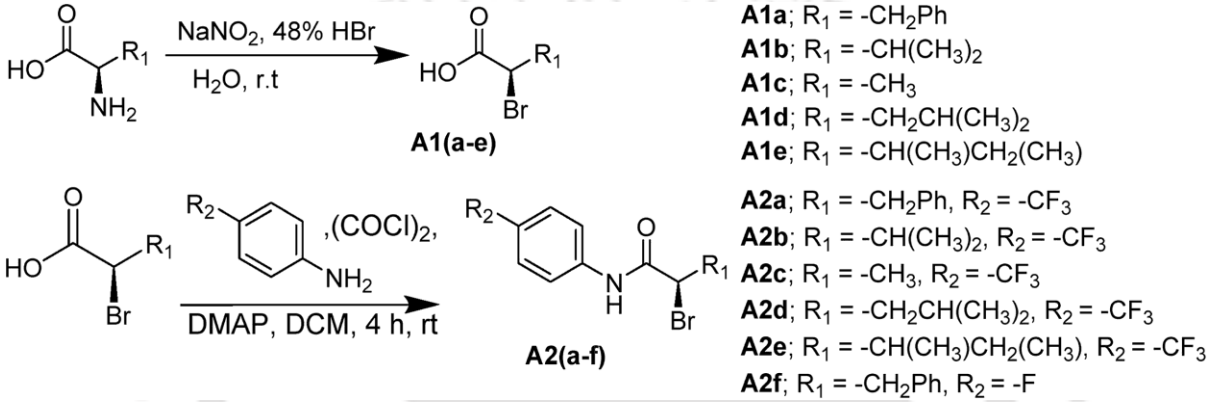

Scheme 2.1. Synthesis of amino acid derivatives.

To obtain corresponding amide derivatives. Finally, the coupling of 4-substituted 7-chloroquinoline with the bromo-containing amide derivatives using K_2CO_3 resulted in the targeted DCQ derivatives (Scheme 2.2). The products were purified in column chromatographic technique and characterized by HRMS and NMR techniques. Further, HPLC-based purification analysis was also performed. The products were isolated with more than 97-98% purity level and used further for biophysical and cellular studies.

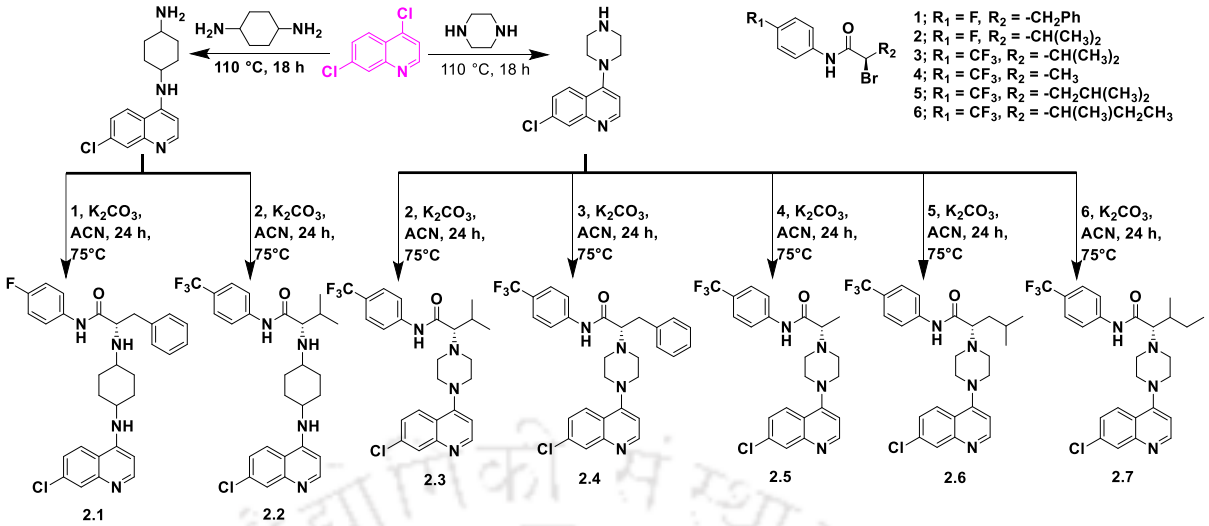

Scheme 2.2. Synthetic routes to DCQ derivatives.

2.2.2. Inhibitory activities against IDO1 enzyme

The initial enzyme activity screening revealed that the compound **2.4** strongly inhibits the IDO1-mediated catabolism of L-trp to *N*-formylkynurenine (IC_{50} = 94 ± 4 M) (Fig. 2.1) [7, 14, 15].

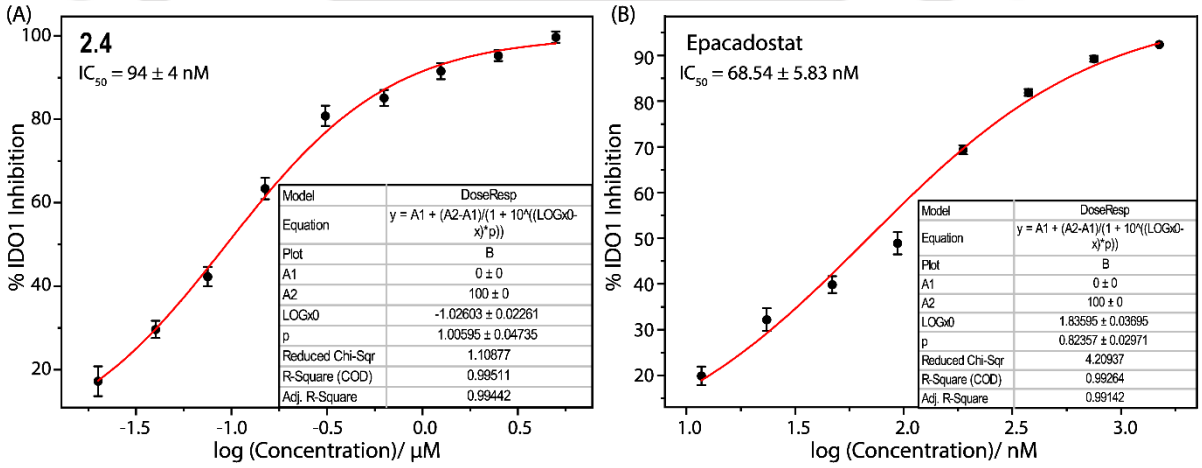

Fig. 2.1. Plots of concentration of *N*-formyl kynurenine in the presence of different concentrations of **2.4**.

The other DCQ derivative sowed much weaker IDO1 inhibitory activity. Tryptophan 2,3-dioxygenase (TDO) is another member of the same enzyme family as that of IDO1 and regulates the initial rate-limiting step in the metabolism of L-trp to *N*-formylkynurenine via the kynurenine pathway. However, the potent compound did not show significant inhibitory activity against the tryptophan 2,3-dioxygenase (TDO) enzyme, suggesting its higher selectivity in inhibiting IDO1 over the TDO enzyme

(Table 2.1 and 2.2). In particular, L-trp and indole derivatives are preferred binding partners for the TDO. On the other hand, various types of small molecules can accommodate within the active site of IDO1 due to its plasticity.[16] Accordingly, the potent DCQ derivative could have higher specificity for the IDO1 over the TDO enzyme. For these measurements the inhibitory activity was measured with 60 min of preincubation of the compound with purified enzyme. The cell viability assay revealed that the potent compound has negligible toxicity for HeLa, MDA-MB-231, and HEK-293 cells, indicating its suitability for IDO1 inhibitory studies (Fig. 2.7).

Table 2.1. IDO1 Inhibition activities of the synthesized compounds.

Compound	%IDO1 inhibition[a]			IC_{50} (nM)
	0.1 µM	1 µM	5 µM	
2.1	6.64	7.02	12.11	
2.2	2.37	6.38	16.68	
2.3	21.86	52.40	69.02	
2.4	51.88	92.51	99.89	94 ±4
2.5	13.80	30.01	42.54	
2.6	18.32	22.82	24.96	
2.7	14.21	23.86	30.94	
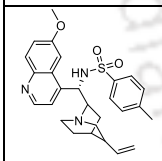 Epacadostat	–	–	–	0.70 ± 0.37

[a] hIDO1 inhibition values are the mean of three independent assays. The activity was measured with 60 min of preincubation of the compound with purified hIDO1 enzyme.

[b] Epacadostat is the reported IDO1 inhibitors

Table 2.2. Inhibitory activity of the **2.4** against purified hIDO1 and hTDO enzymes.

Compound	% Inhibition					
	0.1 µM		1 µM		5 µM	
	IDO1	TDO	IDO1	TDO	IDO1	TDO
2.4	51.88	3.9	92.51	10.57	99.89	14.16

2.2.3. Time and temperature-dependent IDO1 activity

The potent DCQ derivative has no significant similarity to the substrate L-trp or any reported inhibitor; hence we investigated its mechanism of IDO1 inhibition. Initially, the UV-Vis spectral analysis of IDO1 was carried out both in the absence and presence of **2.4** to examine whether removing the heme-cofactor from the IDO1 active site is the vital step for such inhibitory activity (Fig. 2.2A).[17] The temperature and time-dependent inhibition assays were performed without preincubation, and only the incubation times were varied. The spectral analysis revealed a significant reduction of Soret-peak, suggesting the release of the heme-cofactor from holo-IDO1. Conversely, there was no substantial alteration in the Soret-peak of the TDO enzyme. In addition, the other heme-containing proteins, such as hemoglobin and myoglobin, did not significantly alter the Soret-peak, suggesting that the **2.4**-mediated loss of the heme cofactor could be more selective for the IDO1 enzyme. (Fig. 2.2A). Meanwhile, the IDO1 inhibitory activity of **2.4** was examined with different incubation times (10–60 min) at 37 °C. (Fig. 2.2B).

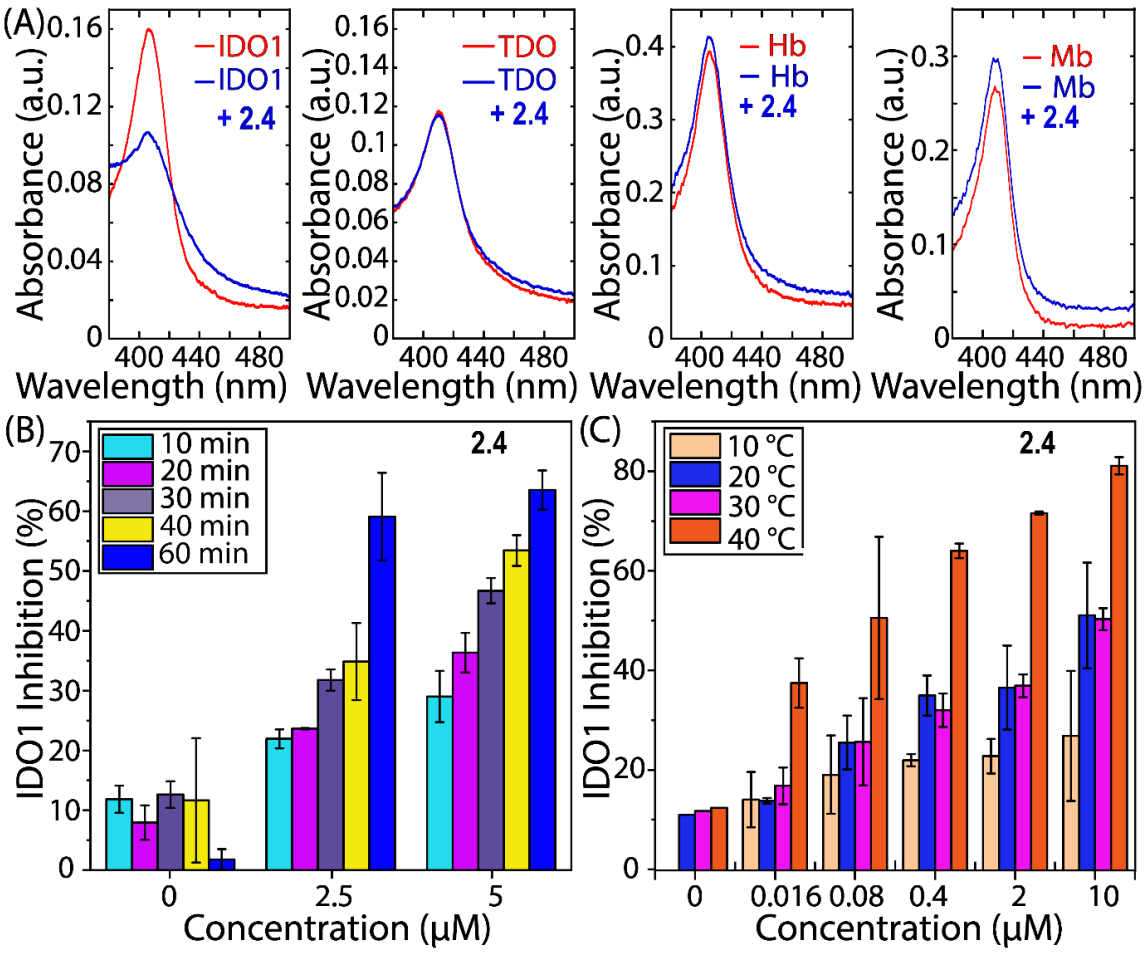

Fig. 2.2. Absorption spectra of the ferric-IDO1 enzyme, ferric-TDO enzyme, hemoglobin, and myoglobin (200 nM) in the absence and presence of the compounds (5 μM) in 100

mM phosphate buffer at pH 6.5 after 60 min of incubation at 37 °C (A). Incubation time was varied to measure the IDO1 (200 nM) activity in the absence and presence of different concentrations of **2.4** (B). Temperature-dependent (C) IDO1 (200 nM) activity in the absence and presence of different concentrations of **2.4** with 60 min of incubation time (C). All of these measurements were performed without any preincubation of enzyme with compound.

Interestingly, an increase in the inhibitory activity was observed with the increase in preincubation time. The maximum inhibitory activity was obtained with 60 min of incubation time. In addition, the IDO1 inhibitory activity of **2.4** was examined at different temperatures with a fixed reincubation time of 60 min (Fig. 2.2C).[17] This temperature-dependent activity assay showed an increase in IDO1 inhibitory activity from 10 to 40 °C, suggesting the probable loss of the heme-cofactor from holo-IDO1 in the presence of the compound. The vicinity of **2.4** to the solvent-exposed surface area of IDO1 could promote partial unfolding of the holo-IDO1, stimulating the release of the heme-cofactor.[5, 13]

2.2.4. Compound-induced heme release property

The protoporphyrin IX (PpIX) quenching experiment was performed to investigate whether **2.4** enhances the release of the heme-cofactor from IDO1. An interaction of PpIX with free heme is known to quench the fluorescence signal of PpIX.[7, 18] Therefore, reducing the PpIX fluorescence signal suggested the **2.4**-mediated release of heme from the IDO1 enzyme and the interaction of the released heme with the PpIX (Fig. 2.3A). In comparison, the PpIX fluorescence signal remained unaltered in the presence of only **2.4**. Meanwhile, the circular dichroism (CD) spectral analysis of IDO1 in the absence and presence of **2.4** did not show any significant change, suggesting a conservation of the structural integrity of the IDO1 even after the loss of the heme-cofactor (Fig. 2.5). Hence, the spectral analyses suggest the possibility of compound-mediated release of heme cofactor from IDO1 plays a crucial role in the.

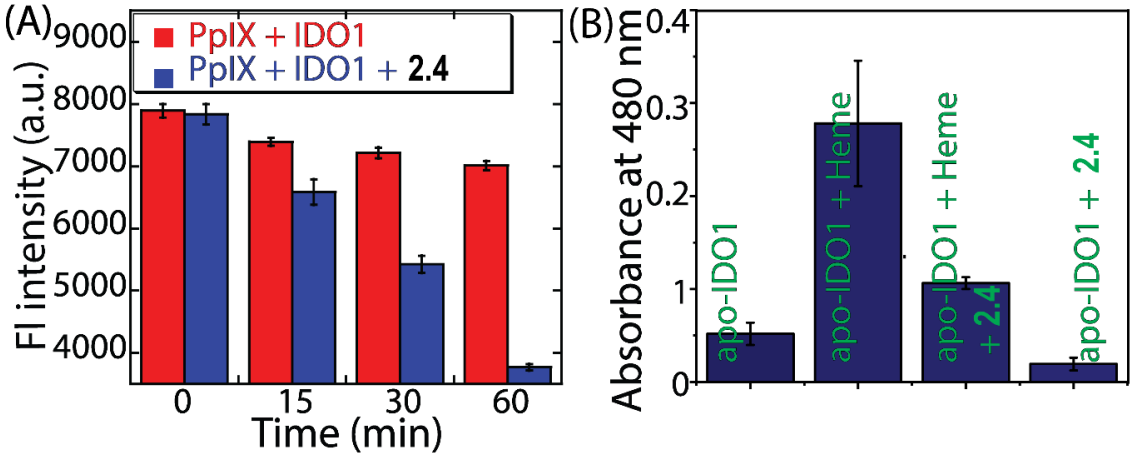

Fig. 2.3. Variation of PpIX fluorescence intensity in the presence of IDO1 or IDO1 equilibrated with **2.4** for different time intervals (A). The activity of apo-IDO1 in the absence and presence of heme and/or **2.4** after equilibration for 60 min (B).

2.4-mediated inhibition studies also indicate that **2.4**-mediated inhibition of IDO1 activity could be due to the conversion of apo-IDO1 from holo-IDO1.[9, 19] To investigate the rate-limiting process of IDO1 inhibition, we performed the activity assay in the presence of different concentrations of **2.4**. The variation of Soret-peak indicates that the extent of heme release efficacy was over 2.2-folds slowed for catalytically active IDO1 than of the inactive IDO1, suggesting that the oxidation state of iron in the heme-cofactor plays a significant role in the heme release profile of IDO1 enzyme in the presence of **2.4** (Fig. 2.4).[19]

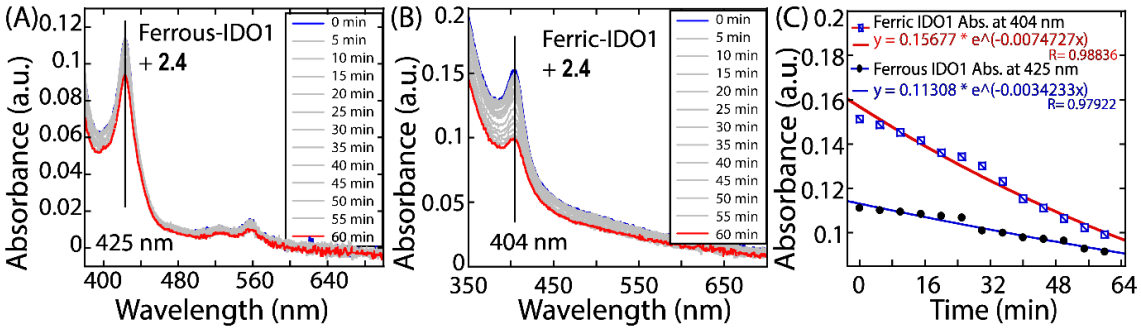

Fig. 2.4. Time-dependent heme dissociation from IDO1 (0.75 μM) in the presence of compound **2.4** (25 μM) at 37 °C. Absorbance spectra of ferrous-IDO1 (A) and ferric-IDO1 (B). The loss in absorbance for ferrous-IDO1 and ferric-IDO1 as a function of time (C). The ferrous-deoxy reaction environment was generated by adding $Na_2S_2O_4$ to the solution under an N_2 atmosphere. Heme dissociation from IDO1 was monitored by the loss of absorbance of the Soret peak: 404 nm for ferric-IDO1 and 425 nm for ferrous-IDO1.

Meanwhile, the inhibitory activity studies of apo-IDO1 in the absence and presence of external heme suggest the recurrence of catalytic IDO1 activity (Fig. 2.3B). The CD analysis also showed that the structural integrity of apo-IDO1 was intact (Fig. 2.5). The control experiment with apo-IDO1 and only **2.4** failed to show any inhibitory activity, even in the presence of external heme. Hence, our systematic biophysical studies revealed that **2.4** promotes the release of heme cofactor from the holo-IDO1 enzyme to produce apo-IDO1 protein.

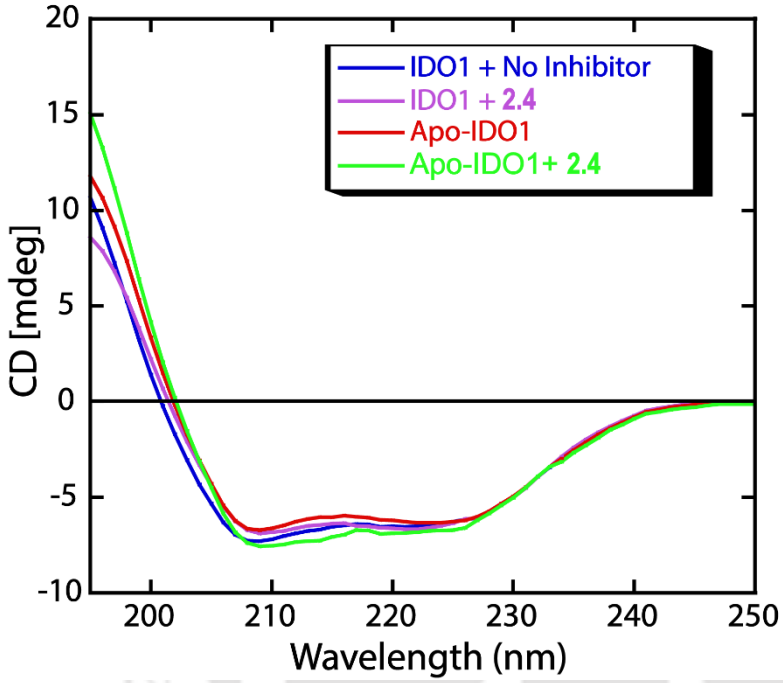

Fig. 2.5. Circular dichroism spectra of apo-IDO1 and IDO1 in the absence and presence of **2.4**.

Table 2.3 Circular dichroism analysis of apo-IDO1 and IDO1 in the absence and presence of **2.4**.

Sl. No.	Sample name	% of secondary structural elements			
		Helix	Beta	Turn	Random
1	IDO1 + No Inhibitor	51.9	0	10.5	37.5
2	IDO1 + 2.4	55.5	0	7.4	33.2
3	Apo-IDO1	56.9	0	11.4	31.7
4	Apo-IDO1 + 2.4	50.4	0	10.6	38.21

2.2.5. Direct apo-IDO1 binding properties of the compound

In the earlier sections, we demonstrated that **2.4** promotes the release of heme cofactor from the holo-IDO1 enzyme to generate apo-IDO1. Consequently, the accretion of free heme in the cytoplasm could stimulate the activity of other heme-containing proteins and heme exporters and alter the turnover.

Rate of the IDO1 enzyme. in free heme-mediated biosynthetic pathways could be stimulated in cancer cells.[7, 20] The **2.4** concentration-dependent decrease of the Soret-peak suggests the interaction of **2.4** with heme (Fig. 2.6).

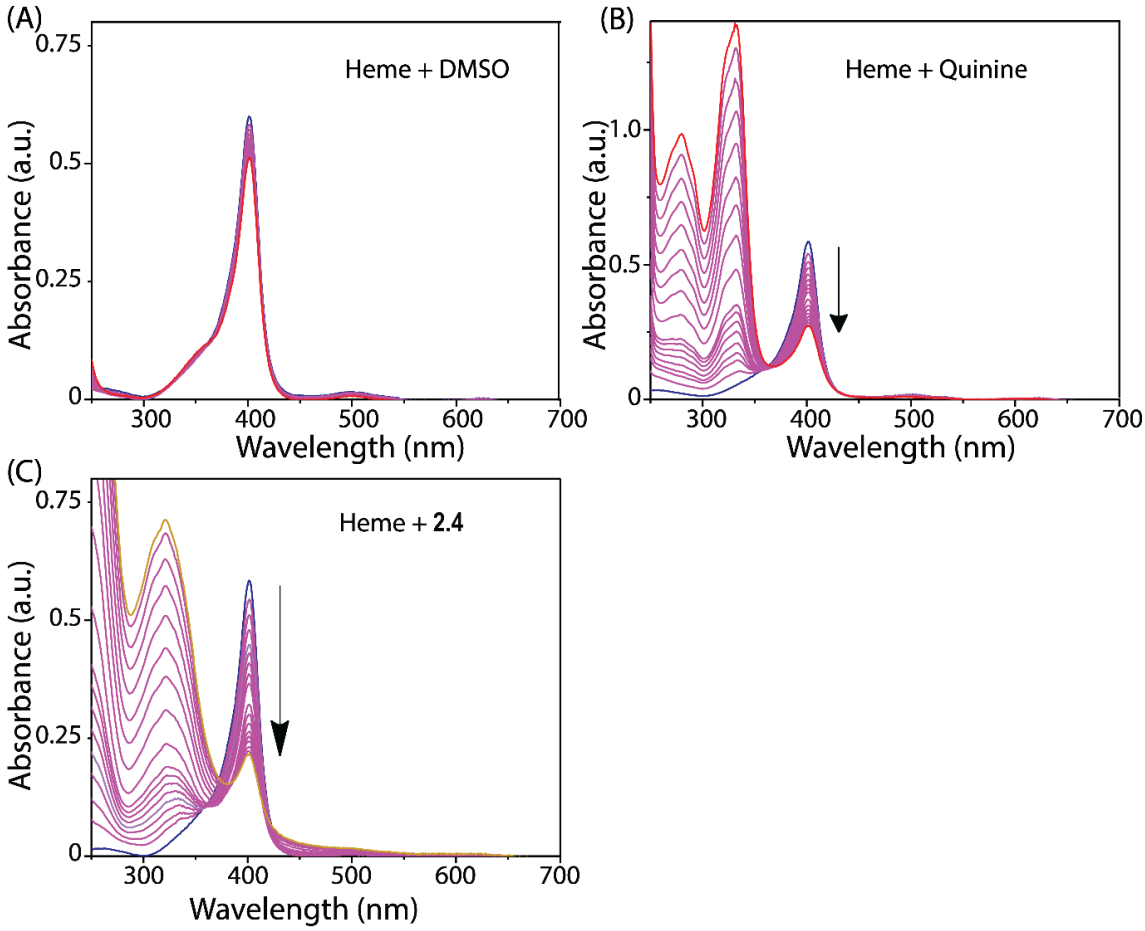

Fig. 2.6. The plot of absorbance of heme (5 µM) in the presence of different concentrations (0-175 µM) of DMSO (A), quinine (B), and **2.4** (C).

The binding affinity of **2.4** for heme is higher than that of quinine, a known heme-binding molecule (Fig. 2.7A). The fluorescence quenching of PpIX in the presence of **2.4** also confirmed the interaction of **2.4** with heme [7, 18]. Additionally, the equilibrated solution of **2.4** and heme significantly affects the PpIX fluorescence quenching and suggests the potential interaction of **2.4** with heme (Fig. 2.7B) [7]. Therefore, these binding

studies indicate that **2.4** could also bind free heme, which could partly suppress the cellular activity of free heme. To investigate whether **2.4** binds to apo-IDO1, we performed surface plasmon resonance (SPR) analysis. The concentration-dependent SPR analysis revealed that **2.4** strongly binds to apo-IDO1 with an affinity (K_D) of 5.98 ± 0.75 μM (Fig. 2.8A), whereas **2.4** weakly binds to IDO1 (K_D = 290.70 M ± 10.45 μM), which could be due to its competition with heme for the same binding site of IDO1 enzyme (Fig. 2.8B).

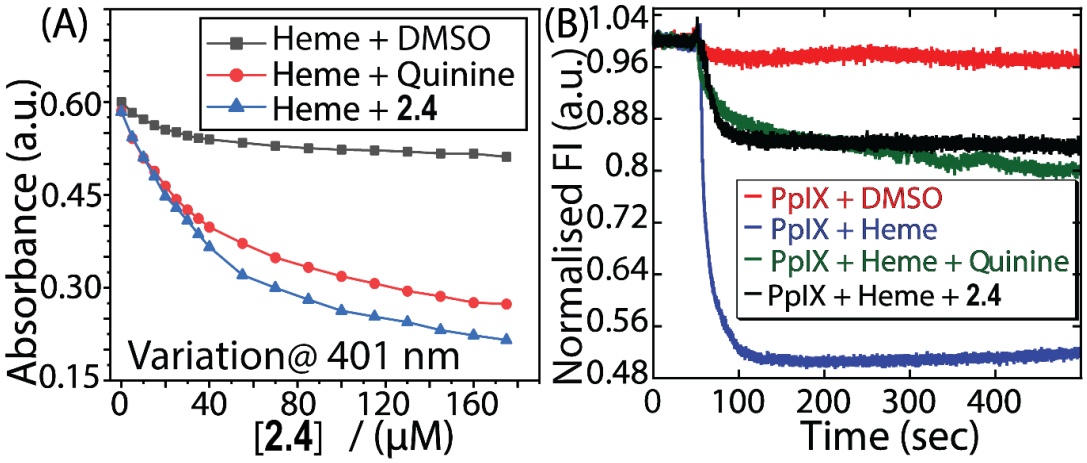

Fig. 2.7. Measurement of heme binding of the compound. Variation of the absorbance at 401 nm of heme (5 μM) in the absence and presence of different concentrations of quinine and **2.4** by spectrophotometric method (A). Variation of PpIX (5 μM) fluorescence in the absence and presence of heme (1.5 μM) or solution of heme (1.5 μM) equilibrated with **2.4** (30 μM) (B).

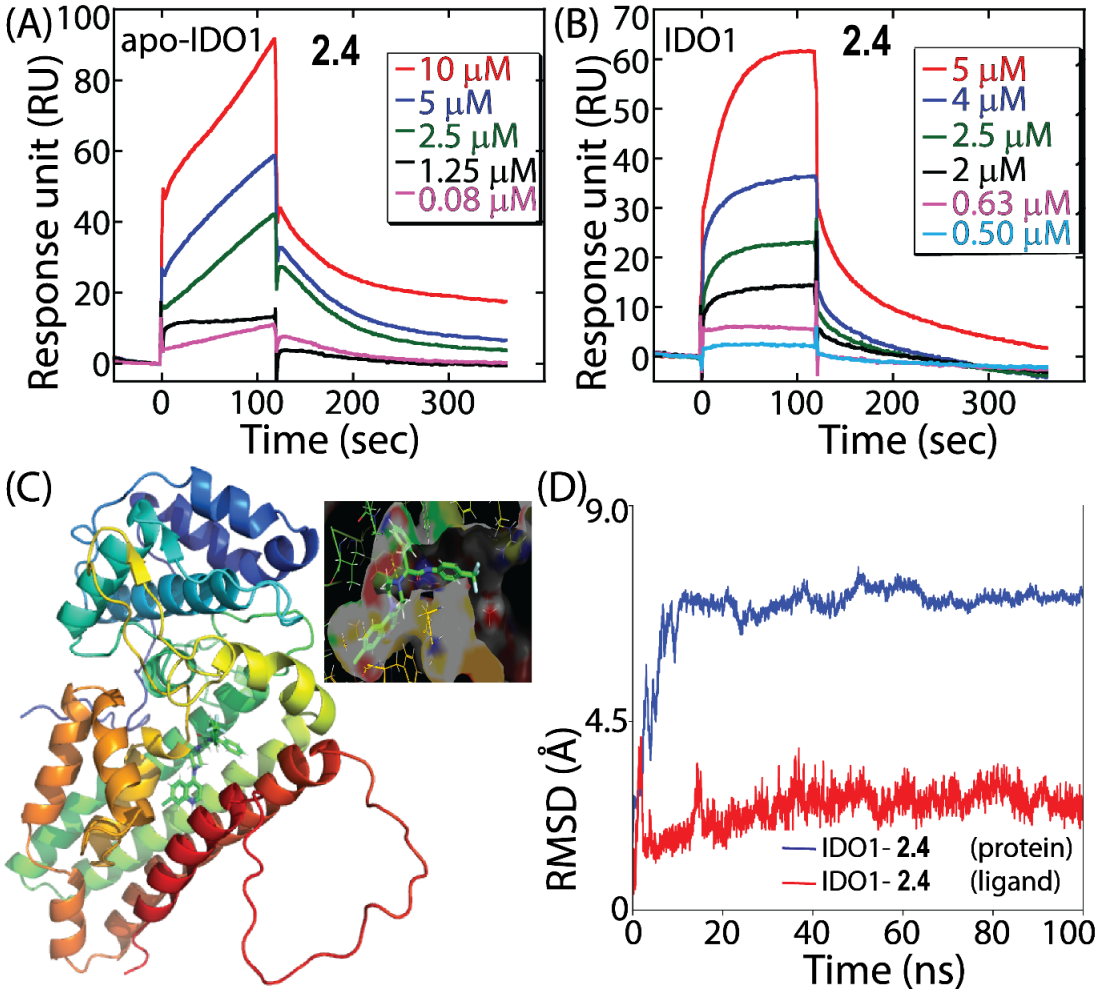

Fig. 2.8. Real-time concentration-dependent binding measurements of the compound, **2.4** with IDO1 enzyme (A) and apo-IDO1 protein by SPR analyses (B). Probable mode of interaction of **2.4** with the apo-IDO1 (PDB ID: 6MQ6) (C). The root-mean-square deviations (RMSD) for protein (apo-IDO1 protein bound to **2.4**; blue) and ligand (**2.4** bound to apo-IDO1; red) (D).

2.2.6. Molecular docking and molecular dynamic simulation studies

Meanwhile, the molecular docking and molecular dynamic simulation studies showed that **2.4** strongly binds to the binding site of apo-IDO1 (PDB ID:6MQ6). The blind-docking results showed that the top pose of the ligand is in the binding site of the IDO1 (Fig. 2.8C). The hydrogen bonding and hydrophobic interactions of **2.4** with the side chain and backbone of apo-IDO1 could be the driving force for such strong interactions. The molecular dynamic results show that the protein reached a stable state with a value of RMSD of 7.2 Å. In comparison, the RMSD of the ligand indicates that **2.4** attained a stable condition with a value of RMSD 4.0 Å (Fig. 2.8D). The RMSF

of the protein shows that the zone with less stability is close to the C-terminal (Fig. 2.9A). The protein-ligand interactions profile of the molecular dynamics diagram generated between apo-IDO1 and **2.4** revealed that the Y114, A198, F202, I205, F214, and F258 residues could be involved in hydrophobic interaction with the protein. Whereas, the H334 could be involved in hydrogen bonding or electrostatic interaction with **2.4** (Fig. 2.9B).

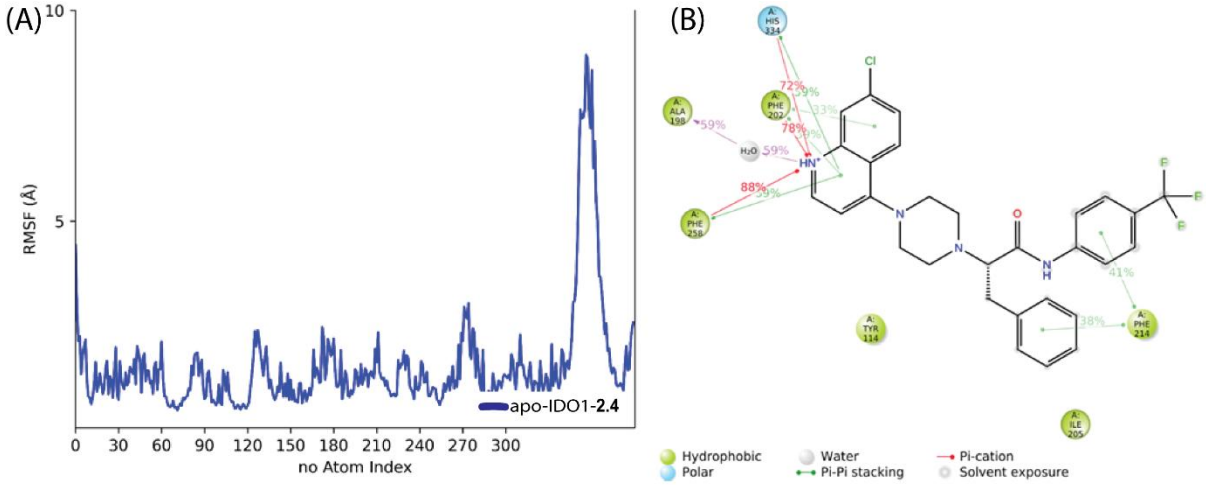

Fig. 2.9. The root-mean-square fluctuation (RMSF) was obtained for apo-IDO1 bound to **2.4** (blue). Two-dimensional protein-ligand interactions of the molecular dynamics diagram generated between apo-IDO1 and **2.4**.

2.2.7. IDO1 activity under cellular environment

The MTT studies were performed to check the toxicity of the compound in HeLa as well as normal cells and found almost negligible toxicity (Fig.2.10).

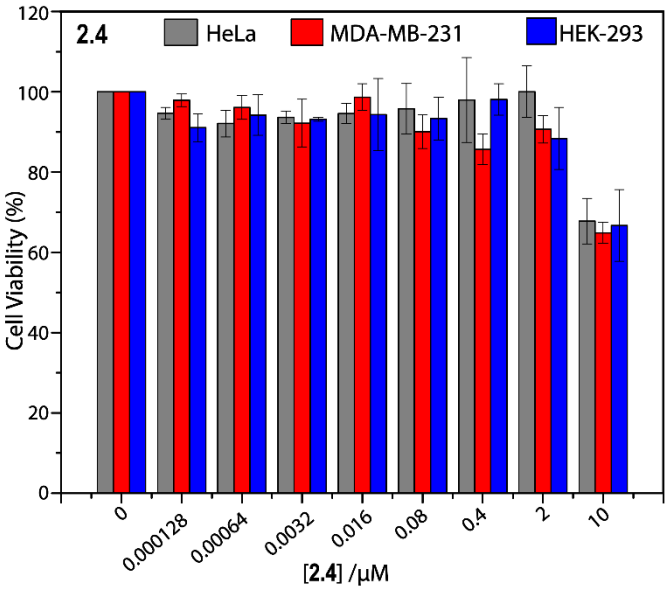

Fig. 2.10. Effect of the potent compound, **2.4,** on the viability of HeLa, MDA-MB-231, HEK-293 cells. The cells were treated with the indicated concentrations of the compounds for 48 h. The MTT assay determined cell viability. Three independent experiments averaged cell viability (%) with standard deviation (error bars).

Finally, the IDO1 inhibitory activity of **2.4** was carried out under a cellular environment in the presence of interferon-gamma (IFN-γ) and external hemin to explore its further applicability (Fig. 2.11). The native IDO1 enzyme is known to be induced from its mRNA by IFN-γ in cancer cells. Hence, HeLa cells were treated with IFN-γ to evaluate the inhibitory activity of **2.4** against cellular IDO1. The EC_{50} value for **2.4** was 326 ± 69 pM in HeLa cells (Fig. 2.11A). However, the dissimilarity of the IDO1 inhibitory activity against purified IDO1 enzyme and cellular IDO1 enzyme could be due to the difficulties in controlling the redox activity of the enzyme under experimental conditions. The cellular environment or the presence of apo-IDO1 could also impact the activity assay. Meanwhile, the treatment of **2.4** equilibrated with heme (1:5; molar ratio) showed a significant decline in cellular IDO1 activity (Fig. 2.11B). Such lower IDO1 activity could be due to the complexation of **2.4** with free heme, significantly affecting the heme binding to the inactive apo-IDO1 protein under the cellular environment. A similar finding was also observed for quinine-based apo-IDO1 inhibitors.[7] Overall, **2.4** showed negligible cytotoxicity and higher selectivity for IDO1 enzyme inhibition, and the IDO1 inhibitory activity of **2.4** could be due to its direct binding to apo-IDO1 protein and formation of **2.4**-heme complex (Fig. 2.11C).

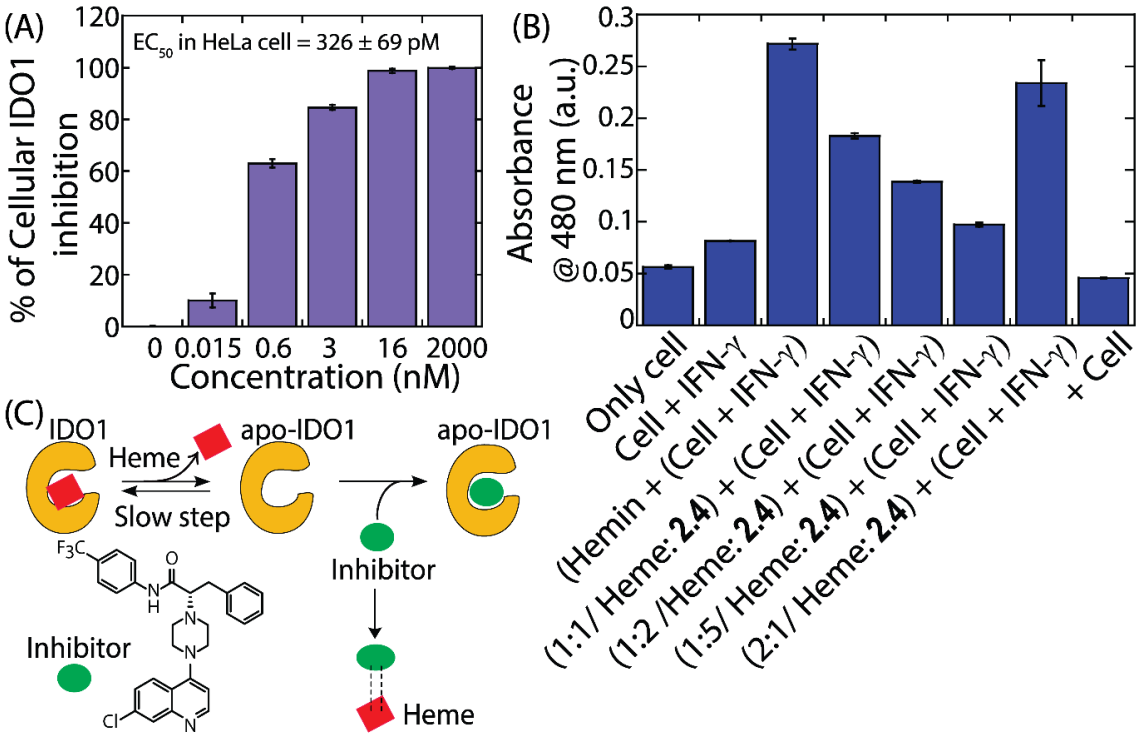

Fig. 2.11. Concentration-dependent cellular IDO1 activity of **2.4** (A). IDO1 activities in the absence and presence of **2.4** and extracellular heme in IFN-γ treated HeLa cells (B). Activities were calculated by HPLC-based kynurenine assay. The schematic diagram depicts the dual mode of action of the **2.4** (C).

Additional theoritical calculations-based on Swiss ADME server revealed the probable advantages and the applicability of **2.4** for future experimental investigations (Fig. 2.12).

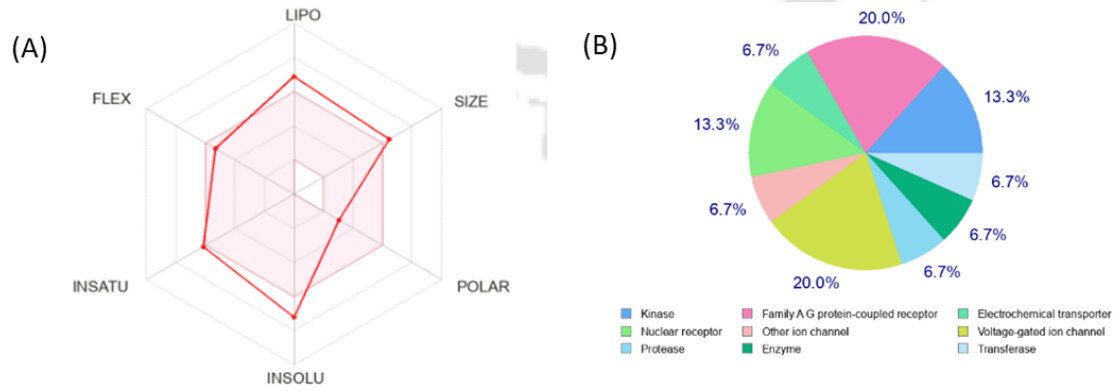

Fig. 2.12. Swiss ADME, pharmacokinetic and drug-likeness properties of **2.4** (A) and Swiss target prediction for **2.4** (B).

Earlier reports demonstrated that the IC_{50} value of linrodostat is 500 pM in HeLa cell lines. The potent DCQ-derivative also exhibited a similar IC_{50} value of 326 pM in HeLa cell lines, indicating its better/comparable efficacy to linrodostat.[19] However, the IC_{50} value of both cannot be compared under similar experimental conditions due to synthetic complexity and the commercial unavailability of linrodostat. It is also demonstrated that linrodostat exerts its inhibitory effect on apo-IDO1 by competing with heme for binding, thereby causing inhibition. In contrast, the potent DCQ-derivatives not only bind to apo-IDO1 but also interact with free heme, effectively preventing any potential reassociation of heme and apo-IDO1. This 'one stone, two bird approach' gives DCQ derivatives a comprehensive advantage for inhibiting the heme-apo-IDO1 rebinding, causing efficient IDO1 inhibition. Hence this strategy might inspire the development of the next generation of IDO1 inhibitors where both apo-enzymes and the cofactors could be targeted by a single potent compound leading to superior results in immunotherapy and other related research areas.

2.3. Summary

In summary, we synthesized DCQ derivatives that showed selective inhibitory activity against purified and cellular IDO1 enzymes. A systematic biophysical analysis revealed that the potent DCQ derivate promotes the release of heme-cofactor from holo-IDO1 to generate apo-IDO1 and strongly bind to the apo-IDO1. The potent compound also binds to free heme-cofactor, minimizes the rebinding efficacy of heme-cofactor to the apo-IDO1, and reduces the catalytic activity of holo-IDO1. The synthesis of potent DCQ derivatives is much simpler and more scalable. Hence, this strategy of designing small molecules-based IDO1 inhibitors that target both apo-IDO1 and free heme-cofactor could provide a peerless advantage over the classical IDO1 inhibitors.

2.4. Experimental section

2.4.1. Synthesis of the compounds

2.4.1.1. Synthesis of compounds A1(a-e)

Sodium nitrite (1.2 equiv.) solution in water (at 0 °C) was added dropwise to a stirring solution of the respective amino acid (1 equiv.) in 48% HBr (3 mL) and water (10 mL). The reaction mixture was then allowed to warm up to room temperature and stirred for 2 hours. The maximum consumption of the starting material in the reaction mixture was then extracted with CH_2Cl_2 (3 × 20 mL), the combined organic layers were dried over anhydrous Na_2SO_4, and the solvent was evaporated under reduced pressure. The crude product was sufficiently pure for the next step (yield: 89.6%).

2.4.1.2. Synthesis of compounds A2(a-e)

To a stirring solution of **A1(a-e)** (1 equiv.) in CH_2Cl_2 (10 mL) oxalyl chloride (4 equiv.) was added under the N_2 atmosphere at 0 °C. DMF (2 drops) was added to the reaction mixture, brought to room temperature, and stirred for 2 hours. After that, unreacted oxalyl chloride was removed under reduced pressure. The residual was then added to a stirring reaction mixture of 4-(trifluoromethyl) aniline (1.5 equiv.) and DMAP (3 equiv.) under an N_2 atmosphere at 0 °C. Then the reaction mixture was warmed to room temperature and stirred for another 2 hours. The reaction mixture was extracted with CH_2Cl_2 (3 × 20 mL). The combined organic layers were washed with water (2 × 20 mL) and dried over anhydrous Na_2SO_4. The solvents were removed under reduced pressure. The reaction mixture was purified through column chromatography using a gradient solvent system of ethyl acetate in hexane (0 – 10%) to obtain the pure product as a crystalline solid (yield: 76%).

2.4.1.3. Synthesis of compound A2f

To a stirring solution of **A1a** (1 equiv.) in CH_2Cl_2 (10 mL), oxalyl chloride (4 equiv.) was added under an N_2 atmosphere at 0 °C. DMF (2 drops) was added to the reaction mixture, and bought to room temperature and stirred for 2 hours. After 2 hours, excess oxalyl chloride was then evaporated under reduced pressure. The residual was then added to a stirring reaction mixture of 4-fluoroaniline (1.5 equiv.) and DMAP (3 equiv.) under an N_2 atmosphere at 0 °C, and then the reaction mixture was warmed up to room temperature and stirred for additional 2 hours. Then the reaction mixture was extracted with CH_2Cl_2 (3 × 20 mL). The combined organic layers were washed with water (2 × 20 mL) and dried over anhydrous Na_2SO_4. The solvents were removed under reduced pressure. The reaction mixture was purified through column chromatography using a gradient solvent system of ethyl acetate in hexane (0 – 10%) to get the pure product as a crystalline solid (yield: 74%).

2.4.1.4. Synthesis of 7-chloro-4-(piperazin-1-yl) quinoline

4,7-Dichloroquinoline (0.5g, 1 equiv, 2.5 mmol) was added to piperazine (0.21 g, 1 equiv., 2.5 mmol) triethylamine (5 mL) and the reaction mixture was stirred under reflux condition at 110 °C for 18 hours. The reaction mixture was then extracted with ethyl acetate (3 × 20 mL) and was dried over anhydrous Na_2SO_4. The solvents were evaporated under reduced pressure. The reaction mixture was purified by column chromatography using a solvent gradient of methanol in CH_2Cl_2 (15-30%) to provide the pure product (yield: 54%, 0.27 g).

2.4.1.5. Synthesis of N^1-(6-chloronaphthalen-1-yl) cyclohexane-1,4-diamine

4,7-Dichloroquinoline (0.5 g, 1 equiv, 2.5 mmol) was added to 1,4-cyclohexanediamine (0.29 g, 1equiv., 2.5 mmol) in triethylamine (5 mL) and the reaction mixture was stirred under reflux condition at 110 °C for 18 hours. The reaction mixture was then extracted with ethyl acetate (3 × 20 mL) and was dried over anhydrous Na_2SO_4. The solvents were evaporated under reduced pressure. The reaction mixture was purified by column chromatography using a solvent gradient of methanol in CH_2Cl_2 (32-40%) to provide the pure product (yield: 49%, 0.24 g).

2.4.1.6. Synthesis of compounds 2.1 and 2.2

To a stirring solution of compound **A2b** or **A2f** (1equiv.) in acetonitrile were added N^1-(6-chloronaphthalen-1-yl) cyclohexane-1,4-diamine (1.5 equiv.) and potassium carbonate (1.5equiv.) under N_2 atmospheric pressure. The reaction mixture was stirred under reflux conditions for 24 hours at 75 °C. After 24 hours, the reaction mixture was extracted with ethyl acetate (3 × 20 mL) and was dried over anhydrous Na_2SO_4. Column chromatography was performed to purify the reaction mixture using a solvent gradient of ethyl acetate in hexane (25-46%) to obtain the respective pure compound.

2.4.1.7. Synthesis of compounds 2.3-2.7

To a stirring solution of compound **A2(a-e)** (1equiv.) in dry acetonitrile was added 7-chloro-4-(piperazin-1-yl)quinoline (1.5 equiv.) and potassium carbonate (1.5 equiv.) under N_2 atmospheric pressure. The reaction mixture was stirred under reflux conditions for 24 hours at 75 °C. After 24 hours, the reaction mixture was extracted with ethyl acetate (3 × 20 mL) and was dried over anhydrous Na_2SO_4. Column chromatography was performed to purify the reaction mixture using a solvent gradient of ethyl acetate in hexane (25-40%) to obtain respective pure compounds.

2.4.2. Characterization of 2.1-2.7 derivatives

2.4.2.1. Characterization of (S)-2-((4-((7-chloroquinolin-4-yl)amino)cyclohexyl)amino)-N-(4-fluorophenyl)-3-phenylpropanamide (2.1)

Following the general procedure as mentioned in section **2.4.1.6.**, the reaction of (*R)*-2-bromo-*N*-(4-fluorophenyl)-3-phenylpropanamide (0.06 g, 0.16 mmol) with N^1-(6-chloronaphthalen-1-yl) cyclohexane-1,4-diamine (0.7 g, 0.25 mmol) to give **2.1** as 63% yield. The product was scrutinized by ^{1}H NMR, ^{13}C NMR, and HRMS analyses. ^{1}H NMR (600 MHz, $CDCl_3$): δ_{ppm} 9.48 (s, 1H), 8.38 (s, 1H), 7.91 (s, 1H), 7.78 (s, 1H), 7.60 - 7.58 (m, 2H), 7.40 - 7.37 (m, 2H), 7.34 - 7.31 (m, 2H), 7.28 -7.27 (m, 2H), 7.08 (t, J = 8.5 Hz, 2H), 6.34 (d, J = 5.6 Hz, 1H), 3.55 – 3.53 (m, 1H), 3.38 – 3.35 (m, 1H), 2.80 – 2.76 (m,

1H), 2.41 – 2.37 (m, 1H), 2.20 -2.13 (m, 1H), 2.00-1.98 (m, 1H), 1.84-1.82 (m, 1H), 1.31 -1.23 (m, 8H). ^{13}C NMR (150 MHz, $CDCl_3$): δ_{ppm} 172.4, 160.1, 158.5, 137.2, 133.7, 133.7, 129.1, 129.0, 127.2, 125.7, 121.0, 120.9, 115.8, 115.7, 98.9, 62.4, 56.0, 51.6, 39.6, 32.7, 31.5, 31.0, 30.9, 29.7, 22.7, 22.7, 14.1. **HRMS (ESI)** calcd. for $C_{30}H_{30}ClFN_4O$ $(M+H)^+$: 517.2165, found: 517.2177.

2.4.2.2. Characterization of (S)-2-((4-((7-chloroquinolin-4-yl)amino)cyclohexyl)amino)-3-methyl-*N*-(4-(trifluoromethyl)phenyl)butanamide (2.2)

Following the general procedure as mentioned in section **2.4.1.6.**, the reaction of (R)-2-bromo-3-methyl-*N*-(4-(trifluoromethyl)phenyl)butanamide (0.1 g, 0.3 mmol) with N^1-(6-chloronaphthalen-1-yl) cyclohexane-1,4-diamine (0.12 g, 0.46 mmol) to give **2.2** as 61% yield. The product was scrutinized by ^{1}H NMR, ^{13}C NMR, and HRMS analyses. ^{1}H NMR (600 MHz, $CDCl_3$): δ_{ppm} 9.76 (s, 1H), 8.45 (d, J = 5.4 Hz, 1H), 7.94 (s, 1H), 7.86 – 7.67 (m, 3H), 7.62-7.61 (m, 2H), 7.39 – 7.30 (m, 1H), 6.40-6.39 (m, 1H), 3.62 – 3.39 (m, 1H), 3.17-3.16 (m, 1H), 2.54-2.50 (m, 1H), 2.34 – 2.21 (m, 3H), 2.06-2.04 (m, 1H), 1.49 – 1.32 (m, 4H), 1.29-1.27 (m, 4H),1.1-1.08 (m, 3H), 0.96-0.95 (m, 3H).^{13}C NMR (150 MHz, $CDCl_3$): δ_{ppm} 173.2, 150.6, 149.3, 140.6, 135.5, 127.6, 126.4, 126.3, 126.0, 125.8, 125.5, 125.0, 123.2, 121.5, 118.9, 116.8, 99.1, 66.9, 56.9, 51.5, 32.8, 32.1, 31.6, 31.2, 29.7, 19.8, 17.5. **HRMS (ESI)** calcd. for $C_{27}H_{30}ClF_3N_4O$ $(M+H)^+$: 519.2133, found: 519.2143.

2.4.2.3. Characterization of (S)-2-(4-(7-chloroquinolin-4-yl)piperazin-1-yl)-3-methyl-*N*-(4(trifluoromethyl)phenyl)butanamide (2.3)

Following the general procedure as mentioned in section **2.4.1.7.**, (R)-2-bromo-3-methyl-*N*-(4-(trifluoromethyl)phenyl)butanamide (0.2 g, 0.6 mmol) was reacted with 7-chloro-4-(piperazin-1-yl)quinoline (0.2 g, 0.9 mmol) to give **2.3** as 59% yield. ^{1}H NMR (600 MHz, $CDCl_3$): δ_{ppm} 8.84 – 8.61 (m, 2H), 8.06 (s, 1H), 7.95-7.93 (m, 1H), 7.74-7.73 (m, 2H), 7.61-7.59 (m, 2H), 7.44-7.42 (m, 1H), 6.86 (d, J = 4.9 Hz, 1H), 3.30- 3.29 (m, 4H), 2.95-2.91 (m, 4H), 2.34 (dd, J = 13.0, 6.6 Hz, 1H), 1.28-1.26 (m, 1H), 1.14-1.13 (m, 3H), 1.03-1.02 (m, 3H). ^{13}C NMR (150 MHz, $CDCl_3$): δ_{ppm} 169.7, 156.7, 151.8, 150.0, 140.5, 135.1, 128.8, 126.4, 126.4, 126.3, 125.1, 121.8, 119.3, 112.9, 109.0, 75.8, 52.5, 50.6, 26.9, 20.2, 17.6. **HRMS (ESI)** calcd. for $C_{25}H_{26}ClF_3N_4O$ $(M+H)^+$: 491.1820, found: 491.1830.

2.4.2.4. Characterization of (S)-2-(4-(7-chloroquinolin-4-yl)piperazin-1yl)-3-phenyl-*N*-(4-(trifluoromethyl)phenyl)propanamide (2.4)

Following the general procedure as mentioned in section **2.4.1.7.**, (R)-2-bromo-3-phenyl-*N*-(4-(trifluoromethyl)phenyl)propanamide (0.2 g, 0.5 mmol) was reacted with 7-chloro-4-(piperazin-1-yl)quinoline (0.199 g, 0.8 mmol) to give **2.4** as 63% yield. The product was scrutinized by ^{1}H NMR, ^{13}C NMR, and HRMS analyses. ^{1}H NMR (600 MHz, $CDCl_3$): δ_{ppm} δ 9.17 (s, 1H), 8.76-8.75 (m, 1H), 8.08 (s, 1H), 7.92-7.91 (m, 1H), 7.67-7.66 (m, 2H), 7.60-7.59 (m, 2H), 7.47-7.46 (m, 1H), 7.40 – 7.36 (m, 4H), 7.29-7.28 (m, 1H), 6.89-6.88 (m, 1H), 3.70-3.68 (m, 1H), 3.47-3.44 (m, 1H), 3.32-3.28 (m, 4H), 3.13-3.10 (m, 1H), 3.00-2.97 (m, 4H). ^{13}C NMR (150 MHz, $CDCl_3$): δ_{ppm} 170.3, 156.5, 151.9, 150.1, 140.6, 139.1, 135.2, 129.2, 128.9, 128.7, 126.6, 126.5, 126.4, 126.3, 125.0, 121.8, 119.0, 109.1, 71.2, 52.7, 32.5. **HRMS (ESI)** calcd. for $C_{29}H_{26}ClF_3N_4O$ $(M+H)^+$: 539.1820, found: 539.1832.

2.4.2.5. Characterization of (S)-2-(4-(7-chloroquinolin-4-yl)piperazin-1-yl)-N-(4-(trifluoromethyl)phenyl)propanamide (2.5)

Following the general procedure as mentioned in section **2.4.1.7.**, (R)-2-bromo-*N*-(4-(trifluoromethyl)phenyl)propenamide (0.1 g, 0.33 mmol) was reacted with 7-chloro-4-(piperazin-1-yl)quinoline (0.2 g, 0.9 mmol) to give **2.5** as 57% yield. The product was scrutinized by ^{1}H NMR, ^{13}C NMR, and HRMS analyses. ^{1}H NMR (600 MHz, $CDCl_3$): δ_{ppm} 9.42 (s, 1H), 8.78-7.74 (m, 1H), 8.09-8.07 (m, 1H), 7.97-7.94 (m, 1H), 7.74 – 7.72 (m, 2H), 7.62 -7.61 (m, 2H), 7.48-7.46 (m, 1H), 6.91 (d, J = 5.0 Hz, 1H), 3.43-3,33 (m, 4H), 3.12 – 3.07 (m, 1H), 2.99 – 2.89 (m, 4H), 1.46 (d, J = 7.1 Hz, 3H). ^{13}C NMR (150 MHz, $CDCl_3$): δ_{ppm} 171.8, 156.5, 151.9, 150.2, 140.7, 135.2, 129.0, 126.5, 126.4, 124.9, 121.8, 118.9, 109.1, 64.6, 57.6, 52.6, 29.7, 11.2. **HRMS (ESI)** calcd. for $C_{23}H_{22}ClF_3N_4O$ $(M+H)^+$: 463.1507, found: 463.1515.

2.4.2.6. Characterization of (S)-2-(4-(7-chloroquinolin-4-yl)piperazin-1-yl)-4-methyl-N-(4-(trifluoromethyl)phenyl)pentanamide (2.6)

Following the general procedure as mentioned in section **2.4.1.7.**, (R)-2-bromo-4-methyl-*N*-(4-(trifluoromethyl)phenyl)pentanamide (0.1 g, 0.33 mmol) was reacted with 7-chloro-4-(piperazin-1-yl)quinoline (0.2 g, 0.9 mmol) to give **2.6** as 57% yield. The product was scrutinized by ^{1}H NMR, ^{13}C NMR, and HRMS analyses. ^{1}H NMR (500 MHz, $CDCl_3$): δ_{ppm} 8.67-8.64 (m, 2H), 7.99-7.98 (m, 1H), 7.87-7.84 (m, 1H), 7.65-7.63 (m, 2H), 7.53-7.50 (m, 2H), 7.37-7.34 (m, 1H), 6.78 (dd, J = 5.0, 2.5 Hz, 1H), 3.30-3.23 (m, 4H), 2.96 (d, J = 5.1 Hz, 1H), 2.88 – 2.79 (m, 4H), 2.02 – 1.94 (m, 1H), 1.63 – 1.56 (m, 1H), 1.32 – 1.24 (m, 1H), 0.99 – 0.89 (m, 6H). ^{13}C NMR (100 MHz, $CDCl_3$): δ_{ppm} 169.8, 156.6, 151.9, 150.1, 140.4, 135.1, 128.9, 126.4, 126.4, 125.0, 121.8, 119.2, 119.2, 109.0, 75.6, 52.5,

34.0, 29.7, 27.0, 24.3, 16.4, 12.2. **HRMS (ESI)** calcd. for $C_{26}H_{28}ClF_3N_4O$ $(M+H)^+$: 505.1977, found: 505.1988.

2.4.2.7. characterization of (2S)-2-(4-(7-chloroquinolin-4-yl)piperazin-1-yl)-3-methyl-N-(4-(trifluoromethyl)phenyl)pentanamide (2.7)

Following the general procedure as mentioned in section **2.4.1.7.** the reaction of (R)-2-bromo-3-methyl-*N*-(4-(trifluoromethyl)phenyl)pentanamide (0.1g, 0.33 mmol) with 7-chloro-4-(piperazin-1-yl)quinoline (0.2 g, 0.9 mmol) to give **2.7** as 57% yield. The product was scrutinized by ^{1}H NMR, ^{13}C NMR, and HRMS analyses. ^{1}H NMR (400 MHz, $CDCl_3$): δ_{ppm} ^{1}H NMR (500 MHz, $CDCl_3$) δ 8.67-8.65 (m, 2H), 8.00-7.98 (m, 1H), 7.86-7.84 (m, 1H), 7.64-7.63 (m, 2H), 7.52-7.50 (m, 2H), 7.36 – 7.33 (m, 1H), 6.78 – 6.77 (m, 1H), 3.23-3.21 (m, 4H), 2.87-2.80 (m, 4H), 1.99 – 1.95 (m, 1H), 1.61 – 1.57 (m, 1H), 1.31 – 1.28 (m, 2H), 1.23-1.18 (m, 3H), 0.94-0.92 (m, 3H)..^{13}C NMR (100 MHz, $CDCl_3$): δ_{ppm} ^{13}C NMR (101 MHz, $CDCl_3$) δ 169.8, 156.7, 151.7, 149.91, 140.4, 135.2, 128.8, 126.5, 126.4, 126.4, 125.1, 121.7, 119.2, 119.2, 108.9, 74.0, 52.5, 50.8, 33.7, 27.0, 14.7, 12.1. **HRMS (ESI)** calcd. for $C_{26}H_{28}ClF_3N_4O$ $(M+H)^+$: 505.1977, found: 505.1985.

2.4.3. Purification of holo-human indoleamine 2,3-dioxygenase 1 and holo-tryptophan 2,3- dioxygenase (TDO) enzymes

Human indoleamine 2,3-dioxygenase 1 (IDO1) and tryptophan 2,3-dioxygenase (TDO) enzymes were purified according to the reported protocols.[7-10, 12, 19, 21, 22] Recombinant human IDO1 and TDO enzymes (with *N*-terminus 6×histidine-tag) were expressed by transforming the cDNAs of human IDO1 and TDO into *Escherichia coli* (BL21-DE3 strain) cells. A single colony of *Escherichia coli* cells was inoculated in 5 mL of Luria-Bertani (LB) medium (containing 50 μg/mL kanamycin), and the cells were grown for 12-14 hours at 37 °C and 180 rpm. The overnight culture (1 mL) was added into 1 L of the same culture media containing antibiotics and incubated at 37 °C and 120 rpm to achieve an OD_{600} of 0.6 of the culture media. Hemin (10 μM) and L-tryptophan (1 mM) were added to the culture medium and incubated at 37 °C for an additional 20–30 min until the OD_{600} reached 0.9–1.0. After cooling the medium, isopropyl β-D-1 thiogalactopyranoside (IPTG, 0.5 mM) was used to promote protein expression. The induced cells were grown for additional 16-18 hours at 22 °C and 120 rpm. The cell pellet was collected by centrifugation and re-suspended in ice-cold phosphate-buffered saline (PBS; 20 mL), centrifuged again to remove hemin (15000 rpm for 10 minutes at 4 °C), and kept at −80 °C.

For enzyme purification, the stored pellet was re-suspended in 15 mL of ice-cold 50 mM potassium phosphate buffer (KPB) at pH 7.2 containing 300 mM potassium chloride (KCl), 10 mM magnesium chloride ($MgCl_2$), 25 mM imidazole, 5% glycerol, protease inhibitors (complete EDTA free), and DNase (<1 mg). Then, the cells were disrupted on ice, and the cell lysate was centrifuged at 20,000 rpm for 30 minutes at 4 °C. The reddish supernatant was then filtered via a 0.22 µm filter. Nickel-nitrilotriacetic acid resin (Qiagen, 1 mL) was added to the reddish supernatant and incubated for 2 hours at 4 °C and 80 rpm. After pouring the liquid into the column, it was equilibrated with 50 mM KPB containing 300 mM KCl, 25 mM imidazole, and 5% glycerol at pH 7.2. The column was progressively washed with 10 mL of KPB at pH 7.2 containing 300 mM KCl, 60 mM imidazole, and 5% glycerol to remove the non-specifically bound protein. The protein was eluted using 50 mM KPB at pH 7.2, 300 mM KCl, 190 mM imidazole, and 5% glycerol. Sephadex-G25 column was used to exchange the IDO1 and TDO proteins' eluted buffer with 50 mM KPB at pH 6.8 with 150 mM KCl and 10% glycerol. The purity of the enzymes was assessed by Coomassie blue-stained SDS-PAGE screening method. Additionally, IDO1 and TDO enzyme purity was measured by the absorbance ratio at 404 nm/280 nm, which was found to be 1.4 and 1.1, respectively.

2.4.4. Expression and purification of apo-indoleamine 2,3-dioxygenase 1 enzyme

Following the same protocol, human apo-IDO1 was expressed and purified. During protein expression, hemin was not added to the medium externally. After nickel-nitrilotriacetic acid resin-based purification, the protein was dialyzed against a buffer containing 25 mM HEPES, 250 mM NaCl, and 100 M tris(2-carboxyethyl)phosphine (TCEP) at pH 7.2. The enzyme was dialyzed and then left to react with 150 mM sodium 2-mercaptoethanesulfonate (MESNA) at room temperature for 6 hours to release the heme cofactor. The apo-IDO1 was then buffer exchanged with 50 mM potassium phosphate buffer at pH 6.8 containing 150 mM KCl and 10% glycerol using a Sephadex-G25 column after being dialyzed in 25 mM HEPES, 250 mM NaCl at pH 7.2. The purified apo-IDO1 enzyme's absorbance ratio at 404 nm/280 nm was used to analyze its heme concentration (around 0.05).

2.4.5. Indoleamine 2,3-dioxygenase 1 and tryptophan 2,3-dioxygenase inhibition assay by the spectrometric method

Following the described methods, the IDO1 and TDO enzyme inhibitory activities were investigated by spectrophotometric measurements. Compounds were initially solubilized in DMSO before diluting with buffer. It was determined that 1% DMSO was

the optimal quantity for the test technique. IDO1 and TDO enzymes were incubated with the drug at the prescribed time and temperature (0 to 60 minutes and 10 to 40 ℃, respectively) before the activity assay. After incubation, a standard reaction mixture consisting of potassium phosphate buffer (100 mM, pH 6.5), sodium ascorbate (20 mM), methylene blue (10 µM), bovine liver catalase (240 nM), and L-Trp (150 µM) was diluted (5×) to 500 µL and analyzed for enzyme inhibition. The inhibitor concentration was adjusted by serial dilution. The reaction mixture was then incubated at 37 ℃ for an hour. After adding trichloroacetic acid (100 µL of 30% (w/v)), we quenched the reaction and incubated the mixture for another 15 minutes at 65 °C. Further addition of paradimethylaminobenzaldehyde (pDMAB; 2% (w/v) in acetic acid) and measurement of the absorbance at 480 nm with a UV-Vis spectrophotometer, we were able to determine the extent of kynurenine production was quantified. In this spectrophotometric analysis of IDO1/TDO activity, the absorption spectra of UV-active DCQ derivatives (50 µM) exhibited no substantial interference.

2.4.6. Cell viability analysis

The viability of HeLa, MDA-MB-231, and HEK-293 cells in the presence and absence of compounds were investigated by using the MTT (3-(4,5-dimethylthiazol-2-yl)-2,5-diphenyltetrazolium bromide) assay. Ten thousand cells were plated in 1 mL of DMEM/F12 complete media at 37 °C with 5% CO_2 in a 96-well tissue culture plate. After 12 hours of culture, the cells were washed in PBS buffer. The compounds (0.1 nM to 50 µM) were then added to the incomplete medium and cultured for an additional 72 hours at 37 °C with 5% CO_2. After that, 100 µL of MTT dye (5 mg/mL in PBS) was added into the culture medium and incubated for an additional 4 hours. The MTT solution was drained, and the formazan crystals were dissolved in 100 µL cell culture grade DMSO. A FLoid® Cell Imaging Station spectrophotometer was used to measure absorbance at 570 and 600 nm. The absorbance of the formazan crystals was used to determine the viability of cells.

2.4.7. Cellular indoleamine 2,3-dioxygenase 1 activity assay:

A. Spectrophotometric cellular IDO1 inhibition assay

The cellular enzyme activity assay was performed according to the reported procedure with minor modifications.[8-10, 17-19, 22] IDO1 mRNA was found in the HeLa cell line; hence, HeLa cells were considered for this assay. HeLa cells were first suspended in DMEM phenol-red free media (including 10% FBS) with 20,000 cells per well and incubated for 3–4 hours at 37 °C with 5% CO_2. Then, the selected compound or solely

heme or heme-incubated compound with different compound-to-heme ratios was incubated with the cells. After 1 h, 50 ng/mL IFN-γ (supplemented in DMEM phenol-red free medium (containing 10% FBS)) was added into the cells and incubated for another 2 hours. Trichloroacetic acid (5% for 0.5 h at 65 °C) was added to the cells to quench the reactions. After sonication, the precipitate was removed by centrifugation (Cells were not washed away before lysis.). The solution was used for further studies. By measuring the reaction mixture's absorbance at 480 nm, the amount of kynurenine production was measured using the pDMAB (2% (w/v)) in acetic acid.

B. HPLC-based cellular IDO1 inhibition assay

The cellular enzyme activity was measured according to the reported procedure.[18] Cells were grown in the presence and absence of compounds according to the method described in section 4.7 and left to grow for 20 hours. After that, clear media was taken for an HPLC analysis. Then 20 µL of the medium was injected through an Ascentis® express C18, 2.7 µm HPLC column. The mobile phase was 50% sodium citrate buffer (40 mM, pH 2.25) and 50% methanol (v/v) with 400 µM SDS and a 0.5 mL/min flow rate. The 365 nm and 280 nm lights were used as detectors.

2.4.8. UV-Vis spectroscopic measurement

To learn more regarding the potent compound's binding ability to the enzyme and the enzyme's heme lability, UV-visible spectroscopic analyses were conducted. EVOLUTION 201 spectrophotometer was used to record the absorbance spectra. All tests were carried out in the presence and absence of the selected compound at 37 °C with 100 mM KPB at pH 6.5 and purified hIDO1 or hTDO enzyme. $Na_2S_2O_6$ was injected into the solution after purging it with N_2 gas to create the deoxy-reaction system. Using the Soret peak, we determined the heme dissociation rate from the IDO1 enzyme (404 nm for IDO1).

2.4.9. Detection of labile heme by fluorescence assay

Protoporphyrin-IX (PpIX) fluorescence signal was utilized to quantify free heme in solution. The presence of heme was investigated by incubating 5 µM IDO1 in 100 mM KPB at pH 6.5 with 50 µM of inhibitor for varying amounts of time (from 0 to 60 minutes). Subsequently, PpIX (5 µM) was added, and the mixture was incubated at room temperature for 5 minutes. The free heme in the solution was measured by monitoring the PpIX fluorescence signal (λ_{ex} = 400 nm, λ_{em} = 615 nm).

2.4.10. Circular Dichroism analysis

The CD spectra of IDO1 and apo-IDO1 were acquired using a Jasco-810 spectropolarimeter. The IDO1 enzyme (200 nM) was incubated in 10 mM Tris buffer at pH 7.2 for one hour with or without the compound of interest (6.25 µM) at 37 °C. Spectra were collected at 17 °C using a 1 mm path length quartz cuvette after incubation with a scan rate of 100 nm/sec and a bandwidth of 1 nm from 195 nm to 250 nm. All final spectra were corrected for buffer background (10 mM Tris buffer at pH 7.2) CD signals. This instrument's built-in software was used to analyze the secondary structure of proteins. Afterward, the BeStSel program was used, and the spectra were examined to determine the secondary structures.

2.4.11. Binding analysis by surface plasmon resonance analysis

The interaction of the compound with apo-IDO1 and IDO1 protein was measured using surface plasmon resonance (SPR) analysis. The Biacore-X100 equipment with the CM5 sensor chip (GE Healthcare) was used for measurements, and the temperature was kept constant at 25 °C. The operating buffer was a phosphate-buffered saline (PBS) solution (pH 7.4) containing 1% DMSO. The surface of the CM5 sensor chip was modified with anti-His antibody using EDC-NHS coupling in both flow cells 1 and 2 (FC-1 and FC-2). The His-tagged IDO1 and apo-IDO1 protein was coated on the same surface in flow cell 2 (FC-2) only. The binding efficacy of **2.4** was then assessed by measuring the change in response unit in both the flow cell and taking the difference, i.e. (FC-2) – (FC-1). This was performed by the inbuilt kinetics/affinity experiment in Biacore X100 control software using a varying concentration of **2.4** i.e., from 0 to 10 µM with a flow rate of 30 µL/minute. The equilibrium dissociation constant (K_D) value of **2.4** to apo-IDO1 and IDO1 was measured using inbuilt Biacore Insight Evaluation software.

2.4.12. Heme binding affinity measurement by UV-Vis method

Heme-inhibitor affinity was determined using a spectrophotometric assay. The heme was dissolved in DMSO and diluted to 5 µM in a 20 mM HEPES buffer, pH 7.2 (containing 40% DMSO). Inhibitors were also dissolved in DMSO to make a stock solution. Inhibitors were then added to the hemin solution. We measured the shift in absorbance of the heme Soret peak at 401 nm as inhibitor concentrations varied from 0 to 175 µM.

2.4.13. PpIX fluorescence-based heme affinity measurement

PpIX fluorescence-based kinetics experiment was conducted to assess the amount of free heme in the solution. PpIX (5 µM) in 20 mM HEPES buffer, pH 7.2 was taken

where heme (1.5 µM) and heme-incubated inhibitor (30 µM) was added at 50 seconds to observe the fluorescence quenching by free heme with time (500 s time period). PpIX: λ_{ex} = 400 nm, λ_{em} = 615 nm.

2.4.14. Cellular apo-indoleamine 2,3-dioxygenase 1 activation assay

The activity of cellular apo-IDO1 was measured using the previously described protocol. However, different ratios of inhibitor and heme were incubated for 4 hours prior to the experiment.

2.4.15. Blind Docking calculations

The blind docking consensus of the IDO1 (PDB ID: 6MQ6) against the compound **2.4** was performed using AutoDock Vina and LeadFinder software.[7] The protein was processed with Maestro software using Protein Preparation Wizard and System Builder tools to obtain the protein in mol2 format. Also, AutoDockTools was used to obtain the protein in pdbqt format. Regarding the ligands, the tool of Maestro: LigPrep was used to obtain both ligands in mol2 format. AutoDockTools was used to obtain the ligands in pdbqt format. Blind Docking runs were performed with a grid box size of 30 $Å^3$ and its default parameters. All the runs of blind docking (BD) and the BD consensus were realized using metascreener (https://github.com/bio-hpc/metascreener).

2.4.16. Molecular Dynamics calculations

Molecular Dynamics simulations were carried out using Maestro-Desmond software (Desmond Molecular Dynamics System, D. E. Shaw Research, New York, NY, 2020. Maestro-Desmond Interoperability Tools, Schrödinger, New York, NY, 2020). The complexes created were immersed in a box filled with water using the simple point charge (SPC) scheme. The size of the box was 10 $Å^3$. Counter ions (1 Cl^-) were added to neutralize charges, and additional Na^+ and Cl^+ were added to obtain a final NaCl of 0.15 M. Energy minimization was carried out by 20000 using the steepest descent method with a threshold of 1.0 kcal/mol/Å. Periodic boundary conditions were used, and a cut off of 9 Å was established for van der Waals interactions. The Particle Mesh Ewald (PME) method with a tolerance of 10^{-9} was used in the electrostatic part. The NPT simulations were realized at 300 K with the Nose-Hoover algorithm, and the pressure was maintained at 1 bar with the Martyna-Tobias-Klein barostat. The force field OPLS3e was used in all runs.

2.4.17. Probable pharmacological properties of the potent compound:

Using the SwissADME server, the ADME parameters, pharmacokinetic characteristics, and drug-likeness of **2.4** were evaluated. The findings showed that the lipophilic nature and substantially decreased solubility of **2.4**, similar to BMS-986205,

might impair its oral bioavailability. However, an exciting result from the Swiss target prediction studies showed that **2.4** demonstrated about 20% glycoprotein target activity. These moderate to low levels of g-protein targets might enhance the absorption and retention of the therapeutic molecule within particular target locations. The hydrophobic properties of **2.4** might facilitate its interaction with these targets. Notably, the compound showed little off-target effects on other human enzymes, including protease enzymes. This suggests a high level of specificity for the desired targets, indicating that **2.4** would be a practical choice for further study.

Overall, based on the forecasts from the Swiss ADME server, the results point to possible advantages and the applicability of **2.4** for future experimental investigations.

2.4.18. NMR spectra of the compounds:

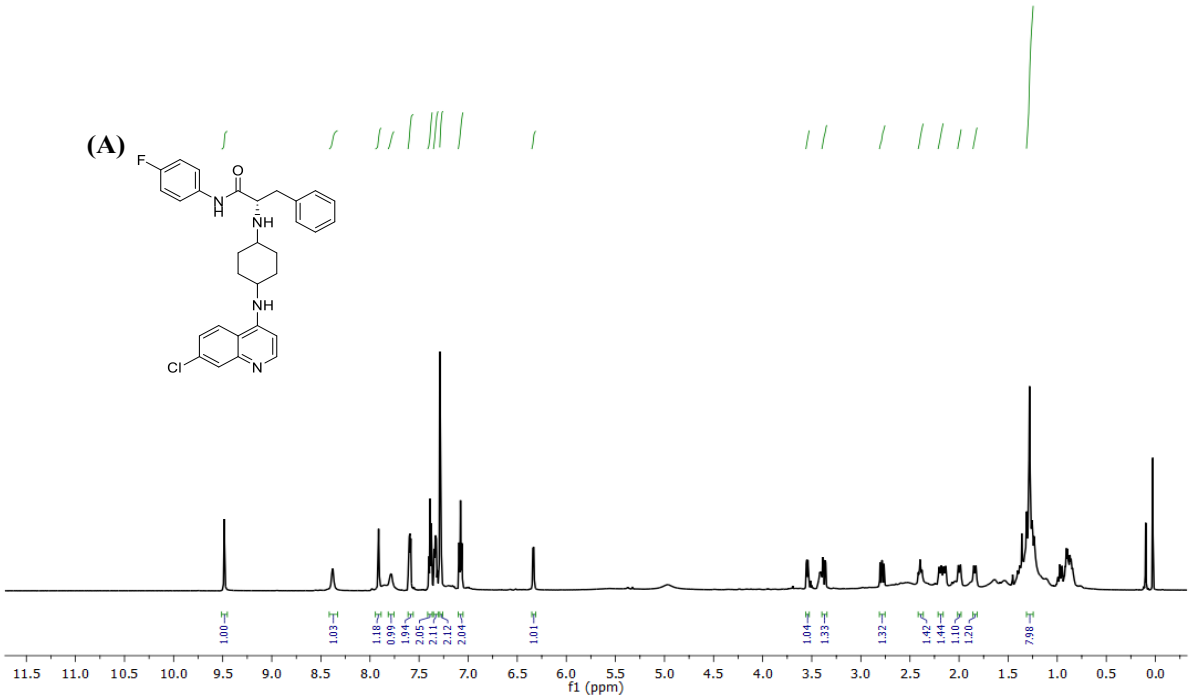

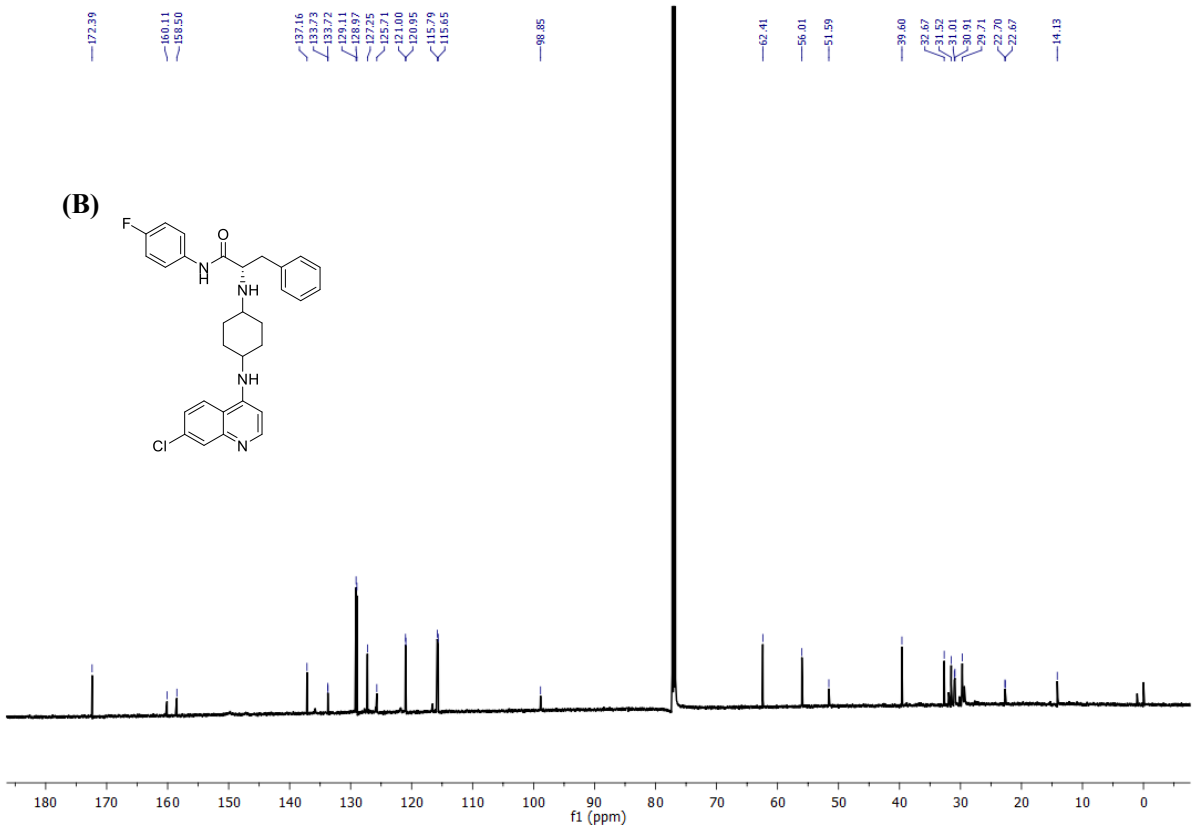

Fig. 2.14. ^{1}H NMR (A) and ^{13}C NMR (B) spectra of compound **2.1.**

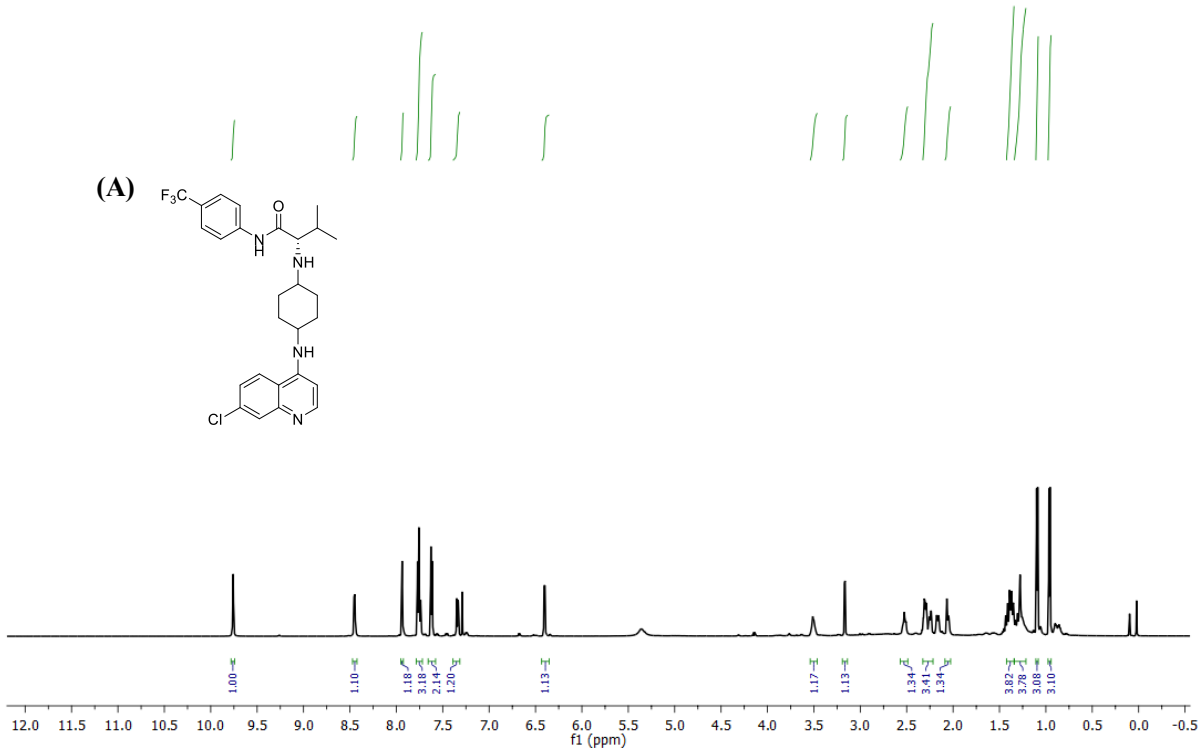

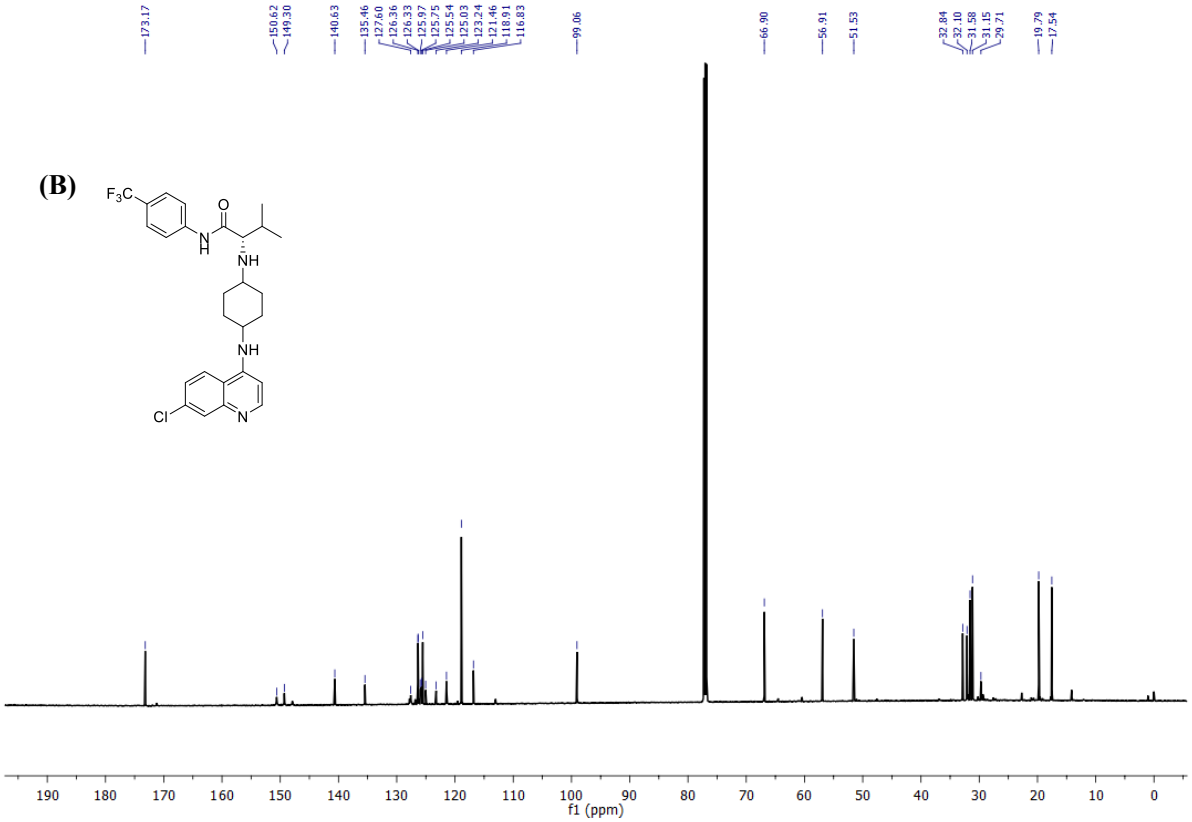

Fig. 2.15. ^{1}H NMR (A) and ^{13}C NMR (B) spectra of compound **2.2.**

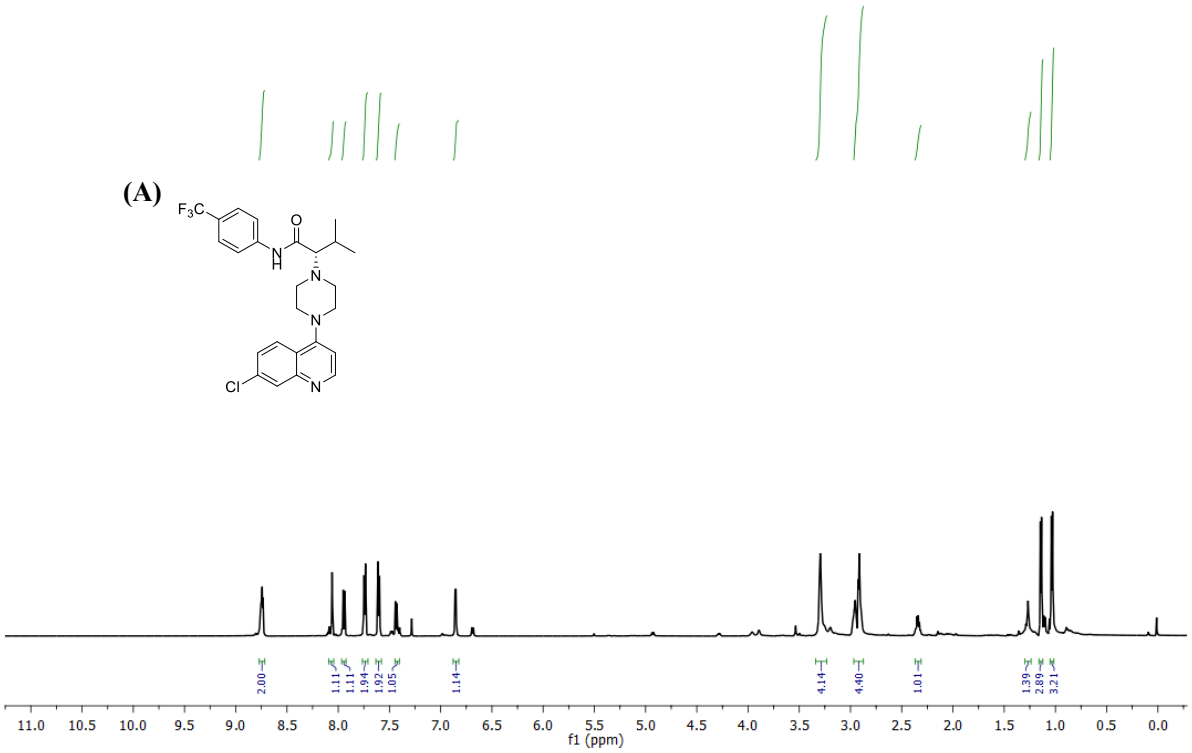

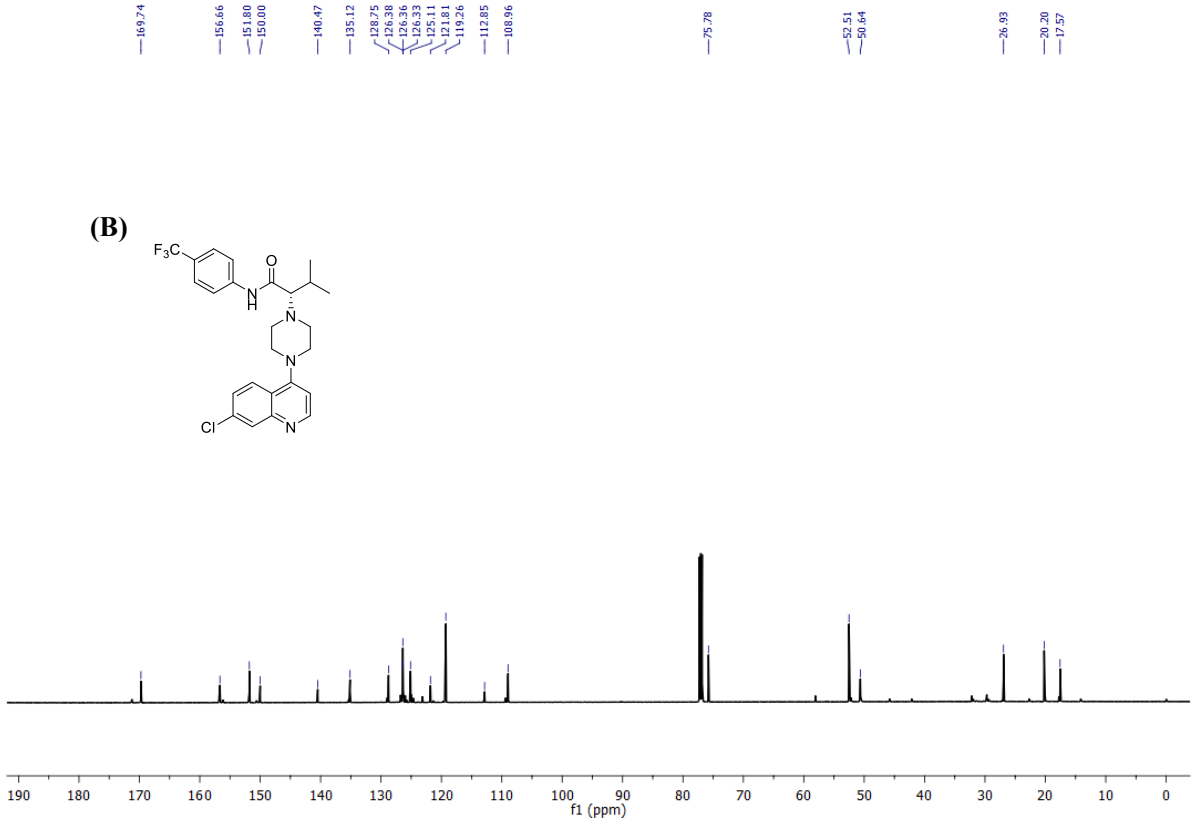

Fig. 2.16. ^{1}H NMR (A) and ^{13}C NMR (B) spectra of compound **2.3.**

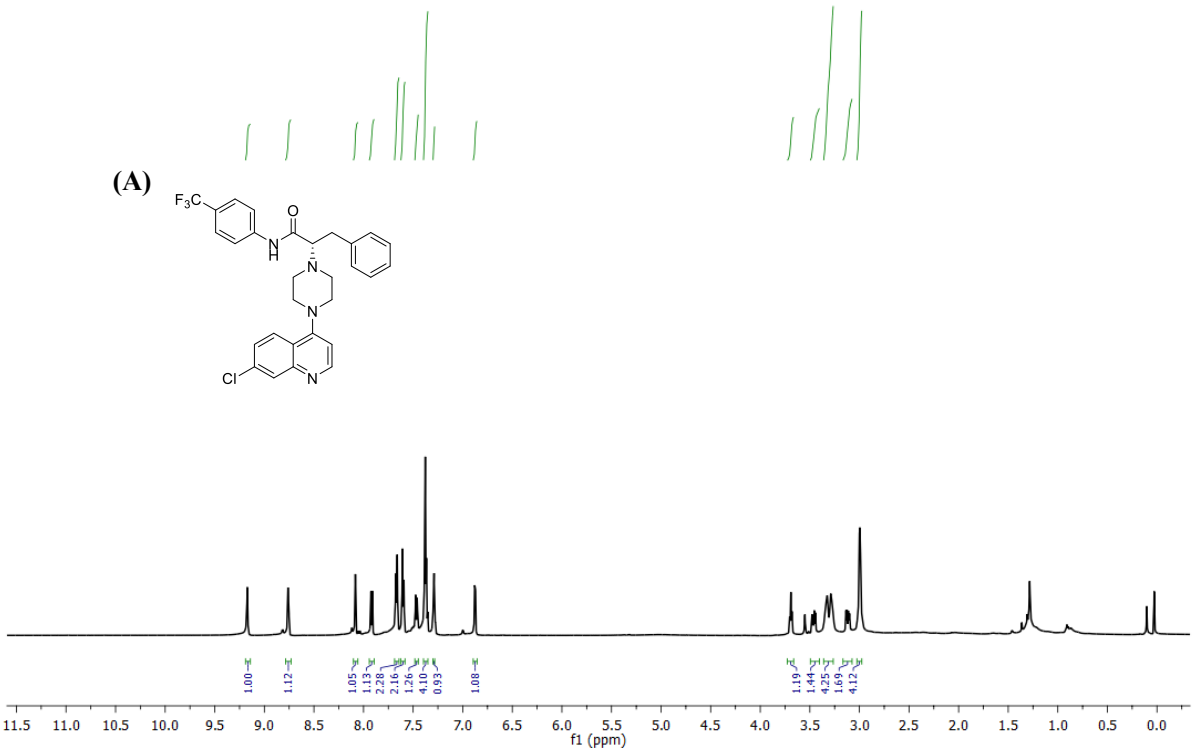

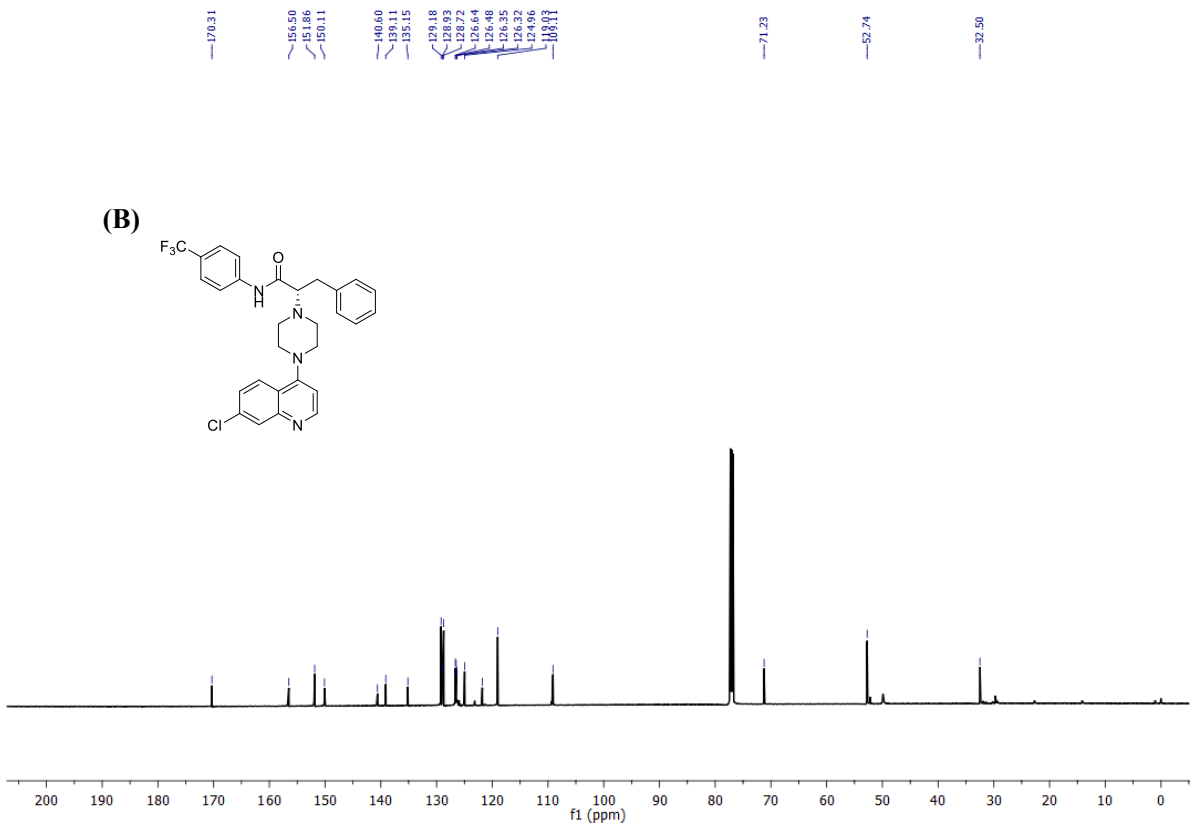

Fig. 2.17. ^{1}H NMR (A) and ^{13}C NMR (B) spectra of compound **2.4.**

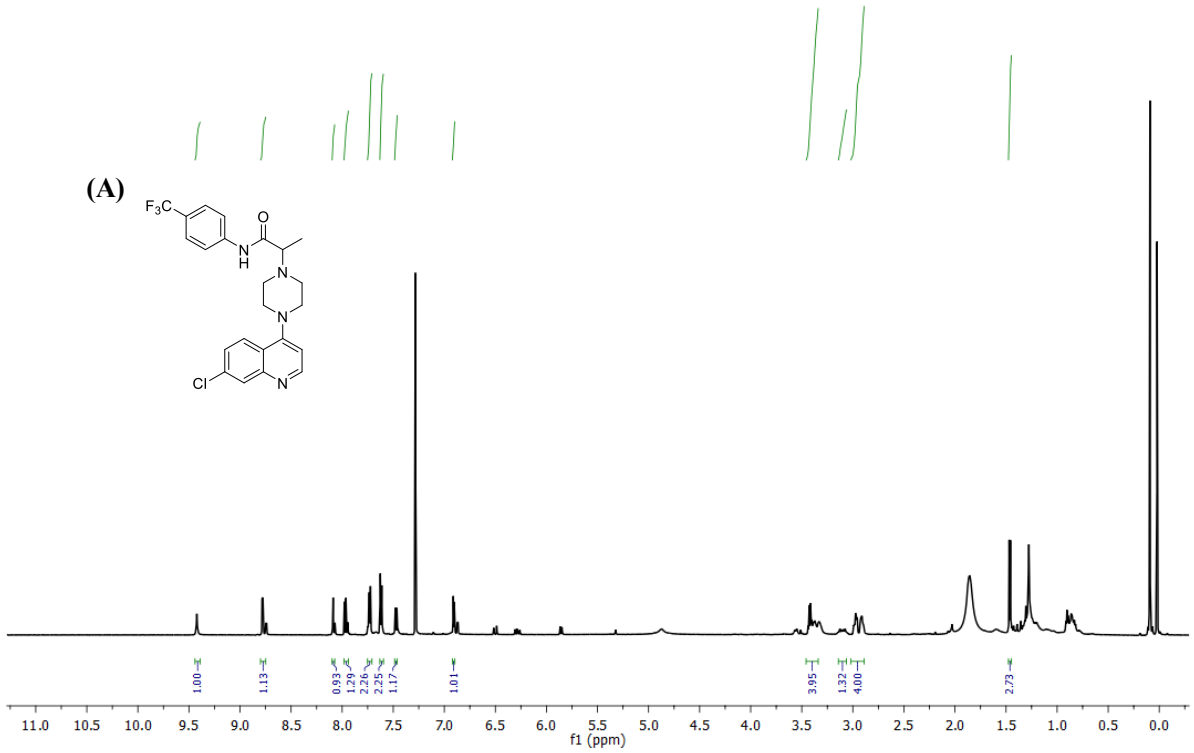

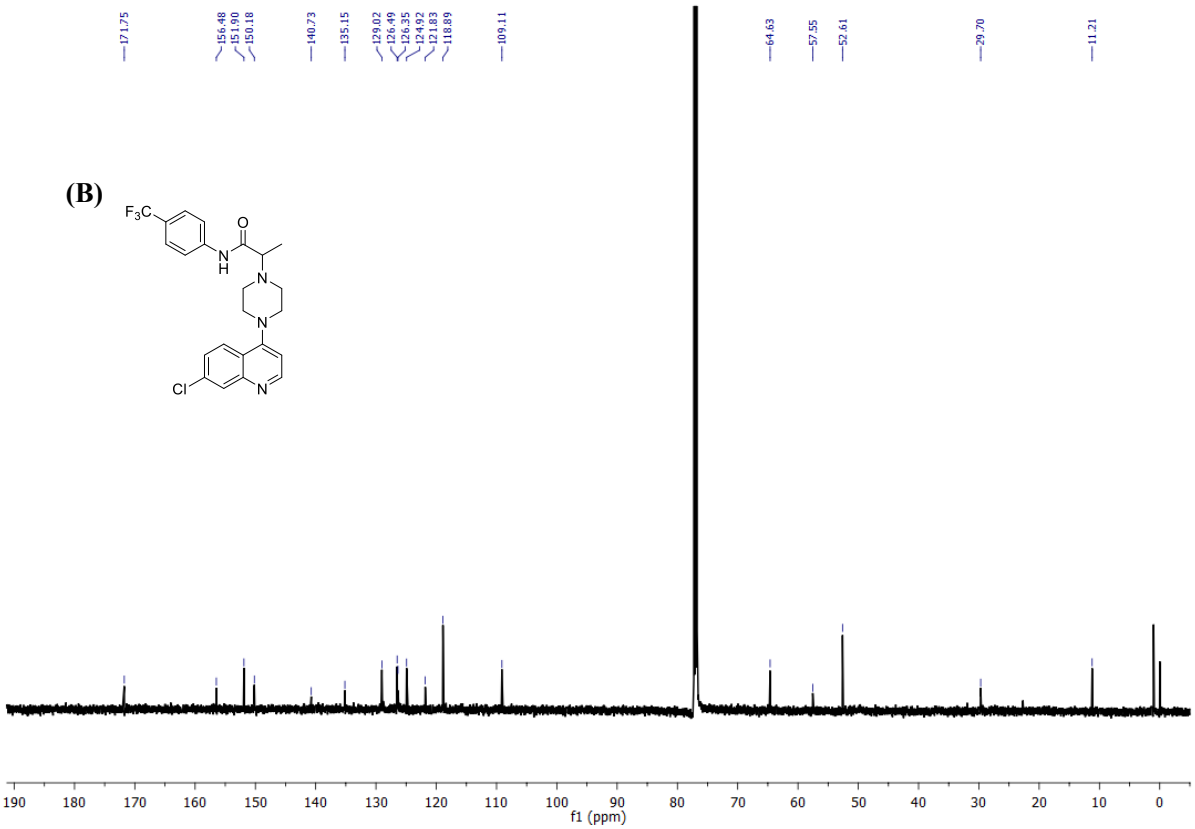

Fig. 2.18. ^{1}H NMR (A) and ^{13}C NMR (B) spectra of compound **2.5.**

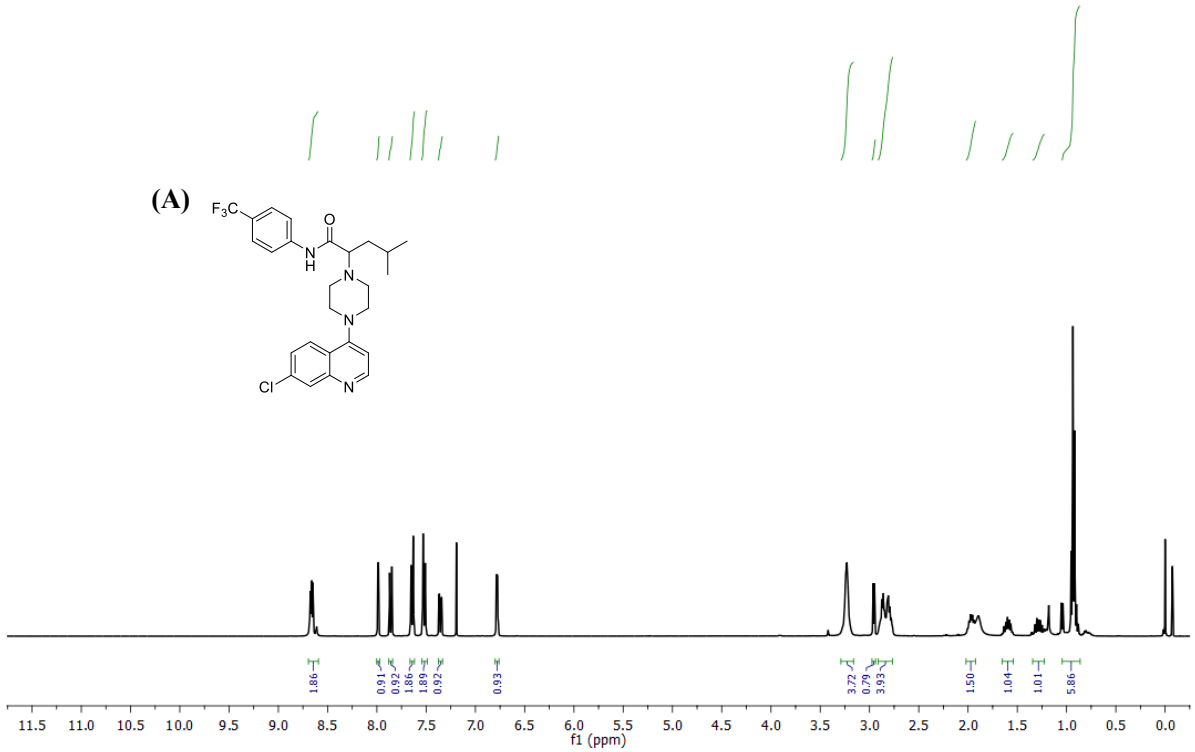

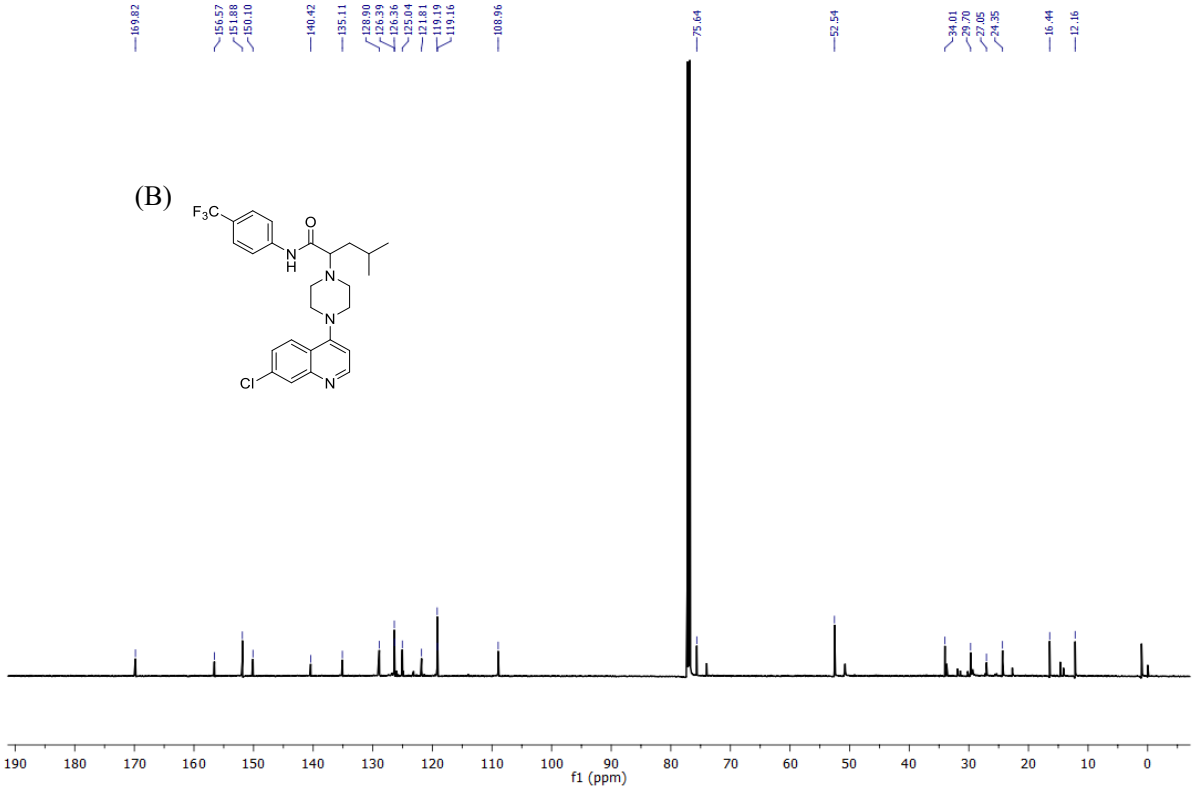

Fig. 2.19. ^{1}H NMR (A) and ^{13}C NMR (B) spectra of compound **2.6.**

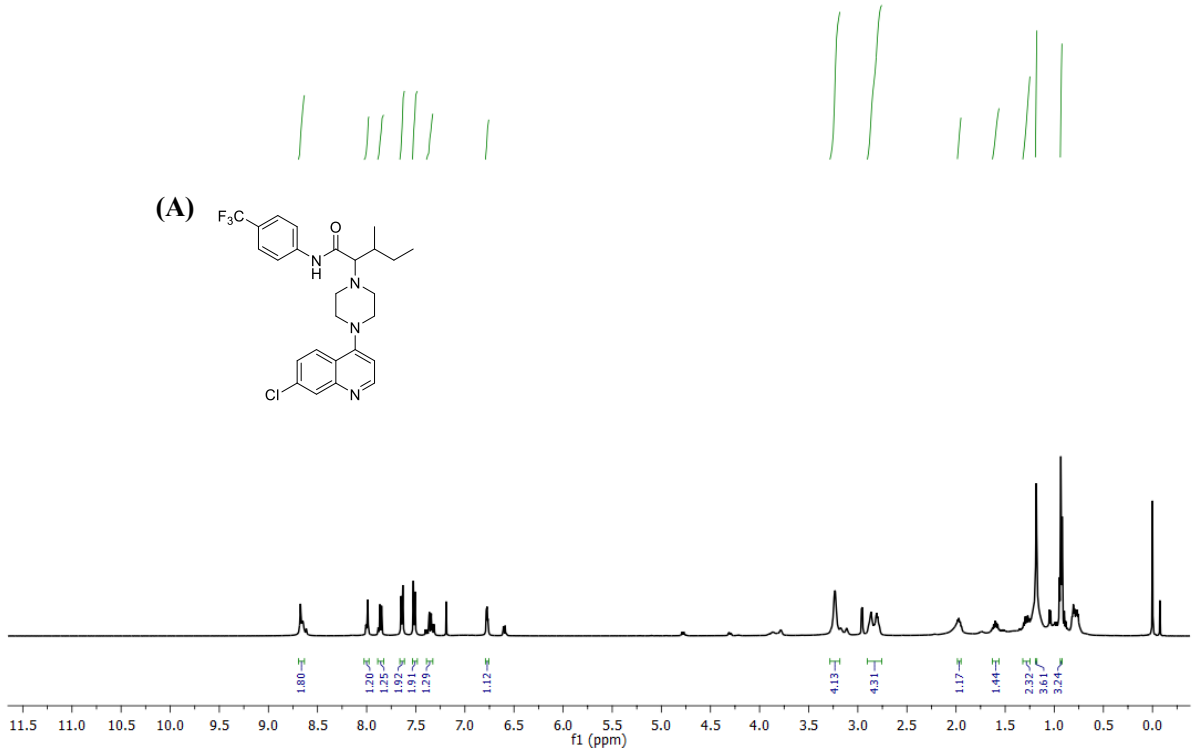

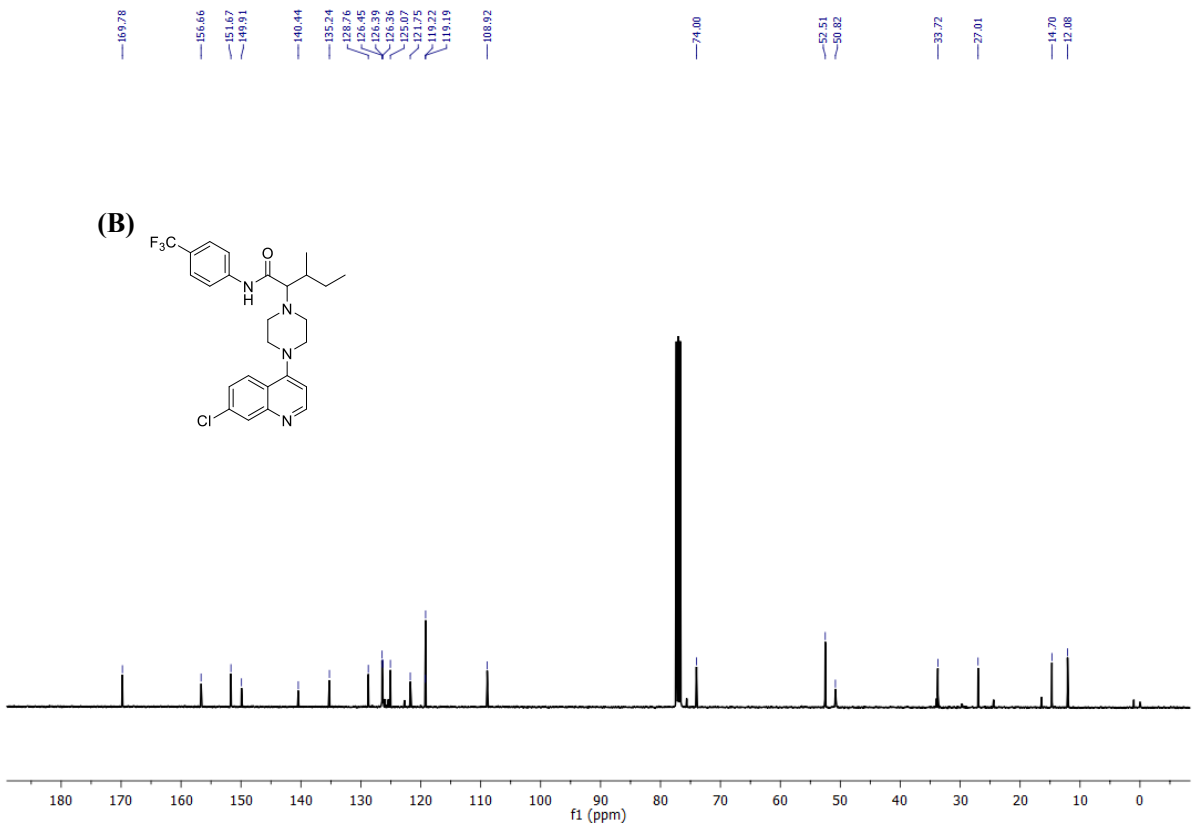

Fig. 2.20. ^{1}H NMR (A) and ^{13}C NMR (B) spectra of compound **2.7.**

2.4.19. Purification of compounds by HPLC analyses:

The purity of compounds was analyzed using a silica-based C18 HPLC column (2.7 µm). ACN/H_2O was used as a mobile phase with optimized step gradient elution methods and a 0.5 mL/minute flow rate. The 365 nm and 254 nm lights were used as the detectors.

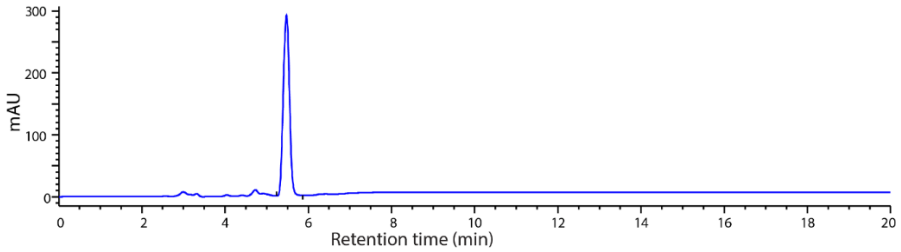

Fig. 2.21. HPLC trace of compound **2.1.**

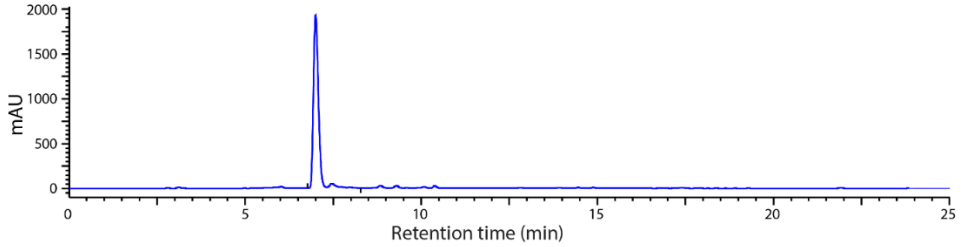

Fig. 2.22. HPLC trace of compound **2.2.**

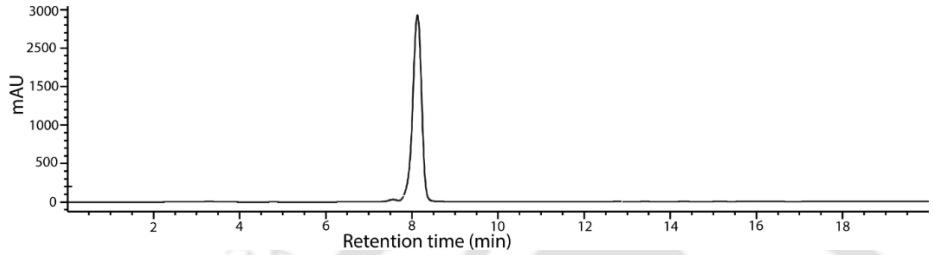

Fig. 2.23. HPLC trace of compound **2.3.**

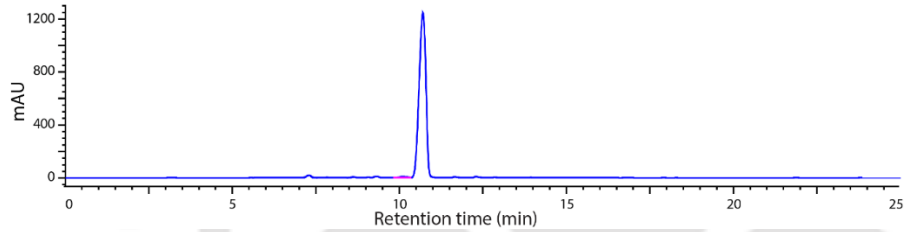

Fig. 2.24. HPLC trace of compound **2.4.**

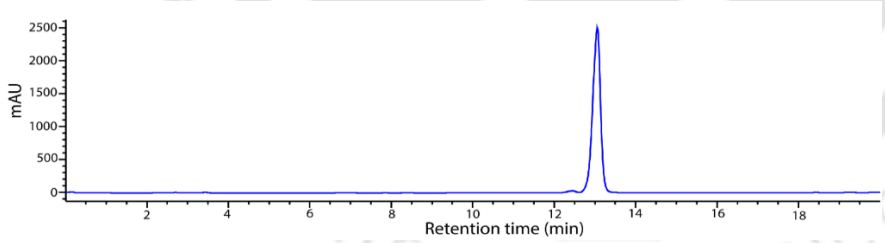

Fig. 2.25. HPLC trace of compound **2.5.**

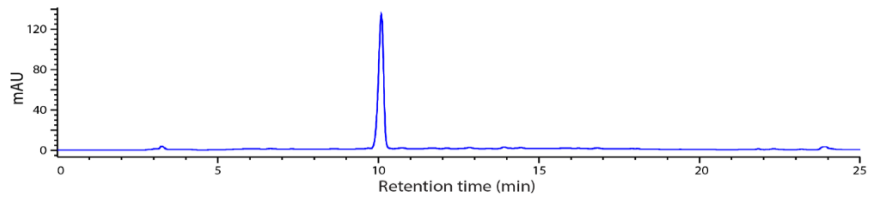

Fig. 2.26. HPLC trace of compound **2.6.**

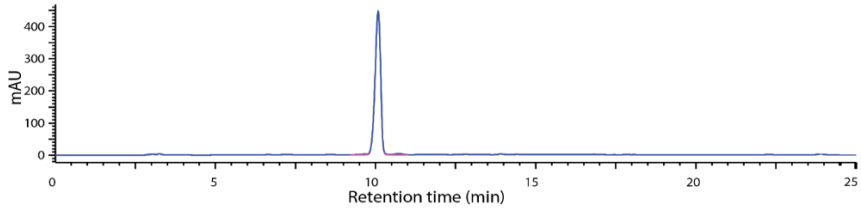

Fig. 2.27. HPLC trace of compound **2.7.**

2.4.20. Optical purity analysis:

The optical purity of the compound was confirmed by HPLC analysis with the chiral column (Chiral Pak AD-H, DAICEL CORPORATION). The mobile phase for the elution technique was iPrOH:n-hexane (20:80), and the flow rate was adjusted at 1.00 mL/min. It was found that the compound has an enantiomeric excess of more than 98%.

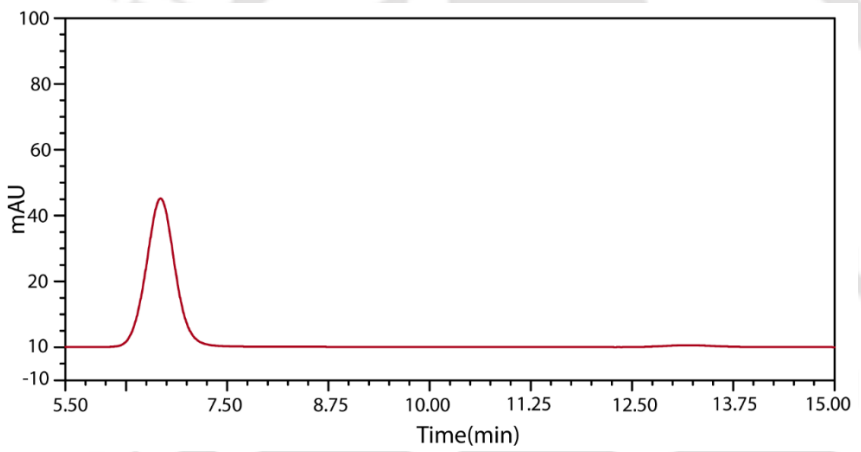

Fig. 2.28. Optical purity analysis of compound **2.4** by chiral column.

All the synthesized compounds are optically active and are single enantiomers. We performed a polarimetric experiment to assess the optical activity of the potent compound, which was found to be $[\alpha]_D^T$ = -45.531 °. Moreover, the biological evaluation was carried out with the single enantiomer of the compound.

2.5. References

1. Zhai, L.; Ladomersky, E.; Lenzen, A.; Nguyen, B.; Patel, R.; Lauing, K. L.; Wu, M.; Wainwright, D. A., IDO1 in cancer: a Gemini of immune checkpoints. *Cell Mol Immunol.* **2018,** *15* (5), 447-457.

2. Yue, E. W.; Sparks, R.; Polam, P.; Modi, D.; Douty, B.; Wayland, B.; Glass, B.; Takvorian, A.; Glenn, J.; Zhu, W., INCB24360 (Epacadostat), a highly potent and selective indoleamine-2, 3-dioxygenase 1 (IDO1) inhibitor for immuno-oncology. *ACS Med. Chem. Lett.* **2017,** *8* (5), 486-491.

3. Crosignani, S.; Bingham, P.; Bottemanne, P.; Cannelle, H.; Cauwenberghs, S.; Cordonnier, M.; Dalvie, D.; Deroose, F.; Feng, J. L.; Gomes, B., Discovery of a novel and selective indoleamine 2, 3-dioxygenase (IDO-1) inhibitor 3-(5-fluoro-1 H-indol-3-yl) pyrrolidine-2, 5-dione (EOS200271/PF-06840003) and its characterization as a potential clinical candidate. *J. Med. Chem.* **2017,** *60* (23), 9617-9629.

4. Kumar, S.; Jaipuri, F. A.; Waldo, J. P.; Potturi, H.; Marcinowicz, A.; Adams, J.; Van Allen, C.; Zhuang, H.; Vahanian, N.; Link Jr, C., Discovery of indoximod prodrugs and characterization of clinical candidate NLG802. *Eur. J. Med. Chem.* **2020,** *198*, 112373.

5. Pham, K. N.; Yeh, S.-R., Mapping the binding trajectory of a suicide inhibitor in human indoleamine 2, 3-dioxygenase 1. *J. Am. Chem. Soc.* **2018,** *140* (44), 14538-14541.

6. Labadie, B. W.; Bao, R.; Luke, J. J., Reimagining IDO pathway inhibition in cancer immunotherapy via downstream focus on the tryptophan–kynurenine–aryl hydrocarbon axis. *Clin Cancer Res.* **2019,** *25* (5), 1462-1471.

7. Pradhan, N.; Akhtar, N.; Nath, B.; Peña-García, J.; Gupta, A.; Pérez-Sánchez, H.; Kumar, S.; Manna, D., Inhibition of immunosuppressive indoleamine 2, 3-dioxygenase by targeting the heme and apo-form. *Chem Commun* **2021,** *57* (3), 395-398.

8. Dodd, E. L.; Bohle, D. S., Orienting the heterocyclic periphery: a structural model for chloroquine's antimalarial activity. *Chem Commun* **2014,** *50* (89), 13765-13768.

9. Shore, N. D.; Redorta, J. P.; Robert, G.; Hutson, T. E.; Cesari, R.; Hariharan, S.; Faba, Ó. R.; Briganti, A.; Steinberg, G. D. In *Non-muscle-invasive bladder cancer: An overview of potential new treatment options*, Urol Oncol, Elsevier: 2021; pp 642-663.

10. Balog, A.; Lin, T.-a.; Maley, D.; Gullo-Brown, J.; Kandoussi, E. H.; Zeng, J.; Hunt, J. T., Preclinical characterization of linrodostat mesylate, a novel, potent, and selective oral indoleamine 2, 3-dioxygenase 1 inhibitor. *Mol. Cancer Ther.* **2021,** *20* (3), 467-476.

11. Fraunhoffer, K. J.; DelMonte, A. J.; Beutner, G. L.; Bultman, M. S.; Camacho, K.; Cohen, B.; Dixon, D. D.; Fan, Y.; Fanfair, D.; Freitag, A. J., Rapid development of a commercial process for linrodostat, an indoleamine 2, 3-dioxygenase (IDO) inhibitor. *Org. Process Res. Dev.* **2019,** *23* (11), 2482-2498.

12. Kayamba, F.; Malimabe, T.; Ademola, I. K.; Pooe, O. J.; Kushwaha, N. D.; Mahlalela, M.; van Zyl, R. L.; Gordon, M.; Mudau, P. T.; Zininga, T., Design and synthesis of quinoline-pyrimidine inspired hybrids as potential plasmodial inhibitors. *Eur. J. Med. Chem.* **2021,** *217*, 113330.

13. Masui, H.; Naito, K.; Minoshima, M.; Kusayanagi, A.; Yosugi, S.; Shoji, M.; Takahashi, T., Efficient synthesis of 5-(hydroxymethyl) piperazin-2-ones using

automatically prepared chiral bromocarboxylic acid and Garner's aldehyde as versatile building blocks. *Bioorg. Med. Chem. Lett.* **2021,** *40*, 127961.

14. Panda, S.; Pradhan, N.; Chatterjee, S.; Morla, S.; Saha, A.; Roy, A.; Kumar, S.; Bhattacharyya, A.; Manna, D., 4, 5-Disubstituted 1, 2, 3-triazoles: effective inhibition of indoleamine 2, 3-dioxygenase 1 enzyme regulates T cell activity and mitigates tumor growth. *Sci. Rep.* **2019,** *9* (1), 18455.

15. Paul, S.; Roy, A.; Deka, S. J.; Panda, S.; Srivastava, G. N.; Trivedi, V.; Manna, D., Synthesis and evaluation of oxindoles as promising inhibitors of the immunosuppressive enzyme indoleamine 2, 3-dioxygenase 1. *Medchemcomm* **2017,** *8* (8), 1640-1654.

16. Röhrig, U. F.; Michielin, O.; Zoete, V., Structure and plasticity of indoleamine 2, 3-dioxygenase 1 (IDO1). *Journal of medicinal chemistry* **2021,** *64* (24), 17690-17705.

17. Wang, T.; Ashrafi, A.; Modareszadeh, P.; Deese, A. R.; Chacon Castro, M. D. C.; Alemi, P. S.; Zhang, L., An analysis of the multifaceted roles of heme in the pathogenesis of cancer and related diseases. *Cancers* **2021,** *13* (16), 4142.

18. Fiorito, V.; Chiabrando, D.; Petrillo, S.; Bertino, F.; Tolosano, E., The multifaceted role of heme in cancer. *Front. Oncol.* **2020,** *9*, 1540.

19. Nelp, M. T.; Kates, P. A.; Hunt, J. T.; Newitt, J. A.; Balog, A.; Maley, D.; Zhu, X.; Abell, L.; Allentoff, A.; Borzilleri, R., Immune-modulating enzyme indoleamine 2, 3-dioxygenase is effectively inhibited by targeting its apo-form. *PNAS* **2018,** *115* (13), 3249-3254.

20. Gorka, A. P.; de Dios, A.; Roepe, P. D., Quinoline drug–heme interactions and implications for antimalarial cytostatic versus cytocidal activities. *J. Med. Chem.* **2013,** *56* (13), 5231-5246.

21. Davis, A. A.; Patel, V. G., The role of PD-L1 expression as a predictive biomarker: an analysis of all US Food and Drug Administration (FDA) approvals of immune checkpoint inhibitors. *JITC* **2019,** *7* (1), 278.

22. Jozefowicz-Korczynska, M.; Pajor, A.; Lucas Grzelczyk, W., The ototoxicity of antimalarial drugs—a state of the art review. *Front. Neurol.* **2021,** *12*, 661740.

CHAPTER 3

Photoresponsive prodrug for regulated inhibition of indoleamine 2,3-dioxygenase 1 enzyme activity

3.1. Background and objective of present work

IDO1 inhibition being a promising therapeutic strategy for both cancer and Alzheimer's disease plays a critical role in modulating immune response and neurodegenerative processes.[1] The development of prodrugs targeting the IDO1 enzyme holds significant promise for advancing targeted drug delivery and selective enzyme inhibition in immunological disorders. While few reports exist on IDO1 prodrugs, earlier efforts, such as an indoximod-based prodrug (NLG802), showed improved IDO1 inhibition and pharmacokinetics but failed in phase II clinical trials.[2] This highlights the need for better prodrug development. Disease conditions and endogenous stimuli such as pH, redox conditions, and enzymes influence the effectiveness of the reported IDO1 selective prodrugs. Consequently, there is a strong demand for prodrugs that can be activated in a controlled manner.[3]

In second chapter, we discussed the development of DCQ derivatives as apo-IDO1 inhibitor exploring a new mechanism of inhibition. It acted as efficient apo IDO1 inhibitor along with its heme binding efficacy but even with good inhibition activity, it lacks target specific drug delivery and spatiotemporal control.[4] To overcome this concern, we hypothesize that designing stimuli-responsive prodrugs may offer a promising strategy for selective inhibition of the IDO1 enzyme. Light, being a versatile and biocompatible external stimulus, has adjustable excitation, remote activation, and high spatial and temporal resolution. The release of active IDO1 inhibitors in targeted tissues, by utilizing light, we can control and disrupt the structure of specially designed prodrugs.[5]

Recently, the role of indole-based IDO1 inhibitors in cancer and Alzheimer's disease have inspired us to develop thiourea derivatives of 1-methyltryptamine.[6] The novelty of our compound design lies in developing thiourea derivatives of 2-azole-substituted 1-methyltryptamine and its photocaged analogue. From consequent biochemical studies, it is confirmed that the potent tryptamine derivative shows moderate inhibitory activity against the purified IDO1 enzyme. The potent compound showed strong IDO1 inhibition activity with an IC_{50} value of 120 nM, whereas the photocaged prodrug showed negligible IDO1 inhibition activity under similar experimental conditions. The photocaged prodrug showed successful regeneration of the active IDO1 inhibitor at visible light irradiation of 400nm light, providing a spatiotemporal control over the drug activation, used to improve the therapeutic efficacy of IDO1 inhibitors.

3.2. Results and discussion

3.2.1. Design and synthesis of 2-azole substituted 1-methyltryptamine derivatives

Indole-based IDO1 inhibitors, such as indoximod, PF06840003 and others, have demonstrated strong anticancer and anti-Alzheimer's activities.[3, 4] This potency may be attributed to their structural similarity to the IDO1 substrate, L-Trp. Additionally, azole-based derivatives offer improved specificity for IDO1 over other heme-containing proteins. The use of indole and azole moieties in IDO1 inhibitors has inspired us to design a new class of 2-azole-substituted 1-methyltryptamine derivatives. We hypothesize that these compounds will exhibit potent and selective inhibitory activity for the IDO1 enzyme by effectively occupying the active site and interacting with the heme group and other neighbouring residues. Whereas most of the reported indole and azole-based compounds, which partially occupy the IDO1 active site, might lack the selectivity and inhibitory activities for the IDO1 enzyme in comparison with the other heme-containing proteins.

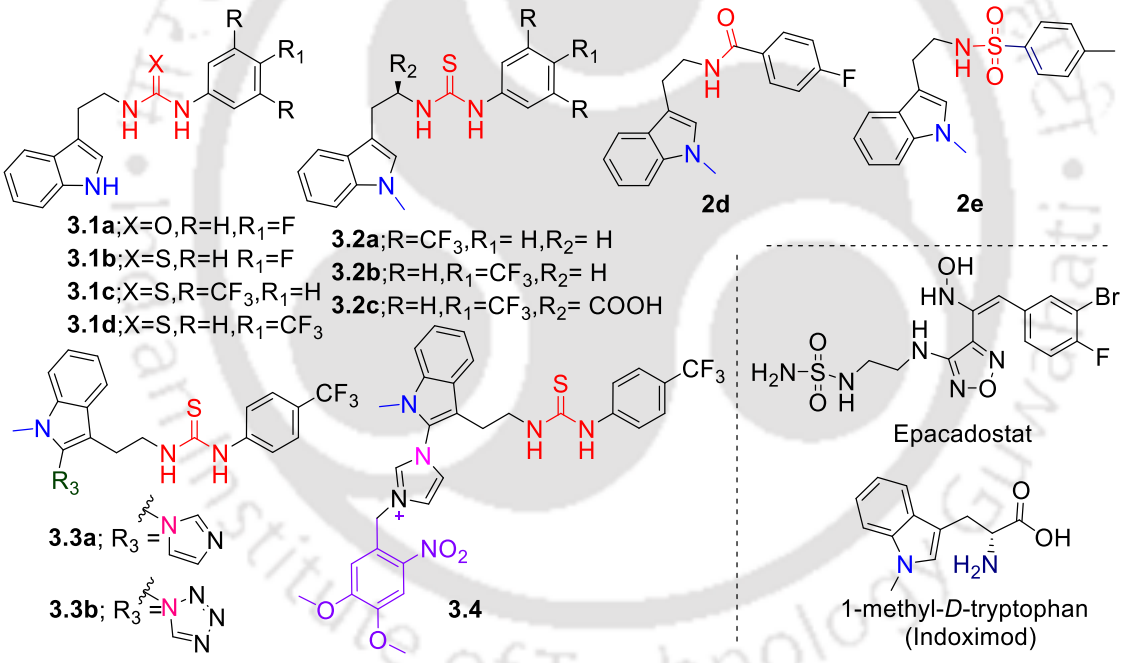

Scheme 3.1. Tryptamine-based azole derivatives.

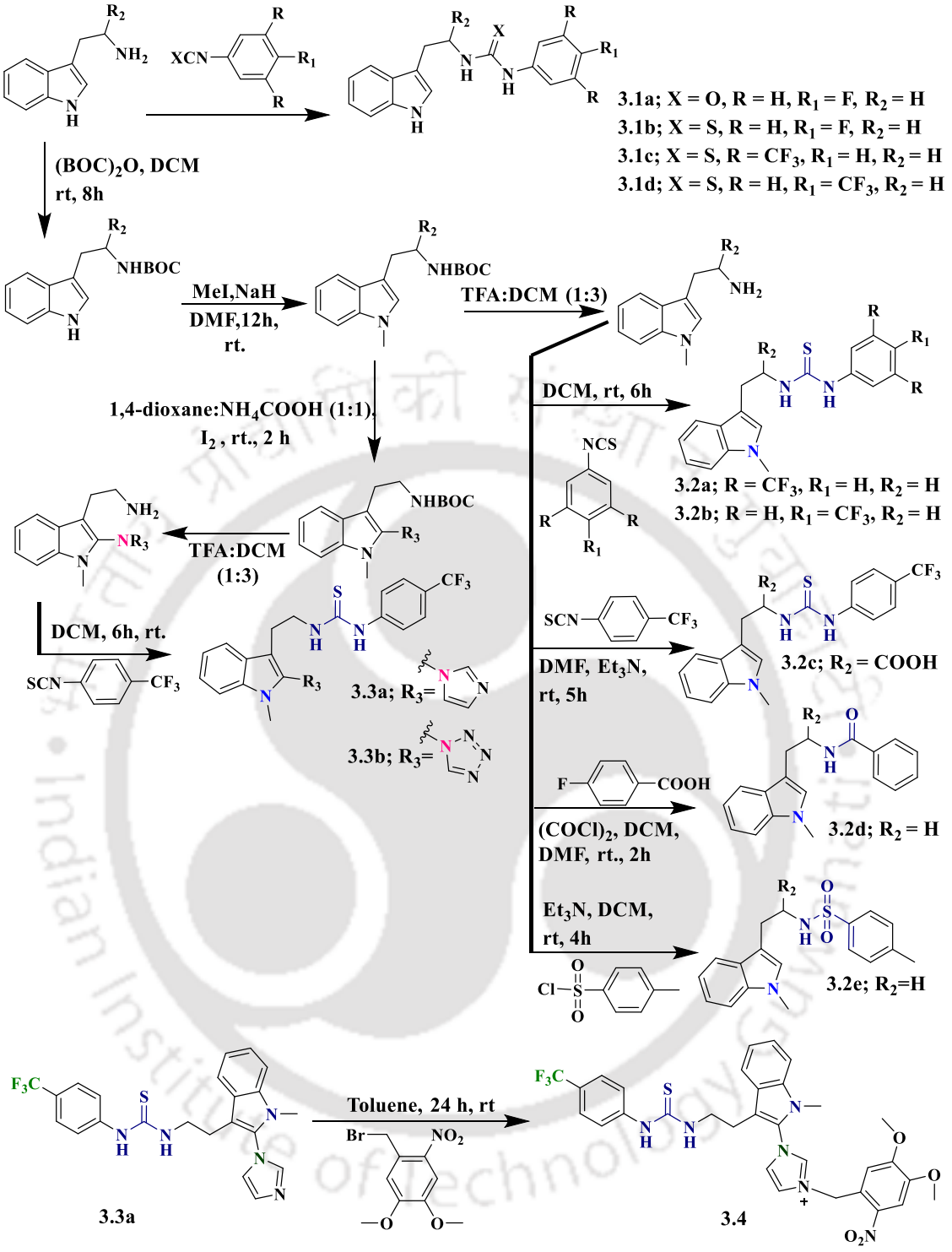

Scheme 3.2. Synthetic routes to various indole derivatives from tryptamine and tryptophan.

In this regard, the tryptamine thiourea derivatives **3.1a–d** were initially synthesized *via* reactions of tryptamine with substituted phenyl isothiocyanate to investigate the role of thiourea moiety in IDO1 inhibition (Table 3.1 and Scheme 3.2). To

improve the IDO1 efficacy of these tryptamine thiourea derivatives, we prepared 1-methyltryptamine thiourea derivatives. The reaction of 1-methyltryptamine and 1-methyltryptophan with substituted phenyl isothiocyanates resulted in the formation of 1-methyltryptamine thiourea **3.2a–c** (Scheme 3.1). We also synthesized 1-methyltryptamine sulphonamide and amide derivatives **3.2d** and **3.2e** *via* reactions of 1-methyltryptamine with tosyl chloride and substituted benzoic acid. For further improvement of IDO1 inhibitory activity, 2-azole-substituted 1-methyltryptamine derivatives were synthesized. The reaction of BOC-protected 1-methyltryptamine with imidazole and tetrazole in the presence of I_2 under 1,4-dioxane and ammonium formate (1 : 1) solvent mixture and subsequent deprotection of the BOC group resulted in the formation of imidazole/tetrazole substituted 1-methyltryptamine derivatives. Finally, coupling of 1-isothiocyanato-4-(trifluoromethyl)benzene with imidazole/tetrazole substituted 1-methyltryptamine derivatives resulted in the targeted products **3.3.3a** and **3.3b**.[7] To develop a photo-responsive prodrug for the IDO1 enzyme, compound **3.4** was synthesized. The reaction of **3.3.3a** with 1-(bromomethyl)-4,5-dimethoxy-2-nitrobenzene produced compound **3.4** (Scheme 3.1).

3.2.2. Inhibitory activities against IDO1 enzyme

Both IDO1 and tryptophan 2,3-dioxygenase (TDO) enzymes are known to regulate the initial rate-limiting step in the metabolism of L-Trp to *N*-formyl kynurenine *via* the kynurenine pathway. The L-Trp and indole derivatives are particularly favoured as binding partners for the active site of the TDO enzyme due to their structural compatibility. In contrast, the active site of the IDO1 enzyme displays a remarkable degree of plasticity, allowing a diverse range of small molecules to interact and accommodate within it. This adaptability results in a broader selection of potential inhibitors and modulators for IDO1, highlighting its versatility in binding interactions. The inhibitory activities of the synthesized compounds on IDO1 were initially assessed using a UV-vis spectrophotometric method.[8]

Table 3.1. Inhibitory activity of the tryptamine derivatives against purified human IDO1 enzyme.

Compounds	IC_{50} values (μM)	%Inhibition	
		1 μM	0.25 μM
3.1a	>10	27 ± 3	8 ± 1
3.1b	>10	36 ± 2	14 ± 1
3.1c	>10	41 ± 1	6 ± 1
3.1d	>10	47 ± 3	16 ± 2
3.2a	0.84 ± 0.09	70 ± 8	38 ± 3
3.2b	0.49 ± 0.05	81 ± 8	44 ± 5
3.2c	>10	45 ± 2	6 ± 2
3.2d	>10	25 ± 1	11 ± 2
3.2e	>10	32 ± 1	11 ± 1
3.3.3a	0.12 ± 0.01	99 ± 1	84 ± 1
3.3b	0.41 ± 0.49	73 ± 1	47 ± 1
3.4	>10	32 ± 3	19 ± 3
Indoximod	>10	29 ± 1	19 ± 2
Epacodastat	0.09 ± 0.02	97 ± 2	80 ± 2

Initial screening of IDO1 enzyme inhibitory activity of the synthesized compounds revealed that compound **3.3a** strongly inhibits the IDO1-mediated catabolism of L-Trp to *N*-formyl kynurenine with an IC_{50} value of 120 ± 3 nM (Table 3.1 and Fig. 3.1A). The other synthesized tryptamine derivatives displayed considerably weaker IDO1 inhibitory activities. The IC_{50} values of the reported compounds epacadostat and indoximod were 90 ± 2 nM and >10 μM, respectively, under similar experimental conditions, which is in accordance with their reported IC_{50} values (Fig. 3.1B and Table 3.1).[9] Meanwhile, the TDO-based enzymatic activity assay of compound **3.3a** showed negligible activity under similar experimental conditions, suggesting its higher selectivity in inhibiting IDO1 over the TDO enzyme (Table 3.2).[8] The UV-vis spectral analyses showed no significant changes in the Soret peak of the TDO enzyme. (Fig. 3.3A)

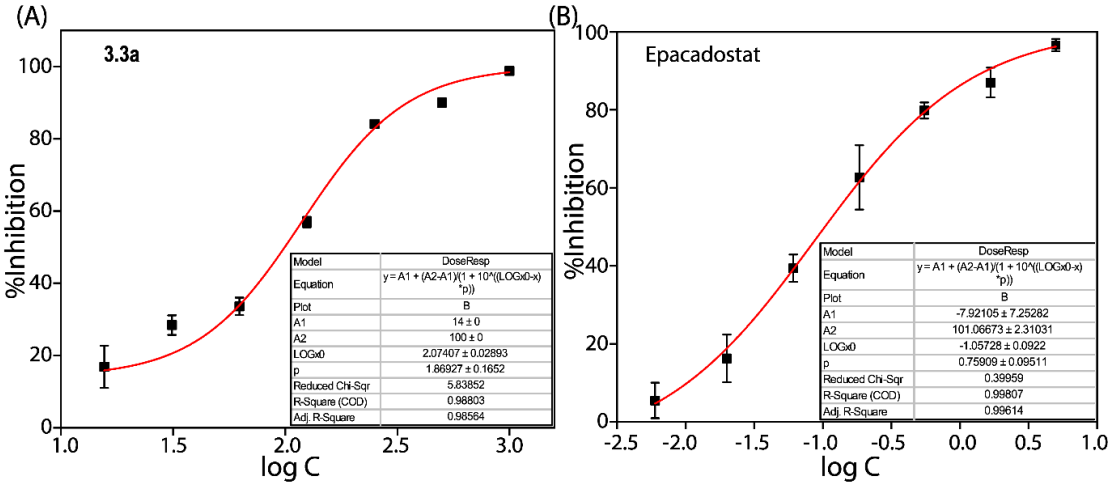

Fig. 3.1. Plots of concentration of *N*-formyl kynurenine in the presence of different concentrations of compound **3.3a** (A) and epacadostat (B).

Table 3.2. Inhibitory activity of the **3.3a** against purified human TDO enzyme.

Compounds	% TDO Inhibition		
	25 µM	50 µM	100 µM
3.3a	4 ± 0.5	17 ± 0.4	48 ± 1

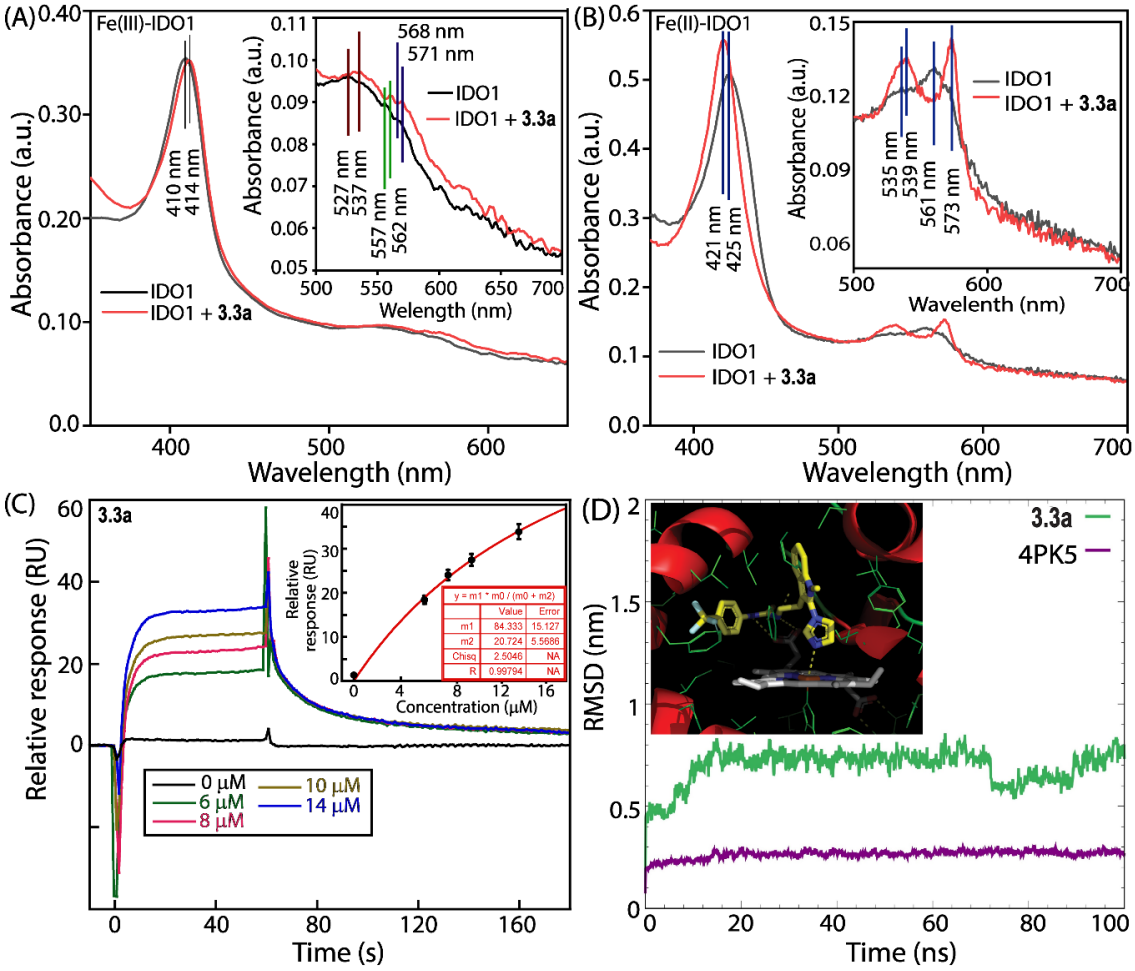

Fig. 3.2. UV-vis spectra of (A) ferric-IDO1 and (B) deoxy-ferrous-IDO1 enzyme in the absence and presence of compound **3.3a** (10 µM) in 100 mM phosphate buffer at pH 6.5. [IDO1] = 0.65 µM. The insets show the zoomed area of the UV-vis spectra within 500–700 nm. (C) Surface plasmon resonance sensorgrams of compound **3.3a** binding to IDO1 enzyme. The inset shows the binding isotherms generated from the response unit (RU) at 60 s (average of triplicate measurements) *versus* the concentration of the compounds. For all SPR measurements, 20 mM HEPES buffer, pH 7.4, with 160 mM KCl was used. (D) Root means square displacement (RMSD) of protein (protein ID: 4PK5; purple) and the ligand (compound **3.3a**; green) in the most stable mode of interaction. Inset demonstrates the probable mode of interaction of the compound **3.3a** with the active site of IDO1 enzyme (4PK5).

Similarly, the analysis of other heme-containing proteins, such as haemoglobin and myoglobin, revealed no notable changes in their Soret peaks. This suggests compound **3.3a** selectively binds to IDO1 (Fig. 3.2A and 3.3A-C). The absorption spectra

of compound **3.3a** exhibited little to no interference with this spectrophotometry-based enzyme activity assay (Fig. 3.3D). One of the prerequisites for the development of IDO1 inhibitor-based immunotherapy for cancer or Alzheimer's disease is minimal cytotoxicity. The cell viability assay of the potent compounds showed minimal toxicity in HEK-293 and HeLa cells, indicating that these compounds are suitable for IDO1 inhibitory studies (Fig. 3.6 C, D and 3.7).

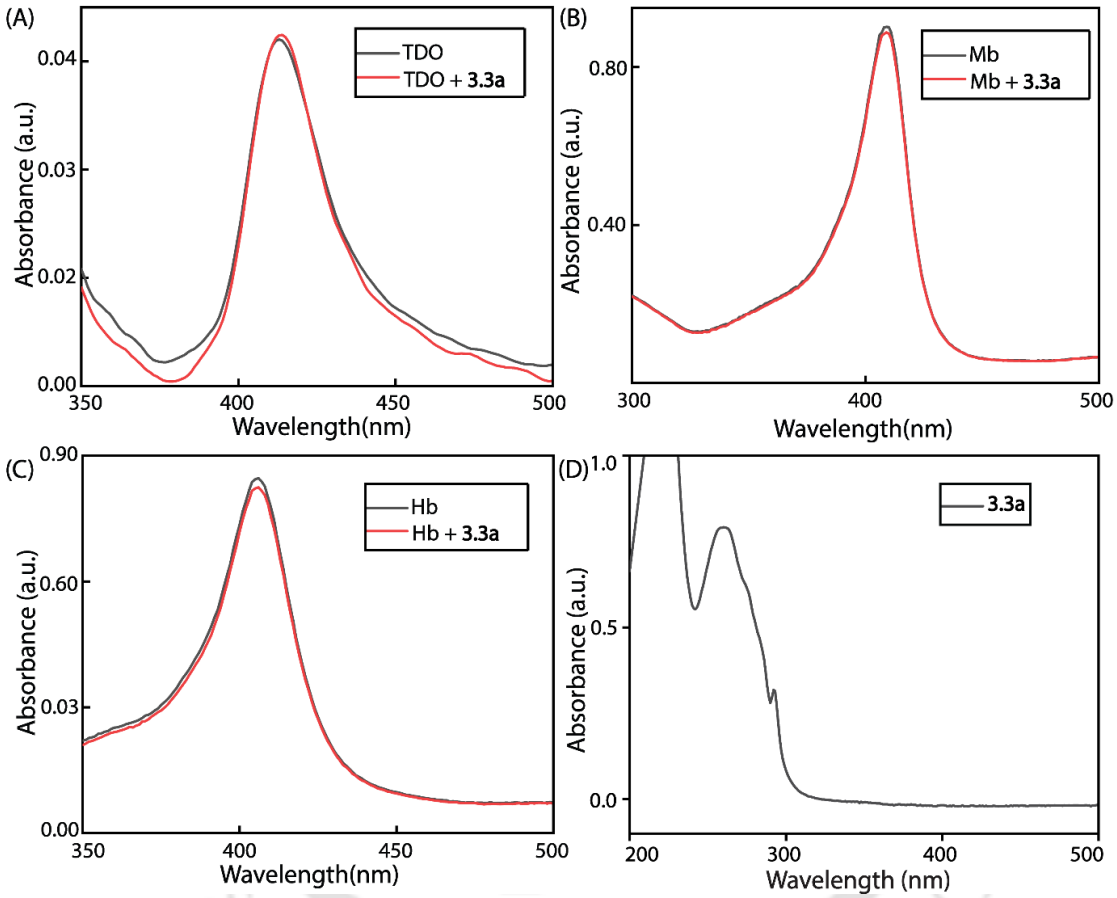

Fig. 3.3. UV-Vis spectra of the TDO (A), myoglobin (B), and hemoglobin (C) proteins (200 nM) in the absence and presence of compound **3.3a** (5 µM) in 100 mM KPB buffer at pH 6.5 after 60 min of incubation at 37 °C (A). UV-Vis spectra of compound **3.3a** (D).

Table 3.3. Characteristic peaks from the UV-Vis measurements of the IDO1 enzyme in the absence and presence of compound **3.3a**.

Sl. No.	Compound	λ_{max} (nm) Fe^{3+} state binding	λ_{max} (nm) Fe^{2+} state binding
1	Only IDO1	410, 527, 557, 568	425, 535, 561
2	IDO1 + **3.3a**	414, 537, 562, 571	421, 539, 573

Enzyme concentration: 650 nM, compound **3.3a** concentration 10 μM

To further explore the interaction of the potent compound with the IDO1 enzyme, UV-vis-based spectral analysis and surface plasmon resonance (SPR) measurements were performed.[4]

The optical properties of the heme group are susceptible to the local environment, which provides strong evidence of the ligand binding aptitude to the IDO1 enzyme. Therefore, the distinctive peaks in the absorbance spectra of the heme group were used to confirm the direct binding of the compound to the heme-containing active site of the IDO1 enzyme. The absorption spectra of ferric IDO1 and deoxy ferrous IDO1 enzymes were recorded in the absence and presence of the selected compound (Fig. 3.2A, B). For the ferric-IDO1 enzyme, the Soret band got red-shifted by 4 nm in the presence of compound **3.3a**, indicating its binding to the heme group. For the deoxy-ferrous-IDO1 enzyme, the Soret band got blue-shifted by 5 nm, and the Q-band at 535 nm and 561 nm (for the only enzyme) got red-shifted by 4 nm and 12 nm, respectively, in the presence of the compound **3.3a**, indicating its binding to Fe^{2+}-IDO1 enzyme (Table 3.3).[1] The SPR measurements showed the binding affinity (K_d) between compound **3.3a** and IDO1 enzyme was within the range of 20.7 ± 5.5 μM (Fig. 3.2C). The absorption spectra of compound **3.3a** did not show any peak in this region. Hence, both absorption spectral analysis and SPR measurements confirm the binding of compound **3.3a** with the IDO1 enzyme.

3.2.3. Docking and MD simulation

To understand the molecular determinants regulating the inhibitory activity of compound **3.3a**, molecular docking analyses were conducted using the X-ray co-crystal structure of the IDO1 complex (PDB code: 4PK5). The molecular docking analysis revealed that the *N*-methyl indole ring of compound **3.3a** could be involved in interaction with the hydrophobic side chains of Y126, F163, F164, L234, and other amino acids present within the hydrophobic 'pocket A' located at the distal heme site (Fig. 3.2D, inset). The imidazole and the thiourea moieties interact with the iron and carboxylate moieties of the heme group. This proposed mode of interaction is in good agreement with the UV-vis spectroscopic-based binding studies. Additionally, the molecular dynamics (MD) simulation studies indicated that the compounds remain strongly bound within the binding site of IDO1. The MD results showed that the protein attained a stable condition at an RMSD of 0.3 nm, while compound **3.3a** stabilized at 0.8 nm (Fig. 3.2D and 3.4).[10] A slight

drift at 70 ns could be due to the conformational change in the ligand. This leads to a decrease in the distance between the iron of heme and the N-atom of the imidazolium ring of the ligand. Overall, the interactions involving hydrophobic forces and hydrogen bonds appear to be the driving factors for the binding of compound **3.3a** to the IDO1 enzyme.

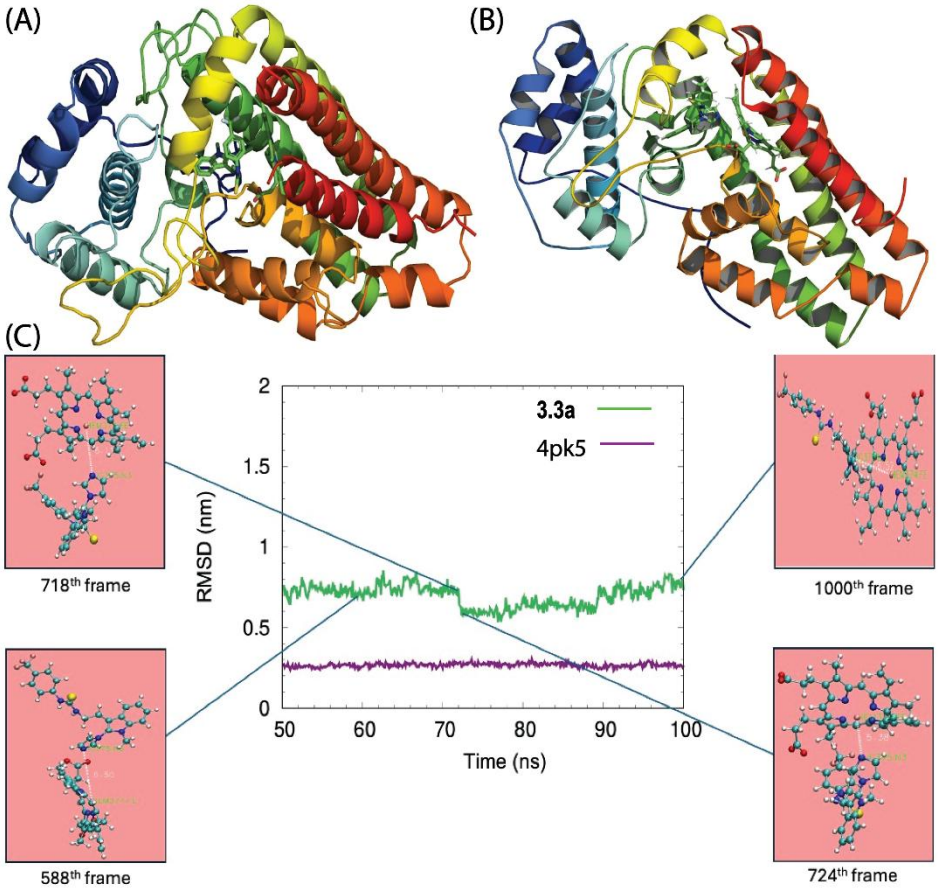

Fig. 3.4. The mode of interaction of compound **3.3a** with the protein 4pk5 in the presence of the heme group after molecular docking (A) and MD simulation (B), respectively. Root means square displacement (RMSD) of protein (protein ID: 4PK5; purple) and the ligand (compound **3.3a**; green) at different time frames.

3.2.4. Photocleavage

Encouraged by the promising IDO1 inhibitory activities of compound **3.3a**, we aimed to enhance its therapeutic potential by introducing a photocage to provide spatiotemporal control over inhibitor release and IDO1 inhibitory activity, enabling more precise targeting and reducing potential off-target effects. Enzyme activity studies showed that prodrug **3.4** exhibited significantly weaker inhibitory activity against IDO1 (Fig. 3.5).

This observed reduction in potency could be due to the modification of the imidazole moiety, which likely affects its binding affinity toward the heme group or fails

to fit the active site of the IDO1 enzyme. The molecular docking analysis of the X-ray co-crystal structure of the IDO1 complex (PDB code: 4PK5) suggests that prodrug **3.4** might be involved in hydrophobic and hydrogen bonding interactions with the amino acids in 'pocket B', which is located near the entrance of the active site. However, no direct interaction between prodrug **3.4** and the heme group of IDO1 was observed (Fig. 3.5). This lack of direct interaction with the heme group could be one of the possible reasons for the low inhibition activity of prodrug **3.4** against IDO1. The treatment of visible light (λ_{ex} = 400 nm) showed the regeneration of the active inhibitor **3.3a**. The regeneration of active inhibitor **3.3a** from prodrug **3.4** was analyzed using HPLC, and the *in-situ* activity of IDO1 was assessed using the UV-vis spectrophotometric method. The HPLC analysis indicated that approximately 90% of prodrug **3.4** was converted to the active inhibitor **3.3a** after 30 minutes of treatment with visible light (Fig. 3.6A). This IDO1 inhibitory activity also showed the regeneration of potent compound **3.3a** after photoirradiation (Fig. 3.6B). The photolysis rate and quantum yield were analysed using HPLC. The photolysis rate was observed to be 4.69×10^{-9} mol s^{-1}, and the apparent quantum yield was found to be 7.82×10^{-5}.

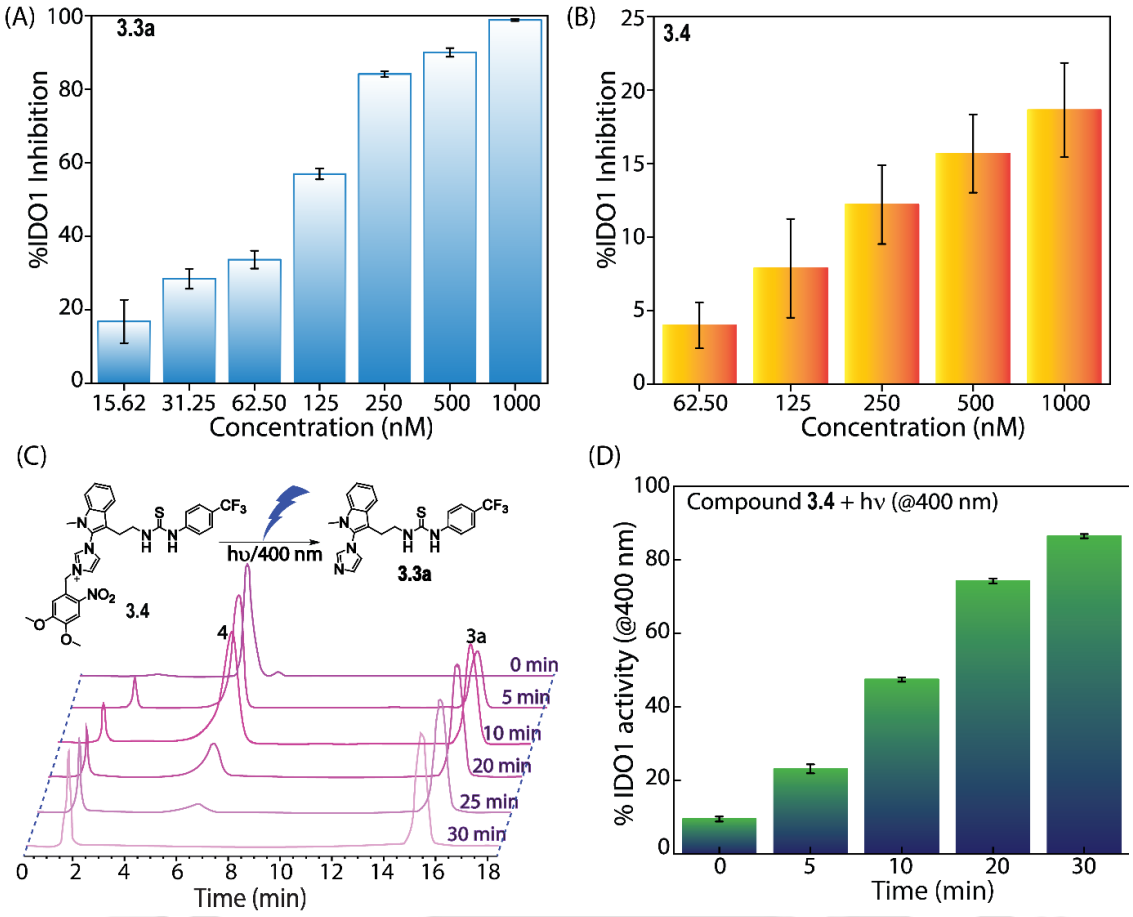

Fig. 3.6. Variation of %IDO1 inhibition in the presence of different concentrations for compound **3.3a** (A) and compound **3.4** (B) in the presence of IDO1 enzyme (650 nM), Photoinduced (λ_{ex} = 400 nm) regeneration of the potent compound **3.3a** from the prodrug **3.4** was analysed by HPLC analysis (C). IDO1 activity assay of prodrug **3.4** at different time intervals after photoinduction (400 nm) (D).

The cell viability assay of the prodrug **3.4** before and after photoirradiation showed minimal toxicity in HEK-293 and HeLa cells (Fig. 3.6C, D). Although this outcome aligns with the intended design of a prodrug for controlled activation, it emphasizes the need to optimize the linker design and assess the activation kinetics of the prodrug. These findings provide valuable insights into the development of photo-responsive IDO1 inhibitors and demonstrate the importance of fine-tuning prodrug strategies to balance controlled enzyme inhibition.

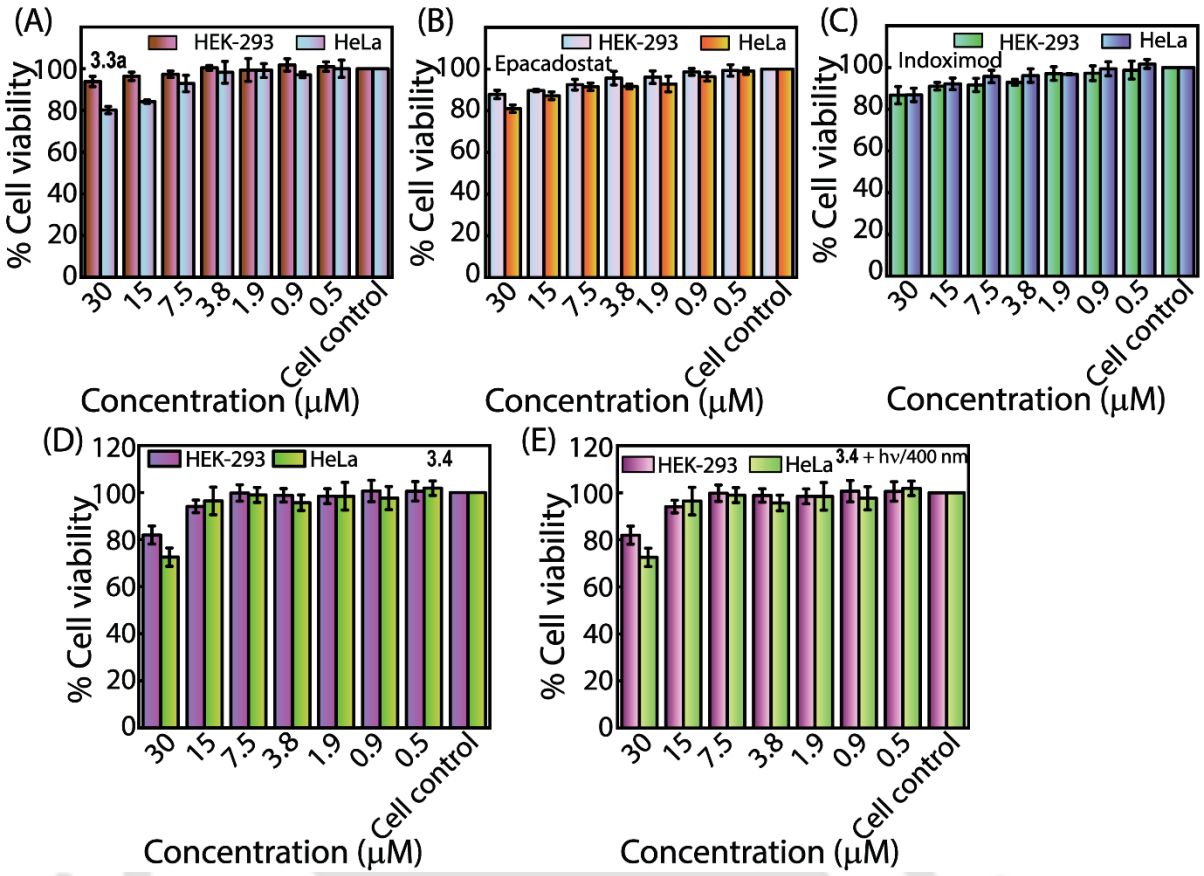

Fig. 3.7. Viability of HEK-293 and HeLa cells in the presence of compound **3.3a** (A), epacadostat (B) and indoximod (C). **3.4** before (D) and after (E) photoirradiation.

3.2.5. Stability study of the prodrug

HPLC-based stability analysis. Compound **3.4** was added to water, DMEM, and DMEF. The stability of the compound was studied at various time intervals using a silica-based C18 HPLC column (2.7 μm). ACN/H_2O was used as a mobile phase with optimized step gradient elution methods and a 0.5 mL per minute flow rate. The 365 nm and 254 nm lights were used as the detectors (Fig. 3.8)

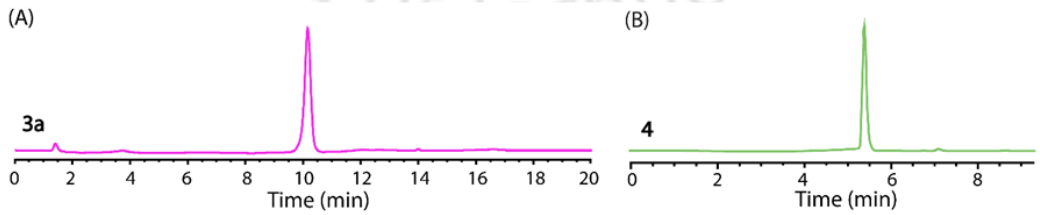

Fig. 3.8. HPLC analysis of **3.3a** (A), and **3.4** (B).

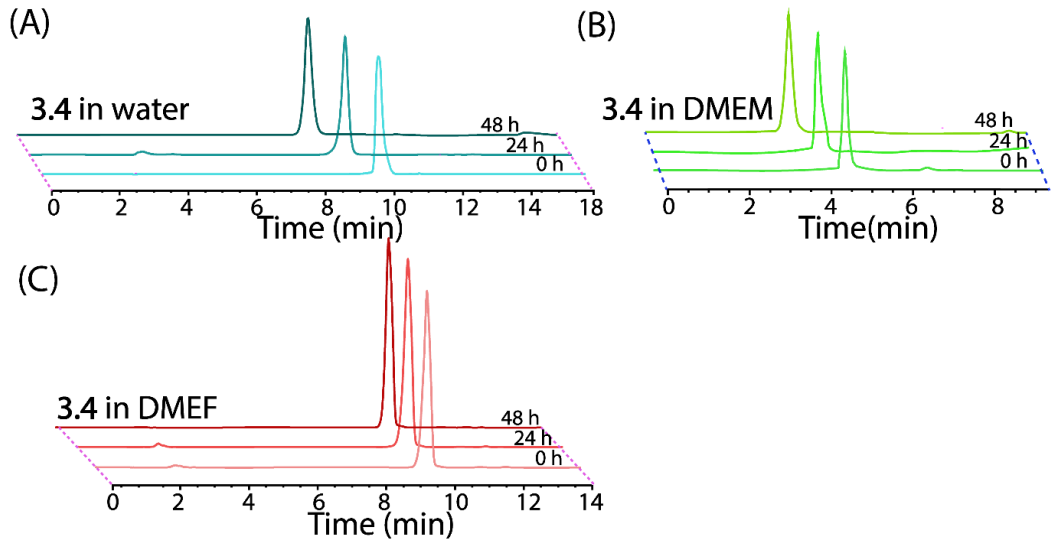

Fig. 3.8. HPLC analysis for the stability of the prodrug (**3.4**) at different time intervals in water (A), DMEM (B), FBS (C).

3.3. Conclusion

This study demonstrated the synthesis of thiourea derivatives of 2-imidazole-substituted 1-methyltryptamine that selectively inhibit IDO1 activity. The UV-vis and SPR-based studies revealed that the potent compound binds to the IDO1 enzyme. We installed a photocage to the potent compound to improve inhibitory efficacy and enable targeted delivery, creating a prodrug. When exposed to visible light, this prodrug regenerates the active inhibitor, allowing for precise, light-controlled inhibition of IDO1 activity. The findings from this study may contribute to the development of photoresponsive prodrugs for IDO1-based immunotherapy aimed at combating cancer and Alzheimer's disease.

3.4. Experimental sections

3.4.1. Synthesis and characterization of compounds

3.4.1.1. General method for the synthesis of compounds 3.1(a–d)

To a stirring solution of tryptamine (1 equiv.) in a dry DCM (4 mL) solvent phenylisothiocyanate or phenylisocyanate (1 equiv.) was added and the solution was stirred for 4 h at room temperature. The reaction mixture was then extracted with EtOAc (3 × 20 mL), the combined organic layers were dried over anhydrous Na_2SO_4, and the solvent was evaporated under reduced pressure. The crude reaction mixture was purified through column chromatography using a gradient solvent system of ethyl acetate (0–5%) in hexane to obtain the pure product (yield: 63–76%).[11]

3.4.1.1.1. Synthesis of 1-(2-(1*H*-indol-3-yl)ethyl)-3-(4-fluorophenyl)urea (3.1a)

Following the general procedure as mentioned above, tryptamine (1 equiv.) and 1-fluoro-4-isocyanatobenzene (1 equiv.) yielded compound **3.1a** as pale-yellow solid with 73% yield. ^{1}H NMR (400 MHz, DMSO-d_6) δ ppm: ^{1}H NMR (400 MHz, DMSO-d_6) δ 10.77 (s, 1H), 8.94 (s, 1H), 7.51 (d, J = 7.8 Hz, 1H), 7.37–7.33 (m, 2H), 7.28 (d, J = 8.0 Hz, 1H), 7.11 (d, J = 2.3 Hz, 1H), 7.03–6.90 (m, 4H), 6.62–6.59 (m, 1H), 3.11 (s, 2H), 2.79 (t, J = 7.3 Hz, 2H). ^{13}C NMR (150 MHz, DMSO-d_6) δ ppm: 180.92, 161.13, 136.77, 127.42, 126.76, 122.68, 121.20, 118.51, 118.32, 115.49, 115.34, 111.75, 111.22, 53.72, 24.33. HRMS calcd. for $C_{17}H_{16}FN_3O$ $(M + H)^+$: 298.1350, obtained: 298.1350.

3.4.1.1.2. Synthesis of 1-(2-(1*H*-indol-3-yl)ethyl)-3-(4-fluorophenyl)thiourea (3.1b)

Following the general procedure, tryptamine (1 equiv.) and 1-fluoro-4-isothiocyanatobenzene (1 equiv.) yielded compound **3.1b** as white solid with 76% yield. ^{1}H NMR (600 MHz, $CDCl_3$) δ ppm: 8.07 (s, 1H), 7.68 (s, 1H), 7.58 (d, J = 7.9 Hz, 1H), 7.39 (d, J = 8.1 Hz, 1H), 7.25–7.22 (m, 1H), 7.14–7.11 (m, 1H), 6.96–6.95 (m, 1H), 6.89–6.88 (m, 4H), 5.88 (s, 1H), 3.98–3.95 (m, 2H), 3.09 (t, J = 6.6 Hz, 2H). ^{13}C NMR (150 MHz, $CDCl_3$) δ ppm: 180.71, 136.33, 127.62, 127.56, 127.15, 122.46, 122.12, 119.80, 118.68, 116.90, 116.75, 112.49, 111.27, 45.68, 24.29. HRMS calcd. for $C_{17}H_{16}FN_3S$ $(M + H)^+$: 328.1270, obtained: 328.1278.

3.4.1.1.3. Synthesis of 1-(2-(1*H*-indol-3-yl)ethyl)-3-(3,5-bis(trifluoromethyl)phenyl)thiourea (3.1c)

Following the general procedure, tryptamine (1 equiv.) and 1-isothiocyanato-3,5-bis(trifluoromethyl)benzene (1 equiv.) yielded compound **3.1c** as yellow solid with 69% yield. ^{1}H NMR (400 MHz, DMSO-d_6) δ ppm: 12.96 (s, 1H), 11.02 (s, 1H), 10.81 (d, J = 8.0 Hz, 1H), 8.49 (s, 2H), 7.60 (d, J = 7.8 Hz, 1H), 7.53 (s, 1H), 7.28 (d, J = 8.0 Hz, 1H), 7.16 (s, 1H), 7.01 (t, J = 7.5 Hz, 1H), 6.92 (t, J = 7.4 Hz, 1H), 3.67 (t, J = 7.8 Hz, 2H), 2.92 (t, J = 7.7 Hz, 2H). ^{13}C NMR (150 MHz, DMSO-d_6) δ ppm: 180.91, 143.86, 136.72, 130.34, 127.73, 124.81, 123.23, 123.01, 121.36, 118.93, 118.66, 115.01, 112.20, 111.81, 44.90, 24.77. HRMS calcd. for $C_{19}H_{15}F_6N_3S$ $(M + H)^+$: 432.0964, obtained: 432.0966.

3.4.1.1.4. Synthesis of 1-(2-(1*H*-indol-3-yl)ethyl)-3-(4-(trifluoromethyl)phenyl)thiourea (3.1d)

Following the general procedure, tryptamine (1 equiv.) and 1-isothiocyanato-4-(trifluoromethyl)benzene (1 equiv.) yielded compound **3.1d** as a pale-yellow solid with 63% yield. ^{1}H NMR (600 MHz, $CDCl_3$) δ ppm: 8.15 (s, 1H), 8.09 (s, 1H), 7.60 (d, J = 7.9 Hz, 1H), 7.41–7.38 (m, 3H), 7.25 (t, J = 7.6 Hz, 1H), 7.12 (t, J = 7.5 Hz, 1H), 6.99 (s, 1H),

6.93 (d, J = 8.1 Hz, 2H), 6.19 (s, 1H), 4.01 (s, 2H), 3.12 (t, J = 6.5 Hz, 2H). ^{13}C NMR (150 MHz, $CDCl_3$) δ ppm: 179.94, 139.32, 136.39, 127.02, 124.58, 123.67, 122.78, 122.65, 122.31, 122.30, 119.94, 118.62, 112.28, 111.40, 45.70, 24.15. HRMS calcd. for $C_{18}H_{16}F_3N_3S$ $(M + H)^+$: 364.1090, obtained: 364.1096.

3.4.1.1.5. General methods for Boc protection of tryptamine and tryptophan compounds (T1–2)

The di-*tert*-butyl decarbonate (1.5 equiv.) was added to the solution of tryptamine/tryptophan (1 equiv.) in DCM (5 mL) and stirred for 8 h at room temperature. The crude reaction mixture was then extracted with EtOAc (3 × 20 mL), the combined organic layers were dried over anhydrous Na_2SO_4, and the solvent was evaporated under reduced pressure. The reaction mixture was pure enough to proceed to the next step of reactions.[11]

3.4.1.1.6. General methods for methylation of Boc-protected tryptamine and tryptophan derivatives (T3–4)

To a stirring solution of **T1–2** (1 equiv.) and NaH (2 equiv.), in dry DMF (3 mL), methyl iodide (2 equiv.) was added dropwise. The reaction mixture was stirred at room temperature until the maximum starting material was consumed. The consumption of the starting was monitored by TLC. The reaction mixture was then extracted with EtOAc (4 × 20 mL), and ice water was used to remove the DMF. The combined organic layers were dried over anhydrous Na_2SO_4, and the solvent was evaporated under reduced pressure. The crude product was sufficient enough to proceed to the next step.[11]

3.4.1.1.7. General methods for deprotection of Boc group from compounds T5 and T6

To a stirring solvent mixture of TFA and DCM (10 mL, 1 : 3, v/v), compound **T3** or **T4** was added, and the reaction mixture was allowed to stir at room temperature until the maximum consumption of the starting material. The conversation of starting to the desired compound was monitored by TLC. TFA solvent was evaporated out from the reaction mixture under reduced pressure. The reaction mixture was then extracted with EtOAc (4 × 20 mL), and water was used to remove the excess TFA. The combined organic layers were dried over anhydrous Na_2SO_4, and the solvent was evaporated under reduced pressure. The crude product was sufficient enough to proceed to the next step.[12]

3.4.1.2. General procedure for the synthesis of thiourea/urea derivatives of *N*-methyltryptamine (3.2a–b)

To a stirring solution of *N*-methyltryptamine (**T6**) (1 equiv.) in dry DCM (3 mL), phenylisothiocyanate (1.2 equiv.) was added. The reaction mixture was allowed to stir for 6 h at room temperature, and thereafter, it was extracted with EtOAc (3 × 20 mL). The crude reaction mixture was purified through column chromatography using a gradient solvent system of ethyl acetate (0–5%) in hexane to obtain the pure product (yield: 60–71%).[11]

3.4.1.2.1. Synthesis of 1-(3,5-bis(trifluoromethyl)phenyl)-3-(2-(1-methyl-1*H*-indol-3-yl)ethyl)thiourea (3.2a)

Following the general procedure, 2-(1-methyl-1*H*-indol-3-yl)ethan-1-amine (**T6**) (1 equiv.) and 1-isothiocyanato-3,5-bis(trifluoromethyl)benzene (1 equiv.) yielded compound **3.2a** as yellow solid with 65% yield. ^{1}H NMR (600 MHz, DMSO-d_6) δ ppm: 11.94 (s, 1H), 10.06 (s, 1H), 8.44 (s, 2H), 7.67 (d, J = 7.7 Hz, 1H), 7.65 (s, 1H), 7.39 (d, J = 8.2 Hz, 1H), 7.21 (s, 1H), 7.15 (t, J = 7.7 Hz, 1H), 7.03 (t, J = 7.5 Hz, 1H), 3.74 (s, 3H), 2.98 (t, J = 7.7 Hz, 2H), 1.78 (s, 2H). ^{13}C NMR (150 MHz, DMSO) δ ppm: 180.91, 143.43, 137.13, 128.03, 127.71, 124.76, 122.96, 121.62, 121.55, 119.17, 118.80, 115.45, 111.43, 110.01, 44.93, 32.71, 24.61. HRMS calcd. for $C_{20}H_{17}F_6N_3S$ $(M + H)^+$: 446.1120, obtained: 446.1118.

3.4.1.2.2. Synthesis of 1-(2-(1-methyl-1*H*-indol-3-yl)ethyl)-3-(4-(trifluoromethyl)phenyl)thiourea (3.2b)

Following the general procedure, 2-(1-methyl-1*H*-indol-3-yl)ethan-1-amine (**T6**) (1 equiv.) and 1-isothiocyanato-4-(trifluoromethyl)benzene (1 equiv.) yielded compound **3.2b** as yellow solid with 62% yield. ^{1}H NMR (600 MHz, $CDCl_3$) δ ppm: 8.37 (s, 1H), 7.58 (d, J = 7.9 Hz, 1H), 7.39 (d, J = 8.2 Hz, 2H), 7.33 (d, J = 8.2 Hz, 1H), 7.29–7.26 (m, 1H), 7.11 (t, J = 7.4 Hz, 1H), 6.96 (d, J = 8.2 Hz, 2H), 6.83 (s, 1H), 6.23 (s, 1H), 3.98 (s, 2H), 3.71 (s, 3H), 3.09 (t, J = 6.6 Hz, 2H). ^{13}C NMR (150 MHz, $CDCl_3$) δ ppm: 179.80, 139.46, 137.18, 127.42, 127.10, 126.93, 124.60, 123.69, 122.80, 122.19, 119.39, 118.74, 110.59, 109.48, 45.74, 32.61, 24.05. HRMS calcd. for $C_{19}H_{18}F_3N_3S$ $(M + H)^+$: 378.1246, obtained: 378.1250.

3.4.1.2.3. Synthesis of 1-methyl-*N*α-((4-(trifluoromethyl)phenyl)carbamothioyl)tryptophan (3.2c)

To a stirring solution of 1-methyl-L-tryptophan (1 equiv.) in dry DMF (10 mL) solvent, 1-isothiocyanato-4-(trifluoromethyl)benzene (1 equiv.) was added. Triethylamine (0.5 mL) was added to the solution, and the reaction mixture was stirred for 5 h at room temperature. After completion of the reaction, it was extracted with EtOAc (3 × 20 mL)

and ice-cold water to remove the DMF from the reaction. The crude reaction mixture was purified through column chromatography using a gradient solvent system of ethyl acetate (0–5%) in hexane to obtain the pure product **3.2c** as a yellow solid with a 60% yield. ^{1}H NMR (600 MHz, DMSO-d_6) δ ppm: 11.15 (s, 1H), 8.55 (s, 1H), 7.92 (d, J = 8.3 Hz, 2H), 7.62 (d, J = 8.0 Hz, 1H), 7.54 (d, J = 8.4 Hz, 2H), 7.27 (d, J = 8.1 Hz, 1H), 7.04 (t, J = 7.5 Hz, 1H), 7.02 (s, 1H), 6.90 (t, J = 7.4 Hz, 1H), 4.65–4.63 (m, 1H), 3.61 (s, 3H), 3.20 (dd, J = 14.3, 3.7 Hz, 1H), 1.74 (s, 1H). ^{13}C NMR (150 MHz, DMSO) δ ppm: 178.44, 143.88, 136.65, 129.88, 129.32, 128.44, 127.18, 125.96, 125.94, 122.14, 121.15, 119.44, 118.53, 110.52, 109.57, 79.36, 49.07, 32.59. HRMS calcd. for $C_{20}H_{18}F_3N_3O_2S$ $(M + H)^+$: 422.1145, obtained: 422.1115.

3.4.1.2.4. Synthesis of 4-fluoro-*N*-(2-(1-methyl-1*H*-indol-3-yl)ethyl)benzamide (3.2d)

To a stirring solution of 2-(1-methyl-1*H*-indol-3-yl)ethan-1-amine (**T6**) (1 equiv.) in dry DCM (10 mL), 4-fluorobenzoic acid (1 equiv.), oxalyl chloride (2 equiv.) were added. To this solution, 20 µL of DMF was added to increase the solubility of the reactants. The reaction mixture was stirred for 2 h at room temperature. After maximum consumption of the starting materials, the reaction mixture was extracted with EtOAc (3 × 20 mL), the combined organic layers were dried over anhydrous Na_2SO_4, and the solvent was evaporated under reduced pressure. The crude reaction mixture was purified through column chromatography using a gradient solvent system of ethyl acetate (0–10%) in hexane to obtain the pure product **3.2d** as a white solid with a yield of 68%. ^{1}H NMR (400 MHz, $CDCl_3$) δ ppm: 7.99 (s, 1H), 7.97–7.94 (m, 2H), 7.65 (d, J = 7.3 Hz, 2H), 7.62 (s, 1H), 7.29 (d, J = 8.2 Hz, 1H), 7.21–7.19 (m, 1H), 7.09–7.06 (m, 1H), 6.94 (d, J = 1.7 Hz, 1H), 3.74 (d, J = 1.6 Hz, 3H), 3.71–3.68 (m, 2H), 3.09–3.05 (m, 2H). ^{13}C NMR (150 MHz, $CDCl_3$) δ ppm: 170.96, 143.12, 141.79, 137.04, 132.67, 132.65131.59, 129.95, 126.37, 123.65, 123.54, 116.53, 114.08, 45.68, 37.37, 29.91. HRMS calcd. for $C_{18}H_{17}FN_2O$ $(M+H)^+$: 297.1398, obtained: 297.1389.

3.4.1.2.5. Synthesis of 4-methyl-*N*-(2-(1-methyl-1*H*-indol-3-yl)ethyl)benzenesulfonamide (3.2e)

To the stirring solution of 2-(1-methyl-1*H*-indol-3-yl)ethan-1-amine (**T6**, 1 equiv.) in dry DCM (10 mL), 4-methylbenzenesulfonyl chloride (1 equiv.) and tryethylamine (1 equiv.) was added. The reaction mixture was stirred for 4 h at room temperature. After maximum consumption of the starting materials, the reaction mixture was extracted with EtOAc (3 × 20 mL), the combined organic layers were dried over anhydrous Na_2SO_4, and the solvent was evaporated under reduced pressure. The crude reaction mixture was

purified through column chromatography using a gradient solvent system of ethyl acetate (0–10%) in hexane to obtain the pure product **3.2e** as a white solid with a yield of 71%. ^{1}H NMR (600 MHz, $CDCl_3$) δ ppm: 7.67 (d, J = 8.3 Hz, 2H), 7.43 (d, J = 7.9 Hz, 1H), 7.31 (d, J = 8.2 Hz, 1H), 7.25 (t, J = 7.4 Hz, 3H), 7.10–7.07 (m, 1H), 6.85 (s, 1H), 4.65 (t, J = 6.1 Hz, 1H), 3.74 (s, 3H), 3.28 (d, J = 6.4 Hz, 2H), 2.94 (t, J = 6.7 Hz, 2H), 2.43 (s, 3H). ^{13}C NMR (150 MHz, $CDCl_3$) δ ppm: 143.30, 137.15, 136.81, 129.65, 127.39, 127.35, 127.06, 121.82, 119.00, 118.65, 109.99, 109.40, 43.25, 32.68, 25.41, 21.56. HRMS calcd. for $C_{18}H_{20}N_2O_2S$ $(M + H)^+$: 329.1318, obtained: 329.1300.[17]

3.4.1.3. General method for synthesis of Boc-protected azole derivatives of *N*-methyltryptamine (T7 and T8)

To the stirring solution of *tert*-butyl(2-(1-methyl-1*H*-indol-3-yl)ethyl)carbamate (**T4**) (1 equiv.) in a solvent mixture of dioxane: NH_4COOH (6 mL; 1 : 1, v/v), imidazole or tetrazole was added in presence of I_2. The reaction mixture was stirred for 2 h at room temperature to get a white solid precipitate as the desired product. The crude solid was sufficiently pure to proceed to the next step.[7]

3.4.1.4. General methods for Boc-deprotection of azole derivatives of *N*-methyltryptamine (T9–10)

To a stirring solvent mixture of TFA and DCM (10 mL; 1 : 3, v/v), compound **T7** or **T8** was added and stirred at room temperature until maximum consumption of the starting material. The conversation of starting to the desired compound was monitored by TLC. TFA solvent was evaporated out from the reaction mixture under reduced pressure. The reaction mixture was then extracted with EtOAc (4 × 20 mL), and water was used to remove the excess TFA. The combined organic layers were dried over anhydrous Na_2SO_4, and the solvent was evaporated under reduced pressure. The crude product was sufficient enough to proceed to the next step.

3.4.1.5. General methods for synthesis of thiourea derivatives of 2-azole substituted tryptamine (3.3a–b)

To the stirring solution of **T9** or **T10** (1 equiv.) in dry DCM (3 mL) 1-isothiocyanato-4-(trifluoromethyl)benzene (1.2 equiv.) was added. The reaction mixture was allowed to stir for 6–7 h at room temperature, and thereafter, it was extracted with EtOAc (3 × 20 mL). The combined organic layers were dried over anhydrous Na_2SO_4, and the solvent was evaporated under reduced pressure. The crude reaction mixture was purified through column chromatography using a gradient solvent system of ethyl acetate (0–5%) in hexane to obtain the pure products.

3.4.1.5.1. Synthesis of 1-(2-(2-(1*H*-imidazol-1-yl)-1-methyl-1*H*-indol-3-yl)ethyl)-3-(4-(trifluoromethyl)phenyl)thiourea (3.3a)

Following the general procedure, 2-(2-(1*H*-imidazol-1-yl)-1-methyl-1*H*-indol-3-yl)ethan-1-amine, (**T9**, 1 equiv.) and 1-isothiocyanato-4-(trifluoromethyl)benzene (1.2 equiv.) yielded compound **3.3a** as a pale-yellow solid with 57% yield. ^{1}H NMR (600 MHz, DMSO-d_6) δ ppm: 9.90 (s, 1H), 9.24 (s, 1H), 8.13–8.10 (m, 2H), 7.76 (d, J = 7.8 Hz, 1H), 7.68 (s, 1H), 7.66 (s, 1H), 7.64 (d, J = 5.1 Hz, 3H), 7.60 (s, 1H), 7.38–7.36 (m, 1H), 7.30 (t, J = 7.4 Hz, 1H), 3.99 (s, 3H), 3.85–3.81 (m, 2H), 3.02 (t, J = 7.2 Hz, 2H). ^{13}C NMR (150 MHz, DMSO-d_6) δ ppm: 180.83, 152.58, 151.32, 143.55, 135.40, 130.67, 126.60, 126.57, 126.15, 125.12, 123.33, 123.28, 122.45, 119.96, 119.11, 118.62, 115.16, 54.45, 43.97, 24.21. ^{19}F NMR (565 MHz, DMSO-d_6) δ ppm: 60.46. HRMS calcd. for $C_{22}H_{20}F_3N_5S$ $(M + H)^+$: 444.1464, obtained: 444.1487.

3.4.1.5.2. Synthesis of 1-(2-(1-methyl-2-(1*H*-tetrazol-1-yl)-1*H*-indol-3-yl)ethyl)-3-(4-(trifluoromethyl)phenyl)thiourea (3.3b)

Following the general procedure, 2-(1-methyl-2-(1*H*-tetrazol-1-yl)-1*H*-indol-3-yl)ethan-1-amine, (**T10**, 1 equiv.) and 1-isothiocyanato-4-(trifluoromethyl)benzene (1.2 equiv.) yielded compound **3.3b** as an off-white solid with 54% yield. ^{1}H NMR (400 MHz, DMSO-d_6) δ ppm: 8.17 (s, 1H), 8.04 (s, 1H), 7.57 (d, J = 7.8, 1H), 7.50 (s, 2H), 7.42 (s, 1H), 7.39–7.35 (m, 1H), 7.28–7.24 (m, 1H), 7.07 (d, J = 8.2 Hz, 2H), 6.19 (s, 1H), 4.03 (s, 3H), 4.01–3.97 (m, 2H), 3.08–3.05 (m, 2H). ^{13}C NMR (150 MHz, $CDCl_3$) δ ppm: 180.32, 139.34, 135.59, 129.97, 127.18, 127.15, 125.19, 124.52, 123.19, 123.08, 122.71, 119.02, 118.07, 115.40, 53.88, 44.97, 24.16. HRMS calcd. for $C_{20}H_{18}F_3N_7S$ $(M + Na)^+$: 468.1189, obtained: 468.1174.

3.4.1.5.3. Synthesis of 3-(4,5-dimethoxy-2-nitrobenzyl)-1-(1-methyl-3-(2-(3-(4-(trifluoromethyl)phenyl)thioureido)ethyl)-1*H*-indol-2-yl)-1*H*-imidazol-3-ium (3.4)

To a stirring solution of 1-(2-(2-(1*H*-imidazol-1-yl)-1-methyl-1*H*-indol-3-yl)ethyl)-3-(4-(trifluoromethyl)phenyl)thiourea (**3.3a**, 1 equiv.) in toluene (5 mL) 1-(bromomethyl)-4,5-dimethoxy-2-nitrobenzene (1.2 equiv.) was added and stirred at room temperature for 24 h. The reaction mixture is extracted with EtOAc (3 × 20 mL). The combined organic layers were dried over anhydrous Na_2SO_4, and the solvent was evaporated under reduced pressure. The crude reaction mixture was purified through column chromatography using a gradient solvent system of ethyl acetate (0–5%) in hexane to obtain the pure product **3.4** as a yellow solid with 47% yield. ^{1}H NMR (600 MHz, $CDCl_3$) δ ppm: 8.17 (s, 1H), 8.07 (s, 1H), 7.59 (s, 2H), 7.49 (d, J = 7.9 Hz, 1H), 7.44

(d, J = 8.3 Hz, 1H), 7.40 (d, J = 8.2 Hz, 2H), 7.35 (d, J = 8.8 Hz, 1H), 7.27 (t, J = 7.6 Hz, 1H), 7.18 (d, J = 7.6 Hz, 1H), 7.07 (d, J = 8.1 Hz, 2H), 6.87 (s, 1H), 6.30 (s, 1H), 4.79 (s, 2H), 3.95 (d, J = 2.2 Hz, 3H), 3.92 (s, 3H), 3.88 (s, 3H), 3.78 (s, 2H), 2.98 (t, J = 6.8 Hz, 2H). ^{13}C NMR (150 MHz, $CDCl_3$) δ ppm: 180.41, 153.26, 151.27, 148.97, 140.27, 140.07, 139.72, 130.02, 127.46, 126.98, 126.82, 126.01, 125.12, 124.58, 123.81, 123.14, 123.06, 119.04, 118.76, 118.12, 115.35, 113.72, 108.60, 56.56, 56.48, 53.84, 44.83, 30.08, 24.19. ^{19}F NMR (565 MHz, DMSO-d_6) δ ppm: 60.47. HRMS calcd. for $C_{31}H_{30}F_3N_6O_4S^+$: 639.1996, obtained: 639.2020.

3.4.2. Enzyme activity assay

3.4.2.1. Purification of holo-human tryptophan 2,3-dioxygenase and human indoleamine 2,3-dioxygenase 1

The enzymes hTDO and hIDO1 were purified according to established protocols.[8, 10, 13] The cDNAs of human IDO1 and TDO were transformed into *Escherichia coli* (BL21-DE3 strain) cells to express recombinant human IDO1 and TDO enzymes (with N-terminus 6× histidine-tag). A single colony of *Escherichia coli* cells was cultured for 12–14 h at 37 °C and 180 rpm after being injected in 5 mL of Luria-Bertani (LB) medium that included 50 μg mL^{-1} kanamycin. To reach an OD_{600} of 0.6 of the culture media, 1 mL of the overnight culture was added to 1 L of the same culture media, including antibiotics and incubated at 37 °C and 120 rpm. After adding hemin (10 μM) and L-tryptophan (1 mM) to the culture medium, the mixture was incubated for 20 to 30 minutes at 37 °C until the OD_{600} reached 0.9 to 1.0. Isopropyl β-D-1 thiogalactopyranoside (IPTG, 0.5 mM) was added to stimulate protein expression after cooling down the culture media. The induced cells were cultured for 16–18 h at 120 rpm and 22 °C. Centrifugation was used to recover the cell pellet, which was then re-suspended in 20 mL of ice-cold phosphate-buffered saline (PBS), centrifuged once more to eliminate hemin (15 000 rpm for 10 minutes at 4 °C), and the cell pellet was stored at −80 °C.

For enzyme purification, the stored pellet was re-suspended in 15 mL of ice-cold 50 mM potassium phosphate buffer (KPB) at pH 7.2 containing 300 mM KCl, 10 mM magnesium chloride ($MgCl_2$), 25 mM imidazole, 5% glycerol, protease inhibitors (complete EDTA free), and DNase (<1 mg). Then, the cells were disrupted on ice, and the cell lysate was centrifuged at 20 000 rpm for 30 minutes at 4 °C. The reddish supernatant was then filtered *via* a 0.22 μm filter. Nickel-nitrilotriacetic acid resin (Qiagen, 1 mL) was added to the reddish supernatant and incubated for 2 h at 4 °C and 80 rpm. After pouring the liquid into the column, it was equilibrated with 50 mM KPB containing 300 mM KCl,

25 mM imidazole, and 5% glycerol at pH 7.2. The non-specifically bound protein was eliminated by gradually washing the column with 10 mL of KPB at pH 7.2, which included 300 mM KCl, 60 mM imidazole, and 5% glycerol. 50 mM KPB at pH 7.2, 300 mM KCl, 190 mM imidazole, and 5% glycerol were used to elute the protein. The eluted buffer of the IDO1 and TDO proteins was exchanged using a Sephadex-G25 column with 50 mM KPB at pH 6.8 with 150 mM KCl and 10% glycerol. The Coomassie blue-stained SDS-PAGE screening method was used to evaluate the purity of enzymes. Furthermore, the absorbance ratio at 404 nm/280 nm was used to test the purity of the IDO1 and TDO enzymes, and the results showed that they were 1.4 and 1.1, respectively.

3.4.2.2. Indoleamine 2,3-dioxygenase 1 and tryptophan 2,3-dioxygenase inhibition assay by the spectrometric method

Following the methods that were described, spectrophotometric measurements were used to examine the inhibitory activities of the IDO1 and TDO enzymes.[4, 8, 10, 13] Before the dilution with buffer, the compounds were first dissolved in DMSO. The ideal amount for the test procedure was found to be 1% DMSO. A standard reaction mixture including KPB buffer (100 mM, pH 6.5), sodium ascorbate (20 mM), methylene blue (10 μM), bovine liver catalase (240 nM), and L-Trp (150 μM) was diluted (5×) to 500 μL. Serial dilution was used to modify the inhibitor concentration. After that, the reaction mixture was incubated for 1 h at 37 °C. After adding 100 μL of 30% (w/v) trichloroacetic acid, we quenched the reaction and allowed the mixture to sit at 65 °C for an additional 15 minutes. By adding paradimethylaminobenzaldehyde (pDMAB; 2% (w/v) in acetic acid) and using a UV-vis spectrophotometer to measure the absorbance at 480 nm, we were able to quantify the amount of kynurenine produced. There was no significant interference in the absorption spectra of UV-active thiourea, urea and azole derivatives (50 μM) in this spectrophotometric study of IDO1/TDO activity.

3.4.3. Protein–ligand binding studies

3.4.3.1. UV-vis spectroscopic measurement

To investigate the binding ability of the potent compound to the enzyme and its aptitude in interacting with the heme group of the enzyme, we conducted UV-vis-based spectroscopic analyses.[8] The absorbance spectra were recorded using an EVOLUTION 201 spectrophotometer. All experiments were performed at 37 °C in a 100 mM KPB buffer at pH 6.5, using purified hIDO1 enzyme. Sodium disulfite (Na_2SO_3) was introduced into the solution after purging it with nitrogen gas to establish a deoxygenation reaction system. We determined the heme dissociation rate from the IDO1 enzyme by measuring the Soret

peak at 404 nm. To assess the absorbance of the compound **3.3a**, we utilized UV-visible spectroscopy to record its absorbance in a 5% DMSO KPB buffer.

3.4.3.2. Binding analysis by surface plasmon resonance analysis

Surface plasmon resonance (SPR) analysis was performed to determine the binding affinity of compound **3.3a** for IDO1 protein.[8] The temperature was maintained at 25 °C while measurements were taken using the Biacore-X100 device with the CM5 sensor chip (GE Healthcare). A phosphate-buffered saline (PBS) solution (pH 7.4) with 1% DMSO was used as the operating buffer. EDC-NHS coupling was used to apply an anti-His antibody to the surface of the CM5 sensor chip in flow cells 1 and 2 (FC-1 and FC-2). The surface was coated with both the His-tagged IDO1 proteins in flow cell 2 (FC-2). By measuring the change in response unit in both the flow cell and taking the difference, *i.e.* (FC-2)–(FC-1), the binding efficacy of compound **3.3a** was then evaluated. This was accomplished by employing a variable concentration of compound **3.3a** (from 0 to 10 μM) at a 30 μL per minute flow rate in the built-in kinetics/affinity experiment in the Biacore X100 control software. Using the built-in Biacore Insight Evaluation program, the equilibrium dissociation constant (K_D) value of compound **3.3a** to IDO1 was calculated.

3.4.4. Cell viability analysis

HeLa and HEK-293 cells were tested for viability assay using the MTT (3-(4,5-dimethylthiazol-2-yl)-2,5-diphenyltetrazolium bromide) assay, both with and without drugs. In a 96-well tissue culture plate, 10 000 cells were plated in 1 mL of DMEM/F12 complete medium at 37 °C with 5% CO_2.[4, 8] The cells were cultured for 12 h before being rinsed in PBS buffer. Following their addition to the incomplete medium, the compounds (0.5 μM to 30 μM) were cultured for 48 h at 37 °C with 5% CO_2. The culture mix was then supplemented with 100 μL of MTT dye (5 mg mL^{-1} in PBS) and incubated for another 4 h. The MTT solution was drained, and the formazan crystals were dissolved in 100 μL cell culture grade DMSO. The absorbance was measured at 570 and 600 nm using a FLoid® Cell Imaging Station spectrophotometer. The absorbance of the formazan crystals was used to determine the viability of cells. The viability of the cells was determined using the absorbance of formazan crystals. The stability of prodrug **3.4** was investigated under various physiological conditions such as water, Dulbecco's modified Eagle medium (DMEM) media, and fetal bovine serum (FBS) containing DMEM media (DMEF). HPLC analysis revealed that the prodrug remains stable in water, DMEM and DMEF for up to 48 hours.

3.4.5. Molecular docking and MD simulation studies

3.4.5.1. Simulation set-up and forcefield details

The Groningen Machine for Chemical Simulations (GROMACS) package version 2023 was used to perform all the molecular dynamics simulations presented in this study.[14] The leapfrog algorithm with a timestep of 2 fs was used to integrate the equation of motions in all the atoms for the protein–ligand in the water system. The cubic simulation box was periodic in all dimensions in all simulations. The CHARMM36 all-atom force field was used to model the protein (PDB ID: 4PK5), and the ligand (**3.3a**).[15, 16] CHARMM-modified TIP3P water model was used to solvate the protein. A cutoff distance of 1.2 nm was used to calculate short-range nonbonded Van der Waals and coulombic interactions. The long-range electrostatic interactions are calculated using the particle mesh Ewald (PME) method.[16] All hydrogen atoms in the protein, heme, and ligand are constrained using the LINCS algorithm.[17] The modified Berendsen thermostat with a time constant of 0.1 ps was used to control the temperature in the simulations in the NVT ensemble. The temperature and pressure in NPT simulations were controlled with a modified Berendsen thermostat and Parrinello-Rahman barostat with a time constant of 0.1 ps and 2 ps, respectively.[18]

3.4.5.2. MD simulation details

Using AutoDock Vina, we first conducted a docking analysis between chain B of IDO1 (PDB ID: 4PK5) and the compound **3.3a** ligand. The docked complex was then subjected to molecular dynamics simulation. This complex was solvated with 24 615 water molecules, and two sodium ions (Na) were added to neutralize the system. We performed energy minimization to eliminate any unfavorable contacts present in the solvated system. The minimized configuration was then equilibrated under NVT (constant number of particles, volume, and temperature) conditions for 0.1 ps, with a simulated temperature set to 300 K. The final configuration from this phase underwent further equilibration under NPT (constant number of particles, pressure, and temperature) conditions for an additional time constant of 0.1 ps and 2 ps respectively. Notably, both the protein and ligand structures were position-restrained during the NVT and initial NPT equilibration stages. Subsequently, we performed a production simulation without any position restraints for 100 ns, recording the trajectory every 100 ps. The simulation trajectory from the production phase was then used to calculate atom-wise distances between the protein and ligand, along with the root-mean-square deviations (RMSD) for both the protein and the ligand.

3.4.6. Photoresponsive prodrug to drug regeneration study

3.4.6.1. HPLC-based compound regeneration analysis

The compound **3.3a** was photoirradiated with light (λ_{ex} 400 nm) for 30 min. The extent of regeneration of compound **3.3a** from compound **3.4** was analyzed using a silica-based C18 HPLC column (2.7 μm). MeOH/H_2O was used as a mobile phase with optimized step gradient elution methods and a 0.5 mL per minute flow rate. The 365 nm and 254 nm lights were used as the detectors. The corresponding eluted solutions of peaks from HPLC traces were further characterized by HRMS analyses.

3.4.7. Stability study of the prodrug

3.4.7.1. HPLC-based stability analysis

Compound **3.4** was added to water, DMEM, and DMEF. The stability of the compound was studied at various time intervals using a silica-based C18 HPLC column (2.7 μm). ACN/H_2O was used as a mobile phase with optimized step gradient elution methods and a 0.5 mL per minute flow rate. The 365 nm and 254 nm lights were used as the detectors.

3.4.8. IDO1 activity study after photoirradiation

Irradiation of compound **3.4** using 400 nm light was conducted with 1 μM compound **3.4** in DMSO solution. The activity assay was performed according to the earlier section. In the activity study process, the concentration of compound **3.4** was kept constant, and the irradiation time was varied. In the activity assay, irradiated compound **3.4** is added to the KPB buffer (100 mM, pH 6.5) in the presence of the IDO1 enzyme. To it, a standard reaction mixture including sodium ascorbate (20 mM), methylene blue (10 μM), bovine liver catalase (240 nM), and L-Trp (150 μM) was diluted (5×) to 500 μL and added. After that, the reaction mixture was incubated for 1 h at 37 °C. Once the incubation was completed, it was followed by adding 100 μL of 30% (w/v) trichloroacetic acid to quench the reaction and allow the mixture to sit at 65 °C for an additional 15 minutes. By adding paradimethylaminobenzaldehyde (pDMAB; 2% (w/v) in acetic acid and using a UV-vis spectrophotometer, we measured the absorbance at 480 nm to quantify the amount of kynurenine produced (the irradiation time was 5, 10, 20, 30 minutes).

3.4.9. ^{1}H and ^{13}C NMR spectra of synthesized compounds

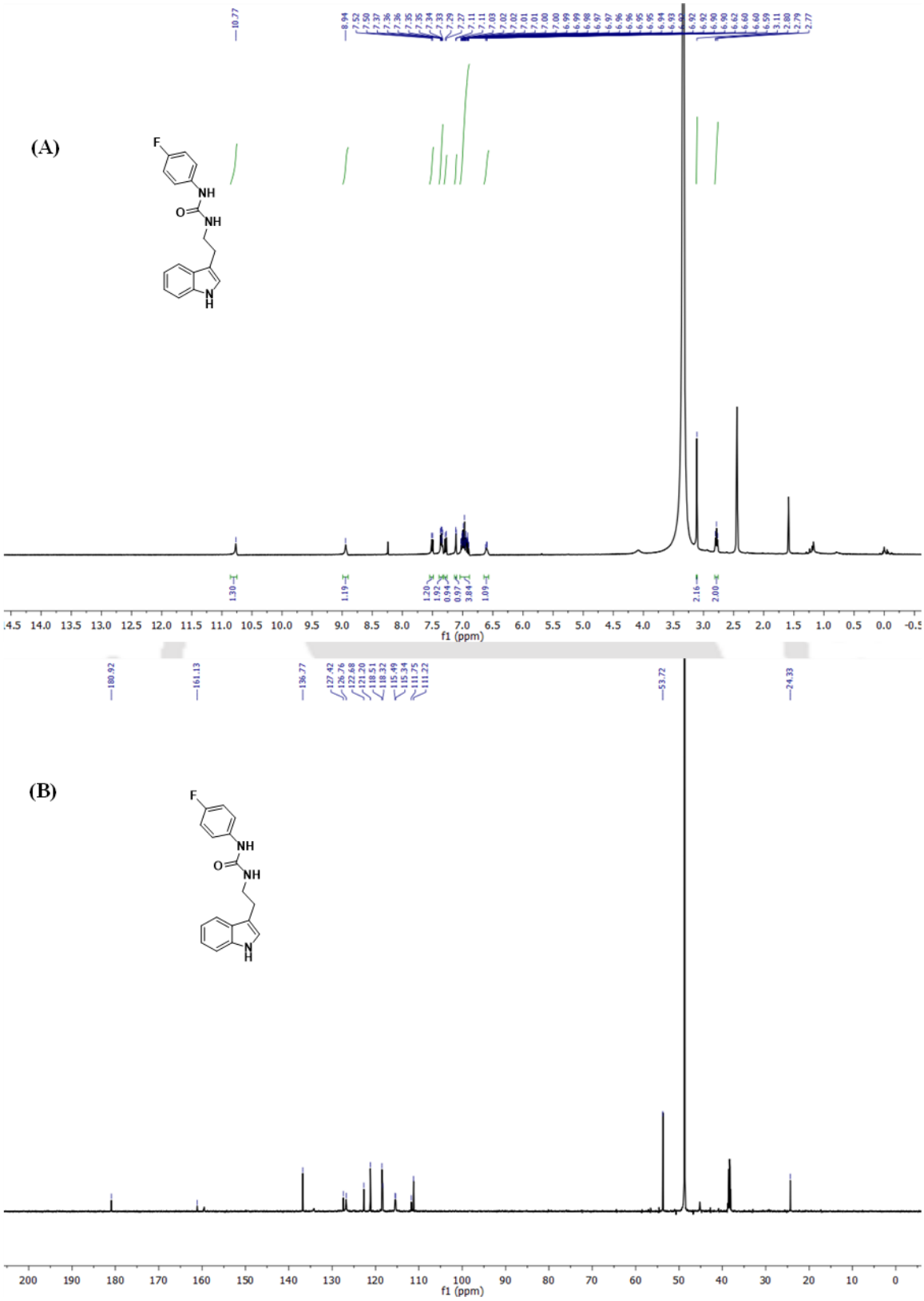

Fig. 3.9. ^{1}H NMR (A) and ^{13}C NMR (B) spectra of 1-(2-(1*H*-indol-3-yl)ethyl)-3-(4-fluorophenyl)urea (**3.1a**) in DMSO-d_6 solvent.

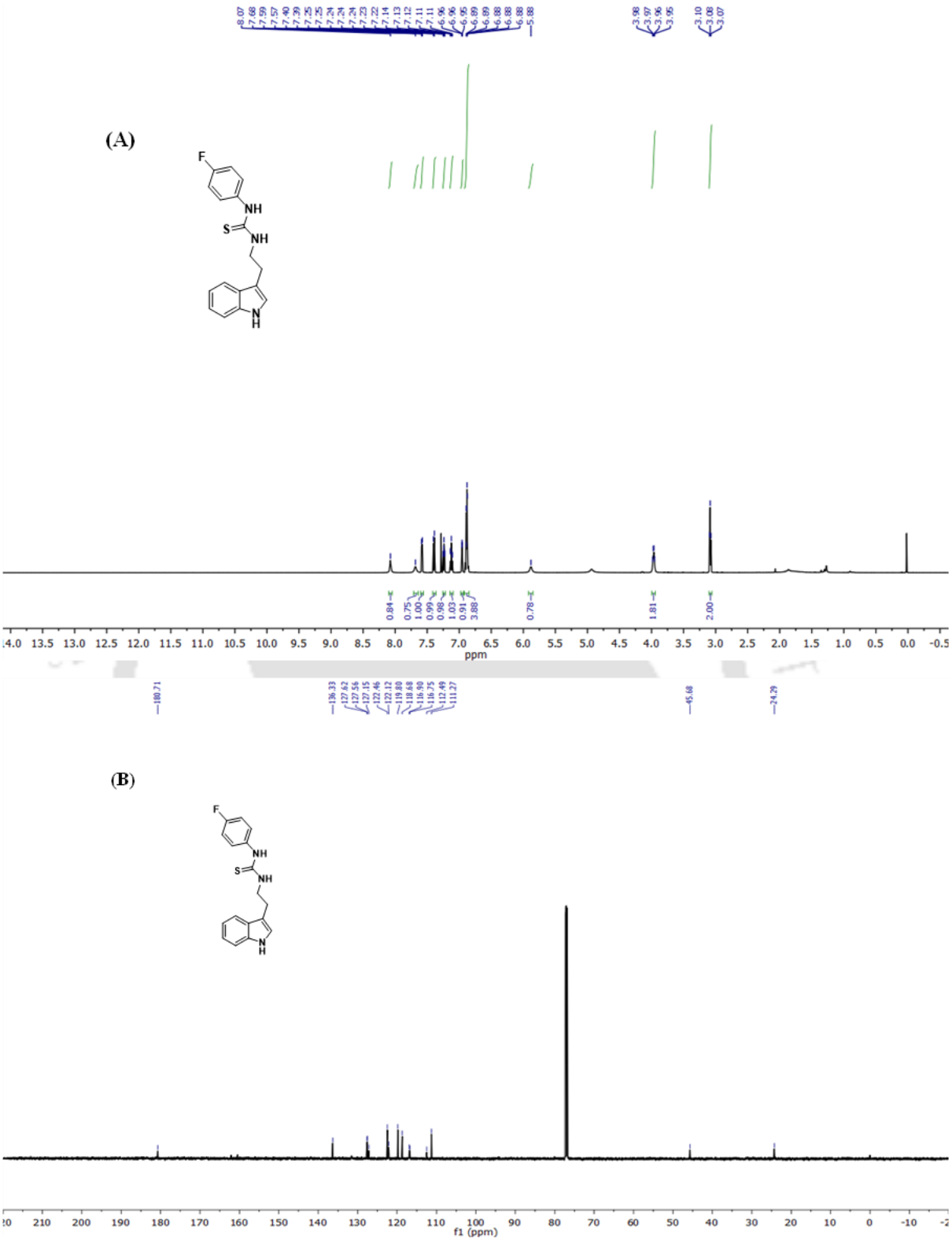

Fig. 3.10. ^{1}H NMR (A) and ^{13}C NMR (B) spectra of 1-(2-(1*H*-indol-3-yl)ethyl)-3-(4-fluorophenyl)thiourea (**3.1b**) in $CDCl_3$ solvent.

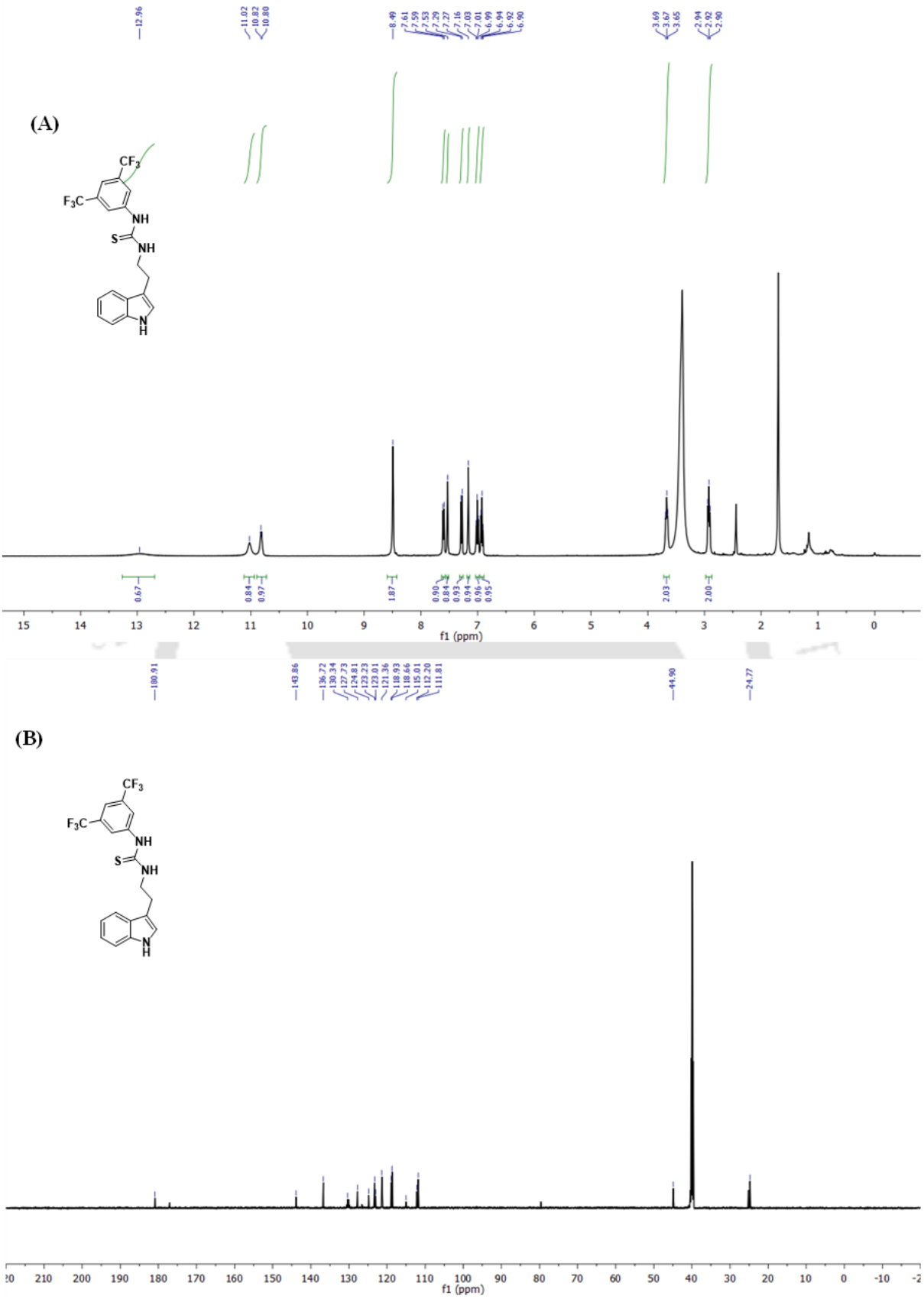

Fig. 3.11. ^{1}H NMR (A) and ^{13}C NMR (B) spectra of 1-(2-(1*H*-indol-3-yl)ethyl)-3-(3,5-bis(trifluoromethyl)phenyl)thiourea (**3.1c**) in DMSO-d_6 solvent.

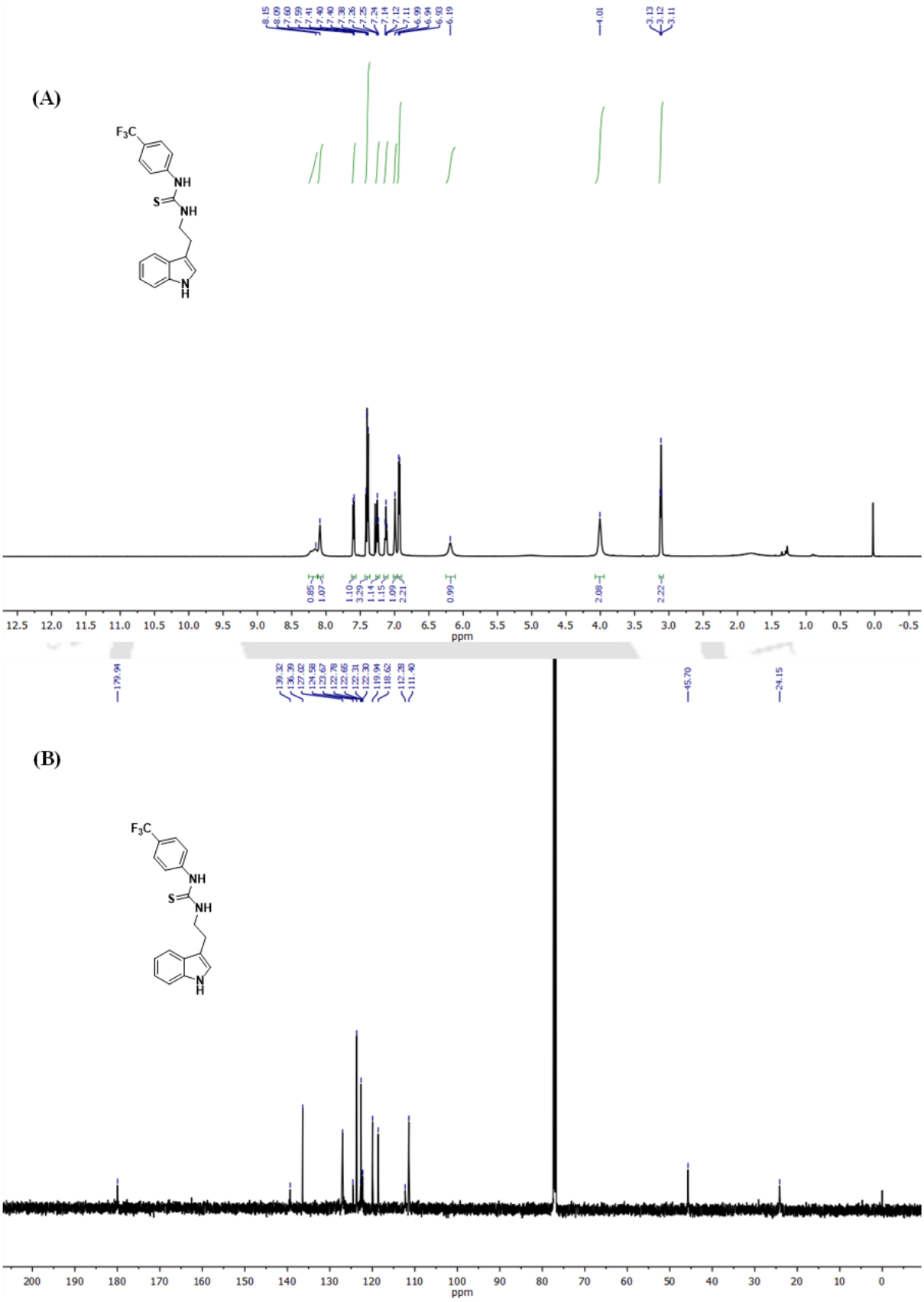

Fig. 3.12. ^{1}H NMR (A) and ^{13}C NMR (B) spectra of 1-(2-(1*H*-indol-3-yl)ethyl)-3-(4-(trifluoromethyl)phenyl)thiourea (**3.1d**) in $CDCl_3$ solvent.

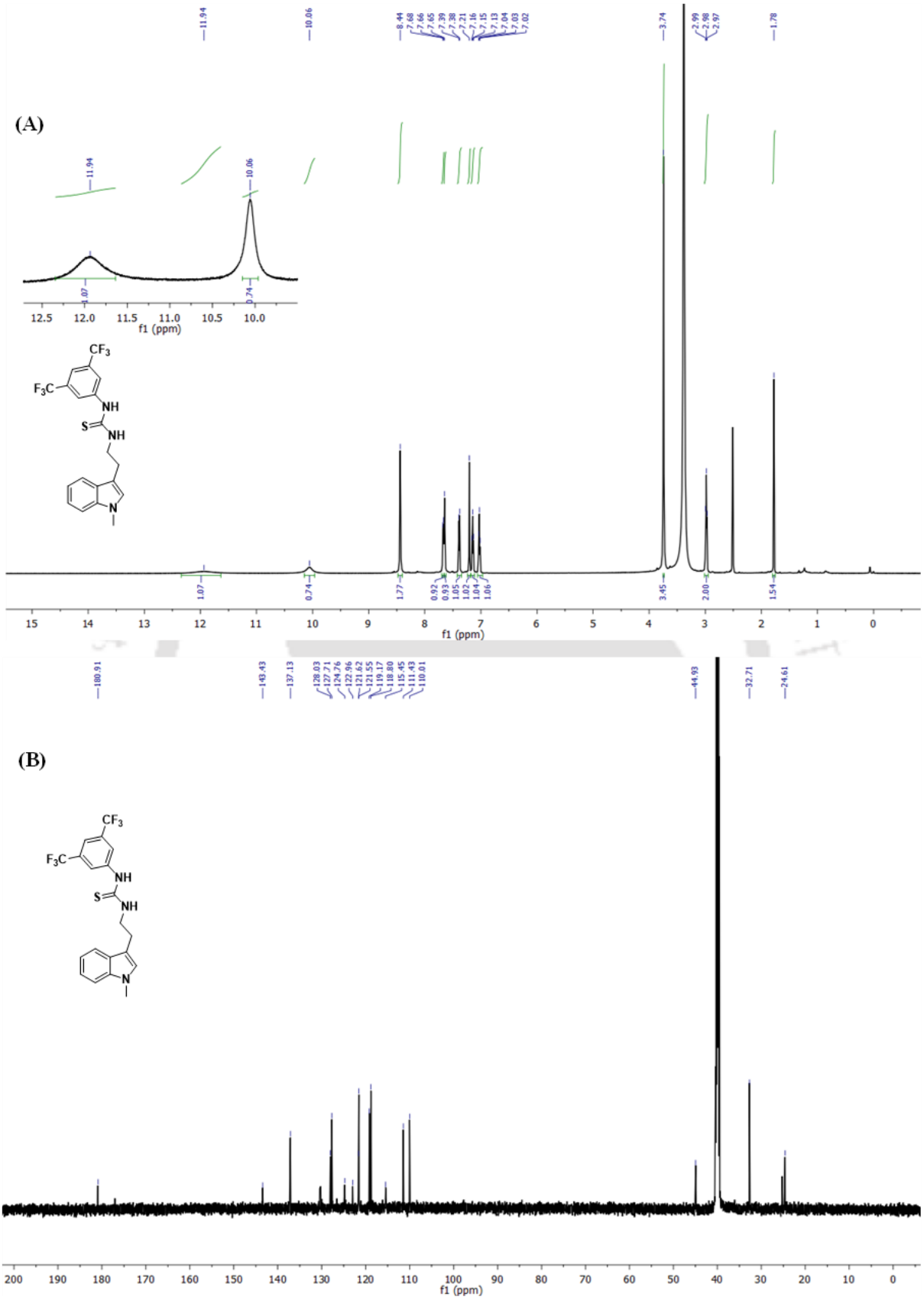

Fig. 3.13. ^{1}H NMR (A) and ^{13}C NMR (B) spectra of 1-(3,5-bis(trifluoromethyl)phenyl)-3-(2-(1-methyl-1*H*-indol-3-yl)ethyl)thiourea (**3.2a**) in DMSO-d_6 solvent.

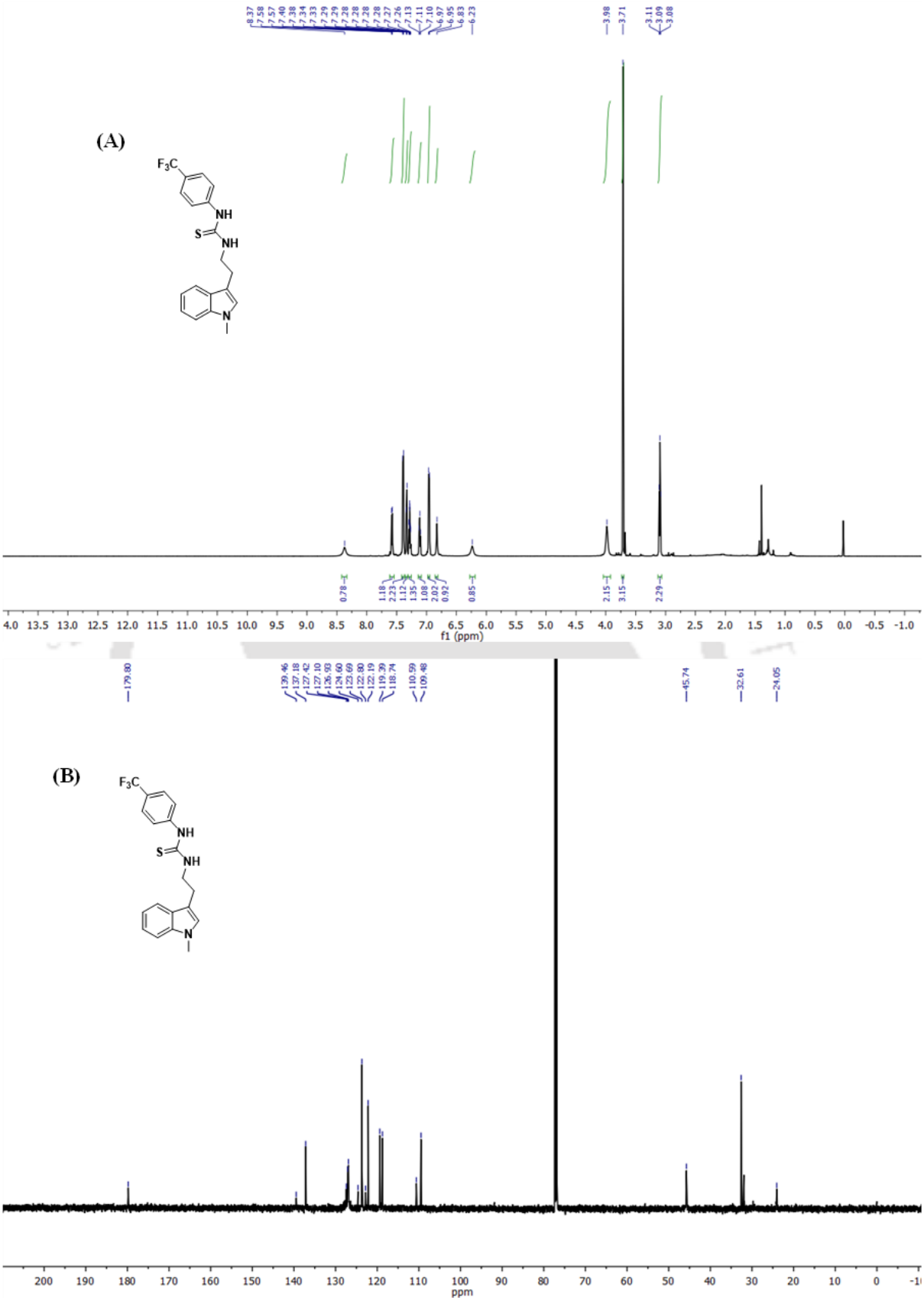

Fig. 3.14. ^{1}H NMR (A) and ^{13}C NMR (B) spectra of 1-(2-(1-methyl-1*H*-indol-3-yl)ethyl)-3-(4-(trifluoromethyl)phenyl)thiourea (**3.2b**) in $CDCl_3$ solvent.

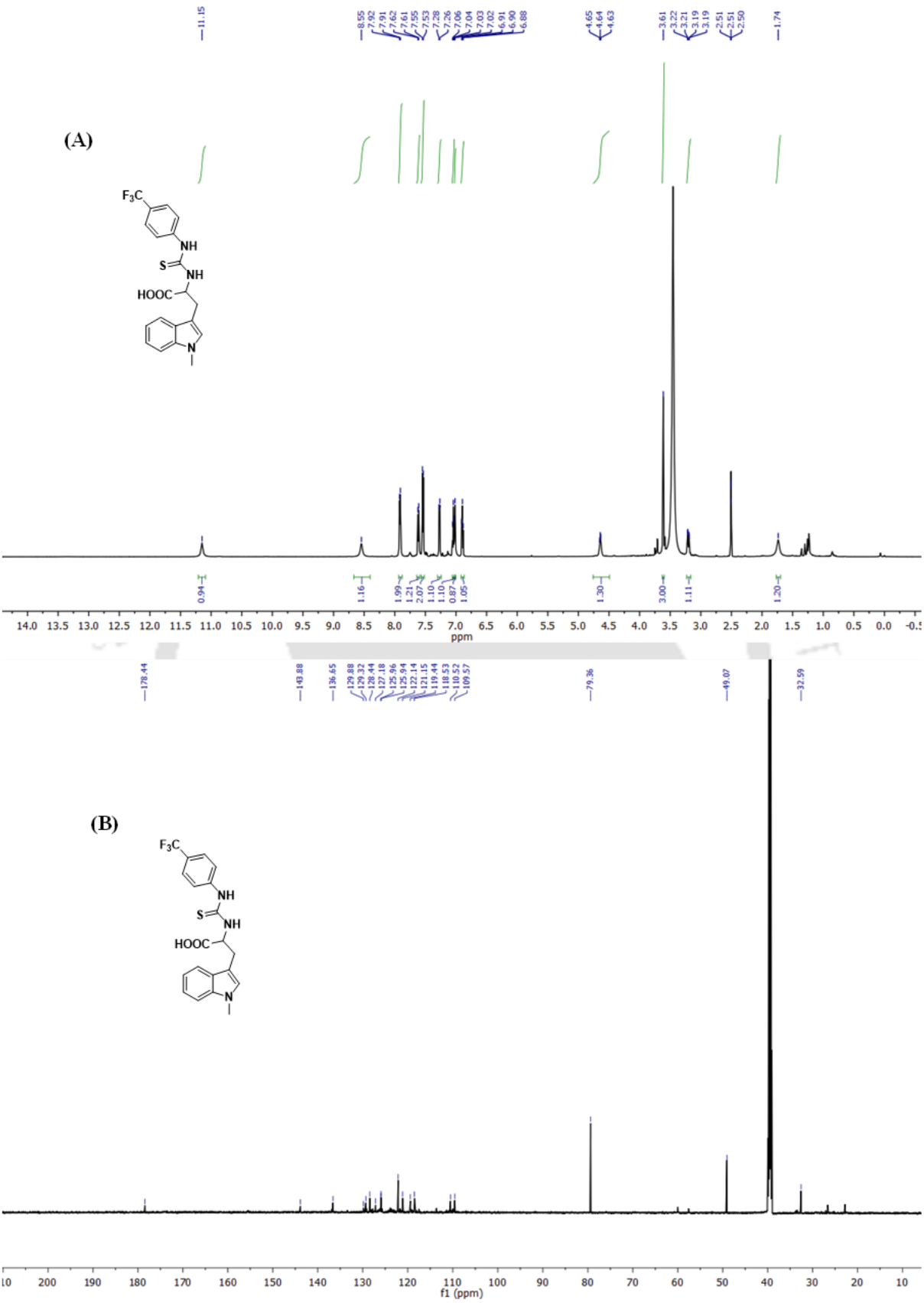

Fig. 3.15. ^{1}H NMR (A) and ^{13}C NMR (B) spectra of ((4-(trifluoromethyl)phenyl)carbamothioyl)tryptophan (**3.2c**) in DMSO-d_6 solvent.

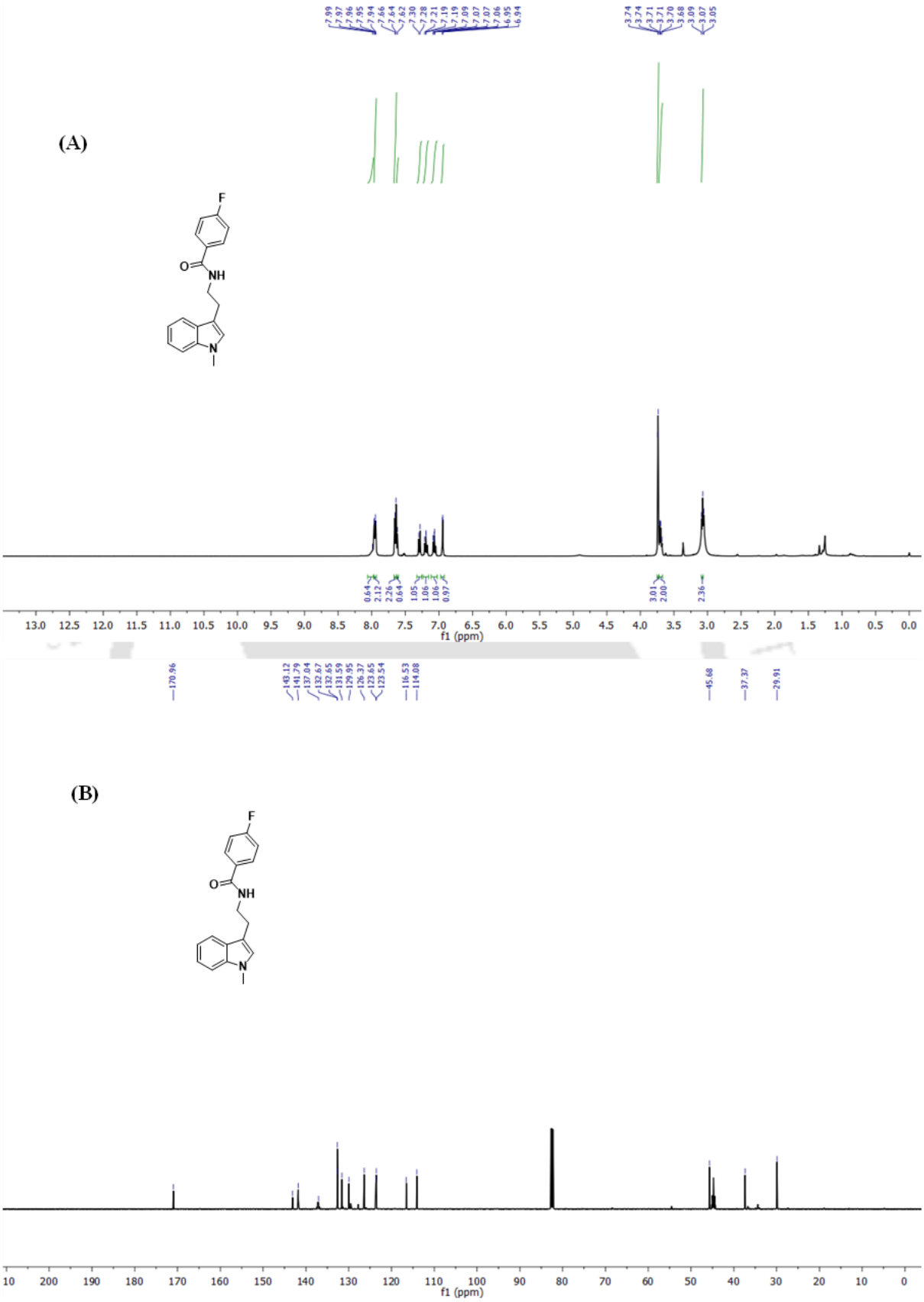

Fig. 3.16. ^{1}H NMR (A) and ^{13}C NMR (B) spectra of 4-fluoro-*N*-(2-(1-methyl-1*H*-indol-3-yl)ethyl)benzamide (**3.2d**) in $CDCl_3$ solvent.

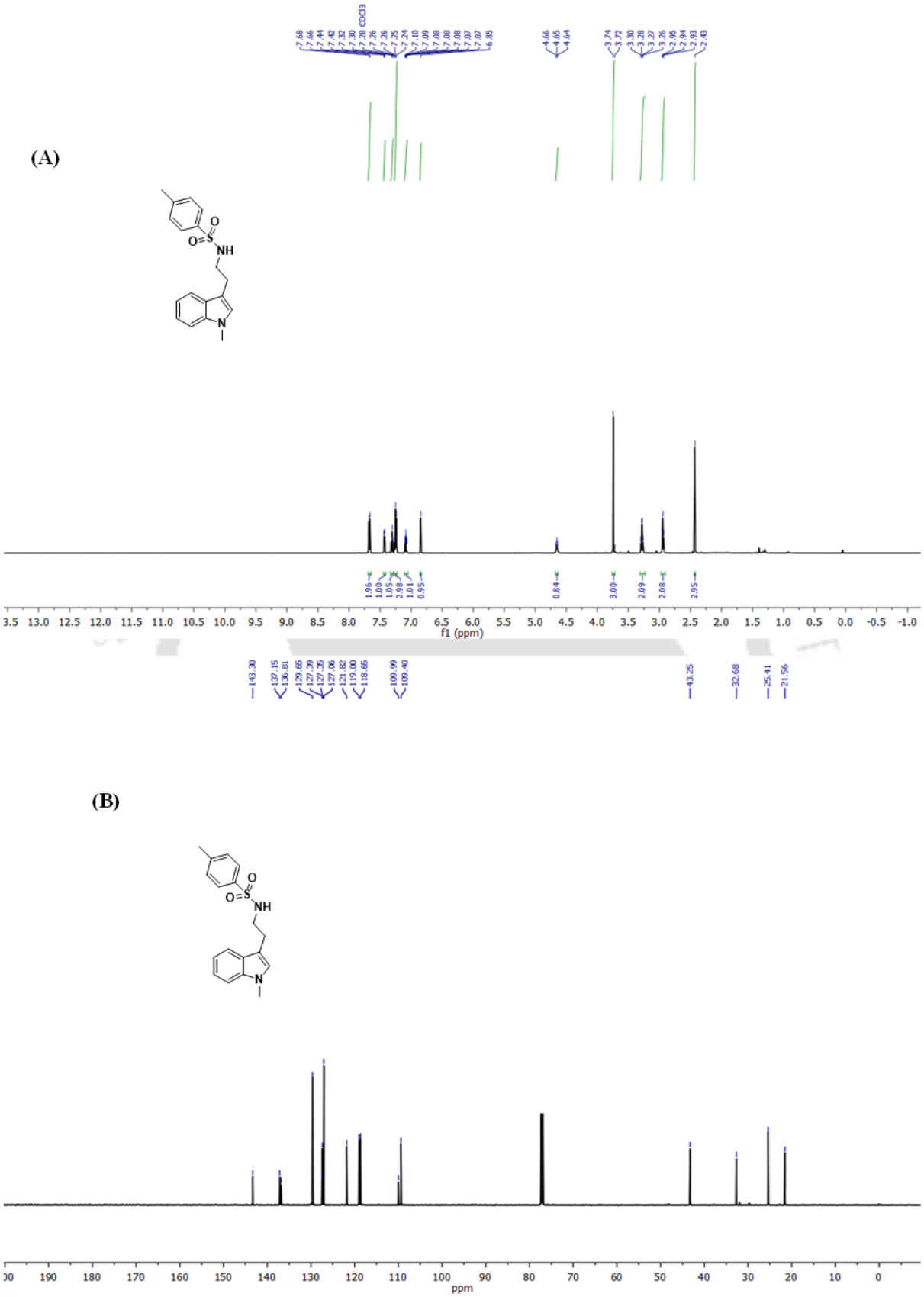

Fig. 3.17. ^{1}H NMR (A) and ^{13}C NMR (B) spectra of 4-methyl-*N*-(2-(1-methyl-1*H*-indol-3-yl)ethyl)benzenesulfonamide (**3.2e**) in $CDCl_3$ solvent.

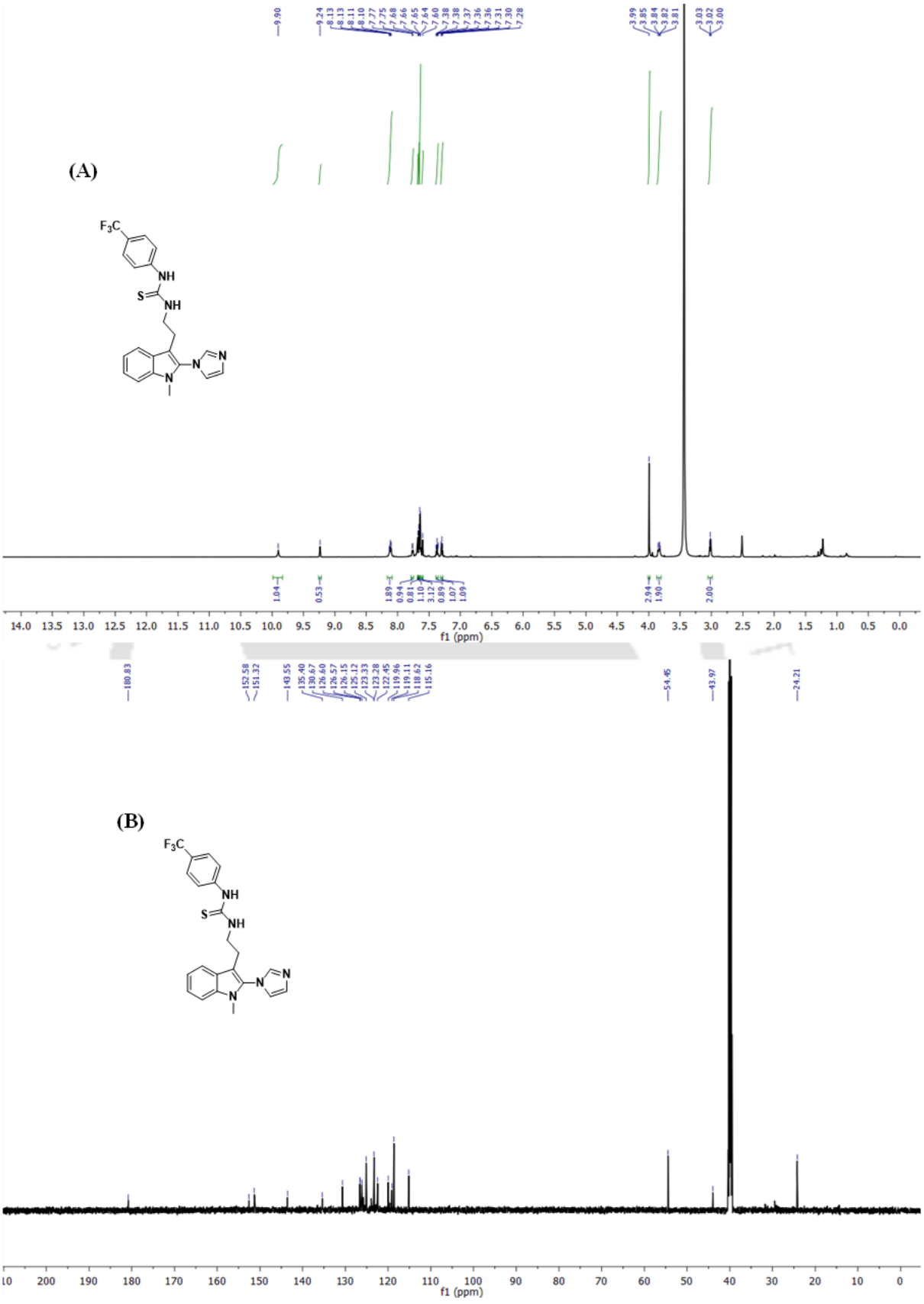

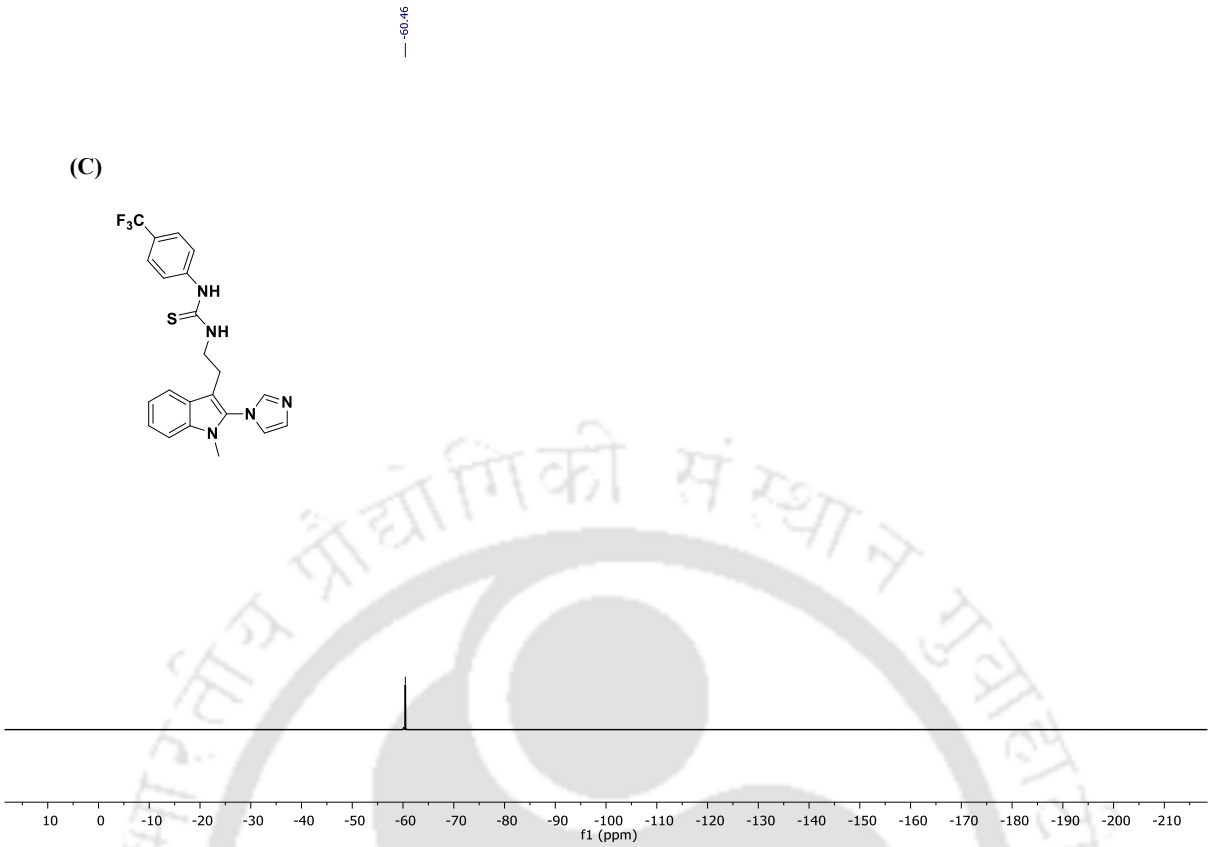

Fig. 3.18. ^{1}H NMR (A), ^{13}C NMR (B) and ^{19}F NMR (C) spectra of 1-(2-(2-(1*H*-imidazol-1-yl)-1-methyl-1*H*-indol-3-yl)ethyl)-3-(4-(trifluoromethyl)phenyl)thiourea (**3.3a**) in DMSO-d_6 solvent.

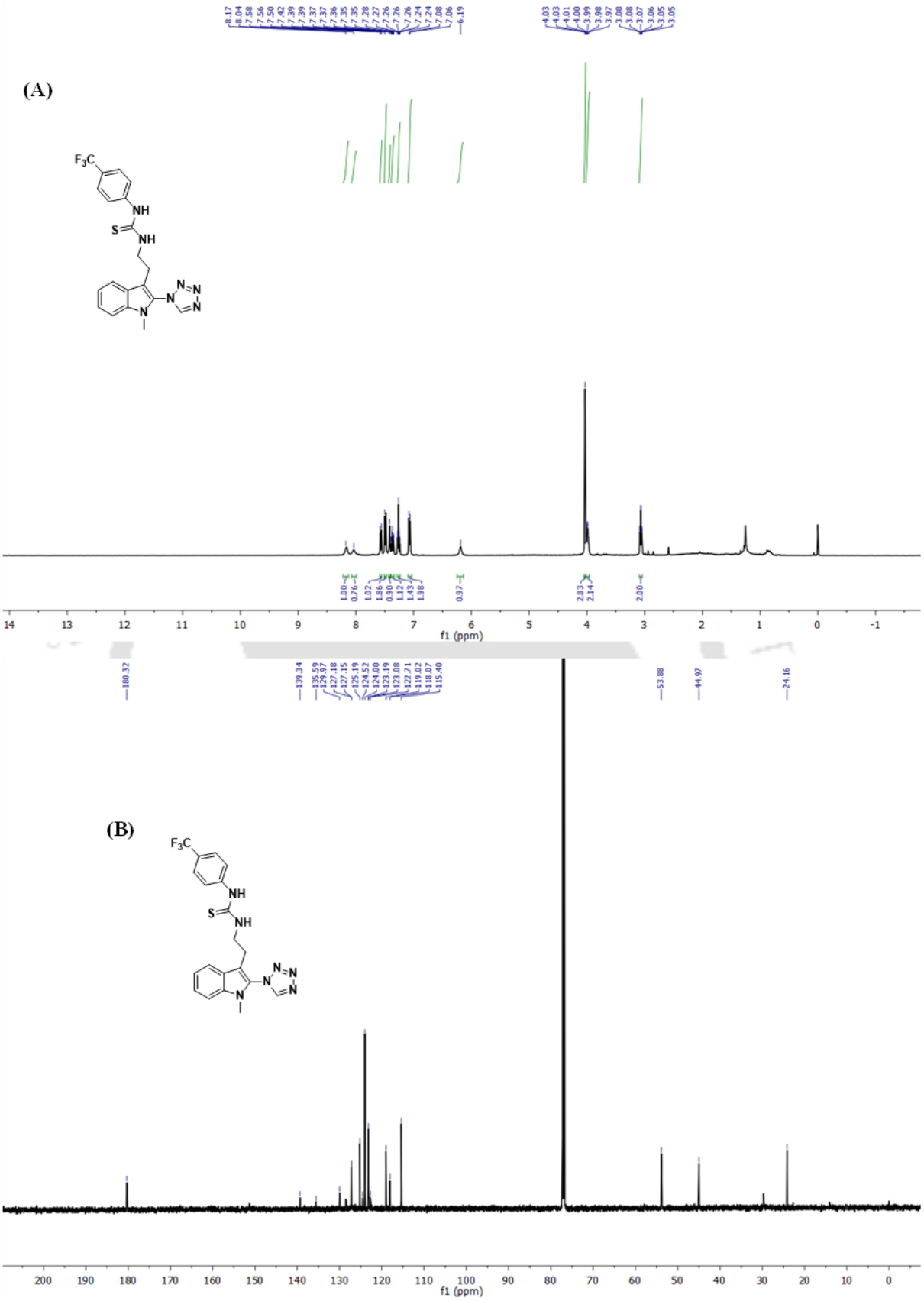

Fig. 3.19. ^{1}H NMR (A) and ^{13}C NMR (B) spectra of 1-(2-(1-methyl-2-(1*H*-tetrazol-1-yl)-1*H*-indol-3-yl)ethyl)-3-(4-(trifluoromethyl)phenyl)thiourea **(3.3b)** in DMSO-d_6 solvent.

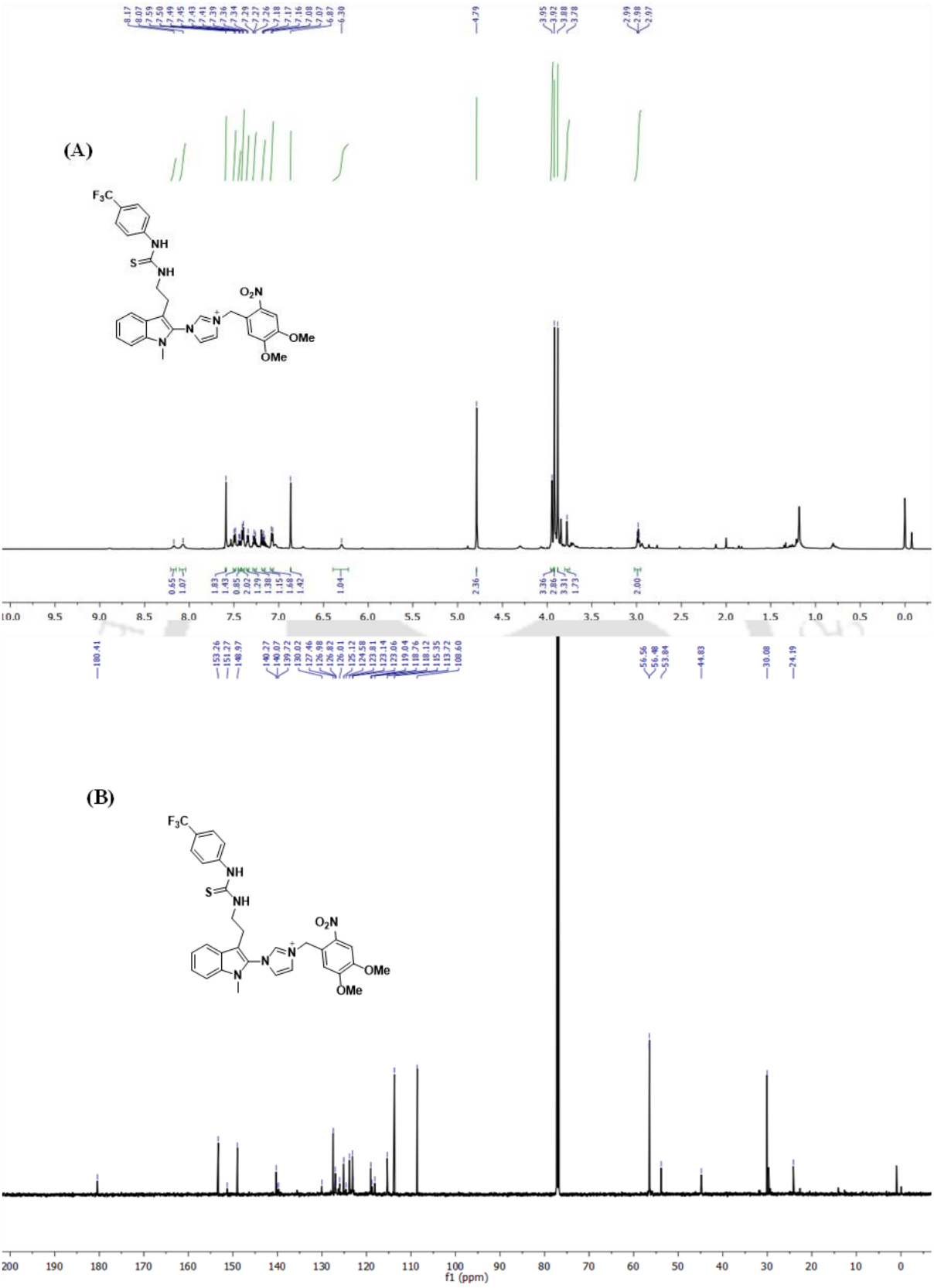

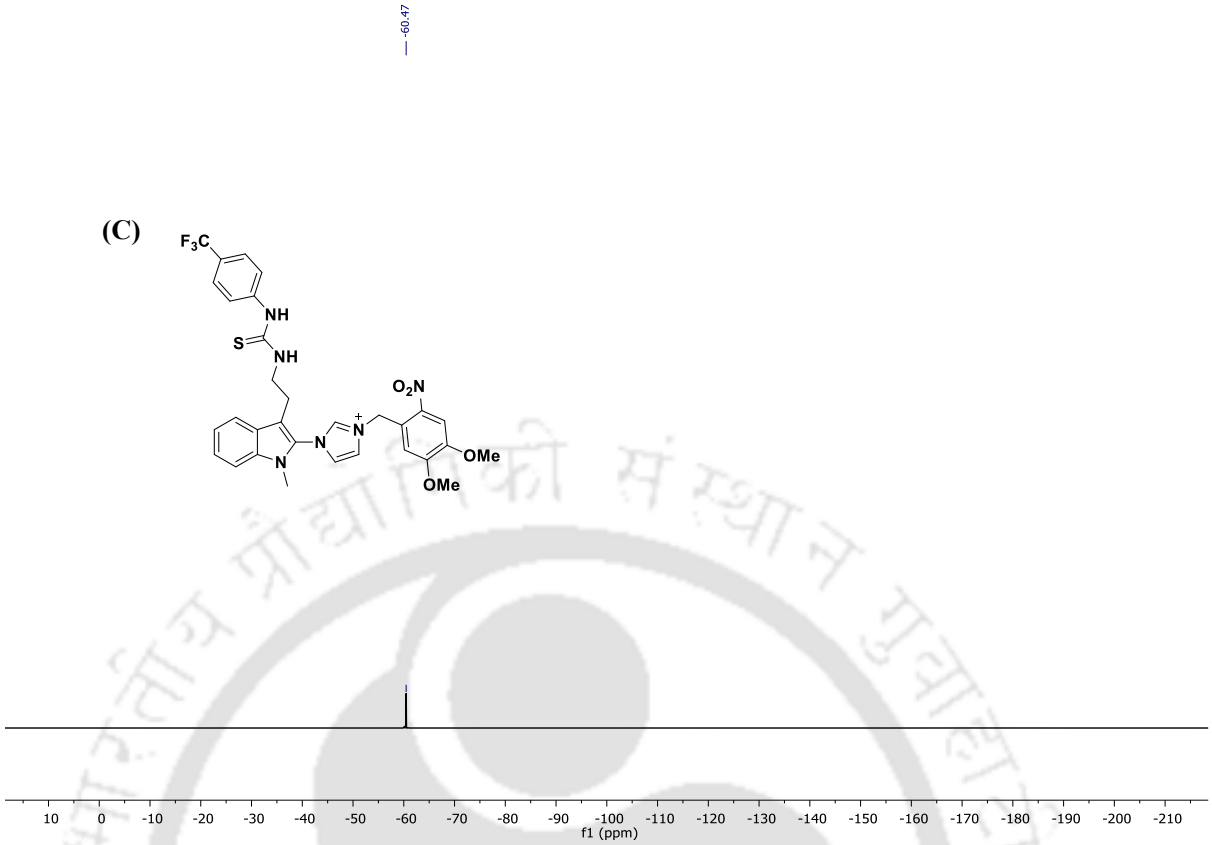

Fig. 3.20. ^{1}H NMR (A) ,^{13}C NMR (B) and ^{19}F NMR (C) spectra of 3-(4,5-dimethoxy-2-nitrobenzyl)-1-(1-methyl-3-(2-(3-(4-(trifluoromethyl)phenyl)thioureido)ethyl)-1*H*-indol-2-yl)-1*H*-imidazol-3-ium (**3.4**) in $CDCl_3$ solvent.

3.4.10. HPLC Traces for purity of the compounds

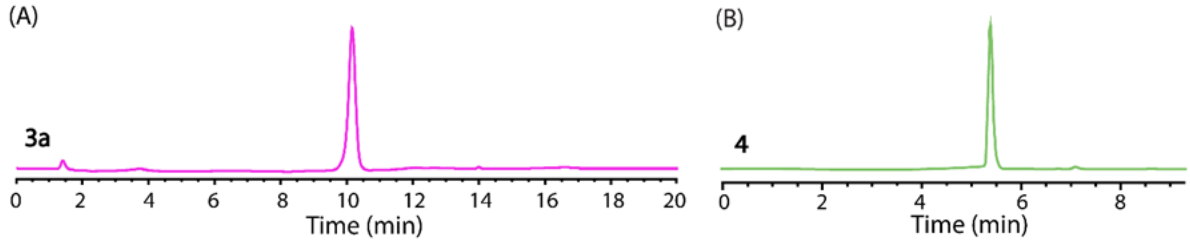

Fig. 3.21. HPLC analysis of **3.3a** (A), and **3.4** (B).

In this chapter, except for 3.2c, in all other compounds R_2 = H, so only 3.2c has one asymmetric center. We conducted an experiment to check the optical activity of 3.2c and found to be $[\alpha]_D^T$ = -37.002 °.

3.5. References

1. Röhrig, U. F.; Majjigapu, S. R.; Vogel, P.; Zoete, V.; Michielin, O. J. J. o. m. c., Challenges in the discovery of indoleamine 2, 3-dioxygenase 1 (IDO1) inhibitors. *J. Med. Chem.* **2015,** *58* (24), 9421-9437.

2. Kumar, S.; Jaipuri, F. A.; Waldo, J. P.; Potturi, H.; Marcinowicz, A.; Adams, J.; Van Allen, C.; Zhuang, H.; Vahanian, N.; Link Jr, C., Discovery of indoximod prodrugs and characterization of clinical candidate NLG802. *Eur. J. Med. Chem.* **2020,** *198*, 112373.

3. Tang, K.; Wu, Y.-H.; Song, Y.; Yu, B., Indoleamine 2, 3-dioxygenase 1 (IDO1) inhibitors in clinical trials for cancer immunotherapy. *J Hematol Oncol.* **2021,** *14* (1), 68.

4. Das, N. M.; Prusty, B. M.; Pradhan, N.; Gupta, A.; Carmena-Bargueño, M.; Karn, R.; Pérez-Sánchez, H.; Kumar, S.; Manna, D., Evaluation of mode of indoleamine 2, 3-dioxygenase 1 inhibition by 4, 7-dichloroquinolines. *Eur. J. Med. Chem. Rep.* **2023,** *9*, 100110.

5. Long, K.; Lv, W.; Wang, Z.; Zhang, Y.; Chen, K.; Fan, N.; Li, F.; Zhang, Y.; Wang, W., Near-infrared light-triggered prodrug photolysis by one-step energy transfer. *Nat. Commun.* **2023,** *14* (1), 8112.

6. Minhas, P. S.; Jones, J. R.; Latif-Hernandez, A.; Sugiura, Y.; Durairaj, A. S.; Wang, Q.; Mhatre, S. D.; Uenaka, T.; Crapser, J.; Conley, T., Restoring hippocampal glucose metabolism rescues cognition across Alzheimer's disease pathologies. *Science* **2024,** *385* (6711), eabm6131.

7. Wu, W.-B.; Huang, J.-M., Highly regioselective C–N bond formation through C–H azolation of indoles promoted by iodine in aqueous media. *Org. Lett.* **2012,** *14* (23), 5832-5835.

8. Panda, S.; Pradhan, N.; Chatterjee, S.; Morla, S.; Saha, A.; Roy, A.; Kumar, S.; Bhattacharyya, A.; Manna, D., 4, 5-Disubstituted 1, 2, 3-triazoles: effective inhibition of indoleamine 2, 3-dioxygenase 1 enzyme regulates T cell activity and mitigates tumor growth. *Sci. Rep.* **2019,** *9* (1), 18455.

9. Yue, E. W.; Sparks, R.; Polam, P.; Modi, D.; Douty, B.; Wayland, B.; Glass, B.; Takvorian, A.; Glenn, J.; Zhu, W., INCB24360 (Epacadostat), a highly potent and selective indoleamine-2, 3-dioxygenase 1 (IDO1) inhibitor for immuno-oncology. *ACS Med. Chem. Lett.* **2017,** *8* (5), 486-491.

10. Pradhan, N.; Akhtar, N.; Nath, B.; Peña-García, J.; Gupta, A.; Pérez-Sánchez, H.; Kumar, S.; Manna, D., Inhibition of immunosuppressive indoleamine 2, 3-dioxygenase by targeting the heme and apo-form. *Chem Commun* **2021,** *57* (3), 395-398.

11. Yu, Z.-L.; Cheng, Y.-F.; Jiang, N.-C.; Wang, J.; Fan, L.-W.; Yuan, Y.; Li, Z.-L.; Gu, Q.-S.; Liu, X.-Y., Desymmetrization of unactivated bis-alkenes via chiral Brønsted acid-catalysed hydroamination. *Chem. Sci.* **2020,** *11* (23), 5987-5993.

12. Lin, H.-C.; McMahon, T. C.; Patel, A.; Corsello, M.; Simon, A.; Xu, W.; Zhao, M.; Houk, K.; Garg, N. K.; Tang, Y., P450-mediated coupling of indole fragments to forge communesin and unnatural isomers. *J. Am. Chem. Soc.* **2016,** *138* (12), 4002-4005.

13. Panda, S.; Roy, A.; Deka, S. J.; Trivedi, V.; Manna, D., Fused heterocyclic compounds as potent indoleamine-2, 3-dioxygenase 1 inhibitors. *ACS Med. Chem. Lett.* **2016,** *7* (12), 1167-1172.

14. Van Der Spoel, D.; Lindahl, E.; Hess, B.; Groenhof, G.; Mark, A. E.; Berendsen, H. J., GROMACS: fast, flexible, and free. *J. Comput. Chem.* **2005,** *26* (16), 1701-1718.

15. Best, R. B.; Zhu, X.; Shim, J.; Lopes, P. E.; Mittal, J.; Feig, M.; MacKerell Jr, A. D., Optimization of the additive CHARMM all-atom protein force field targeting improved sampling of the backbone ϕ, ψ and side-chain χ1 and χ2 dihedral angles. *J Chem Theory Comput* **2012,** *8* (9), 3257-3273.

16. Vanommeslaeghe, K.; Hatcher, E.; Acharya, C.; Kundu, S.; Zhong, S.; Shim, J.; Darian, E.; Guvench, O.; Lopes, P.; Vorobyov, I., CHARMM general force field: A force field for drug-like molecules compatible with the CHARMM all-atom additive biological force fields. *J. Comput. Chem.* **2010,** *31* (4), 671-690.

17. Hess, B., P-LINCS: A parallel linear constraint solver for molecular simulation. *J Chem Theory Comput* **2008,** *4* (1), 116-122.

18. Berjanskii, M. V.; Wishart, D. S., A simple method to predict protein flexibility using secondary chemical shifts. *J. Am. Chem. Soc.* **2005,** *127* (43), 14970-14971.

CHAPTER 4

Photoswitchable Inhibitors: Temporally Regulated Inhibition of IDO1 Enzyme Using Photoactive Merocyanine Derivatives

4.1. Background and objective of present work

IDO1, being one of the crucial enzymes in tumor microenvironment, has always been in explored in preclinical studies. Though various potential traditional IDO1 inhibitors are developed but their effect has been limited due to lack of precise control over the drug delivery, leading to various side effects in immune system.[1] Moreover, they fail to target IDO1 cells in immune system, where its efficiency is more adverse. Hence, more dynamic, advanced and target specific approach for IDO1 inhibition is needed. This is where the need for stimuli responsive drug delivery arises.

In third chapter, we discussed about tryptamine-based azole derivatives as IDO1 inhibitor and photocaged it with a light cleavable moiety to get a prodrug.[2] It showed moderate efficiency as well as spatiotemporal control over drug delivery. Although it behaves as photo-responsive prodrug but the photo cleavable linker can be toxic in long run as well as it is not reversible once the linker in cleaved. In this regard, we assume compounds like spiropyran that shows light as well as pH response can be incorporated for the development of target specific IDO1 inhibitors.[3-5] Spiropyran, versatile organic compound, undergoes reversible isomerisation on irradiation of UV-Vis light or in acidic environment, to its merocyanine (coloured form).[6, 7] This characteristics of spiropyran motivated us to design and develop both light, external stimuli, and pH, internal stimuli (as tumour microenvitonment is acidic in nature), responsive IDO1 inhibitors.[7] This spatio-temporal and controlled property allows for more effective targeting of immune suppression within tumors, which enhance the effectiveness of cancer immunotherapy and minimizes systemic side effects. Additionally, these inhibitors could be activated in specific inflamed tissues, involving chronic inflammation or autoimmune diseases, offering a controlled way to regulate the immune response.[8] Additionally, the dual responsive ability, light and pH responsiveness, in spiropyran-based inhibitors also enables a temporal aspect of control, where the inhibitor can be turned on or off in real-time. This provides the flexibility to align treatment with circadian rhythms or specific therapeutic windows. This level of precision would represent a significant improvement over current approaches, offering a more dynamic and targeted method of IDO1 inhibition.[9]

4.2. Results and Discussions

4.2.1. Synthesis of spiropyran derivatives

Inspired by the benefits of photopharmacology in drug discovery, we designed and synthesized a series of spiropyran derivatives from *N*-alkylated 2,3,3-trimethylindolenine derivatives.[10, 11] The cyclocondensation of *N*-alkylated 2,3,3-trimethylindolenine with substituted 2-hydroxy benzaldehyde or 2-hydroxy-1-napthaldehyde under basic conditions provided the targeted spiropyran derivatives **2a-2e** and **3a-4.3e** (Scheme 4.1). Spectral studies of **4.3e** demonstrated photo-responsive (λ_{ex} = 400 nm) isomerization, transitioning from the closed-ring spiropyran to the open-ring merocyanine isomer and its reversal upon photoirradiation (λ_{ex} = 545 nm) or under dark ambient conditions (Fig. 4.1A). The spectral studies also revealed the pH-dependent reversible isomerization of **4.3e** (Fig. 4.1).[9]

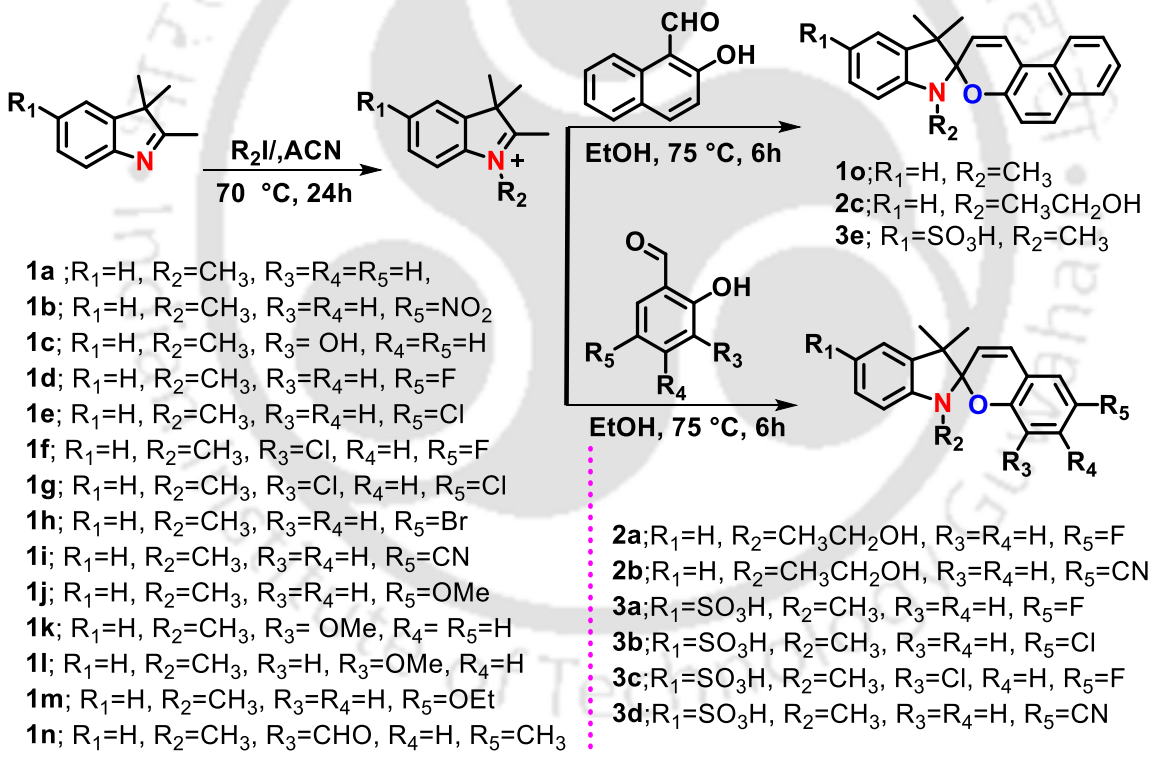

Scheme 4.1. Synthetic routes to spiropyran derivatives from 2,3,3-trimethyl-3*H*-indole.

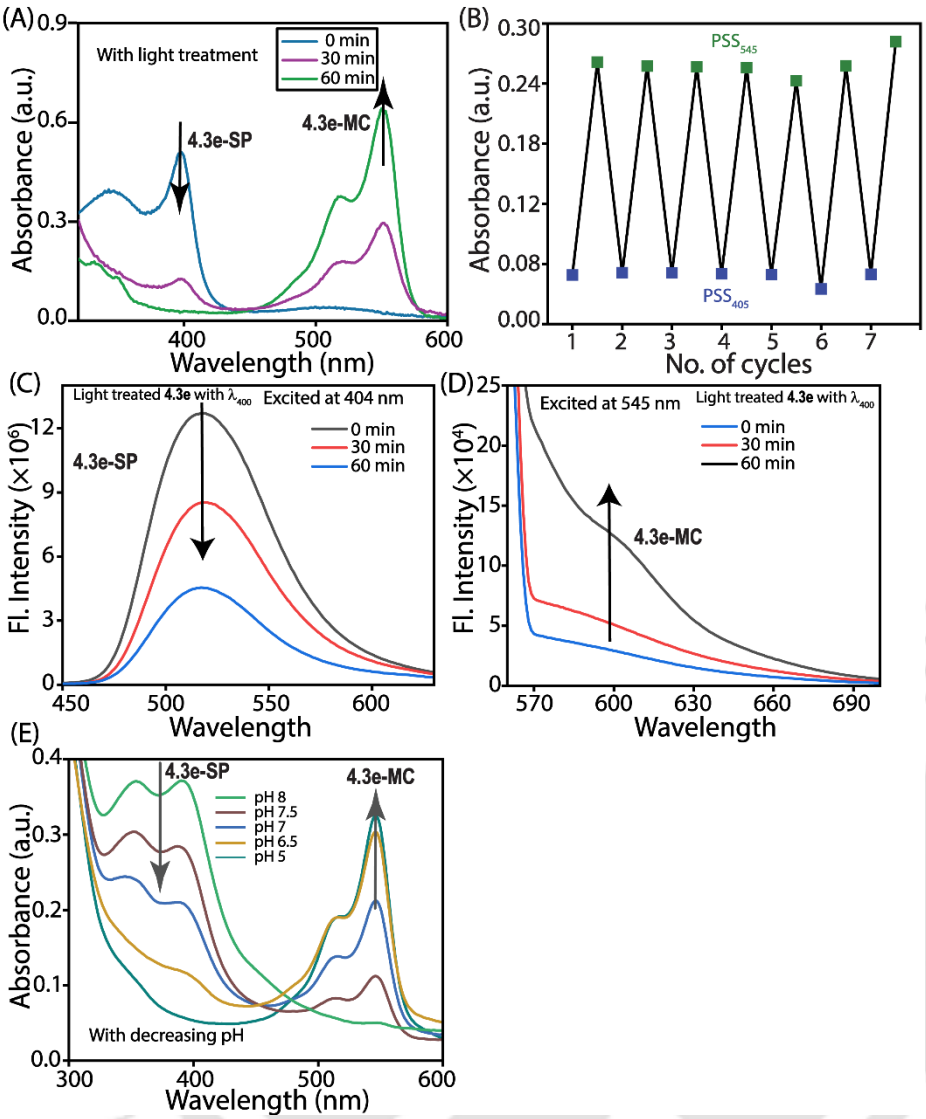

Fig. 4.1. Absorbance spectra demonstrating the conversion of spiropyran to merocyanine isoforms of **4.3e** at different time intervals after photo-irradiation with 404 nm light (A). Photo reversibility of **4.3e** among spiropyran and merocyanine conformation (B). Photo-irradiated (400 and 545 nm) fluorescence spectra of **4.3e** at different time intervals (C, D). Conversion of spiropyran to merocyanine isoforms of **4.3e** at different pH (E).

4.2.2. Inhibitory activities against IDO1 enzyme

The initial screening of the synthesized compounds using the HPLC-based kynurenine assay revealed that the merocyanine (MC) form of **4.3e** (**4.3e-MC**) strongly inhibits the activity of the IDO1 enzyme, with an IC_{50} value of 53.9 ± 2 nM (Fig. 4.2A-B, Table 4.1, and Table 4.2). The **4.3e-MC** also showed stronger IDO1 inhibitory activity under the acidic environment (Fig. 4.2F). In contrast, the spiropyran derivative isomer of **4.3e** (**4.3e-SP**) exhibited significantly weaker IDO1 inhibitory activity (IC_{50} > 10 μM)

(Fig. 4.2E). The other synthesized merocyanine derivatives showed much lower inhibitory activities against IDO1. The potent **4.3e-MC** exhibited no significant inhibitory activity against the tryptophan 2,3-dioxygenase (TDO) enzyme, which belongs to the same enzyme family as IDO1 (Table 4.3).

Table 4.1. Inhibitory activity of the spiropyran and merocyanine derivatives against purified human IDO1 enzyme.

Compounds	IC_{50} values (nM)	% Inhibition	
		0.25 µM	1 µM
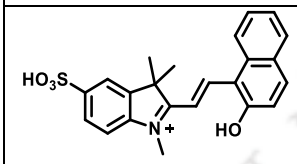	54 ± 2	83 ± 1.5	97 ± 1
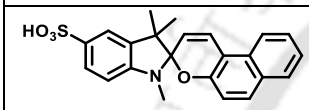	>10000	9 ± 1	21 ± 9
Epacadostat	61 ± 6	76 ± 4	96 ± 2

Table 4.2. Inhibitory activity of the synthesized compounds against purified human IDO1 enzyme measured by the HPLC method.

Compound (Spiropyran form)	% Inhibition	Compound (merocyanine form)	% Inhibition	
	1 µM		1 µM	0.25 µM
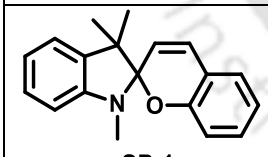 SP-1a	7 ± 0.3	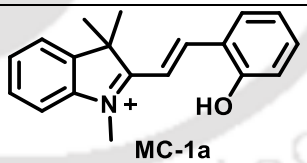 MC-1a	29 ± 7	12 ± 2
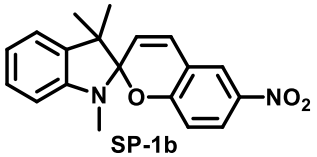 SP-1b	9 ± 2	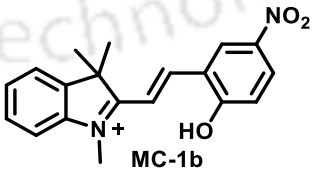 MC-1b	24 ± 7	3 ± 1
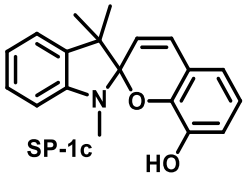 SP-1c	13 ± 1	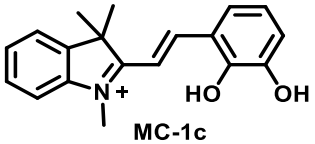 MC-1c	22 ± 4	7 ± 1

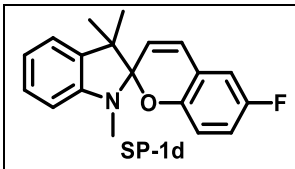 SP-1d	21 ± 3	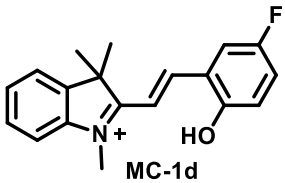 MC-1d	70 ± 9	38 ± 3
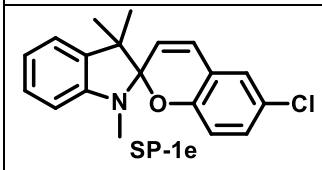 SP-1e	19 ± 0.7	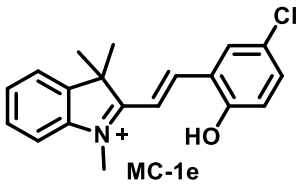 MC-1e	49 ± 7	23 ± 2
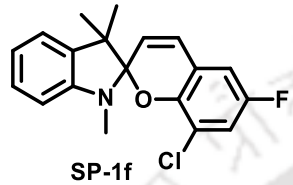 SP-1f	8 ± 1	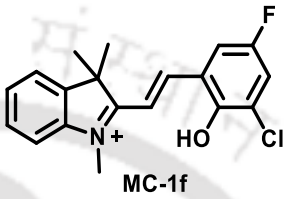 MC-1f	48 ± 5	12 ± 3
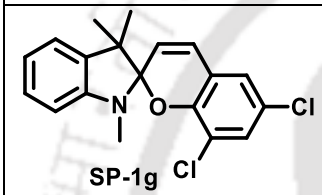 SP-1g	15 ± 2	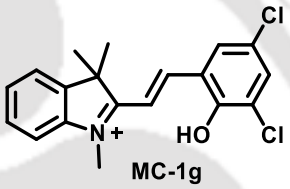 MC-1g	43 ± 8	14 ± 3
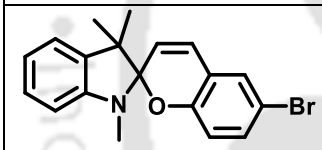 SP-1h	12 ± 0.9	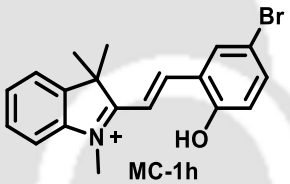 MC-1h	31 ± 5	9 ± 3
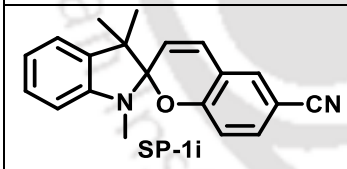 SP-1i	18 ± 3	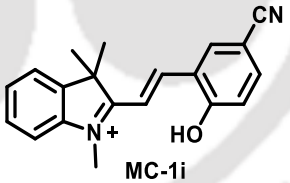 MC-1i	69 ± 12	43 ± 5
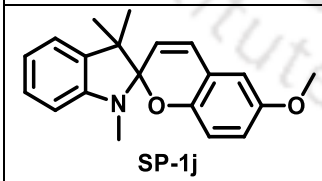 SP-1j	16 ± 3	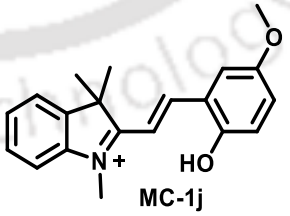 MC-1j	45 ± 12	21 ± 4
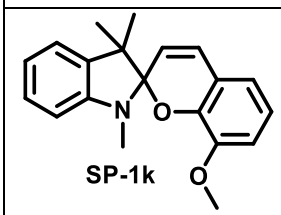 SP-1k	18 ± 2	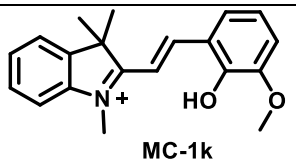 MC-1k	37 ± 6	13 ± 6

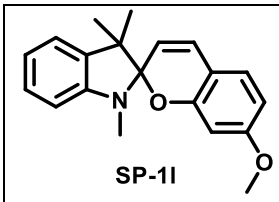 SP-1l	14 ± 3	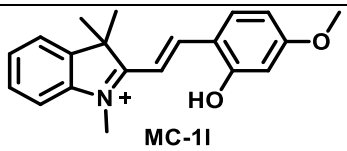 MC-1l	30 ± 9	6 ± 2
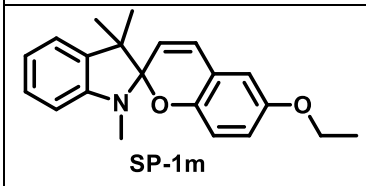 SP-1m	15 ± 1	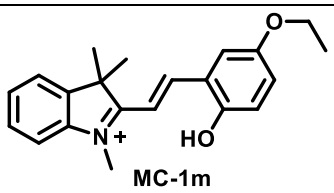 MC-1m	39 ± 7	11 ± 1
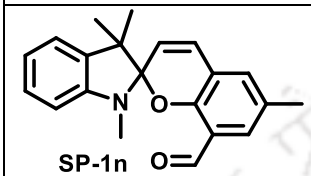 SP-1n	6 ± 0.4	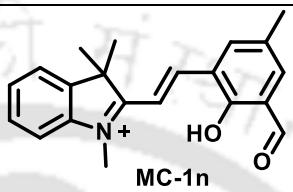 MC-1n	23 ± 3	11 ± 4
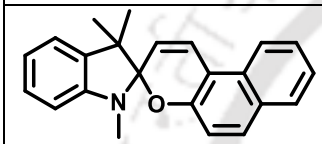 SP-1o	19 ± 2	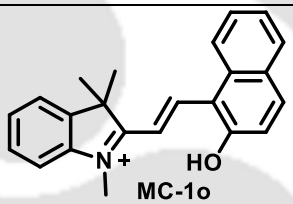 MC-1o	73 ± 4	30 ± 7
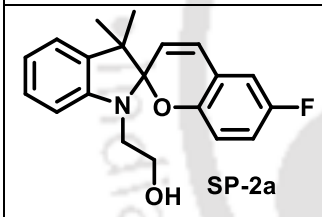 SP-2a	11 ± 0.4	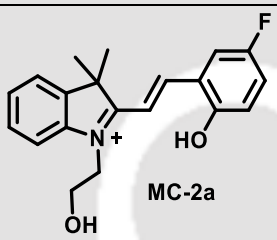 MC-2a	25 ± 4	5 ± 0.3
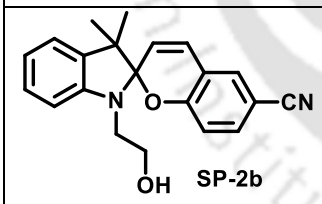 SP-2b	13 ± 0.8	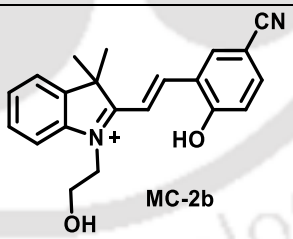 MC-2b	34 ± 7	18 ± 1
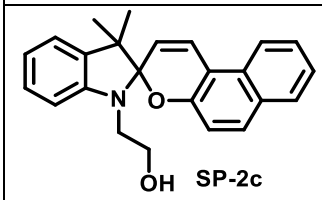 SP-2c	9 ± 0.6	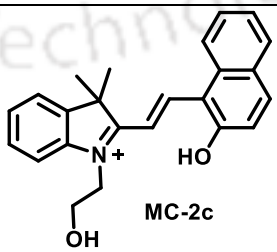 MC-2c	55 ± 7	32 ± 1
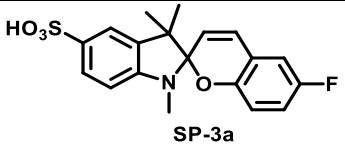 SP-3a	28 ± 3	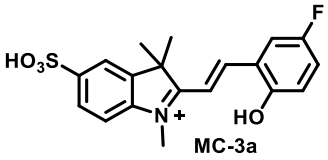 MC-3a	67 ± 9	34 ± 4

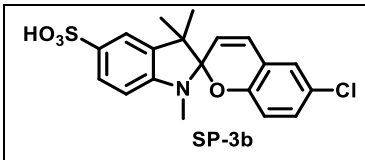 SP-3b	8 ± 0.7	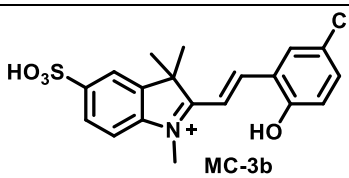 MC-3b	58 ± 5	27 ± 3
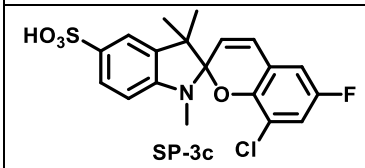 SP-3c	14 ± 3	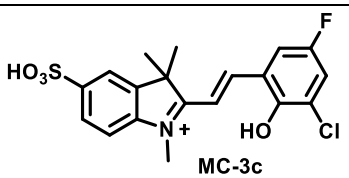 MC-3c	55 ± 6	16 ± 3
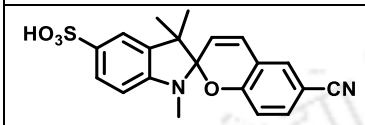 Sp-3d	16 ± 1	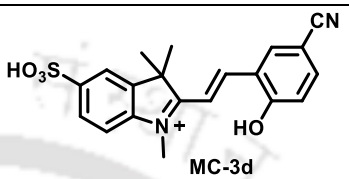 MC-3d	80 ± 9	52 ± 4
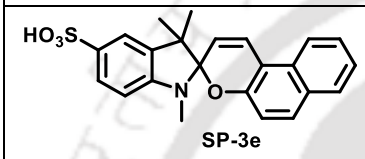 SP-3e	21 ± 9	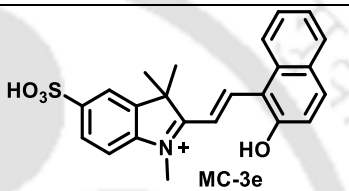 MC-3e	97 ± 1	83 ± 1.5

Table 4.3. Inhibitory activity of the compounds against purified human TDO enzyme using pDMAB assay.

Compound	% enzyme inhibition			
	0.25 µM of **4.3e-MC**		1 µM of **4.3e-MC**	
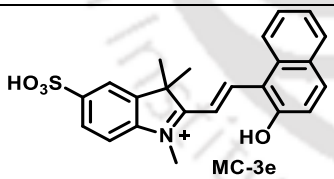 MC-3e	IDO1	TDO	IDO1	TDO
	83 ± 2	9 ± 4	97 ± 1	24 ± 4
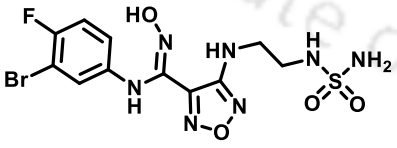 Epacadostat	76 ± 4	5 ± 1	96 ± 2	16 ± 4

4.2.3. Time and temperature-dependent IDO1 activity

The activity of **4.3e-MC** encouraged us to explore its detailed inhibitory mechanism on IDO1. A variation in the pre-incubation time period of **4.3e-MC** with IDO1 enzyme at 37 °C demonstrated a significant increase in its inhibitory activity over time, reaching maximum activity (>90%) at 60 minutes (Fig. 4.2C). The temperature-dependent

activity assays showed that the inhibition of IDO1 by **4.3e-MC** increased when the temperature was raised from 20 °C to 37 °C. These results indicate that the inhibition process may involve time and temperature-sensitive events, such as the dissociation of the heme cofactor from the IDO1 enzyme (Fig. 4.2C).[12, 13]

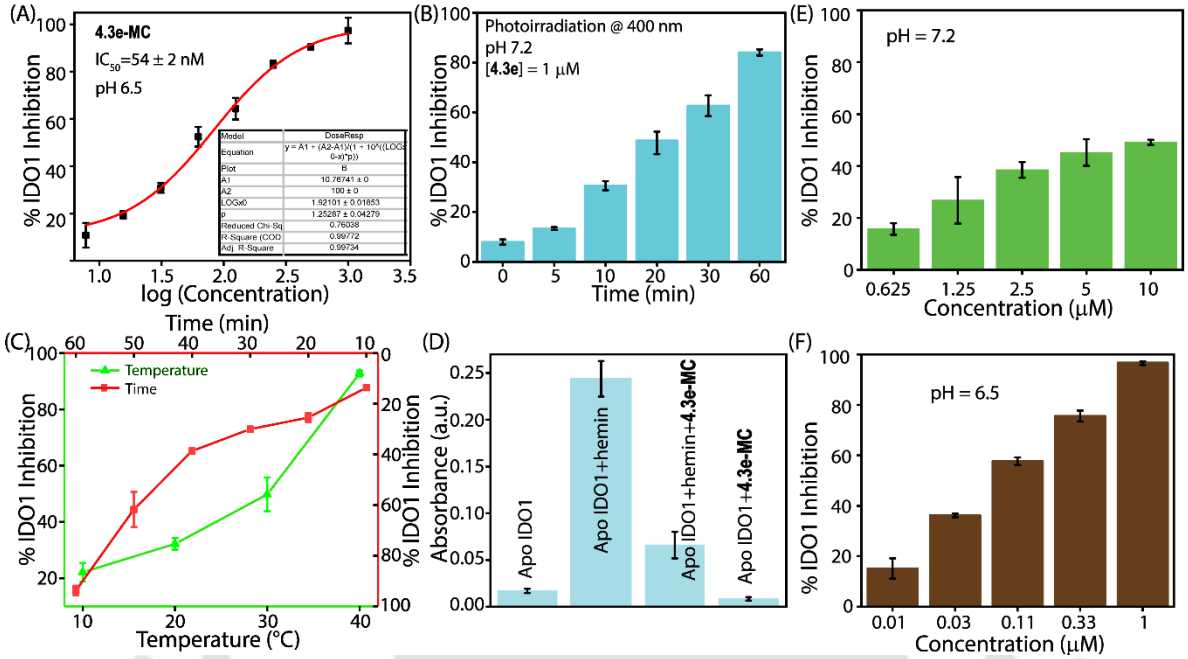

Fig 4.2. Inhibitory activities of IDO1 at different concentrations of **4.3e-MC** at pH 6.5 (A), after photoirradiation of **4.3e** with 400 nm light at different time intervals (B). IDO1 inhibitory activities at different temperatures and time intervals with **4.3e-MC** at pH 6.5 (C). The activity of apo-IDO1 in the absence and presence of the compound and/or hemin (D). IDO1 inhibitory activities at different pH in presence of **4.3e** (10 and 1µM) (E, F).

4.2.4. Compound-induced heme release property

The binding of **4.3e-MC** to "pocket C" near the solvent-exposed regions of the IDO1 enzyme could induce partial unfolding of the enzyme, promoting heme release. To determine whether the loss of heme-cofactor is a decisive step in the inhibition process of IDO1 enzyme, we performed UV-Vis spectroscopic analysis both in the presence and absence of **4.3e-MC**. The results showed a decrease in the Soret peak in the presence of **4.3e-MC**, indicating that heme was released from IDO1(Fig. 4.3A).[12] Notably, no significant changes were observed in the Soret peaks of TDO or other heme-containing proteins, such as hemoglobin and myoglobin, suggesting that the hemin loss induced by **4.3e-MC** is selective for IDO1 enzyme (Fig. 4.3B-D).

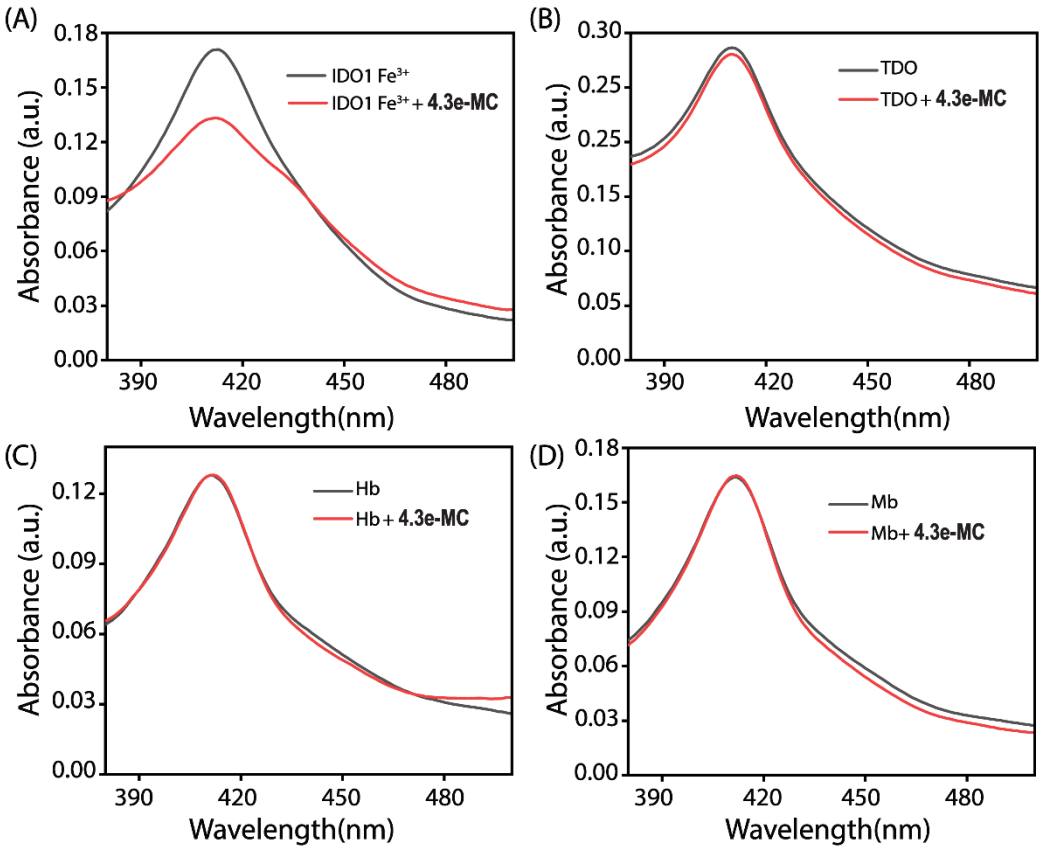

Fig. 4.3. Absorption spectra of the ferric-IDO1 enzyme(A), ferric-TDO enzyme (B), hemoglobin (C), and myoglobin (0.9 μM) (D) in the absence and presence of the compound **4.3e-MC** (10 μM) in 100 mM phosphate buffer at pH 6.5 after 15 min incubation at 37 °C.

For further investigation of the **4.3e-MC**-mediated release of the heme cofactor from the IDO1 enzyme, the protoporphyrin IX (PpIX)-based fluorescence quenching assay was performed. A significant decrease in the PpIX fluorescence upon the addition of **4.3e-MC** indicated the interaction between PpIX and hemin. In contrast, no observable change in the PpIX fluorescence signal was detected in the presence of **4.3e-SP** (Fig. 4.4). Thus, these UV-Vis and fluorescence spectral changes of the IDO1 enzyme and PpIX suggest the potential for **4.3e-MC**-mediated release of the heme from IDO1.

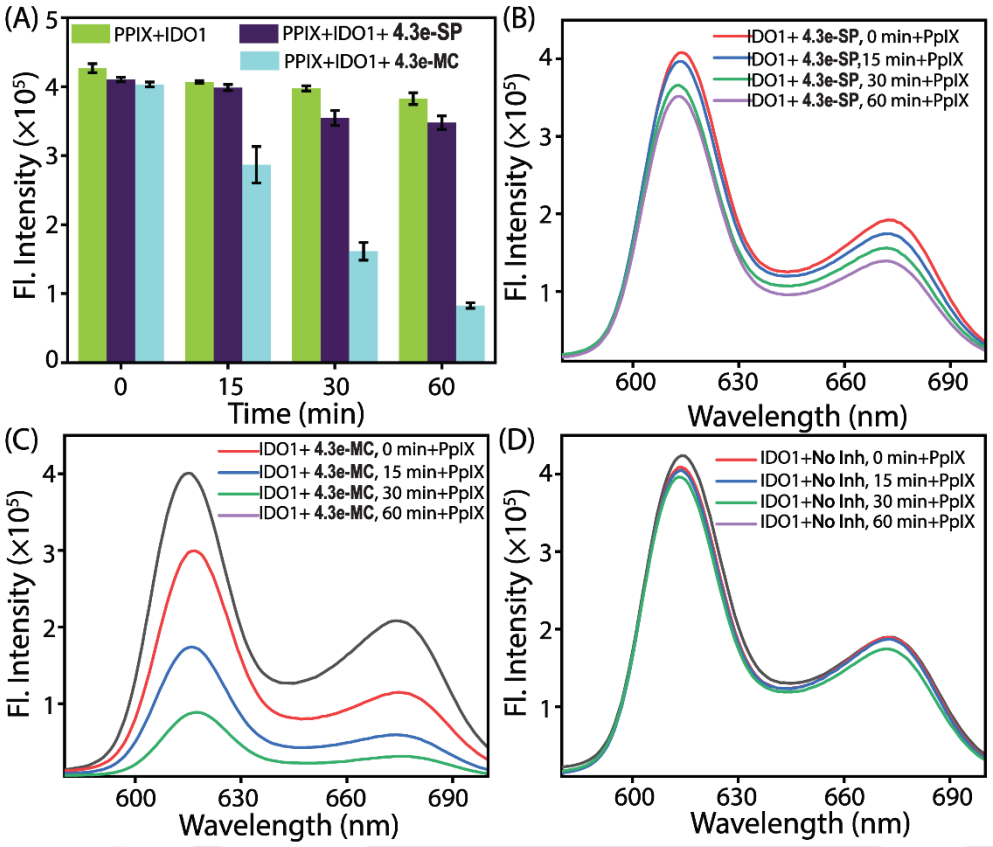

Fig. 4.4. Extent of heme release from IDO1 enzyme (0.75 µM) in the absence and presence of compounds at different time intervals (A, B, C, and D), measured by monitoring the fluorescence intensity of PpIX (615 nm).

Additionally, we did not observe any significant changes in the circular dichroism (CD) spectra of IDO1 before and after incubation with **4.3e-MC**, indicating the compound-mediated release of the heme cofactor from the IDO1 active site is not caused by any significant alteration in its structural integrity (Fig. 4.5 and Table 4.4). Therefore, removing the heme-cofactor from the IDO1 enzyme and generating apo-IDO1 are the crucial steps in the IDO1 inhibitory activity of **4.3e-MC**.

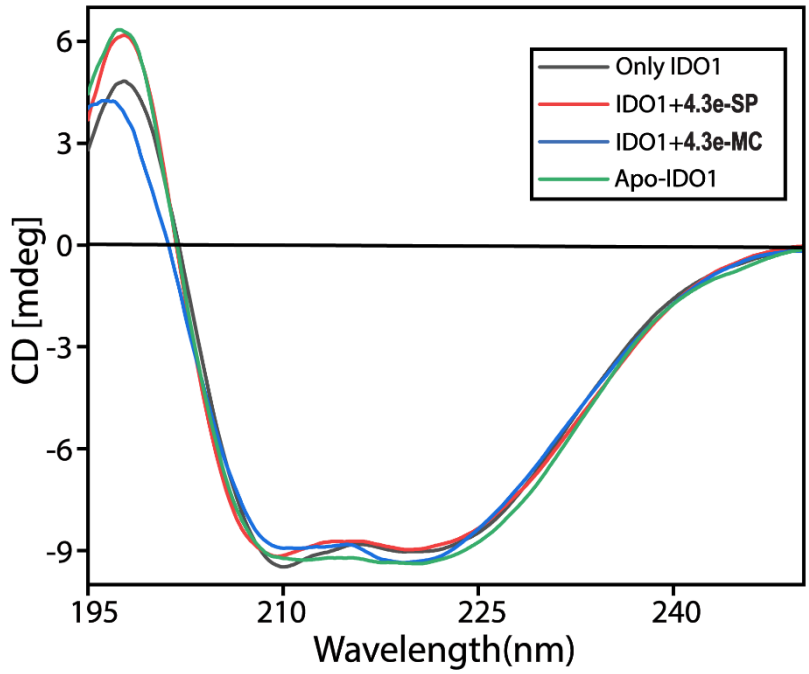

Fig. 4.5. Circular dichroism spectra of apo-IDO1 protein and IDO1 enzyme in the absence and presence of compound **4.3e-MC**.

Table 4.4. Circular dichroism analysis of apo-IDO1 protein and IDO1 enzyme in the absence and presence of compound **4.3e-MC.**

Sl. No.	Sample Name	% of secondary structural elements			
		Helix	Beta	Turn	Other
1	IDO1	62.3	0.0	14.6	23.1
2	IDO1 + **4.3e-SP**	60.6	0.0	14.7	25.2
3	IDO1 + **4.3e-MC**	53.2	0.0	15.7	31.1
4	Apo IDO1	52.4	0.0	13.8	33.8

The concentration-dependent activity assay was performed to investigate the rate-limiting process of **4.3e-MC**-mediated IDO1 inhibition. The activity assay was performed after incubating the IDO1 enzyme with **4.3e-MC** for 60 minutes. The IDO1 activity at various concentrations of **4.3e-MC** exhibited a non-linear relationship. The IDO1 inhibition assay in the presence of L-Trp and the reducing agents (ascorbate, methylene blue, and catalase) against different concentrations of **4.3e-MC** also showed a nonlinear inhibition profile, suggesting that the oxidation state of iron does not influence the **4.3e-MC**-mediated IDO1 inhibitory activity in the hemin group. Therefore, releasing the heme cofactor or generating the apo-IDO1 protein is the rate-limiting step of the **4.3e-MC**-

mediated IDO1 inhibition mechanism. The UV-Vis spectral analysis showed that the extent of reduction of the Soret peak was quite similar for both catalytically active and inactive IDO1 enzyme, indicating that the release capability of the heme cofactor was nearly the same (Fig. 4.6). The apo-IDO1 protein equilibrated with external hemin regained its catalytic activity, whereas the apo-IDO1 protein equilibrated with **4.3e-MC** failed to show any significant activity even after adding external hemin (Fig. 4.2D).

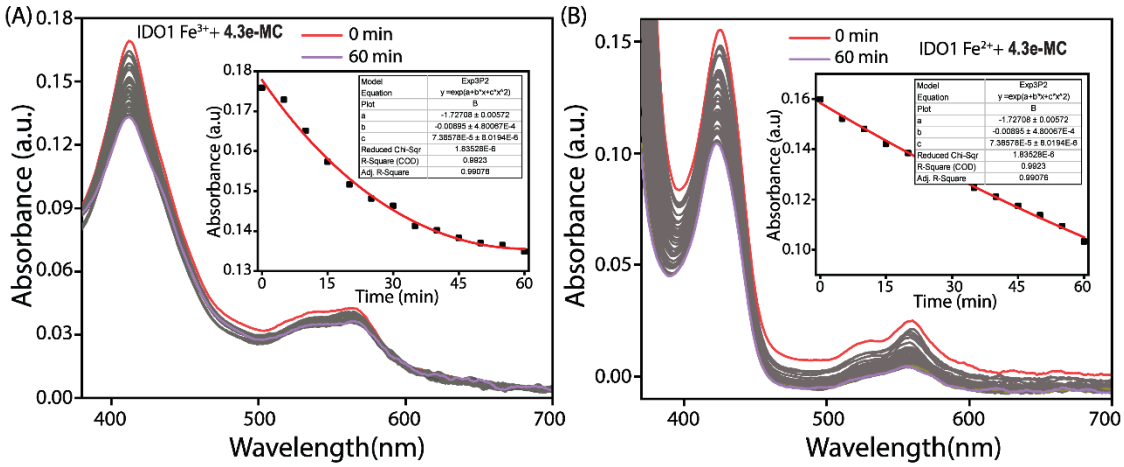

Fig. 4.6. Time-dependent heme dissociation from IDO1 enzyme (0.75 µM) in the presence of compound **4.3e-MC** (25 µM) at 37 °C. Absorbance spectra of ferric-IDO1 enzyme. The inset shows the loss in absorbance for ferric-IDO1 as a function of time (A). Absorbance spectra of ferrous-IDO1 enzyme (B). The ferrous-deoxy reaction environment was generated by adding $Na_2S_2O_4$ to the solution under an N_2 atmosphere. The inset shows the loss in absorbance for ferrous-IDO1 as a function of time. Heme dissociation from IDO1 was monitored by the loss of absorbance of the Soret peak: 404 nm for ferric-IDO1 and 425 nm for ferrous-IDO1.

4.2.5. Heme binding properties of the compound

Recent studies indicate that free hemin is necessary for cellular homeostasis and plays a dual role in cancer, where its accumulation and metabolic dysregulation promote tumor growth by generating oxidative stress and inflammation. However, hemin deficiency also impairs critical cellular functions, necessitating careful regulation of hemin metabolism. Various spectrometric techniques were employed to investigate whether **4.3e-MC** exhibits hemin-binding properties. The concentration-dependent decrease of the Soret peak indicated that **4.3e-MC** also interacts with the free heme cofactor. The binding affinities of these **4.3e-MC** are similar to quinine, a known hemin-binding molecule (Fig. 4.7).

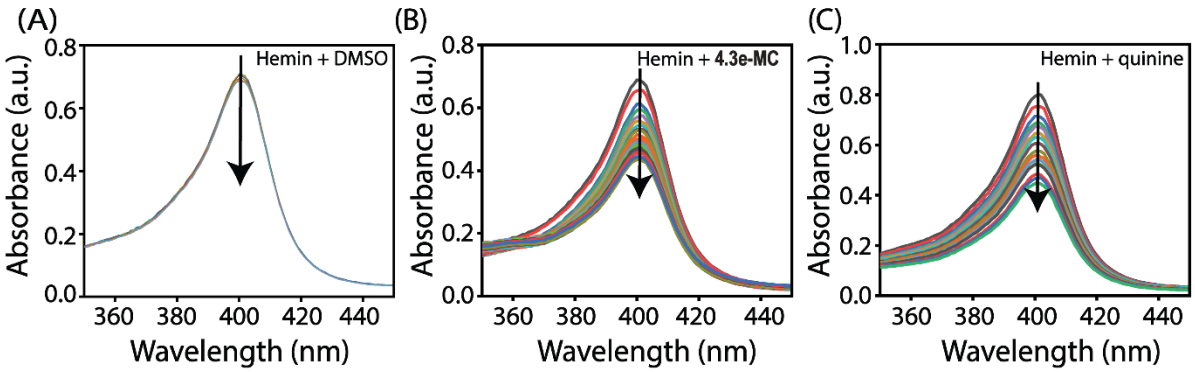

Fig. 4.7. The plot of absorbance of heme (5 µM) in the presence of different concentrations (0- 175 µM) of DMSO (A), **4.3e-MC** (B), and Quinine (C).

The time-dependent decrease in PpIX fluorescence in the presence of hemin indicates the interaction of PpIX with hemin. However, the addition of **4.3e-MC**, in combination with hemin, significantly alters the degree of PpIX fluorescence quenching induced by hemin, indicating the potential interaction of **4.3e-MC** with PpIX (Fig. 4.8). In contrast, the addition of **4.3e-SP**, in combination with hemin, did not result in any significant alterations in the PpIX fluorescence quenching caused by hemin. Thus, the PpIX-based fluorescence studies indicate that **4.3e-MC** could inhibit the activity of overproduced labile hemin, while **4.3e-SP** failed to do so. The photo or pH-induced conversion of **4.3e-SP** to **4.3e-MC** and the interaction between **4.3e-MC** and apo-IDO1 were examined using various spectroscopic studies.

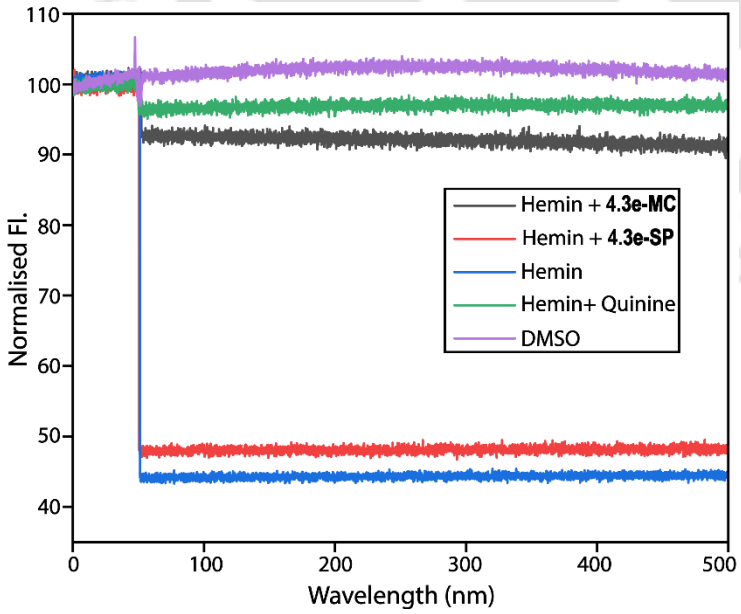

Fig. 4.8. The plot of PpIX fluorescence (5 mM) in the absence or presence of only heme or a solution of heme (1.5 mM) equilibrated with compounds (30 mM).

4.2.6. Apo-IDO1 binding properties of the compound

The steady-state fluorescence anisotropy measurements of **4.3e-MC** showed a significant increase in anisotropy with increasing concentrations of apo-IDO1, resulting in a binding affinity (K_d) of 3.9 ± 0.58 μM (Fig. 4.9A).[14] Additionally, the introduction of NaCl led to a concentration-dependent decrease in the steady-state anisotropy value, indicating that the interaction between **4.3e-MC** and apo-IDO1 is reversible (Fig. 4.9A).

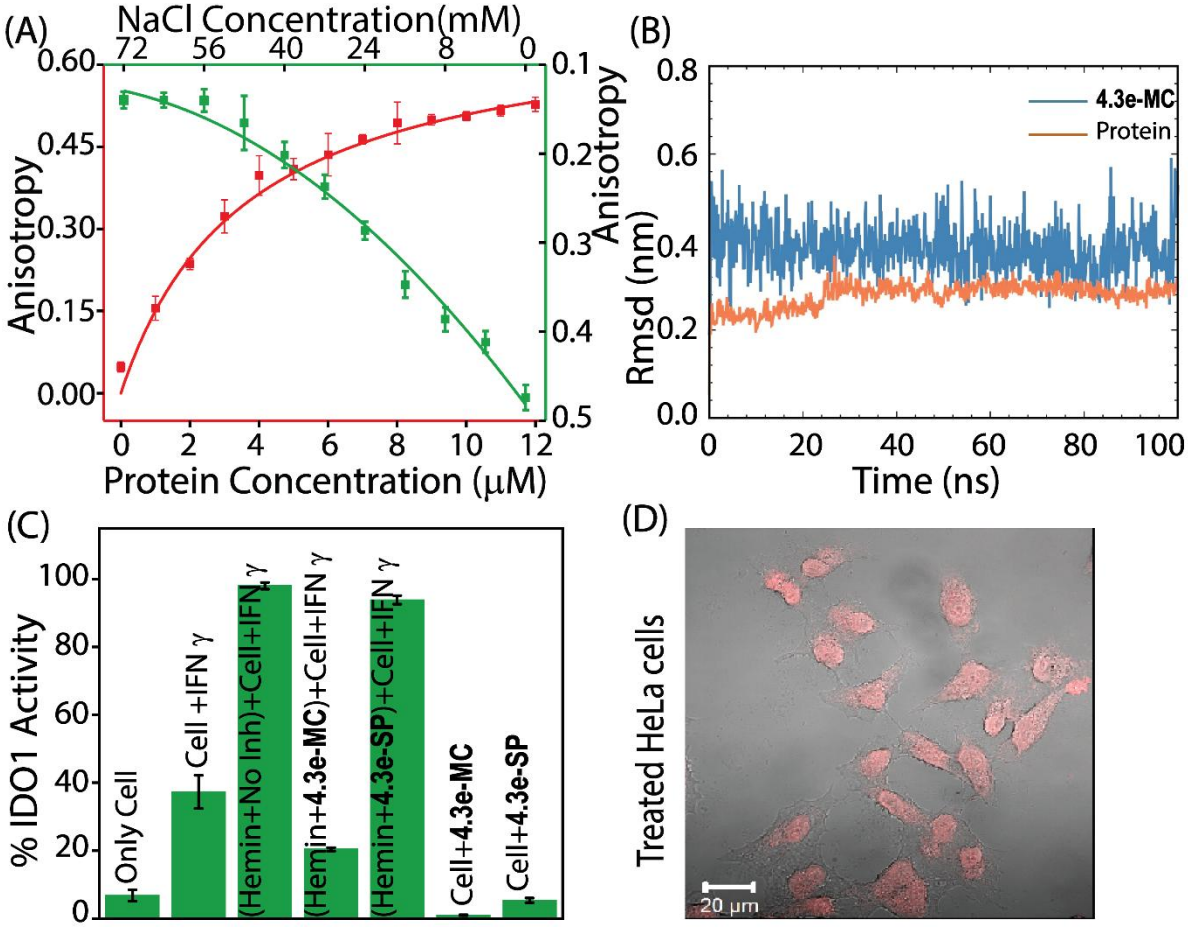

Fig. 4.9. Steady-state fluorescence anisotropy measurements of **4.3e-MC** (500 nM) in the presence of various concentrations of apo-IDO1 protein (0-12 μM) and in the absence and presence of different concentrations of NaCl (0-75 mM) (A). The variation in RMSD obtained for apo IDO1 (orange) and **4.3e-MC** (blue) (B). IDO1 inhibition activity in cells with and without IFN-γ treatment in the presence and absence of the isoforms of **4.3e** (C)**.** Confocal microscopic image of **4.3e-MC**-treated HeLa cells (D).

The time-dependent UV-Vis spectral studies of **4.3e-MC** in equilibrium with apo-IDO1 were conducted under neutral and dark conditions. The absorbance profiles of **4.3e-MC** in the presence of apo-IDO1 exhibited minimal variation over time. This indicates

that the **4.3e-MC** isomer remains stable within the binding site of apo-IDO1 and does not experience significant photochemical or structural changes during a prolonged incubation period of up to 10 h (Fig. 4.10A-B). However, the control study without apo-IDO1 showed the spontaneous conversion of the merocyanine (**4.3e-MC**) to the spiropyran isomer (**4.3e-SP**) under similar experimental conditions (Fig. 4.10C-D). Hence, these spectral studies suggest a strong and persistent interaction of **4.3e-MC** with the apo-IDO1, which is crucial for the **4.3e-MC**-mediated IDO1 inhibitory activity.

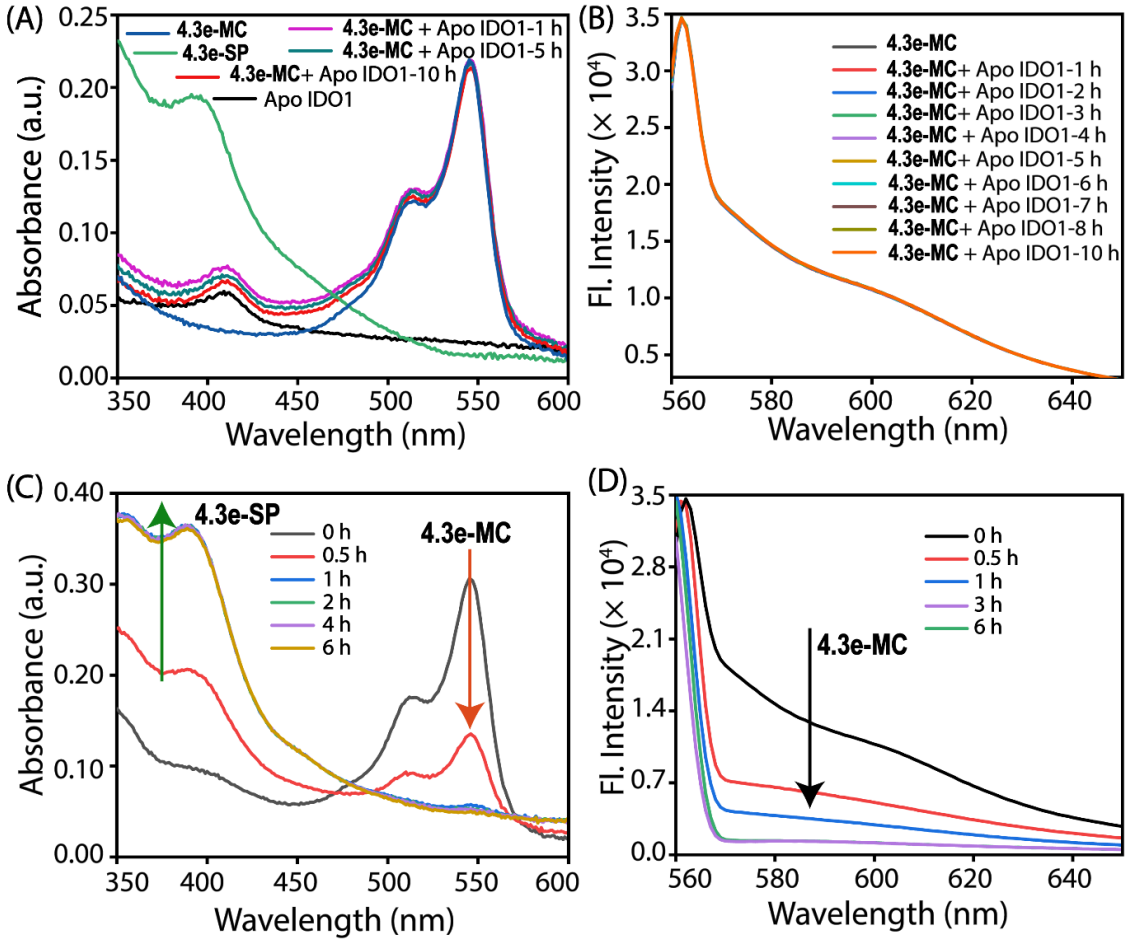

Fig. 4.10. Absorption (A) and emission spectra (B) of the IDO1 enzyme incubated with 4.3e-MC at different time intervals. Absorption (C) and emission spectra (D) of **4.3e-MC** without IDO1 enzyme under similar experimental conditions.

4.2.7. Molecular docking and molecular dynamic simulation studies

To investigate the molecular determinants responsible for the binding of **4.3e-MC** to the apo-IDO1, molecular docking and molecular dynamics (MD) simulations were performed.[13] The molecular docking analysis of **4.3e-MC** with the X-ray co-crystal structure of the apo-IDO1 protein **(PDB ID: 6AZW)** revealed that the resulting top poses

are located within the binding site of the apo-IDO. The MD simulation studies (100 ns) of the best pose showed that **4.3e-MC** remains strongly bound within the binding site of apo-IDO1, with an RMSD of 0.143 nm, while **4.3e-MC** stabilized at 0.191 nm**.** The slight drifts in RMSD values could be due to changes in the conformation of **4.3e-MC** within the binding site. Further molecular docking analysis indicated that the hydrophobic, hydrogen bond, pi-pi stacking, pi-cation and water bridge interactions could primarily drive the binding of **4.3e-MC** to the apo-IDO1 protein. The napthyl and 2,2-dimethyl indolenine moieties of **4.3e-MC** could be involved in hydrophobic interactions with the residues T117, P117, P217, L225, A255 and I345, respectively. The hydroxyl group of the naphthalene ring and sulfonic acid **4.3e-MC** could be involved in hydrogen bond interactions with the backbone of I345 and G355 residues. There is a water bridge between the residue A255 and the ligand, which helps to keep the ligand in place by adding more flexibility to the binding **(**Fig. 4.9B).

4.2.8. IDO1 activity under cellular environment

The viability assay of **4.3e-MC** showed low toxicity in HeLa and HEK-293 cells (after 48 h), indicating that this compound is suitable for IDO1 inhibitory studies (Fig. 4.11). Initially, **4.3e-SP** was converted to **4.3e-MC** through light or acidic treatment; however, the following 48 h incubation period with HeLa cells could allow for partial thermal reversal of **4.3e-MC** back to **4.3e-SP**. Consequently, the observed cell viability outcomes likely reflect the combined effects of merocyanine and spiropyran isomers, rather than only **4.3e-MC**.

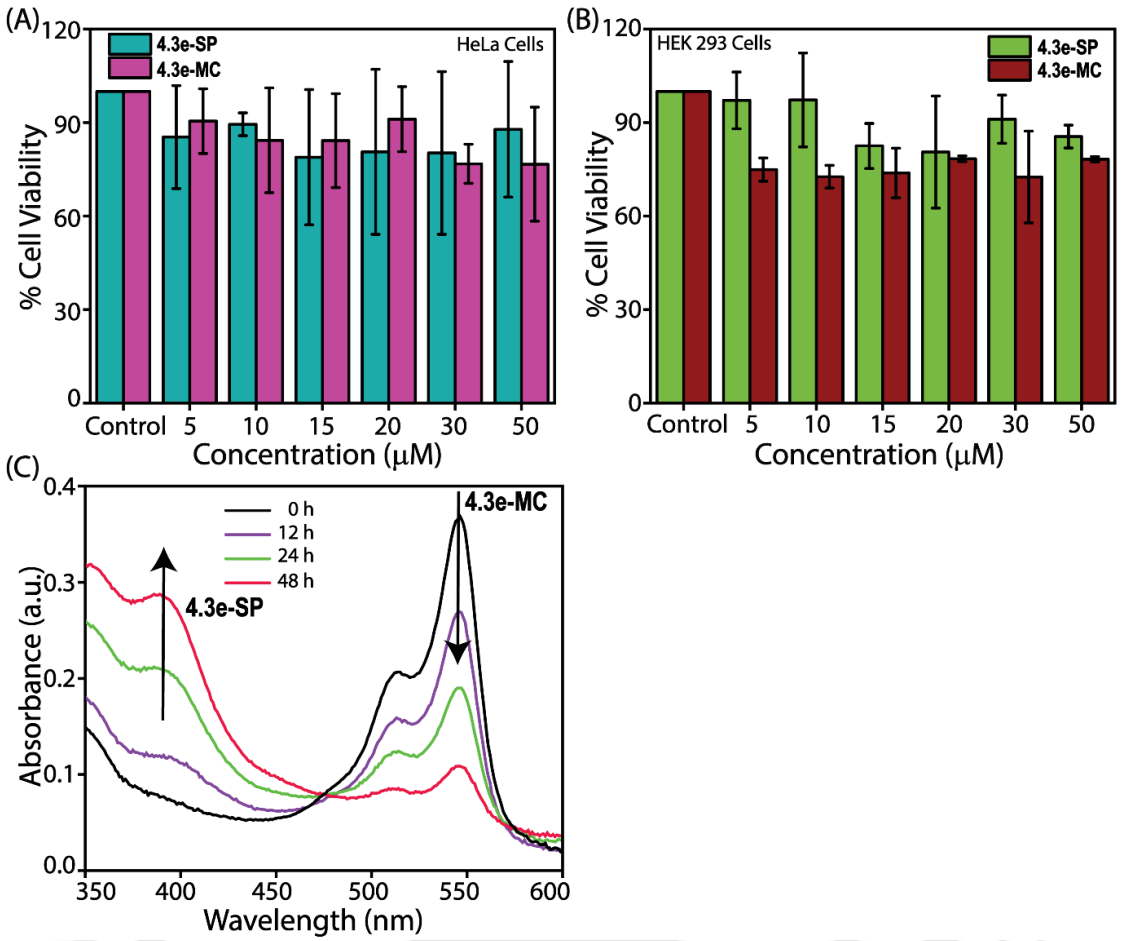

Fig. 4.11. Effect of the compounds on the viability of HeLa cells (A) and HeK cells (B). The cells were treated with the indicated concentrations of the compounds for 48 h. The MTT assay determined cell viability. Cell viability (%) is averaged with standard deviation (error bars) from three independent experiments. Conversion of **4.3e-MC** to **4.3e-SP** in 48 h during the MTT assay (C).

The cellular IDO1 activity assays demonstrated a considerable increase in IDO1 activity when treated with external IFN-γ and hemin, suggesting a notable amount of apo-IDO1 is present in the cellular environment. Under similar experimental conditions, hemin, which was equilibrated with the potent compound, demonstrated a significant decrease in IDO1 activity. This suggests that the complexation of hemin with the **4.3e-MC** hinders the ability of apo-IDO1 to rebind hemin (Fig. 4.9C and 4.12). Therefore, compound binding to the apo-IDO1 and the formation of the hemin-**4.3e-MC** complex could inhibit the cellular IDO1 activity. The confocal microscopic images revealed distinct red fluorescent puncta in treated HeLa cells, confirming internalization of **4.3e-MC**, while untreated control cells showed no fluorescence (Fig. 4.9D and 4.13).

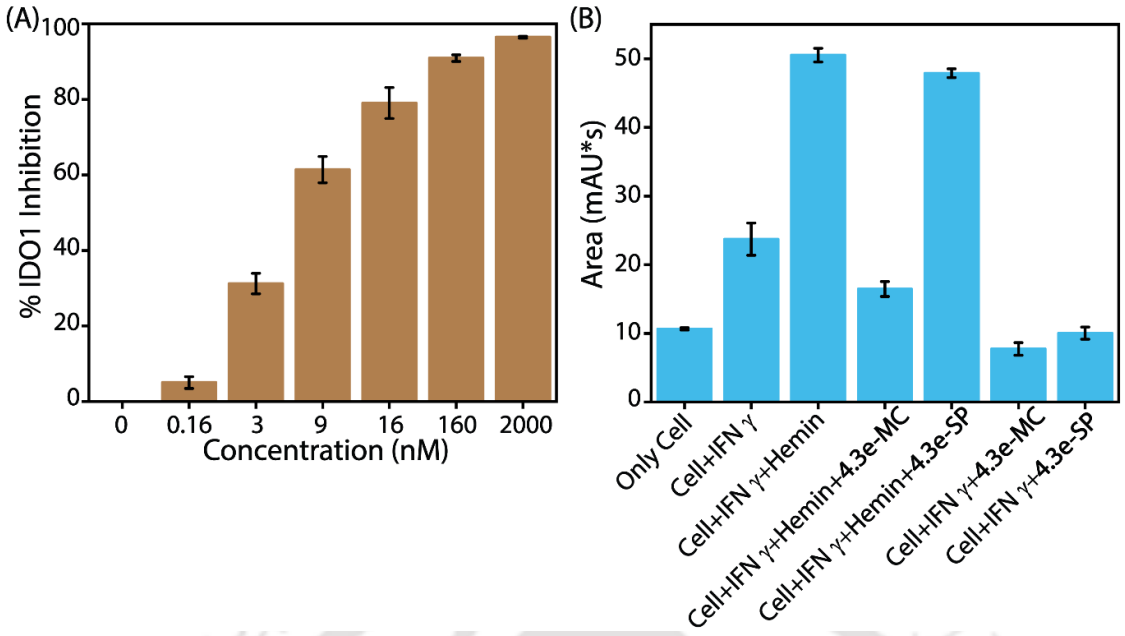

Fig. 4.12. Concentration-dependent cellular IDO1 enzyme activity in the absence and presence of compound **4.3e-MC** (A). IDO1 enzyme activities in the absence and presence of **4.3e** and extracellular heme in the IFN-γ-treated HeLa cells (B). Activities were calculated by HPLC-based kynurenine assay.

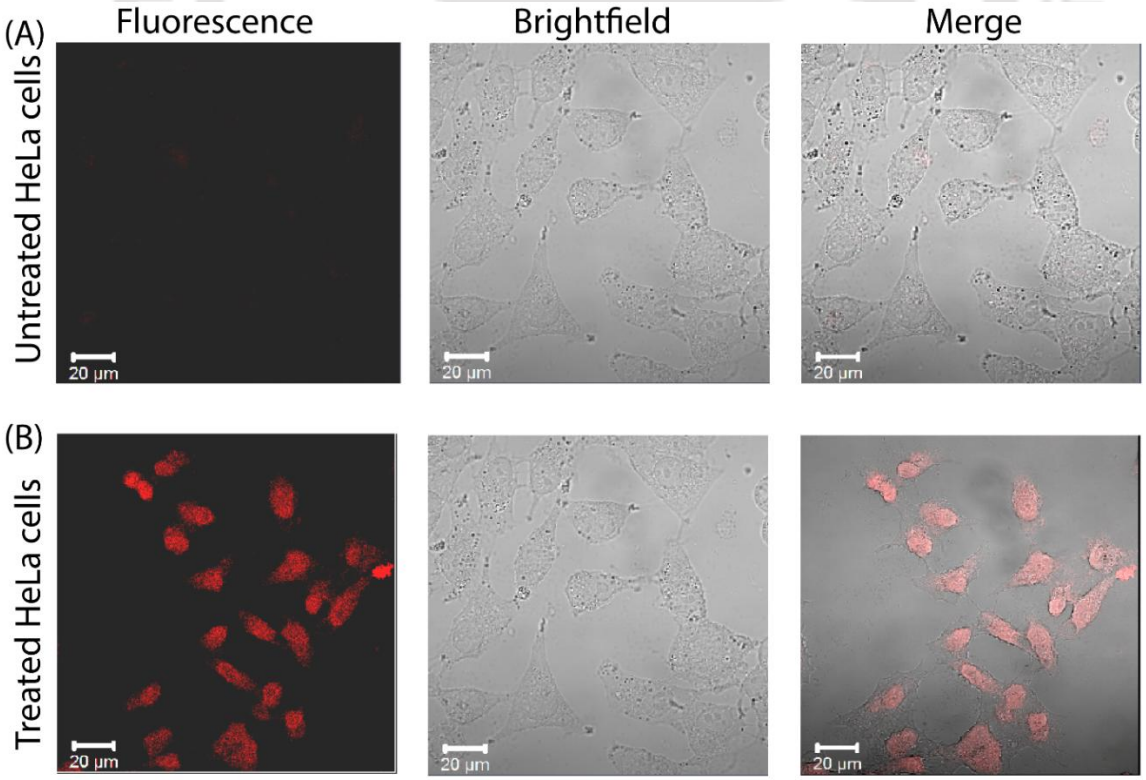

Fig. 4.13. Representative confocal microscopic images of untreated (A) and **4.3e-MC**-treated (B) HeLa cells.

The ability to respond to visible light and changes in pH provides a mechanism for controlled IDO1 enzyme inhibition and offers the prospect of targeted therapeutic intervention with minimized off-target effects. The acidic pH-dependent isomerization of **4.3e** from inactive (**4.3e-SP**) to active (**4.3e-MC**) IDO1 enzyme inhibitor offers a significant advantage, because a lower extracellular pH typically characterizes the tumor microenvironment compared to healthy tissues.[15] The visible light can serve as an external stimulus to convert an inactive inhibitor of the IDO1 enzyme into an active one. This approach also offers significant advantages for biomedical applications, as it has relatively low phototoxicity and allows for deeper tissue penetration compared to ultraviolet light.[16] Therefore, the inherent properties of spiropyran derivatives make them a promising scaffold for the development of smart drugs that effectively respond to specific stimuli in a spatiotemporally controlled manner, particularly in the field of immunotherapy.

4.3. Summary

In summary, we synthesized a series of spiropyran derivatives and identified **4.3e** as a potent and stimuli-responsive inhibitor of IDO1. Upon exposure to light, **4.3e** undergoes conversion to the photoactive **4.3e-MC** isoform, which exhibits strong IDO1 inhibitory activity in comparison to that of the photoinactive **4.3e-SP** isoform. By facilitating the release of heme from holo-IDO1 and transforming it into the apo form, the **4.3e-MC** exhibits the ability to bind both apo-IDO1 protein and free hemin. These findings highlight a novel strategy for spatiotemporal regulation of IDO1 activity by utilizing light and pH as the external stimuli. Compared to traditional IDO1 inhibitors, this photoresponsive approach offers significant potential for the development of spatiotemporally regulated therapies for cancer, Alzheimer's disease, and other pathological conditions, enabling greater specificity and safety.

4.4. General information

The required chemicals were all acquired from Sigma Aldrich, Merck, and various sources and utilized directly without any purification. The thin-layer chromatography (TLC) was prepared using silica gel 60 F254 (0.25 mm) on glass plates and used to monitor the progress of the reaction. Column chromatography was carried out using 60-120 mesh silica gels. With the help of 600, 400, and 150 MHz Bruker spectrometer, the ^{1}H NMR and ^{13}C NMR were obtained, respectively. The chemical shift (δ_{ppm}) and the coupling constants (J values) were mentioned in parts per million (ppm) and Hertz (Hz), respectively, downfield from tetramethylsilane using $CDCl_3$ and DMSO-d_6 as the internal solvent. The residual chloroform (d = 7.28 ppm for ^{1}H NMR, d = 77.23 ppm for ^{13}C NMR)

was used as an internal standard. Multiplicities were designated as follows: s (singlet), d (doublet), t (triplet), m (multiplet), and br (broadened). The Agilent Q-TOF mass spectrometer was used to record the high-resolution mass spectra (HRMS) of the synthesized compounds.

4.5. Experimental section

4.5.1. Synthesis and characterization of compounds

4.5.1.1. General method for the synthesis of N-alkylated 2,3,3-trimethylindolenine derivatives

To the stirring solution of 2,3,3-trimethyl-3*H*-indole (1equiv.) in CAN (25 mL), methyl iodide/ iodoethanol (2 equiv.) was added. The reaction mixture was stirred under reflux conditions for 24 hours. A pink precipitate formed in the mixture, which was subsequently filtered out and washed with acetone to yield the desired product with around 95% yield. The product obtained was sufficiently pure to proceed to the next reaction without further purification.[17]

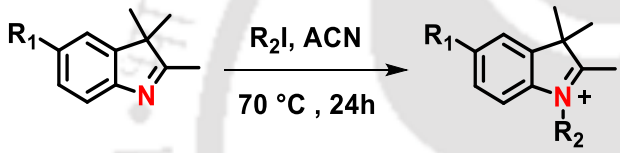

Scheme 4.2. Synthetic routes to *N*-alkylated 2,3,3-trimethylindolenine derivatives.

4.5.1.2. General method for the synthesis of spiropyran derivatives

To a stirring solution of *N*-alkylated 2,3,3-trimethylindolenine derivative (1.14 equiv) in EtOH (10 mL), salicylaldehyde derivatives (1.08 equiv.) To the reaction mixture, NaOAc (2 equiv.) was added and stirred for 6 hours at 75 °C. The reaction mixture was then extracted with EtOAc (3 × 20 mL), and the combined organic layers were dried over anhydrous Na_2SO_4, and the solvent was evaporated under reduced pressure. The reaction mixture was purified through column chromatography using a gradient solvent system of EtOAC/Hexane (0-15%) to obtain the pure product.[18]

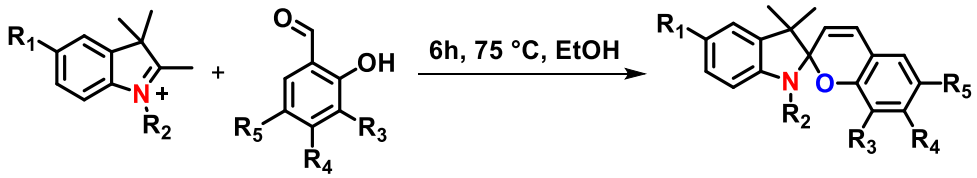

Scheme 4.3. General method for the synthesis of spiropyran derivatives.

4.5.1.2.1. Synthesis of 1',3',3'-trimethylspiro[chromene-2,2'-indoline] (1a*)*

The targeted compound (76% yield) was synthesized from 1,2,3,3-tetramethyl-3*H*-indol-1-ium and 2-hydroxybenzaldehyde following the general procedure as mentioned in section 4.5.1. **^{1}H NMR (600 MHz, DMSO-*d*$_6$) δ$_{ppm}$** 7.17 (dd, *J* = 7.6, 1.7 Hz, 1H), 7.12 - 7.08 (m, 3H), 7.02 (d, *J* = 10.2 Hz, 1H), 6.83 (t, *J* = 7.4 Hz, 1H), 6.77 (t, *J* = 7.4 Hz, 1H), 6.66 (d, *J* = 8.1 Hz, 1H), 6.56 (d, *J* = 7.7 Hz, 1H), 5.76 (d, *J* = 10.2 Hz, 1H), 2.65 (s, 3H), 1.21 (s, 3H), 1.09 (s, 3H). **^{13}C NMR (150 MHz, DMSO-*d*$_6$) δ$_{ppm}$** 154.41, 148.31, 136.75, 130.25, 129.80, 127.91, 127.39, 121.92, 120.67, 119.70, 119.39, 119.08, 114.79, 107.25, 104.29, 51.82, 29.04, 26.13, 20.35. **HRMS (ESI)** calcd. for **$C_{19}H_{19}NO$** $(M+H)^+$: 278.1539, found: 278.1507.

4.5.1.2.2. Synthesis of 1',3',3'-trimethyl-6-nitrospiro[chromene-2,2'-indoline] (1b)

The targeted compound (71% yield) was synthesized from 1,2,3,3-tetramethyl-3*H*-indol-1-ium and 2-hydroxy-5-nitrobenzaldehyde following the general procedure as mentioned in section 4.5.1. **^{1}H NMR (400 MHz, DMSO-*d*$_6$) δ$_{ppm}$** 8.16 (d, J = 2.8 Hz, 1H), 7.94 (dd, J = 9.0, 2.9 Hz, 1H), 7.17 (d, J = 10.4 Hz, 1H), 7.06 (d, J = 7.4 Hz, 2H), 6.83 (dd, J = 9.0, 0.7 Hz, 1H), 6.75 (td, J = 7.4, 1.0 Hz, 1H), 6.56 (dt, J = 7.3, 1.0 Hz, 1H), 5.93 (d, J = 10.4 Hz, 1H), 2.62 (s, 3H), 1.16 (s, 3H), 1.05 (s, 3H). **^{13}C NMR (150 MHz, DMSO-*d*$_6$) δ$_{ppm}$** 159.87, 147.88, 140.95, 136.29, 128.75, 128.13, 126.20, 123.28, 122.03, 121.90, 119.90, 119.39, 115.85, 107.51, 106.61, 52.33, 28.97, 26.14, 20.12. **HRMS (ESI)** calcd. for **$C_{19}H_{18}N_2O$** $(M+H)^+$: 323.1390, found: 323.1358.

4.5.1.2.3. Synthesis of 1',3',3'-trimethylspiro[chromene-2,2'-indolin]-8-ol (1c)

The targeted compound (73% yield) was synthesized from 1,2,3,3-tetramethyl-3*H*-indol-1-ium and 2,3-dihydroxybenzaldehyde following the general procedure as mentioned in section 4.5.1. **^{1}H NMR (600 MHz, CDCl$_3$) δ$_{ppm}$** 7.22 (td, J = 7.6, 1.3 Hz, 1H), 7.12 (dd, J = 7.3, 1.3 Hz, 1H), 6.91 – 6.88 (m, 2H), 6.82 (dd, J = 8.0, 1.6 Hz, 1H), 6.78 (t, J = 7.7 Hz, 1H), 6.68 (dd, J = 7.5, 1.6 Hz, 1H), 6.57 (d, J = 7.7 Hz, 1H), 5.73 (d, J = 10.3 Hz, 1H), 5.56 (s, 1H), 2.79 (s, 3H), 1.34 (s, 3H), 1.22 (s, 3H). **^{13}C NMR (150 MHz, CDCl$_3$) δ$_{ppm}$** 147.98, 143.23, 140.82, 136.56, 129.57, 127.75, 121.68, 120.36, 119.49, 119.35, 118.96, 118.05, 115.61, 106.98, 105.35, 51.76, 28.88, 25.91, 19.92. **HRMS (ESI)** calcd. for **$C_{19}H_{19}NO_2$** $(M+H)^+$: 294.1489, found: 294.1491.

4.5.1.2.4. Synthesis of 6-fluoro-1',3',3'-trimethylspiro[chromene-2,2'-indoline] (1d)

The targeted compound (80% yield) was synthesized from 1,2,3,3-tetramethyl-3*H*-indol-1-ium and 5-fluoro-2-hydroxybenzaldehyde following the general procedure as mentioned in section 4.5.1. **^{1}H NMR (400 MHz, CDCl$_3$) δ$_{ppm}$** 7.18 (td, *J* = 7.6, 1.3 Hz, 1H), 7.07 (dd, *J* = 7.2, 1.3 Hz, 1H), 6.84 (td, *J* = 7.4, 1.0 Hz, 1H), 6.80 – 6.75 (m, 3H),

6.65-6.62 (m, 1H), 6.52 (d, *J* = 7.7 Hz, 1H), 5.74 (d, *J* = 10.2 Hz, 1H), 2.72 (s, 3H), 1.30 (s, 3H), 1.16 (s, 3H). **^{13}C NMR (150 MHz, CDCl$_3$) δ$_{ppm}$** 157.34, 155.76, 150.43, 148.11, 136.65, 128.67, 127.64, 121.51, 120.89, 119.20, 115.81, 112.62, 112.46, 106.82, 104.22, 51.82, 28.93, 25.84, 20.20. **HRMS (ESI)** calcd. for **$C_{19}H_{18}FNO$** $(M+H)^+$: 296.1445, found: 296.1416.

4.5.1.2.5. Synthesis of 6-chloro-1',3',3'-trimethylspiro[chromene-2,2'-indoline] (1e)

The targeted compound (78% yield) was synthesized from 1,2,3,3-tetramethyl-3*H*-indol-1-ium and 5-chloro-2-hydroxybenzaldehyde following the general procedure as mentioned in section 4.5.1. **^{1}H NMR (400 MHz, CDCl$_3$) δ$_{ppm}$** 7.10 (td, *J* = 7.6, 1.3 Hz, 1H), 6.99 (dd, *J* = 7.3, 1.3 Hz, 1H), 6.94 (dq, *J* = 4.7, 2.6 Hz, 2H), 6.77 (td, *J* = 7.4, 1.0 Hz, 1H), 6.70 (d, *J* = 10.3 Hz, 1H), 6.57 – 6.54 (m, 1H), 6.44 (d, *J* = 7.7 Hz, 1H), 5.65 (d, *J* = 10.2 Hz, 1H), 2.64 (s, 3H), 1.21 (s, 4H), 1.08 (s, 3H). **^{13}C NMR (150 MHz, CDCl$_3$) δ$_{ppm}$** 153.06, 148.08, 136.58, 129.36, 128.51, 127.70, 126.18, 124.64, 121.54, 120.76, 120.06, 119.32, 116.38, 106.90, 104.55, 51.91, 28.94, 25.88, 20.16. **HRMS (ESI)** calcd. for **$C_{19}H_{18}ClNO$** $(M+H)^+$: 312.1150, found: 312.1150

4.5.1.2.6. Synthesis of 8-chloro-6-fluoro-1',3',3'-trimethylspiro[chromene-2,2'-indoline] (1f)

The targeted compound (76% yield) was synthesized from 1,2,3,3-tetramethyl-3*H*-indol-1-ium and 3-chloro-5-fluoro-2-hydroxybenzaldehyde following the general procedure as mentioned in section 4.5.1. **^{1}H NMR (400 MHz, CDCl$_3$) δ$_{ppm}$** 7.16 (td, *J* = 7.6, 1.3 Hz, 1H), 7.06 (dd, *J* = 7.3, 1.3 Hz, 1H), 6.90 (dd, *J* = 8.3, 3.0 Hz, 1H), 6.84 (td, *J* = 7.4, 1.0 Hz, 1H), 6.76 (d, *J* = 10.2 Hz, 1H), 6.69 (dd, *J* = 8.0, 3.0 Hz, 1H), 6.52 (d, *J* = 7.6 Hz, 1H), 5.79 (d, *J* = 10.2 Hz, 1H), 2.72 (s, 3H), 1.30 (s, 3H), 1.17 (s, 4H). **^{13}C NMR (150 MHz, CDCl$_3$) δ$_{ppm}$** 156.37, 154.78, 147.89, 146.30, 146.28, 136.41, 128.18, 127.60, 122.24, 121.45, 119.35, 116.84, 111.25, 106.88, 105.30, 51.94, 28.89, 25.77, 20.26. **HRMS (ESI)** calcd. for **$C_{19}H_{17}ClFNO$** $(M+H)^+$: 330.1055, found: 330.1038.

4.5.1.2.7. Synthesis of 6,8-dichloro-1',3',3'-trimethylspiro[chromene-2,2'-indoline] (1g)

The targeted compound (81% yield) was synthesized from 1,2,3,3-tetramethyl-3*H*-indol-1-ium and 3,5-dichloro-2-hydroxybenzaldehyde following the general procedure as mentioned in section 4.5.1. **^{1}H NMR (400 MHz, CDCl$_3$) δ$_{ppm}$** 7.09 (dd, *J* = 7.6, 1.3 Hz, 1H), 7.06 (dd, *J* = 3.5, 1.9 Hz, 1H), 6.98 (dd, *J* = 7.3, 1.3 Hz, 1H), 6.86 (d, *J* = 2.5 Hz, 1H), 6.76 (td, *J* = 7.4, 1.0 Hz, 1H), 6.68 (d, *J* = 10.3 Hz, 1H), 6.45 (d, *J* = 7.7 Hz, 1H), 5.70 (d, *J* = 10.2 Hz, 1H), 2.63 (s, 3H), 1.21 (s, 3H), 1.08 (s, 3H). **^{13}C NMR (150 MHz,**

$CDCl_3$) δ_{ppm} 148.67, 147.83, 136.33, 131.14, 129.39, 128.01, 127.63, 124.71, 124.45, 122.03, 121.46, 121.07, 119.45, 106.93, 105.69, 52.03, 28.88, 25.80, 20.21. **HRMS (ESI)** calcd. for **$C_{19}H_{18}Cl_2NO$** $(M+H)^+$: 346.076, found: 346.0740.

4.5.1.2.8. Synthesis of 6-bromo-1',3',3'-trimethylspiro[chromene-2,2'-indoline] (1h)

The targeted compound (78% yield) was synthesized from 1,2,3,3-tetramethyl-3*H*-indol-1-ium and 5-bromo-2-hydroxybenzaldehyde following the general procedure as mentioned in section 4.5.1. **^{1}H NMR (400 MHz, DMSO-d_6) δ_{ppm}** 7.33 (dd, *J* = 28.1 Hz, 2.8Hz, 1H), 7.17 (dd, *J* = 8.6, 2.6 Hz, 1H), 7.11 – 7.02 (m, 2H), 6.96 (d, *J* = 10.3 Hz, 1H), 6.72 (t, *J* = 7.3 Hz, 1H), 6.59 (d, *J* = 8.6 Hz, 1H), 6.48 (dd, *J* = 22.1, 8.4 Hz, 1H), 5.79 (d, *J* = 10.3 Hz, 1H), 2.58 (s, 3H), 1.14 (s, 3H), 1.03 (s, 3H). **^{13}C NMR (150 MHz, DMSO-d_6) δ_{ppm}** 153.63, 148.13, 137.95, 136.57, 132.49, 129.56, 128.76, 127.98, 121.94, 121.16, 119.55, 117.13, 111.69, 107.31, 104.77, 52.01, 29.00, 24.06, 20.27. **HRMS (ESI)** calcd. for **$C_{19}H_{18}BrNO$** $(M+H)^+$: 356.0645, found: 356.0600.

4.5.1.2.9. Synthesis of 1',3',3'-trimethylspiro[chromene-2,2'-indoline]-6-carbonitrile (1i)

The targeted compound (74% yield) was synthesized from 1,2,3,3-tetramethyl-3*H*-indol-1-ium and 3-formyl-4-hydroxybenzonitrile following the general procedure as mentioned in section 4.5.1. **^{1}H NMR (400 MHz, $CDCl_3$) δ_{ppm}** 7.38 – 7.35 (m, 2H), 7.20 (td, *J* = 7.7, 1.3 Hz, 1H), 7.08 (dd, *J* = 7.2, 1.2 Hz, 1H), 6.89 – 6.83 (m, 2H), 6.76 – 6.74 (m, 1H), 6.55 (d, *J* = 7.7 Hz, 1H), 5.81 (d, *J* = 10.3 Hz, 1H), 2.73 (s, 3H), 1.29 (s, 3H), 1.17 (s, 3H). **^{13}C NMR (150 MHz, $CDCl_3$) δ_{ppm}** 158.00, 147.79, 136.19, 133.84, 130.76, 128.03, 127.82, 121.57, 121.42, 119.67, 119.55, 119.18, 116.13, 107.03, 105.76, 103.26, 52.21, 28.88, 25.86, 19.99. **HRMS (ESI)** calcd. for **$C_{20}H_{18}N_2O$** $(M+H)^+$: 303.1492, found: 303.1461.

4.5.1.2.10. Synthesis of 6-methoxy-1',3',3'-trimethylspiro[chromene-2,2'-indoline] (1j)

The targeted compound (75% yield) was synthesized from 1,2,3,3-tetramethyl-3*H*-indol-1-ium and 2-hydroxy-5-methoxybenzaldehyde following the general procedure as mentioned in section 4.5.1. **^{1}H NMR (400 MHz, $CDCl_3$) δ_{ppm}** 7.16 (td, *J* = 7.6, 1.3 Hz, 1H), 7.06 (dd, *J* = 7.3, 1.3 Hz, 1H), 6.83 (dd, *J* = 7.4, 1.0 Hz, 1H), 6.79 (d, *J* = 10.2 Hz, 1H), 6.65 – 6.64 (m, 2H), 6.60 – 6.59 (m, 1H), 6.51 (d, *J* = 7.9 Hz,1H), 5.69 (d, *J* = 10.2 Hz, 1H), 3.74 (s, 3H), 2.71 (s, 3H), 1.30 (s, 3H), 1.15 (s, 3H). **^{13}C NMR (150 MHz, $CDCl_3$) δ_{ppm}** 153.15, 148.63, 148.28, 136.88, 129.34, 127.61, 121.53, 120.33, 119.12,

119.07, 115.56, 115.28, 111.49, 106.80, 103.89, 55.82, 51.67, 29.00, 25.90, 20.29. **HRMS (ESI)** calcd. for **$C_{20}H_{21}NO_2$** (M+ H)$^+$: 308.1645, found: 308.1646.

4.5.1.2.11. Synthesis of 8-methoxy-1',3',3'-trimethylspiro[chromene-2,2'-indoline] (1k)

The targeted compound (73% yield) was synthesized from 1,2,3,3-tetramethyl-3*H*-indol-1-ium and 2-hydroxy-3-methoxybenzaldehyde following the general procedure as mentioned in section 4.5.1. **^{1}H NMR (400 MHz, $CDCl_3$) δ_{ppm}** 7.05 (td, *J* = 7.6, 1.3 Hz, 1H), 6.96 (dd, *J* = 7.2, 1.3 Hz, 1H), 6.74 – 6.72 (m, 1H), 6.70 (d, *J* = 1.6 Hz, 1H), 6.65 (d, *J* = 6.0 Hz, 2H), 6.60 – 6.58 (m, 1H), 6.41 (d, *J* = 7.7 Hz, 1H), 5.57 (d, *J* = 10.2 Hz, 1H), 3.55 (s, 3H), 2.65 (s, 3H), 1.23 (s, 3H), 1.08 (s, 3H). **^{13}C NMR (150 MHz, $CDCl_3$) δ_{ppm}** 148.16, 147.09, 143.98, 136.81, 129.21, 127.44, 121.50, 119.83, 119.69, 119.60, 119.28, 118.87, 114.10, 106.65, 104.31, 56.59, 51.64, 28.88, 25.79, 20.32. **HRMS (ESI)** calcd. for **$C_{20}H_{21}NO_2$** (M+ H)$^+$: 308.1645, found: 308.1614.

4.5.1.2.12. Synthesis of 7-methoxy-1',3',3'-trimethylspiro[chromene-2,2'-indoline] (1l)

The targeted compound (72% yield) was synthesized from 1,2,3,3-tetramethyl-3*H*-indol-1-ium and 2-hydroxy-4-methoxybenzaldehyde following the general procedure as mentioned in section 4.5.1. **^{1}H NMR (600 MHz, $CDCl_3$) δ_{ppm}** 7.22 (td, *J* = 7.6, 1.3 Hz, 1H), 7.12 (dd, *J* = 7.2, 1.3 Hz, 1H), 6.98 (d, *J* = 8.3 Hz, 1H), 6.89 (td, *J* = 7.4, 1.0 Hz, 1H), 6.84 (d, *J* = 10.2 Hz, 1H), 6.57 (d, *J* = 7.7 Hz, 1H), 6.43 (dd, *J* = 8.3, 2.4 Hz, 1H), 6.35 – 6.34 (m, 1H), 5.57 (d, *J* = 10.2 Hz, 1H), 3.74 (s, 2H), 2.78 (s, 3H), 1.36 (s, 3H), 1.20 (s, 3H). **^{13}C NMR (150 MHz, $CDCl_3$) δ_{ppm}** 161.09, 155.86, 148.29, 136.93, 129.10, 127.60, 127.37, 121.54, 119.10, 116.22, 112.26, 106.84, 106.64, 104.64, 100.12, 55.31, 51.57, 28.92, 25.93, 20.11. **HRMS (ESI)** calcd. for **$C_{20}H_{21}NO_2$** (M+ H)$^+$: 308.1645, found: 308.1624.

4.5.1.2.13. Synthesis of 6-ethoxy-1',3',3'-trimethylspiro[chromene-2,2'-indoline] (1m)

The targeted compound (72% yield) was synthesized from 1,2,3,3-tetramethyl-3*H*-indol-1-ium and 5-ethoxy-2-hydroxybenzaldehyde following the general procedure as mentioned in section 4.5.1. **^{1}H NMR (600 MHz, $CDCl_3$) δ_{ppm}** 7.19 (t, *J* = 7.7 Hz, 1H), 7.10 (d, *J* = 7.2 Hz, 1H), 6.87 (t, *J* = 8.5 Hz, 2H), 6.85 – 6.82 (m, 1H), 6.79 – 6.75 (m, 2H), 6.53 (d, *J* = 7.7 Hz, 1H), 5.73 (d, *J* = 10.1 Hz, 1H), 3.93 (p, *J* = 6.9 Hz, 2H), 2.76 (s, 2H), 1.37 (s, 3H), 1.23 (s, 3H), 1.14 (t, *J* = 7.0 Hz, 3H). **^{13}C NMR (150 MHz, $CDCl_3$) δ_{ppm}** 148.12, 146.04, 145.00, 136.91, 129.42, 127.42, 121.43, 120.06, 120.05, 119.63,

119.36, 118.97, 118.07, 106.64, 104.23, 66.27, 51.42, 28.93, 25.78, 20.32, 14.96. **HRMS (ESI)** calcd. for **$C_{21}H_{23}NO_2$** $(M+H)^+$: 322.1802, found: 322.1802.

4.5.1.2.14. Synthesis of 1',3',3',6-tetramethylspiro[chromene-2,2'-indoline]-8-carbaldehyde (1n)

The targeted compound (72% yield) was synthesized from 1,2,3,3-tetramethyl-3*H*-indol-1-ium and 2-hydroxy-5-methylisophthalaldehyde following the general procedure as mentioned in section 4.5.1. **^{1}H NMR (400 MHz, $CDCl_3$) δ_{ppm}** 10.03 (s, 1H), 7.36 (dd, *J* = 2.3, 0.9 Hz, 1H), 7.07 (td, *J* = 7.6, 1.3 Hz, 1H), 7.01 (d, *J* = 2.3 Hz, 1H), 6.97 (dd, *J* = 7.1, 1.3 Hz, 1H), 6.79 – 6.74 (m, 2H), 6.43 (d, *J* = 7.7 Hz, 1H), 5.70 (d, *J* = 10.3 Hz, 1H), 2.66 (s, 4H), 2.18 (s, 4H), 1.24 (s, 4H), 1.11 (s, 4H). **^{13}C NMR (150 MHz, $CDCl_3$) δ_{ppm}** 189.08, 155.59, 147.81, 136.36, 133.55, 129.32, 128.85, 127.69, 127.39, 122.24, 121.44, 120.38, 120.00, 119.55, 106.96, 105.47, 52.03, 28.98, 25.82, 20.44, 20.30. **HRMS (ESI)** calcd. for **$C_{21}H_{21}NO_2$** $(M+H)^+$: 320.1645, found: 320.1642.

4.5.1.2.15. Synthesis of 1',3',3'-trimethylspiro[benzo[f]chromene-2,2'-indoline] (1o)

The targeted compound (68% yield) was synthesized from 1,2,3,3-tetramethyl-3*H*-indol-1-ium and 1-hydroxy-2-naphthaldehyde following the general procedure as mentioned in section 4.5.1. **^{1}H NMR (400 MHz, DMSO-d_6) δ_{ppm}** 8.14 (d, *J* = 8.5 Hz, 1H), 7.77 – 7.74 (m, 2H), 7.66 (d, *J* = 8.9 Hz, 1H), 7.47 (ddd, *J* = 8.4, 6.8, 1.4 Hz, 1H), 7.30 (ddd, *J* = 8.0, 6.8, 1.1 Hz, 1H), 7.08 – 7.04 (m, 2H), 6.92 (d, *J* = 8.9 Hz, 1H), 6.73 (td, *J* = 7.4, 1.0 Hz, 1H), 6.53 – 6.50 (m, 1H), 5.81 (d, *J* = 10.4 Hz, 1H), 2.60 (s, 3H), 1.19 (s, 3H), 1.09 (s, 3H**). ^{13}C NMR (150 MHz, DMSO-d_6) δ_{ppm}** 152.45, 148.15, 136.69, 130.62, 129.86, 128.89, 128.82, 127.96, 127.43, 125.60, 123.94, 121.97, 121.57, 119.50, 118.21, 117.36, 110.95, 107.26, 104.39, 51.66, 29.00, 26.05, 20.41. **HRMS (ESI)** calcd. for **$C_{23}H_{21}NO$** $(M+H)^+$: 328.1696, found: 328.1672.

4.5.1.2.16. Synthesis of 2-(6-fluoro-3',3'-dimethylspiro[chromene-2,2'-indolin]-1'-yl)ethan-1-ol (2a)

The targeted compound (78% yield) was synthesized from 1,2,3,3-tetramethyl-3*H*-indol-1-ium and 5-fluoro-2-hydroxybenzaldehyde following the general procedure as mentioned in section 4.5.1. **^{1}H NMR (600 MHz, $CDCl_3$) δ_{ppm}** 7.20 (td, *J* = 7.6, 1.3 Hz, 1H), 7.11 (d, *J* = 7.2 Hz, 1H), 6.89 (t, *J* = 7.4 Hz, 1H), 6.83 – 6.78 (m, 3H), 6.68 – 6.65 (m, 2H), 5.77 (d, *J* = 10.2 Hz, 1H), 3.79 – 3.77 (m, 2H), 3.56 – 3.51 (m, 1H), 3.36 (dt, *J* = 15.0, 5.2 Hz, 1H), 1.33 (s, 3H), 1.20 (s, 3H). **^{13}C NMR (150 MHz, $CDCl_3$) δ_{ppm}** 157.57, 156.00, 149.86, 147.24, 136.29, 128.78, 128.77, 127.66, 121.88, 121.24, 119.44, 116.19,

112.89, 106.65, 104.69, 60.79, 52.45, 46.13, 25.82, 20.38. **HRMS (ESI)** calcd. for **$C_{20}H_{20}FNO_2$** $(M+H)^+$: 326.1551, found: 326.1532.

4.5.1.2.17. Synthesis of 1'-(2-hydroxyethyl)-3',3'-dimethylspiro[chromene-2,2'-indoline]-6-carbonitrile (2b)

The targeted compound (64% yield) was synthesized from 1-(2-hydroxyethyl)-2,3,3-trimethyl-3*H*-indol-1-ium and 3-formyl-4-hydroxybenzonitrile following the general procedure as mentioned in section 4.5.1. **^{1}H NMR (400 MHz, $CDCl_3$) δ_{ppm}** 7.38 – 7.34 (m, 2H), 7.18 (td, *J* = 7.6, 1.3 Hz, 1H), 7.09 (dd, *J* = 7.3, 1.3 Hz, 1H), 6.89 (td, *J* = 7.4, 1.0 Hz, 1H), 6.83 (d, *J* = 10.4 Hz, 1H), 6.74 (d, *J* = 8.4 Hz, 1H), 6.66 (d, *J* = 7.8 Hz, 1H), 5.83 (d, *J* = 10.3 Hz, 1H), 3.82 – 3.70 (m, 2H), 3.45 (ddd, *J* = 14.9, 7.4, 5.5 Hz, 1H), 3.32 (dt, *J* = 14.8, 5.2 Hz, 1H), 1.28 (s, 3H), 1.18 (s, 3H). **^{13}C NMR (150 MHz, $CDCl_3$) δ_{ppm}** 157.52, 147.06, 135.90, 133.99, 130.87, 128.03, 127.82, 121.90, 121.74, 119.89, 119.41, 119.03, 116.17, 106.85, 106.15, 103.60, 60.84, 52.76, 46.11, 25.87, 20.08. **HRMS (ESI)** calcd. for **$C_{21}H_{20}N_2O_2$** $(M+H)^+$: 333.1598, found: 333.1579.

4.5.1.2.18. Synthesis 2-(3',3'-dimethylspiro[benzo[f]chromene-3,2'-indolin]-1'-yl)ethan-1-ol (2c)

The targeted compound (67% yield) was synthesized from 1-(2-hydroxyethyl)-2,3,3-trimethyl-3*H*-indol-1-ium and 2-hydroxy-1-naphthaldehyde following the general procedure as mentioned in section 4.5.1. **^{1}H NMR (400 MHz, $CDCl_3$) δ_{ppm}** 7.93 (d, *J* = 8.5 Hz, 1H), 7.65 – 7.63 (m, 1H), 7.51 (dd, *J* = 19.9, 9.7 Hz, 2H), 7.42 (ddd, *J* = 8.4, 6.8, 1.3 Hz, 1H), 7.25 (ddd, *J* = 8.1, 6.8, 1.1 Hz, 1H), 7.09 (td, *J* = 7.7, 1.3 Hz, 2H), 7.01 (dd, *J* = 7.2, 1.3 Hz, 1H), 6.88 (d, *J* = 8.9 Hz, 1H), 6.79 (t, *J* = 7.4 Hz, 1H), 6.56 (d, *J* = 7.8 Hz, 1H), 5.71 (d, *J* = 10.5 Hz, 1H), 3.66 (ddq, *J* = 16.5, 11.1, 5.9, 5.3 Hz, 2H), 3.45 (ddd, *J* = 14.9, 7.2, 5.3 Hz, 1H), 3.26 (dt, *J* = 14.8, 5.2 Hz, 1H), 1.25 (s, 3H), 1.13 (s, 3H). **^{13}C NMR (150 MHz, $CDCl_3$) δ_{ppm}** 152.13, 147.32, 136.40, 130.30, 129.74, 128.89, 128.64, 127.61, 126.85, 125.05, 123.49, 121.92, 120.69, 119.43, 118.04, 117.29, 110.50, 106.63, 104.74, 60.93, 52.16, 46.11, 25.73, 20.37. **HRMS (ESI)** calcd. for **$C_{24}H_{23}NO_2$** $(M+H)^+$: 358.1802, found: 358.1783.

4.5.1.2.19. Synthesis of 6-fluoro-1',3',3'-trimethylspiro[chromene-2,2'-indoline]-5'-sulfonic acid (3a)

The targeted compound (54% yield) was synthesized from 1,2,3,3-tetramethyl-5-sulfo-3*H*-indol-1-ium and 5-fluoro-2-hydroxybenzaldehyde following the general procedure as mentioned in section 4.5.1. **^{1}H NMR (400 MHz, DMSO-d_6) δ_{ppm}** 7.33 (dd, *J* = 8.0, 1.7 Hz, 1H), 7.24 (d, *J* = 1.7 Hz, 1H), 7.02 (dd, *J* = 8.7, 3.1 Hz, 1H), 6.95 (d, *J* =

10.2 Hz, 1H), 6.86 (td, *J* = 8.7, 3.1 Hz, 1H), 6.67 (dd, *J* = 8.9, 4.6 Hz, 1H), 6.42 (d, *J* = 8.0 Hz, 1H), 5.81 (d, *J* = 10.2 Hz, 1H), 2.59 (s, 3H), 1.16 (s, 3H), 1.04 (s, 3H). **^{13}C NMR (150 MHz, DMSO-*d*$_6$) δ$_{ppm}$** 150.57, 148.37, 140.39, 135.79, 129.22, 125.81, 121.08, 119.81, 116.31, 116.06, 116.00, 113.36, 113.20, 105.83, 104.73, 51.82, 29.15, 25.95, 20.26. **HRMS (ESI)** calcd. for **$C_{19}H_{18}FNO_4S$** $(M-H)^-$: 374.0868, found: 374.0892.

4.5.1.2.20. Synthesis of 6-chloro-1',3',3'-trimethylspiro[chromene-2,2'-indoline]-5'-sulfonic acid (3b)

The targeted compound (57% yield) was synthesized from 1,2,3,3-tetramethyl-5-sulfo-3*H*-indol-1-ium and 5-chloro-2-hydroxybenzaldehyde following the general procedure as mentioned in section 4.5.1. **^{1}H NMR (400 MHz, DMSO-*d*$_6$) δ$_{ppm}$** 7.54 (dd, J = 8.0, 1.7 Hz, 1H), 7.44 (t, J = 2.1 Hz, 2H), 7.25 (dd, J = 8.7, 2.6 Hz, 1H), 7.17 (d, J = 10.3 Hz, 1H), 6.89 (d, J = 8.7 Hz, 1H), 6.63 (d, J = 8.0 Hz, 1H), 6.01 (d, J = 10.3 Hz, 1H), 2.80 (s, 3H), 1.36 (s, 3H), 1.24 (s, 3H). **^{13}C NMR (150 MHz, DMSO-*d*$_6$) δ$_{ppm}$** 153.15, 148.32, 140.42, 135.71, 129.66, 128.97, 126.72, 125.84, 124.15, 120.99, 120.72, 119.82, 116.70, 105.88, 105.05, 51.89, 29.12, 25.96, 20.19. **HRMS (ESI)** calcd. for **$C_{19}H_{18}ClNO_4S$** $(M-H)^-$: 390.0572, found: 390.0595.

4.5.1.2.21. Synthesis of 8-chloro-6-fluoro-1',3',3'-trimethylspiro[chromene-2,2'-indoline]-5'-sulfonic acid (3c)

The targeted compound (52% yield) was synthesized from 1,2,3,3-tetramethyl-5-sulfo-3*H*-indol-1-ium and 3-chloro-5-fluoro-2-hydroxybenzaldehyde following the general procedure as mentioned in section 4.5.1. **^{1}H NMR (600 MHz, DMSO-*d*$_6$) δ$_{ppm}$** 7.43 (d, *J* = 8.0 Hz, 1H), 7.33 (d, *J* = 1.7 Hz, 1H), 7.24 (dd, *J* = 8.5, 3.0 Hz, 1H), 7.15 (dd, *J* = 8.5, 3.0 Hz, 1H), 7.06 (d, *J* = 10.2 Hz, 1H), 6.53 (d, *J* = 8.0 Hz, 1H), 5.97 (d, *J* = 10.2 Hz, 1H), 2.67 (s, 3H), 1.23 (s, 3H), 1.11 (s, 3H). **^{13}C NMR (150 MHz, DMSO-*d*$_6$) δ$_{ppm}$** 156.32, 154.74, 148.11, 146.21, 140.19, 135.52, 128.80, 128.78, 126.02, 122.42, 121.20, 119.78, 116.79, 112.49, 105.77, 52.00, 29.02, 26.04, 20.20. **HRMS (ESI)** calcd. for **$C_{19}H_{17}ClFNO_4S$** $(M+H)^+$: 410.0624, found: 410.0606.

4.5.1.2.22. Synthesis 6-cyano-1',3',3'-trimethylspiro[chromene-2,2'-indoline]-5'-sulfonic acid (3d)

The targeted compound (59% yield) was synthesized from 1,2,3,3-tetramethyl-5-sulfo-3*H*-indol-1-ium and 3-formyl-4-hydroxybenzonitrile following the general procedure as mentioned in section 4.5.1. **^{1}H NMR (400 MHz, DMSO-*d*$_6$) δ$_{ppm}$** 7.66 (d, *J* = 2.1 Hz, 1H), 7.49 (dd, *J* = 8.5, 2.2 Hz, 1H), 7.37 (dd, *J* = 8.0, 1.7 Hz, 1H), 7.28 (d, *J* = 1.7 Hz, 1H), 7.03 (d, *J* = 10.4 Hz, 1H), 6.83 (d, *J* = 8.5 Hz, 1H), 6.47 (d, *J* = 8.1 Hz, 1H),

5.89 (d, *J* = 10.3 Hz, 1H), 2.61 (s, 3H), 1.73 (s, 3H), 1.06 (s, 3H). **^{13}C NMR (150 MHz, DMSO-*d*$_6$) δ$_{ppm}$** 157.94, 148.25, 140.31, 135.56, 134.52, 131.59, 128.63, 125.99, 121.37, 120.03, 119.85, 119.46, 116.37, 106.18, 106.07, 102.97, 52.12, 29.06, 25.94, 20.03. **HRMS (ESI)** calcd. for **$C_{20}H_{18}N_2O_4S$** $(M-H)^-$: 381.0915, found: 381.0925.

4.5.1.2.23. Synthesis 1',3',3'-trimethylspiro[benzo[f]chromene-3,2'-indoline]-5'-sulfonic acid (4.3e)

The targeted compound (61% yield) was synthesized from 1,2,3,3-tetramethyl-5-sulfo-3*H*-indol-1-ium and 2-hydroxy-1-naphthaldehyde following the general procedure as mentioned in section 4.5.1. **^{1}H NMR (400 MHz, DMSO-*d*$_6$) δ$_{ppm}$** 8.15 (d, J = 8.5 Hz, 1H), 7.78 – 7.74 (m, 2H), 7.66 (d, J = 8.9 Hz, 1H), 7.48 (dd, J = 8.5, 6.9 Hz, 1H), 7.35 (dd, J = 8.0, 1.7 Hz, 1H), 7.30 (t, J = 7.5 Hz, 1H), 7.27 (d, J = 1.7 Hz, 1H), 6.97 (d, J = 8.9 Hz, 1H), 6.43 (d, J = 8.0 Hz, 1H), 5.83 (d, J = 10.5 Hz, 1H), 2.61 (s, 3H), 1.20 (s, 3H), 1.10 (s, 3H). **^{13}C NMR (150 MHz, DMSO-*d*$_6$) δ$_{ppm}$** 152.45, 148.30, 140.42, 135.80, 130.66, 129.85, 128.90, 128.85, 127.42, 125.82, 125.73, 123.94, 121.57, 119.85, 117.97, 117.40, 110.90, 105.82, 104.69, 51.54, 29.11, 25.91, 20.31. **HRMS (ESI)** calcd. for **$C_{23}H_{21}NO_4S$** $(M)^-$: 407.1197, found: 407.1183.

4.5.2. Purity Assessment by HPLC Analysis

HPLC analyses were performed to assess the purity of the synthesized compounds. Compound solution (20 µL of 100 µM) was injected into a 2.7 µm Ascentis® Express C18 HPLC column. The mobile phase, comprising 50% sodium citrate buffer (40 mM, pH 2.25), 50% methanol (v/v) containing 400 µM SDS, was used to perform HPLC analyses with a flow rate of 0.5 mL/minute. The HPLC traces were monitored using a 254 and 360 nm light source. The purity of the potent compounds was found to be 95-98%.

4.5.3. Light- and pH-modulated conformational switching of the compound

The photoswitchable properties of **4.3e** were examined under light irradiation and varying pH conditions using UV–Vis spectroscopy. A solution of **4.3e** in DMSO (100 µM) was irradiated at a wavelength of 400 nm. The resulting photochemical response was monitored using UV–Vis absorption spectroscopy with an EVOLUTION 201 spectrophotometer. We also investigated the photo reversibility of the **4.3e** between merocyanine and spiropyran conformation up to 7 cycles. Spectroscopic measurements were conducted across different pH levels to assess the pH-dependent switching behavior. Both UV–Vis and fluorescence spectroscopy were employed to monitor the changes in optical properties. Fluorescence measurements were performed for two distinct forms of the compound: **4.3e-SP** (λ_{ex} = 400 nm, λ_{em} = 510 nm) and **4.3e-MC** (λ_{ex} = 545 nm, λ_{em} =

603 nm). These spectral analyses demonstrated the reversible isomerization of **4.3e** in response to external stimuli, such as light and pH.

4.5.4. Purification of human tryptophan 2,3-dioxygenase (TDO) and indoleamine 2,3-dioxygenase 1 enzymes

The tryptophan 2,3-dioxygenase (TDO) and human indoleamine 2,3-dioxygenase 1 (IDO1) enzymes were purified following established protocols.[2, 12, 19] Recombinant human IDO1 and TDO enzymes, each engineered with an N-terminal 6×histidine tag, were expressed in *Escherichia coli* BL21 (DE3) cells. For culture initiation, a single transformed colony was inoculated into 5 mL of Luria–Bertani (LB) medium with kanamycin (50 μg/mL) and incubated overnight at 37 °C with shaking at 180 rpm. The resulting preculture (1 mL) was used to seed 1 L of fresh LB medium containing kanamycin, and the culture was maintained at 37 °C with shaking at 120 rpm until an optical density at 600 nm (OD_{600}) of approximately 0.6 was attained. To facilitate proper heme incorporation into the enzymes, hemin (10 μM) and L-tryptophan (1 mM) were introduced, and cells were allowed to grow further until reaching an OD_{600} of 0.9–1.0. Induction of protein expression was achieved by adding isopropyl β-D-1-thiogalactopyranoside (IPTG, 0.5 mM) following a cooling step, after which cultures were incubated at 22 °C with shaking at 120 rpm for 16–18 h to promote soluble protein expression. Cells were subsequently harvested by centrifugation, resuspended in 20 mL of ice-cold phosphate-buffered saline (PBS), and re-centrifuged at 15,000 rpm for 10 minutes at 4 °C to remove excess hemin. The resulting pellet was stored at –80 °C until further processing. The frozen cell pellet was resuspended in 15 mL of ice-cold potassium phosphate buffer (50 mM, pH 7.2) containing 300 mM KCl, 10 mM $MgCl_2$, 25 mM imidazole, 5% glycerol, a protease inhibitor cocktail (EDTA-free), and DNase (<1 mg) to facilitate protein purification. Cell disruption was carried out on ice, and the resulting lysate was centrifuged at 20,000 rpm for 30 minutes at 4 °C. The reddish supernatant was clarified through a 0.22 μm filter and subsequently incubated with 1 mL of nickel–nitrilotriacetic acid (Ni–NTA) resin (Qiagen) for 2 h at 4 °C with gentle agitation (80 rpm). The resin–protein suspension was transferred to an affinity column pre-equilibrated with potassium phosphate buffer (50 mM, pH 7.2) containing 300 mM KCl, 25 mM imidazole, and 5% glycerol. Unbound and weakly associated proteins were removed by sequential washing with 10 mL of equilibration buffer supplemented with 60 mM imidazole. Bound protein was eluted using phosphate buffer (50 mM, pH 7.2) containing 300 mM KCl, 190 mM imidazole, and 5% glycerol. IDO1 and TDO samples were passed through a Sephadex

G-25 desalting column equilibrated with phosphate buffer (50 mM, pH 6.8) to exchange the elution buffer containing 150 mM KCl and 10% glycerol. Protein purity was initially assessed by SDS-PAGE followed by Coomassie brilliant blue staining. Spectroscopic evaluation of enzyme quality was performed by calculating the absorbance ratio at 404 nm to 280 nm, yielding values of 1.1 for IDO1 and 0.8 for TDO, confirming the presence of heme-bound protein with satisfactory purity.

4.5.5. Expression and purification of apo-indoleamine 2,3-dioxygenase 1 enzyme

With a similar procedure, as described earlier, human apo-IDO1 was expressed and purified.[19] No external hemin was supplemented during protein expression. Following Ni–NTA affinity purification, the protein was dialyzed against 25 mM HEPES buffer (pH 7.2) containing 250 mM NaCl and 100 µM tris(2-carboxyethyl)phosphine (TCEP) to ensure a reducing environment. The enzyme was subsequently incubated overnight at room temperature with 150 mM sodium 2-mercaptoethanesulfonate (MESNA) to remove the bound heme cofactor. The resulting apo-IDO1 was dialyzed again in 25 mM HEPES buffer (pH 7.2) with 250 mM NaCl, and its buffer was further exchanged through a Sephadex G-25 column equilibrated with 50 mM potassium phosphate buffer (pH 6.8) containing 150 mM KCl and 10% glycerol. The efficiency of heme removal was assessed by calculating the absorbance ratio at 404 nm/280 nm for the purified apo-IDO1, which was approximately 0.06, indicating successful depletion of the heme cofactor.

4.5.6. Indoleamine 2,3-dioxygenase 1 and tryptophan 2,3-dioxygenase inhibition assay by the HPLC method

The HPLC analyses were performed to investigate the inhibitory activities of the IDO1 and TDO enzymes, following previously described protocols.[12, 19] Compounds were initially dissolved in DMSO and subsequently diluted with buffer, with 1% DMSO identified as the optimal concentration for the assay conditions. The inhibitors were pre-incubated with IDO1 and TDO enzymes for 1 hour prior to the activity assay. Following incubation, the reaction mixture was diluted 5-fold to a final volume of 500 µL in potassium phosphate buffer (100 mM, pH 7.2) supplemented with sodium ascorbate (20 mM), methylene blue (10 µM), bovine liver catalase (240 nM), and L-tryptophan (150 µM). Enzyme inhibition was assessed using a series of inhibitor concentrations prepared by serial dilution. The reaction mixtures were then incubated at 37 °C for 1 hour. To terminate the reaction, 100 µL of 30% (w/v) trichloroacetic acid was added, followed by incubation at 65 °C for 15 minutes to ensure complete quenching. The resulting precipitate was removed by centrifugation, and the supernatant was collected for HPLC analysis. A

20 µL aliquot was injected onto a 2.7 µm Ascentis® Express C18 column. The mobile phase consisted of a 1:1 (v/v) mixture of 40 mM sodium citrate buffer (pH 2.25) and methanol containing 400 µM SDS, delivered at a flow rate of 0.5 mL/min. Chromatograms were monitored at 365 nm and 280 nm to quantify kynurenine formation and tryptophan depletion, respectively.

4.5.7. Enzyme binding selectivity studies

To investigate the selectivity of **4.3e-MC** towards IDO1 in comparison with other heme-containing enzymes, the UV-Vis spectroscopic analyses of the purified hIDO1, hTDO, myoglobin, and hemoglobin enzymes were performed to investigate the ability of the potent compound to bind to the enzymes and interact with their heme groups.[19] A solution of **4.3e-MC** (10 µM) prepared in phosphate buffer (pH 6.5) was incubated separately with TDO, hemoglobin, and myoglobin for 15 min at 37 °C. The absorption spectra of the only enzymes, as well as the mixture of protein/enzyme and 4.3e-MC, were recorded using a UV–Vis spectrophotometer.

4.5.8. Detection of released heme from IDO1 enzyme using fluorescence assay

The **4.3e-MC**-induced release of heme cofactor from the IDO1 enzyme in solution was detected by monitoring the fluorescence signal of protoporphyrin-IX (PpIX; λ_{ex} = 400 nm, λ_{em} = 615 nm).[20, 21] To determine whether heme was present in the solution, 5 µM of IDO1 was first incubated in 100 mM potassium phosphate buffer at pH 6.5 with 50 µM of inhibitors for different times (0–60 minutes) at 37 °C. The solution was then mixed with PpIX (5 µM) and allowed to sit at room temperature for five minutes. We also conducted UV- Vis spectroscopic studies to further investigate the spectral relationship among PpIX, 4.3e-MC, and 4.3e-SP. The results revealed no overlap between the absorption spectra of PpIX with **4.3e-MC**. In contrast, a significant overlap was observed between the spectra of PpIX and **4.3e-SP**, accounting for their similar excitation profiles. However, the emission spectrum of PpIX was distinctly different from that of **4.3e-SP**, with no spectral overlap between the two.

4.5.9. Circular Dichroism analysis

Circular dichroism (CD) spectra of IDO1 enzyme and apo-IDO1 protein were recorded using a Jasco-810 spectropolarimeter. The IDO1 enzyme (200 nM) was incubated at 37 °C for one hour either in the presence or absence of the compound **4.3e-MC** (6.25 µM) in 10 mM tris buffer (pH 7.2). Following incubation, CD spectra were collected at 17 °C using a quartz cuvette with a 1 mm path length. Measurements were performed over a wavelength range of 195 to 250 nm with a 1 nm bandwidth and a scan

rate of 100 nm/sec. Background signals from the corresponding buffer (10 mM Tris, pH 7.2) were subtracted from all spectra. The secondary structure determination of the enzyme or protein was initially assessed using the in-built analysis software of the instrument and further verified through spectral deconvolution with the BeStSel program.

4.5.10. UV Vis spectral analysis for both catalytically active and inactive forms of IDO1

The UV-Vis spectroscopy was used to investigate the activity of catalytically active and inactive forms of IDO1 and the release of heme from IDO1.[3, 22, 23] Absorbance spectra were acquired using an EVOLUTION 201 spectrophotometer. All measurements were performed at 37 °C in 100 mM potassium phosphate buffer at pH 6.5. To create a deoxygenated environment, the solutions were purged with nitrogen gas, followed by the addition of sodium dithionate ($Na_2S_2O_4$). The dissociation rate of the heme cofactor from the IDO1 enzyme was determined by monitoring the Soret peak absorption at 404 nm. Additionally, the absorbance spectrum of the compound **4.3e-MC** was recorded in 5% DMSO-containing potassium phosphate buffer.

4.5.11. Heme binding affinity of the compound investigated by the UV-Vis method

The heme binding affinity of the compounds was evaluated by UV-Vis spectrophotometric analysis. Hemin was initially dissolved in DMSO and subsequently diluted to a final concentration of 5 µM in 20 mM HEPES buffer (pH 7.2) containing 40% DMSO. The stock solutions of the compounds were also prepared in DMSO. Hemin solutions were titrated with increasing concentrations of the compound, ranging from 0 to 175 µM. The extent of interaction was monitored by recording changes in the absorbance of the heme Soret peak at 401 nm as a function of compound concentration, allowing assessment of inhibitor binding affinity. Quinine and DMSO were used as positive and negative controls.

4.5.12. PpIX fluorescence-based heme binding affinity measurement

To investigate the heme binding affinity of the compounds, the fluorescence-based (λ_{ex} = 400 nm, λ_{em} = 615 nm) kinetic measurements were performed in the absence and presence of compounds (quinine, **4.3e-SP**, and **4.3e-MC**). Freshly prepared stock solution of hemin (0.5 mM in DMSO) in 20 mM HEPES buffer (pH 7.2) was incubated for 1 h at room temperature with and without the compounds.

4.5.13. Protein-ligand binding affinity measurement by Steady-state fluorescence anisotropy measurements

Steady-state fluorescence anisotropy measurements were performed using a Fluoromax-4 spectrofluorometer to determine the binding affinity between the potent compound and apo-IDO1 protein. A solution of **4.3e-MC** (500 nM) was prepared in potassium phosphate buffer (pH 6.5), and steady-state fluorescence anisotropy was recorded upon successive additions of varying concentrations of the apo-IDO1 protein. All anisotropy values of the **4.3e-MC** (λ_{ex} =545 nm; λ_{em} = 603 nm) in the absence or presence of apo-IDO1 protein are the mean values of three individual determinations. The degree (r) of anisotropy in the **4.3e-MC** fluorescence was calculated using the following equation.

$$r = \frac{(I_{VV} - GI_{VH})}{(I_{VV} + 2GI_{VH})}$$

The I_{VV} and I_{VH} are the fluorescence intensities of the emitted light polarized parallel and perpendicular to the excited light, respectively, and G = I_{VH}/I_{HH} is the instrumental grating factor.[24]

Similar steady-state fluorescence anisotropy measurements were performed in the presence of NaCl to investigate whether the interaction of 4.3e-MC with apo-IDO1 is governed by covalent or non-covalent interaction. The **4.3e-MC** (500 nM) was equilibrated with apo-IDO1 (12 µM) protein, 600 µL of potassium phosphate buffer (pH 6.5) for 1 h. Following incubation, the steady-state fluorescence anisotropy (λ_{ex} = 545 nm; λ_{em} = 603 nm) of the mixture was measured in the absence or presence of NaCl (0-75 µM).

4.5.14. Effect of apo-IDO1 protein on the spyropyran-merocyanine isomerization

To evaluate the stability of compound **4.3e-MC** within the IDO1 active site, UV–Vis spectroscopic measurements were performed. **4.3e-MC** (10 µM) was incubated with IDO1 enzyme (0.9 µM) in potassium phosphate buffer (100 mM, pH 7.2) at 37 °C for 1 h. Absorption spectra were recorded at defined time intervals to monitor potential changes in the spectral profile of the **4.3e-MC**, hence assessing the stability of the compound in the enzyme-bound state. The **4.3e-MC,** in the absence of apo-IDO1protein, readily converted to **4.3e-SP,** whereas the **4.3e-MC** remained stable in the presence of apo-IDO1 protein under similar experimental conditions.

4.5.15. Molecular docking and molecular dynamics simulations

4.5.15.1. Simulation setup and force field details

Molecular dynamics simulations were conducted using GROMACS (version 2023). The velocity Verlet scheme was employed for numerical integration with a timestep of 2 fs. The protein–ligand system was placed in a cubic box with periodic boundary

conditions in all directions. For the protein (PDB ID: 6AZW), the AMBER99SB-ILDN force field was applied, while the ligand (mero) was described using the General AMBER Force Field (GAFF). Ligand topologies were generated in *Antechamber* and converted to a GROMACS-compatible format with ACPYPE. The system was solvated with TIP3P water molecules. Non-bonded van der Waals and electrostatic short-range interactions were truncated at 1.2 nm, whereas long-range electrostatics were computed using the particle mesh Ewald (PME) approach. Bond lengths involving hydrogen atoms were constrained with the LINCS algorithm. Temperature was regulated with the modified V-rescale thermostat (relaxation time: 0.1 ps). During equilibration, pressure control was carried out with the C-rescale barostat (time constant: 2 ps), while the production stage employed the Parrinello–Rahman barostat with the same coupling constant.

4.5.15.2. MD simulation details

Before the simulations, docking was performed between chain B of 6AZW and the ligands (mero) using SwissDock with the AutoDock Vina scoring engine. The 6AZW–mero complex was selected for subsequent MD simulations. The solvated system consisted of 25,702 water molecules and a single chloride ion to neutralize the overall charge. Following solvation, steepest-descent energy minimisation was carried out to eliminate steric clashes and high-energy contacts. Equilibration was then performed in two steps: (i) NVT equilibration at 300 K for 0.1 ps, and (ii) NPT equilibration for 2 ps. During both stages, heavy atoms of the protein and ligand were restrained. Finally, a 100 ns production run was conducted under NPT conditions without restraints, and system coordinates were saved every 100 ps for analysis.

4.5.16. Cell viability analysis

Human cervical cancer cells (HeLa) and human embryonic kidney cells (HEK 293) were purchased from the National Centre for Cell Science (NCCS), Pune, India, and were used for this study. Cell lines were maintained with Dulbecco's Modified Eagle's Medium (DMEM) supplemented with 10% fetal bovine serum (FBS), Sodium bicarbonate, and 1% Antibiotic-antimycotic and were incubated in a 5% CO_2 humidified incubator at 37 °C. Trypsin-EDTA was used for further subculture and maintenance of the cells.[25, 26] For the cell viability assay, 5×10^3 cells of each cell line were seeded in 96-well plates, followed by 48h treatment with **4.3e-SP** and **4.3e-MC** in increasing concentration. The 3-(4,5-dimethylthiazol-2-yl)-2,5-diphenyltetrazolium bromide (MTT) dye was used to estimate the viability of the cells. Treated cells were incubated in the presence of MTT for 3h, for the dye to interact with the mitochondrial dehydrogenase enzymes, which is a direct

indication of live viable cells. After that, the MTT-containing media were removed, and 100 µL of MTT solvent composed of 100% isopropanol, 4 mM HCl, and 0.1% Triton X-100 was added to each well. The plates were then incubated for 15 minutes at room temperature in the dark, with slight shaking. Finally, the absorbance was recorded at 560 nm with the reference filter at 600 nm (GloMax® Discover). The data were analyzed using GraphPad Prism 8 software, and the half-maximal inhibitory concentrations (IC_{50}) for the compounds were calculated (if achieved). Cell viability was calculated using the following formula.

$$Cell\ viability\ \% = \frac{(Abs\ 560 - Abs\ 600)Treated\ cells}{(Abs\ 560 - Abs\ 600)\ Untreated\ cells}\ X\ 100$$

4.5.17. Cellular Indoleamine 2,3-dioxygenase 1 activity assay

The cellular enzyme activity assay was performed according to the reported procedure with minor modifications.[19] The HeLa cells were selected for this experiment because of the presence of IDO1 mRNA in this cell line.[27] First, HeLa cells (20,000 cells per well) were suspended in DMEM phenol-red-free medium (containing 10% FBS) and incubated for 3-4 h at 37 °C with 5% CO_2. After that, different compounds or only hemin or hemin-incubated compounds were dispensed into the previously incubated cells. After 1h, 50 ng/mL IFN-γ (supplemented in DMEM phenol-red free medium (containing 10% FBS)) was added to the cells. The treated cells were further incubated for 20 h. Reactions were terminated by the addition of trichloroacetic acid (5% for 0.5 h at 65 °C) into the incubated cells. After sonication, the precipitate was removed by centrifugation (Cells were not washed away before lysis). After that, clear media was taken for HPLC analysis. 20 µL of the media was then injected through Ascentis® express C18, 2.7 µm HPLC column. The mobile phase was 50% sodium citrate buffer (40 mM, pH 2.25) and 50% methanol (v/v) containing 400 µM SDS with a flow rate of 0.5 mL/minute.

4.5.18. Cellular internalization study

HeLa cells (1×10^5) were seeded in a 35 mm glass-bottom dish and incubated for 24 h to allow for cell adhesion. After this period, the cells were treated with compound **4.3e-MC** (final concentration of 50 µM) for 6 h. Incubated cells were washed three times with 1X PBS and then fixed using a 4% formaldehyde solution, followed by a PBS wash. Cells were visualized using a confocal microscope (Zeiss LSM 880).

4.5.19. NMR spectra of the synthesized compound

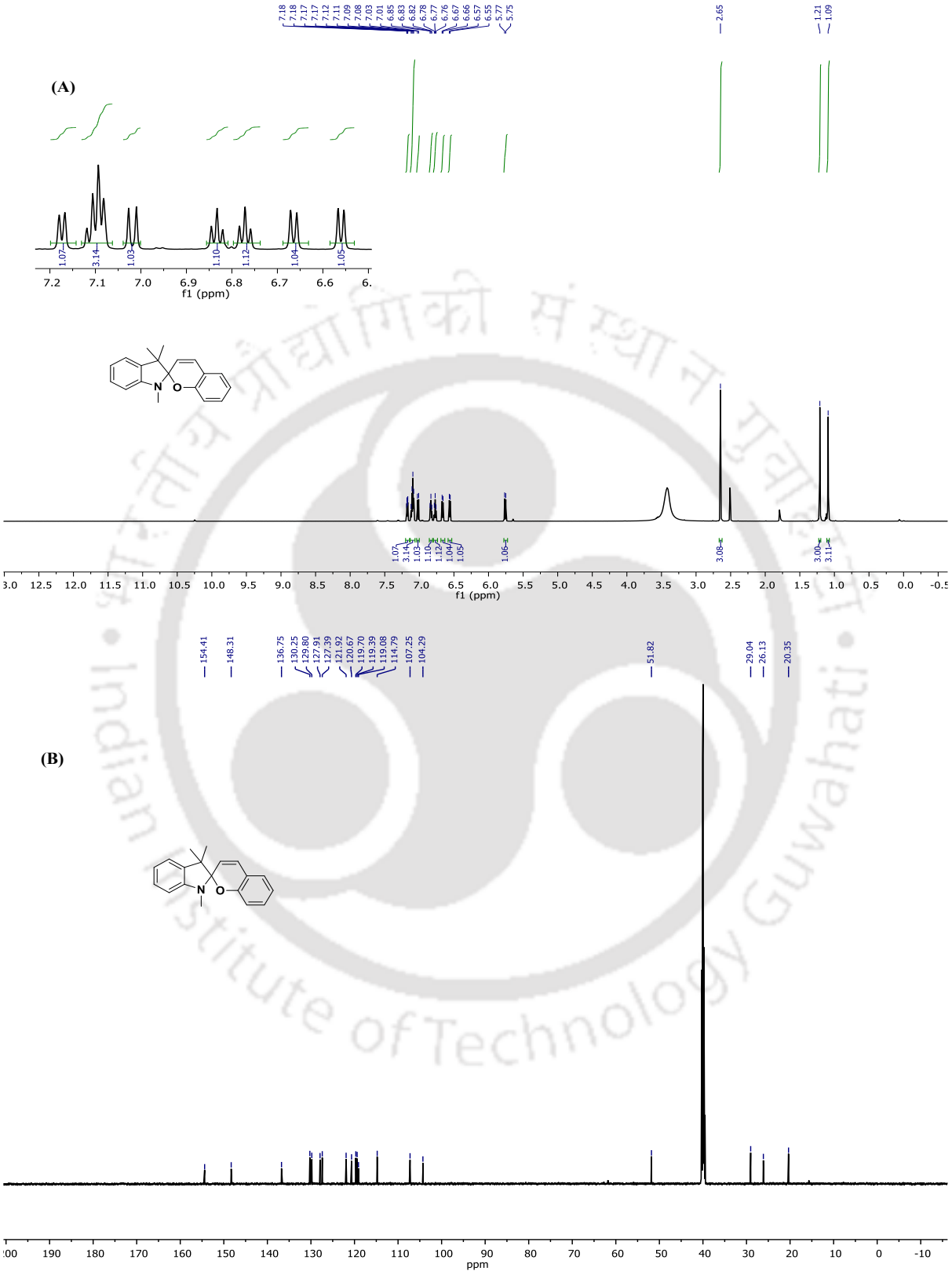

Fig. 4.14. ^{1}H NMR (A) and ^{13}C NMR (B) spectra of compound **1a.**

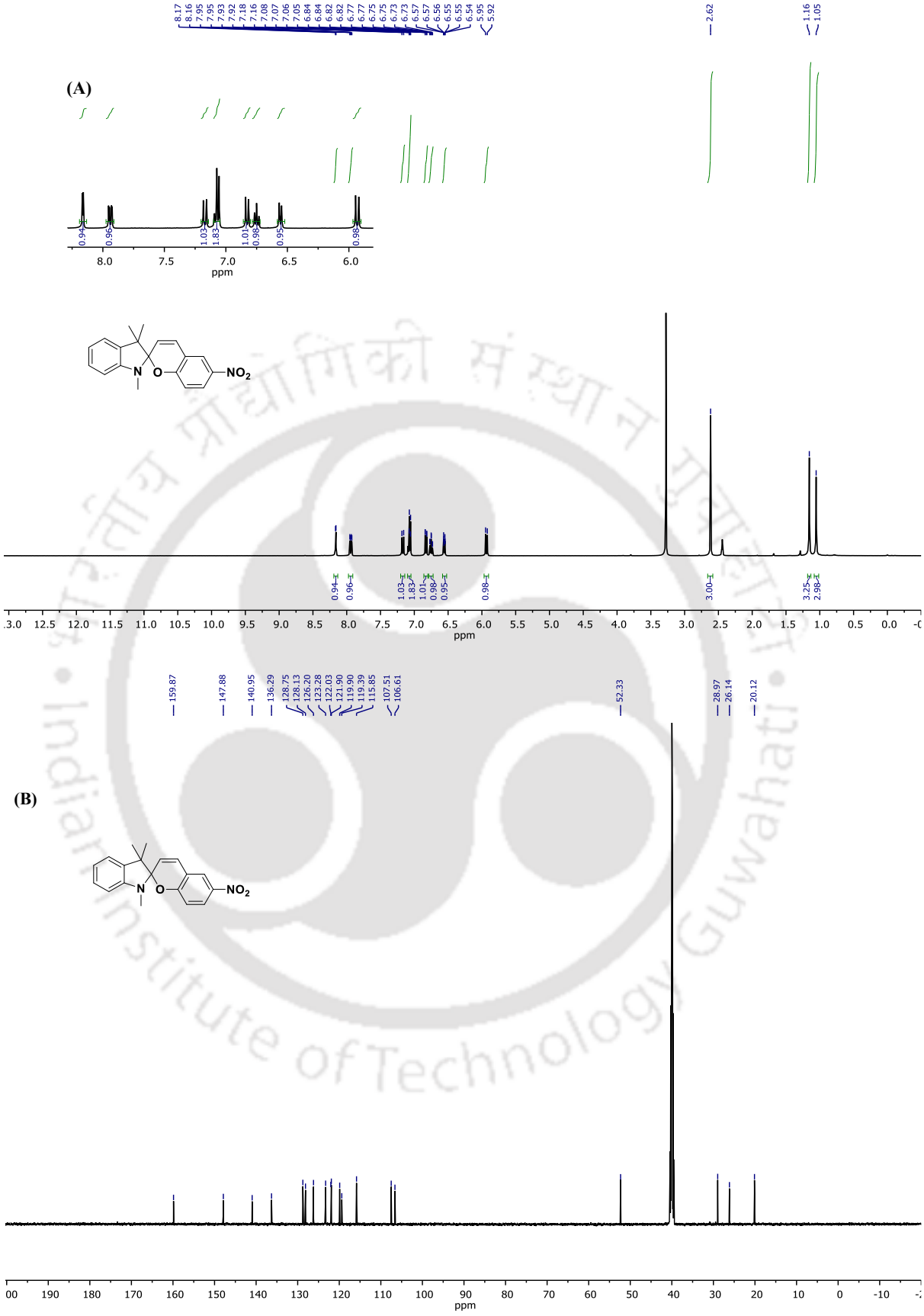

Fig. 4.15. ^{1}H NMR (A) and ^{13}C NMR (B) spectra of compound **1b**.

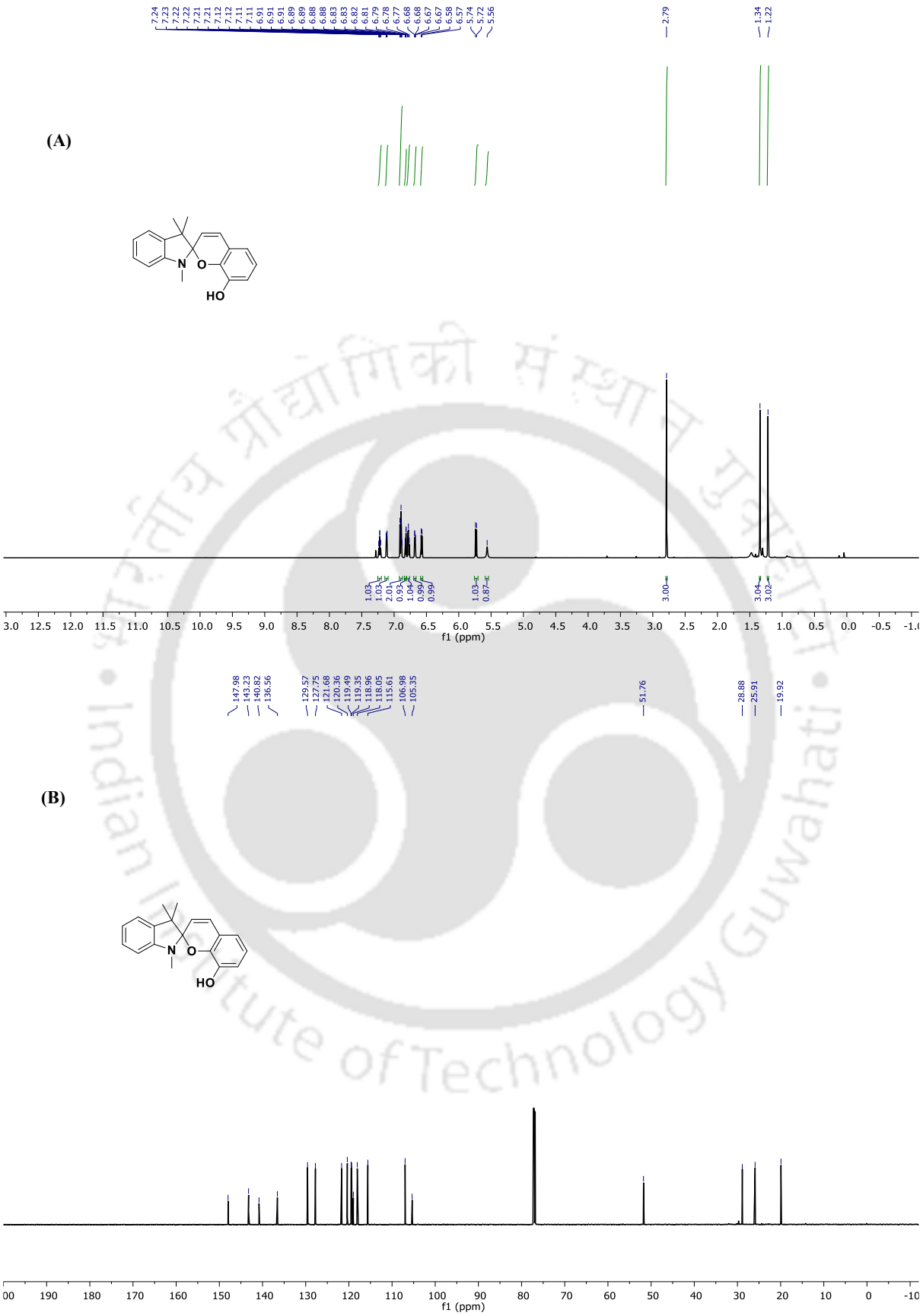

Fig. 4.16. ^{1}H NMR (A) and ^{13}C NMR (B) spectra of compound **1c**.

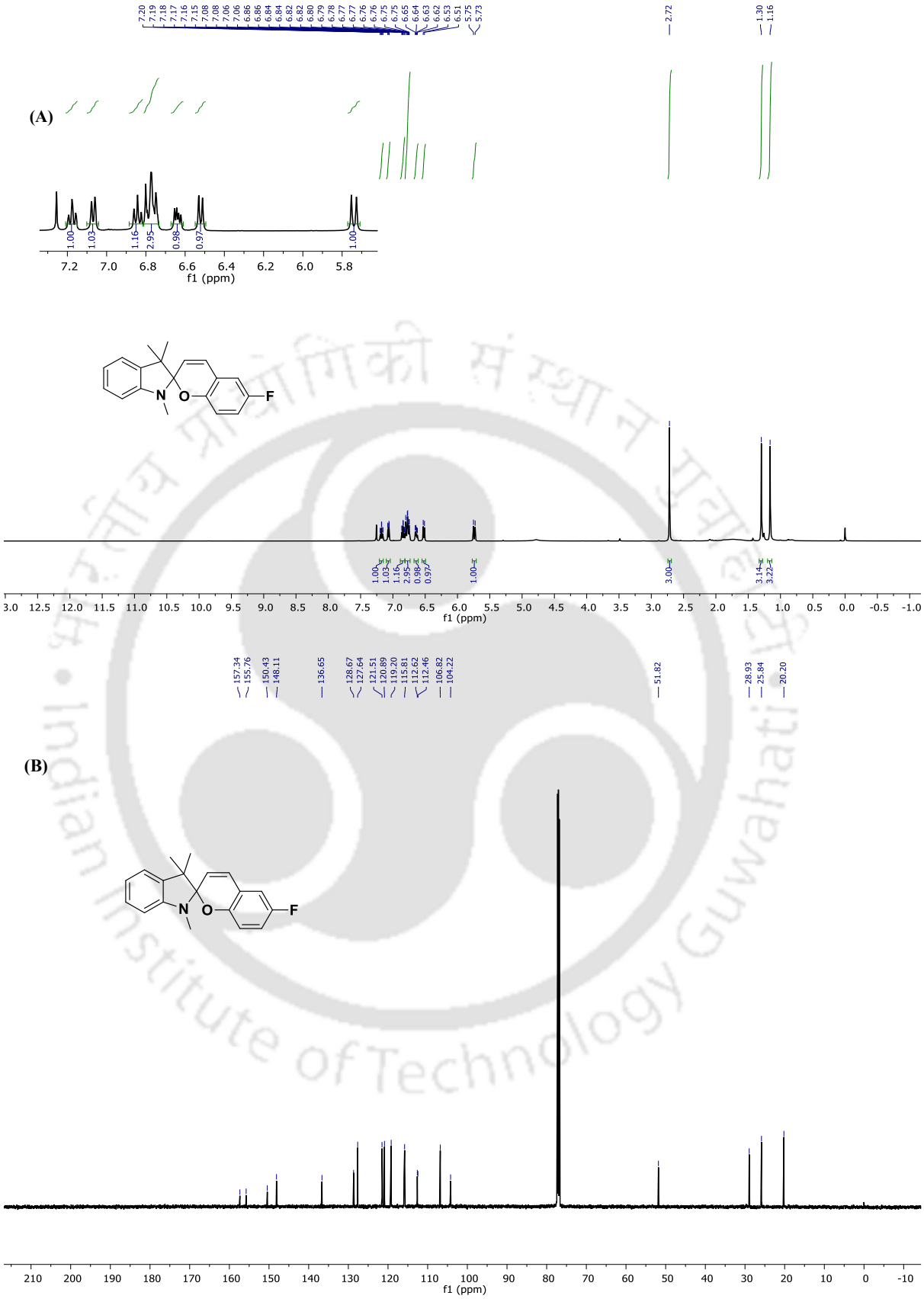

Fig. 4.17. ^{1}H NMR (A) and ^{13}C NMR (B) spectra of compound **1d**.

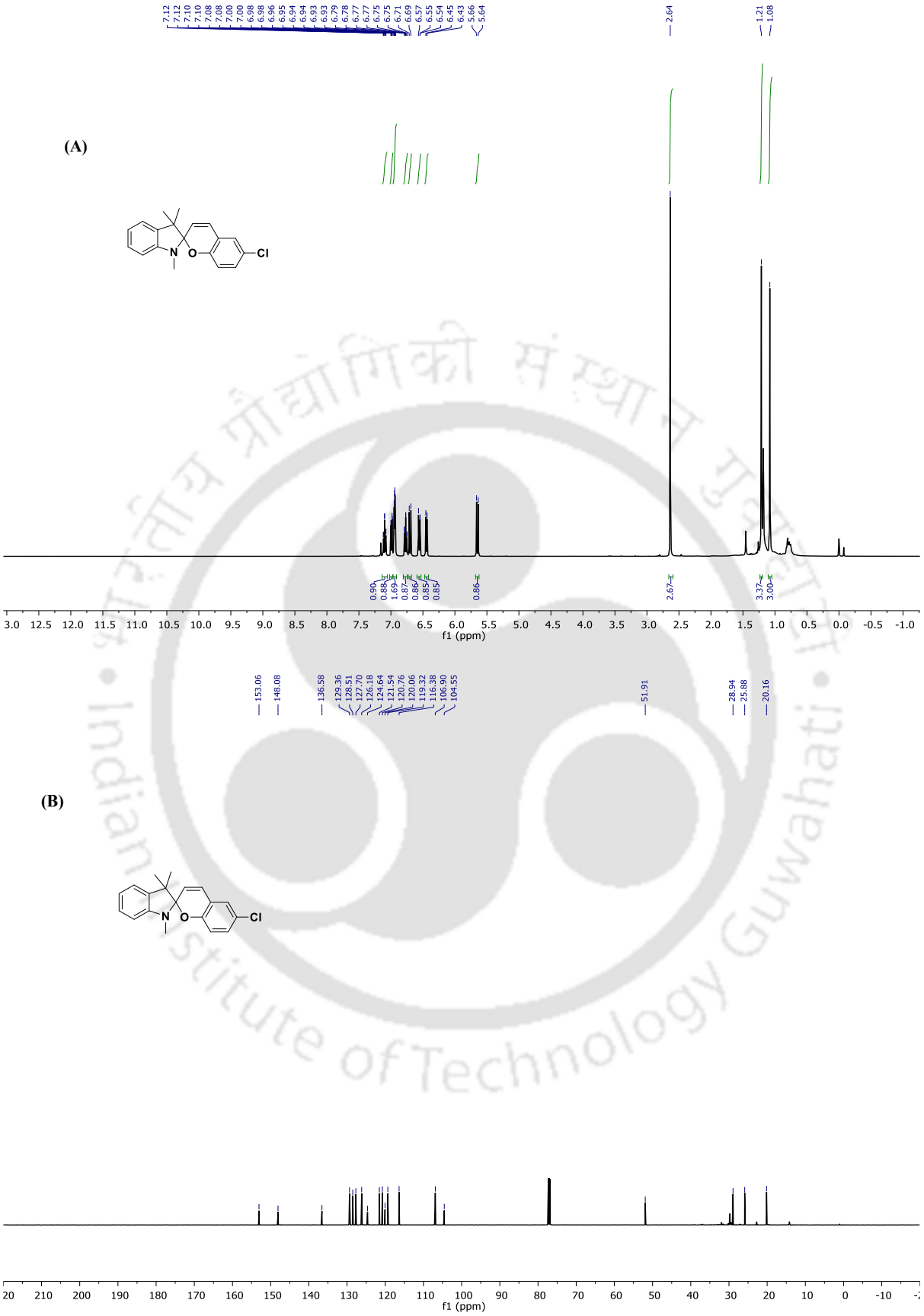

Fig. 4.18. ^{1}H NMR (A) and ^{13}C NMR (B) spectra of compound **1e**.

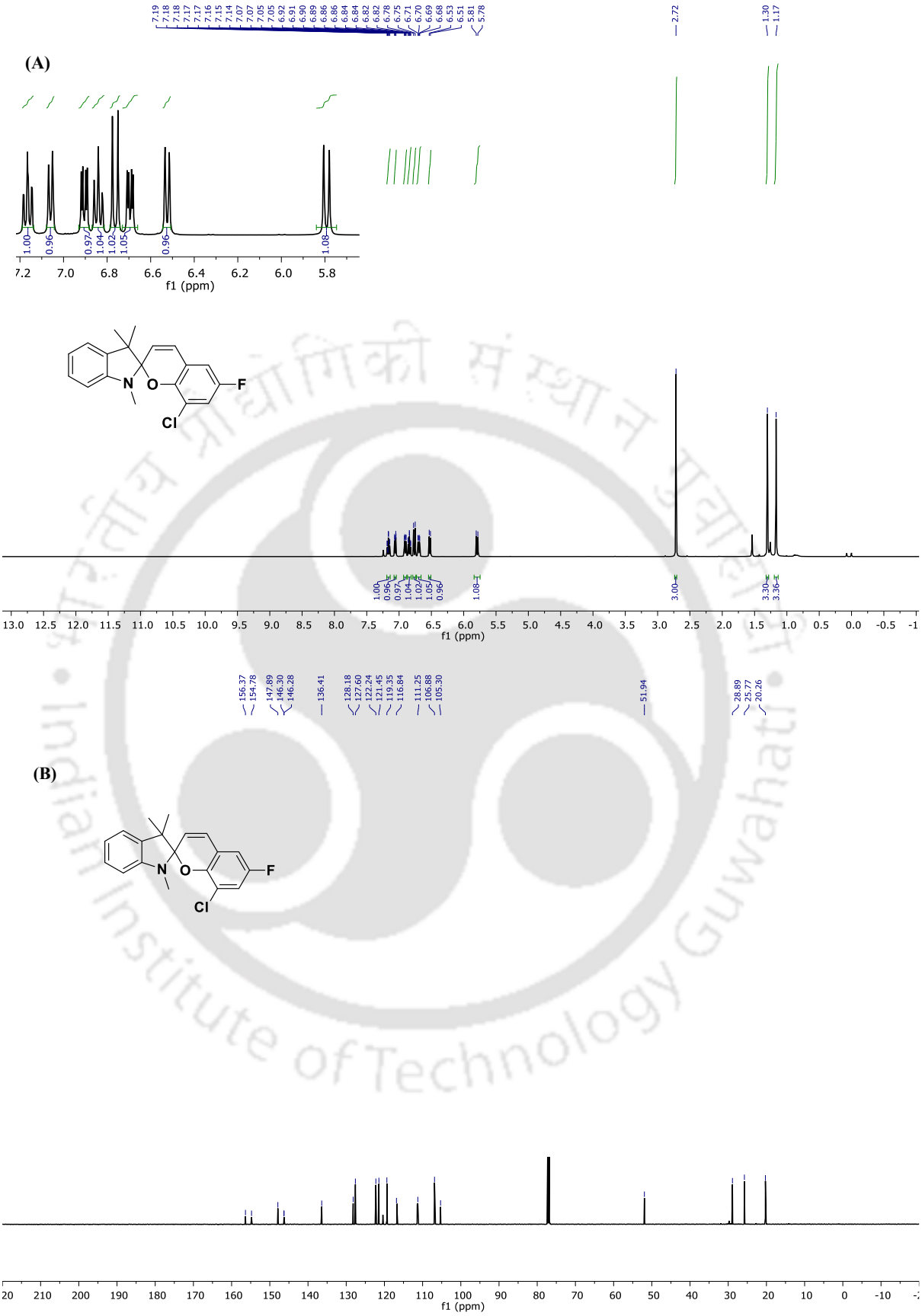

Fig. 4.19. ^{1}H NMR (A) and ^{13}C NMR (B) spectra of compound **1f.**

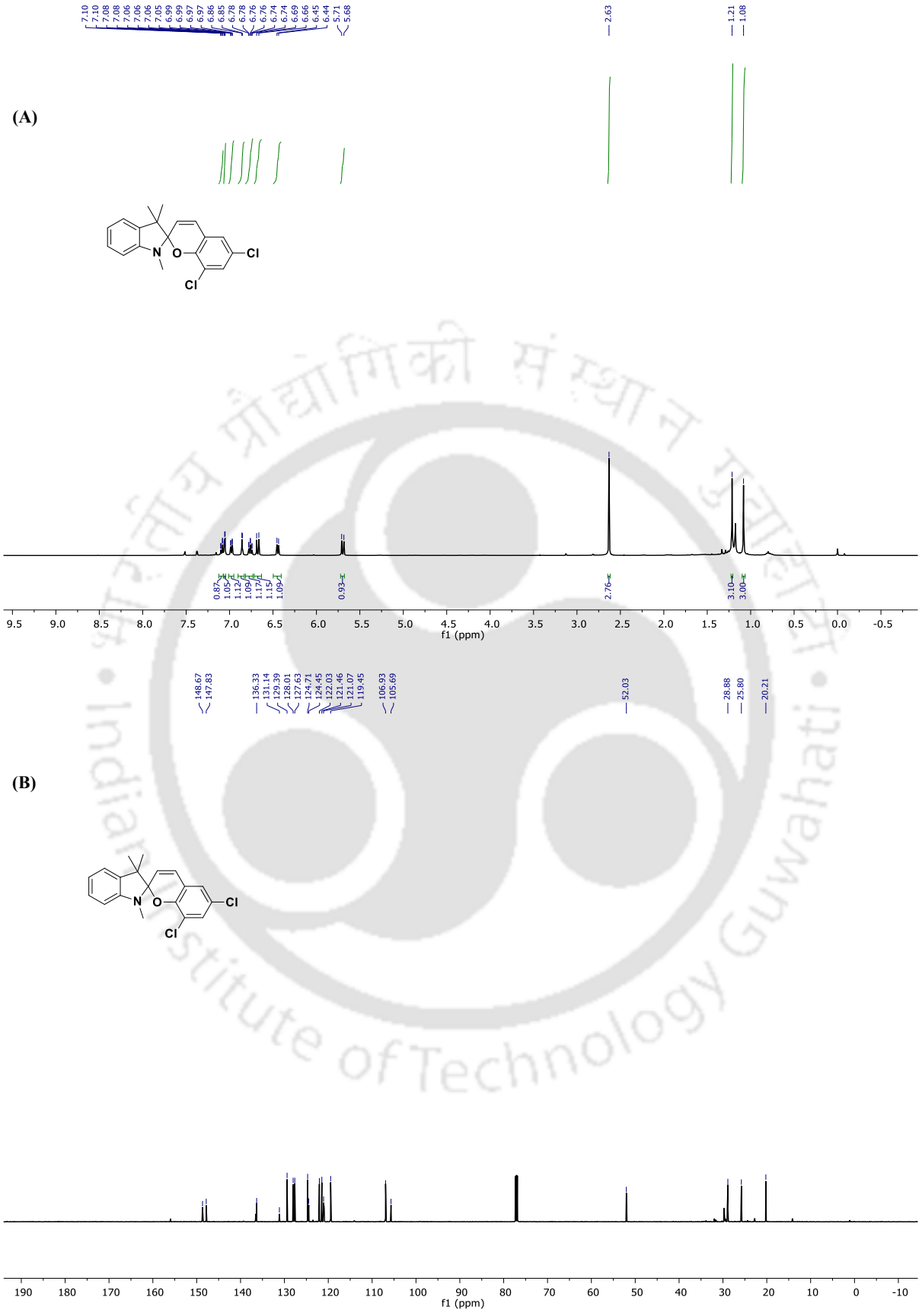

Fig. 4.20. ^{1}H NMR (A) and ^{13}C NMR (B) spectra of compound **1g.**

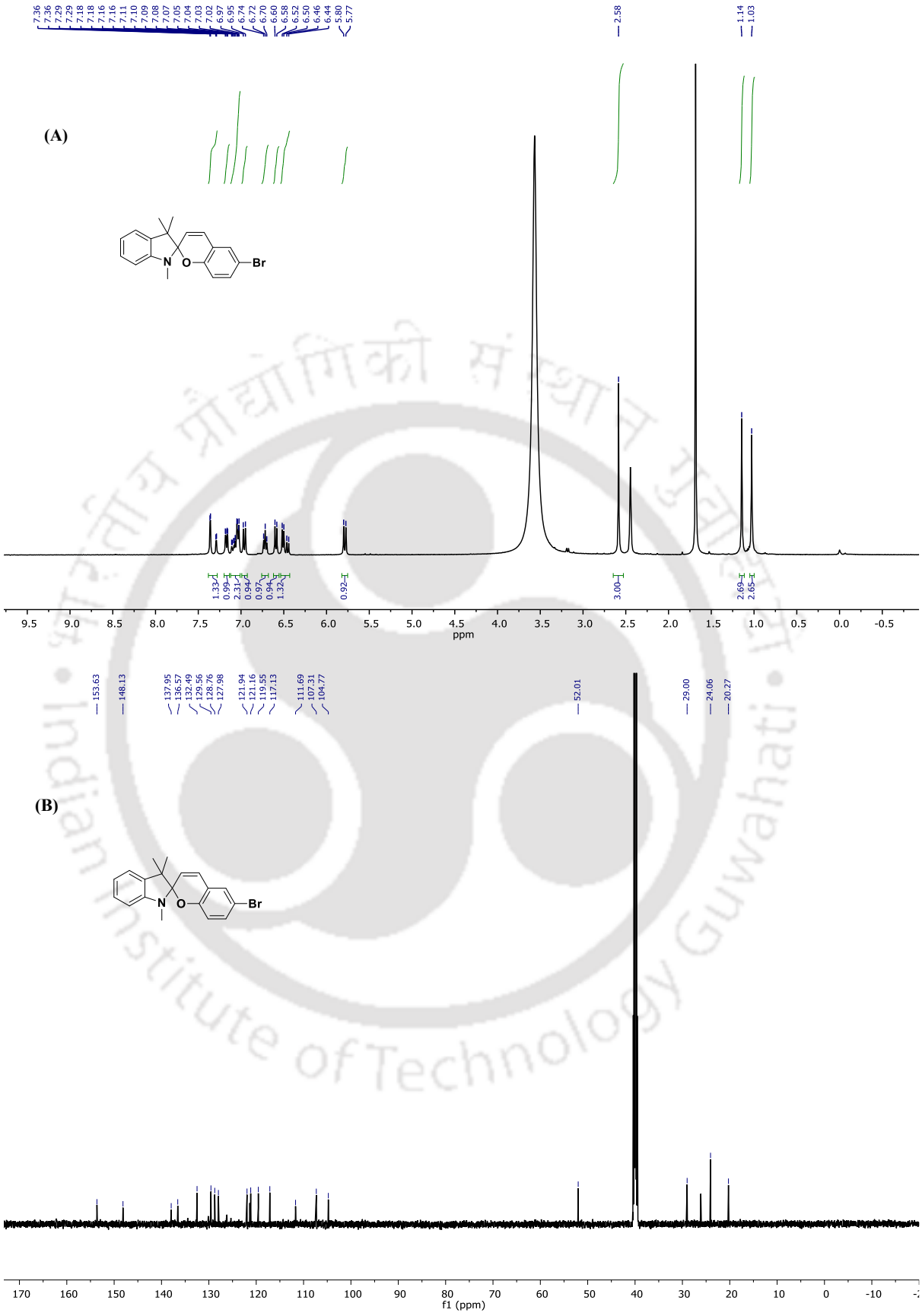

Fig. 4.21. ^{1}H NMR (A) and ^{13}C NMR (B) spectra of compound **1h**.

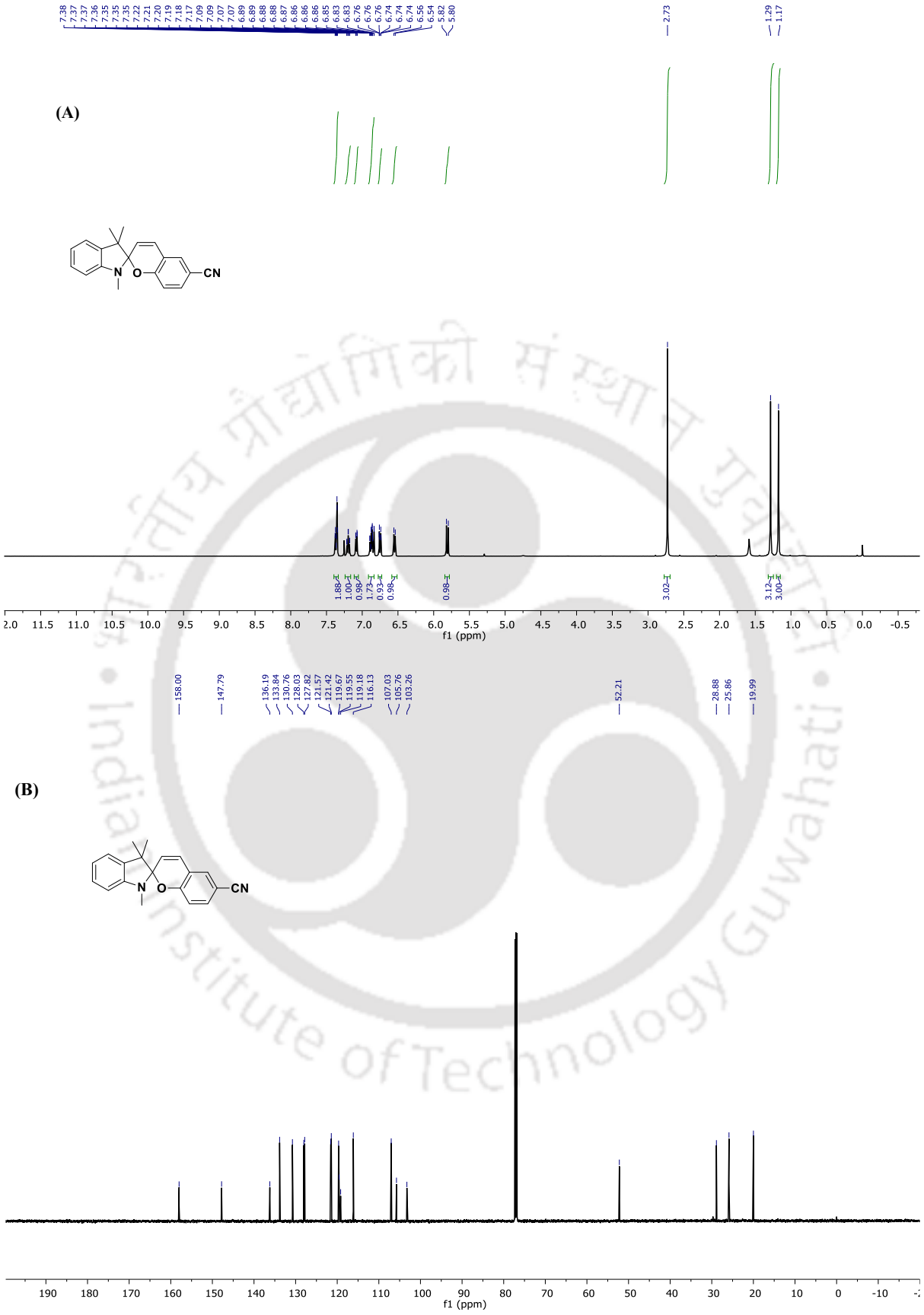

Fig. 4.22. ^{1}H NMR (A) and ^{13}C NMR (B) spectra of compound **1i**.

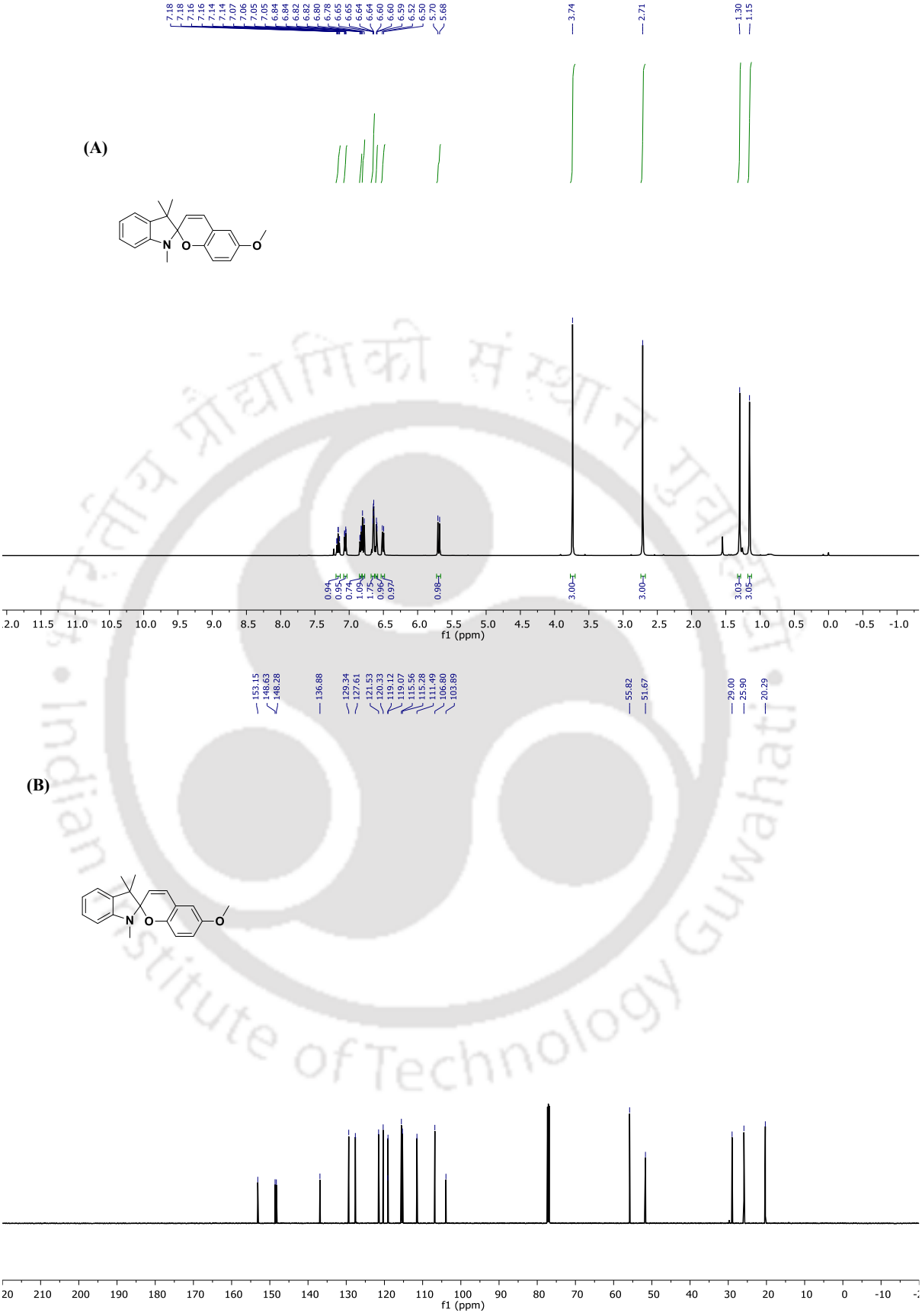

Fig. 4.23. ^{1}H NMR (A) and ^{13}C NMR (B) spectra of compound **1j**.

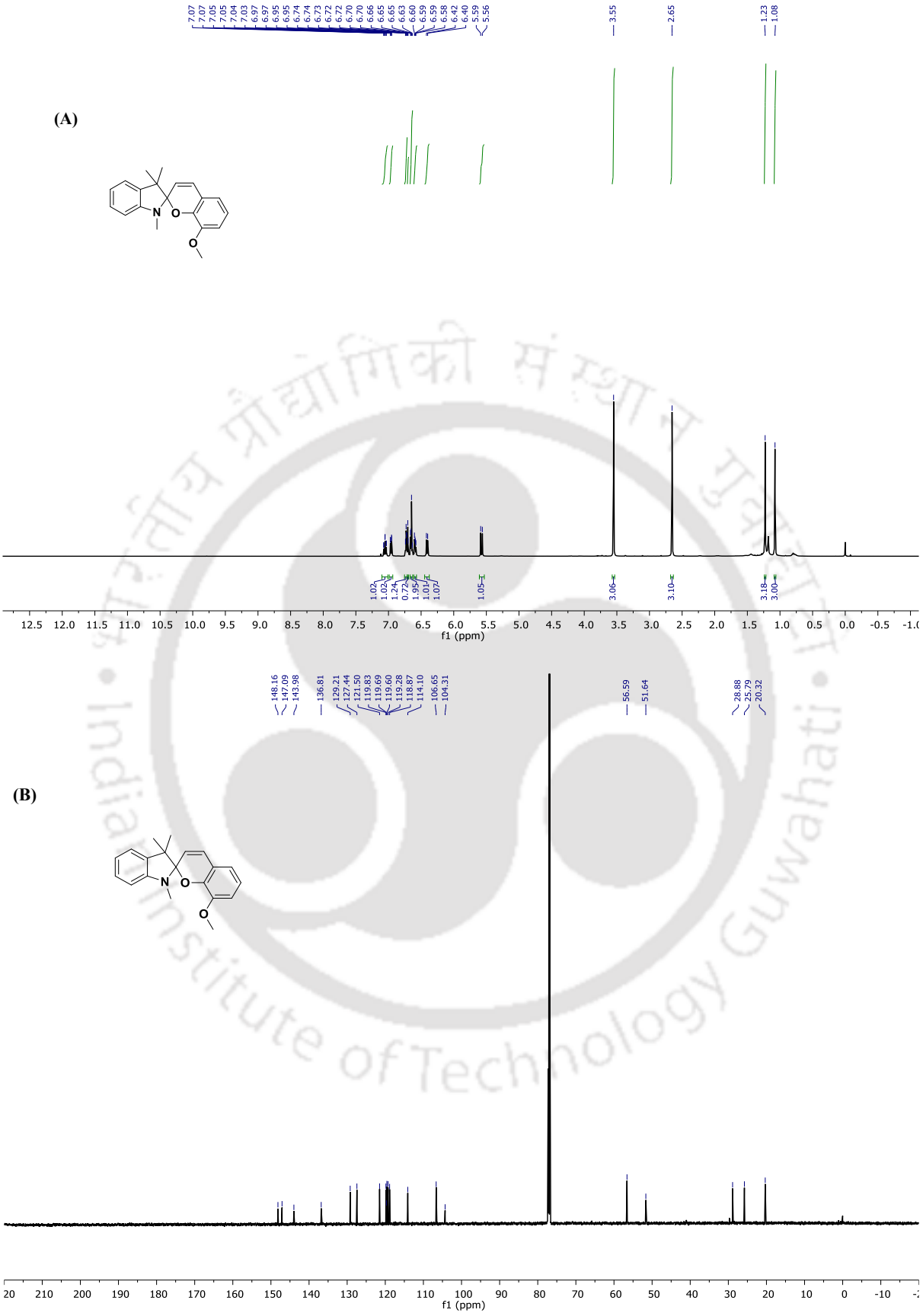

Fig. 4.24. ^{1}H NMR (A) and ^{13}C NMR (B) spectra of compound **1k.**

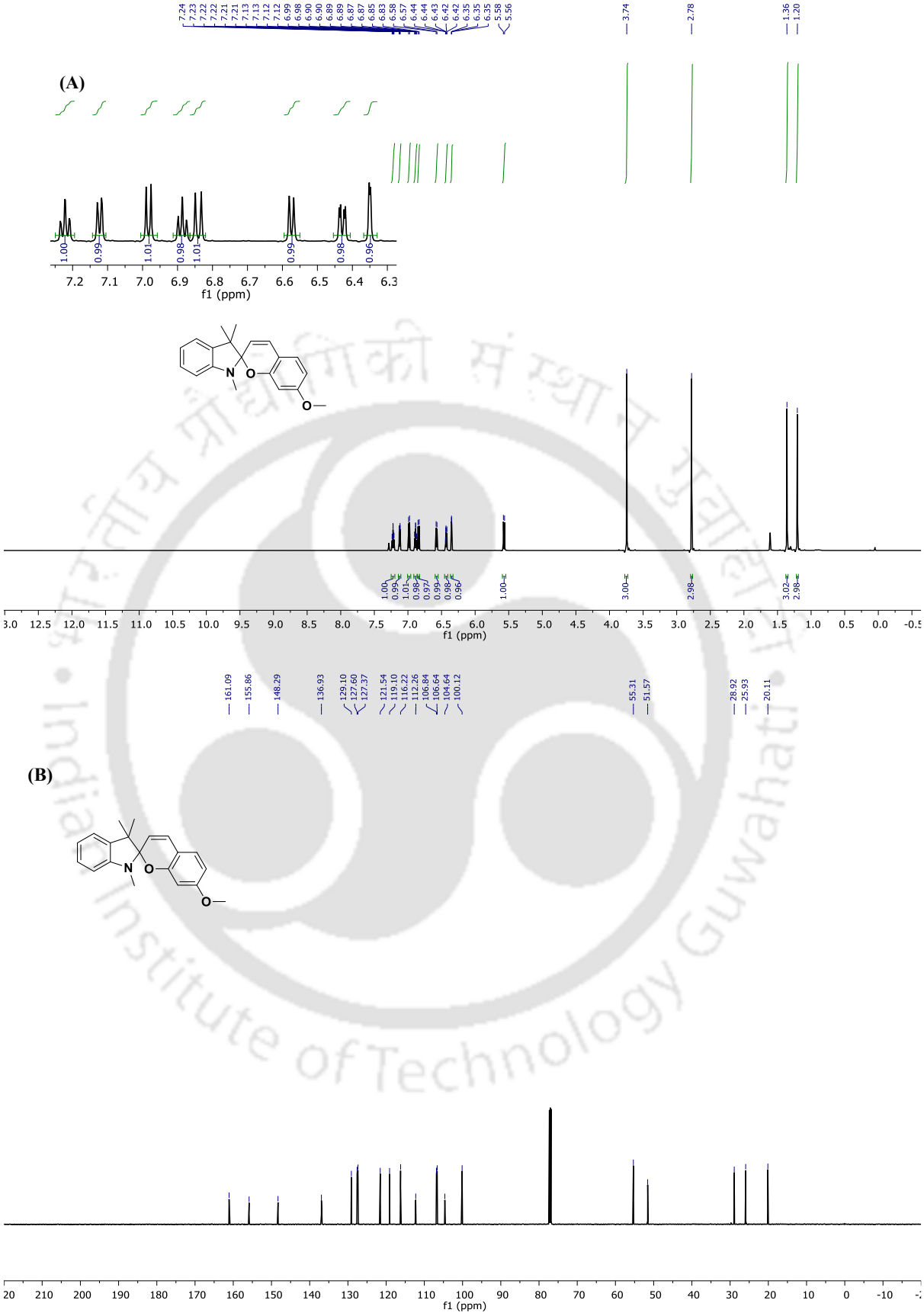

Fig. 4.25. ^{1}H NMR (A) and ^{13}C NMR (B) spectra of compound **1l.**

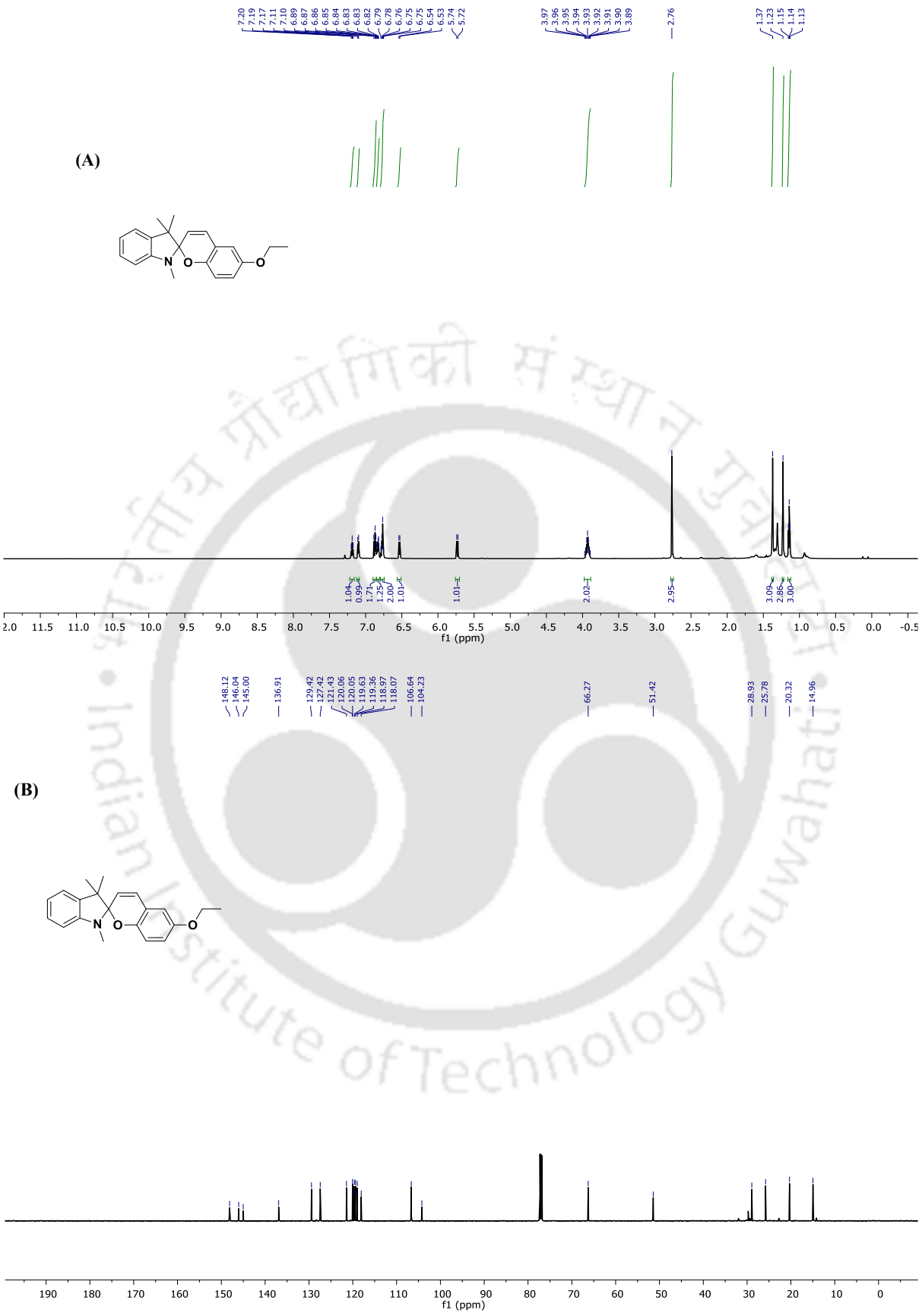

Fig. 4.26. ^{1}H NMR (A) and ^{13}C NMR (B) spectra of compound **1m.**

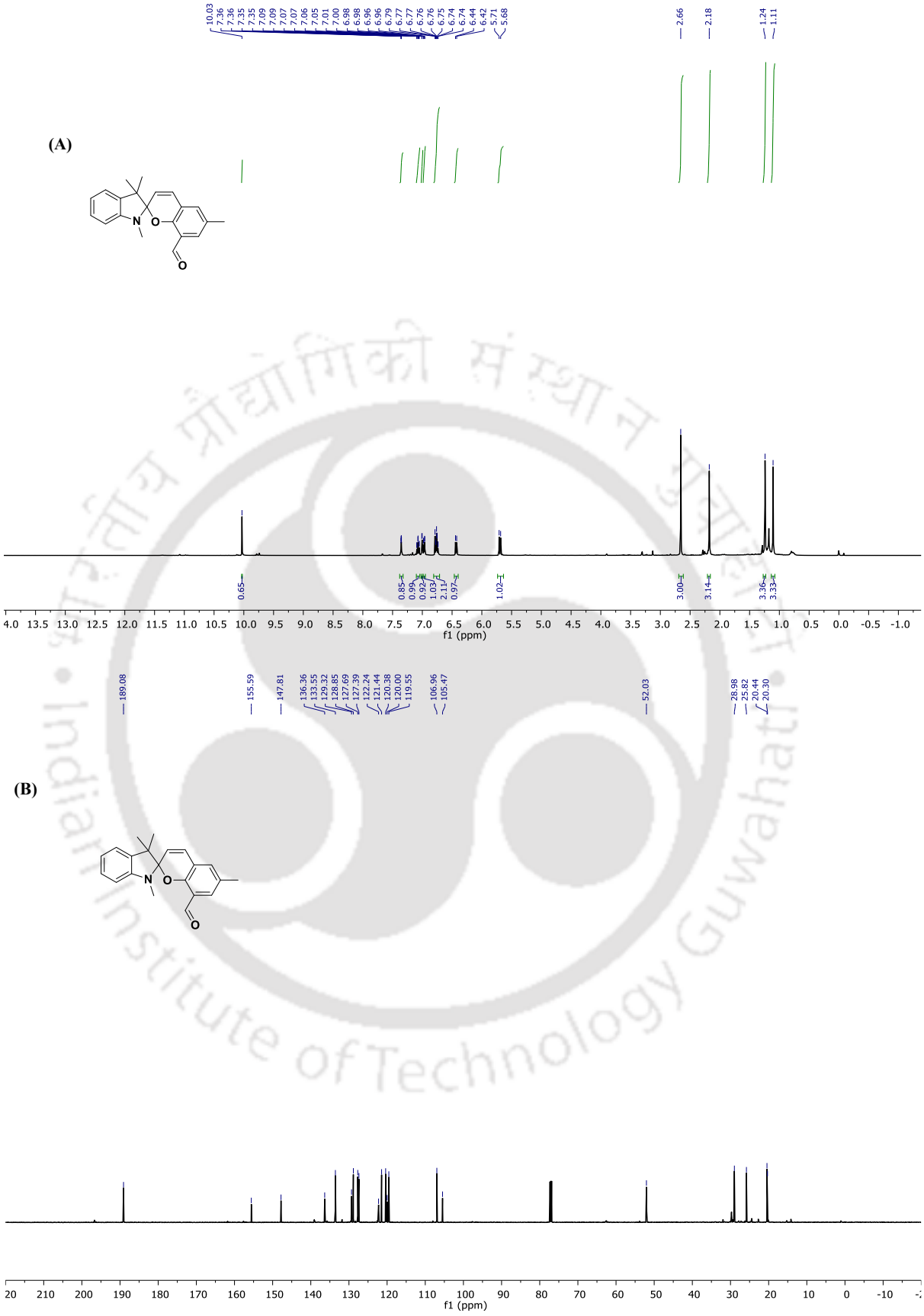

Fig. 4.27. ^{1}H NMR (A) and ^{13}C NMR (B) spectra of compound **1n.**

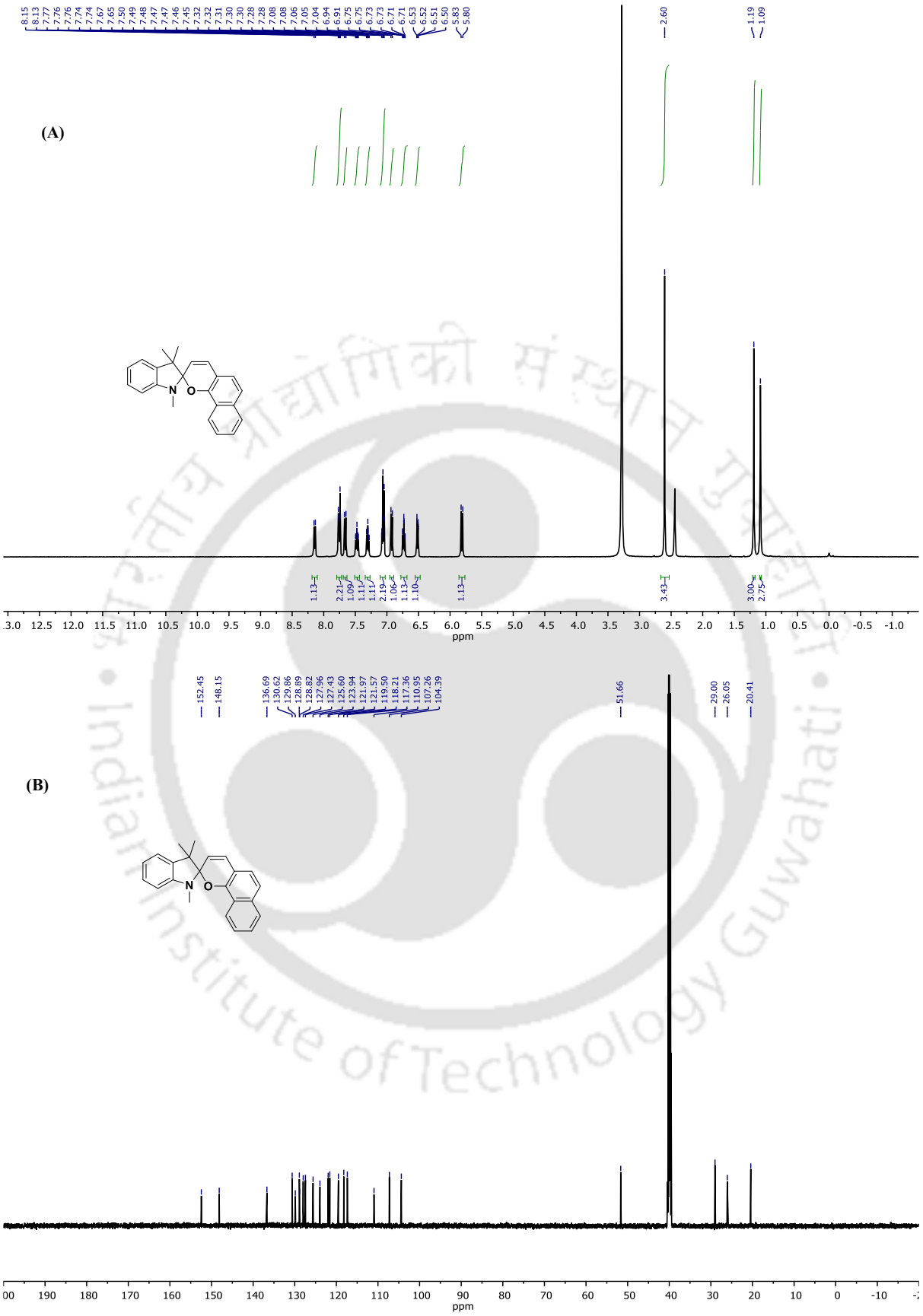

Fig. 4.28. ^{1}H NMR (A) and ^{13}C NMR (B) spectra of compound **1o.**

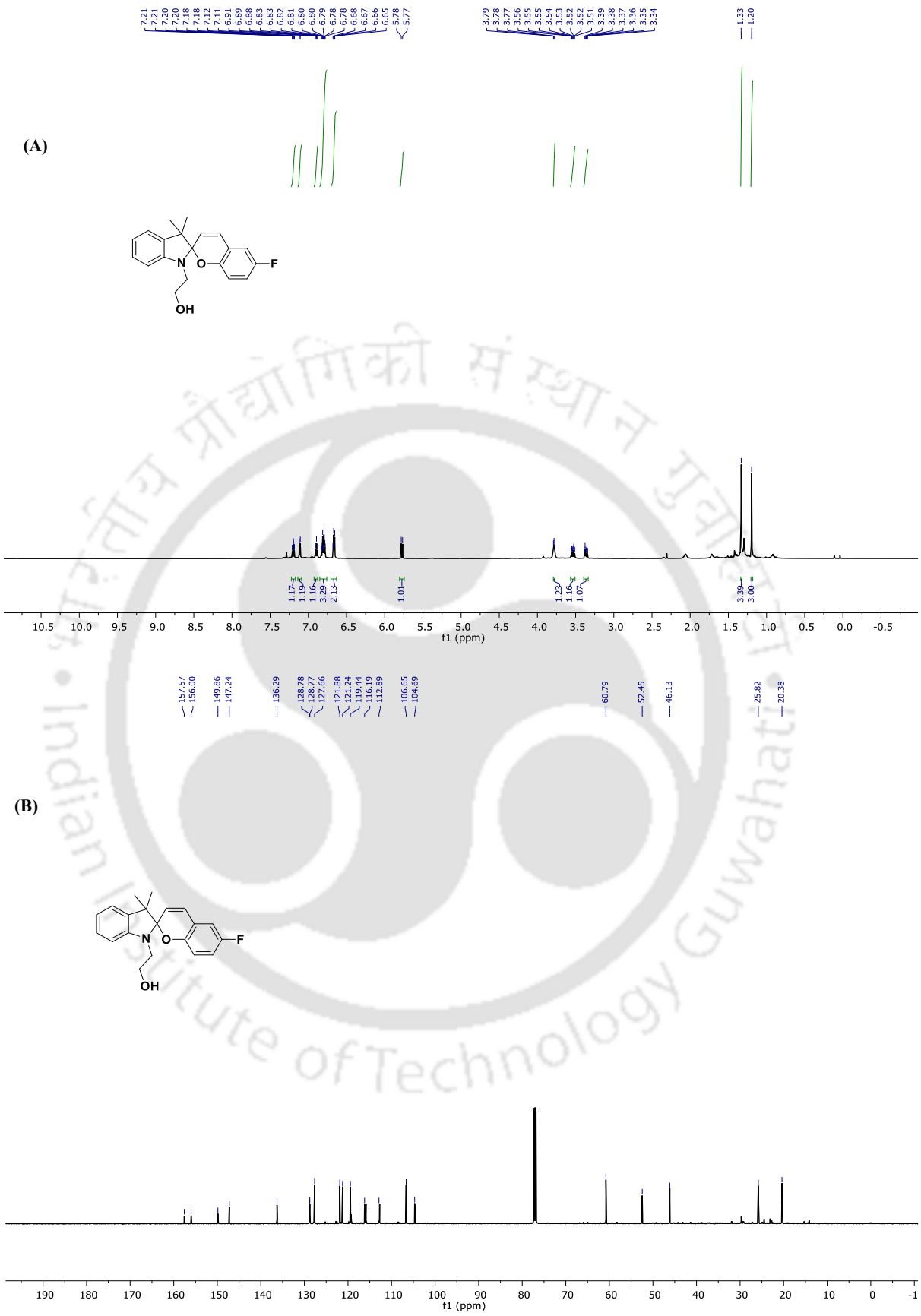

Fig. 4.29. ^{1}H NMR (A) and ^{13}C NMR (B) spectra of compound **2a.**

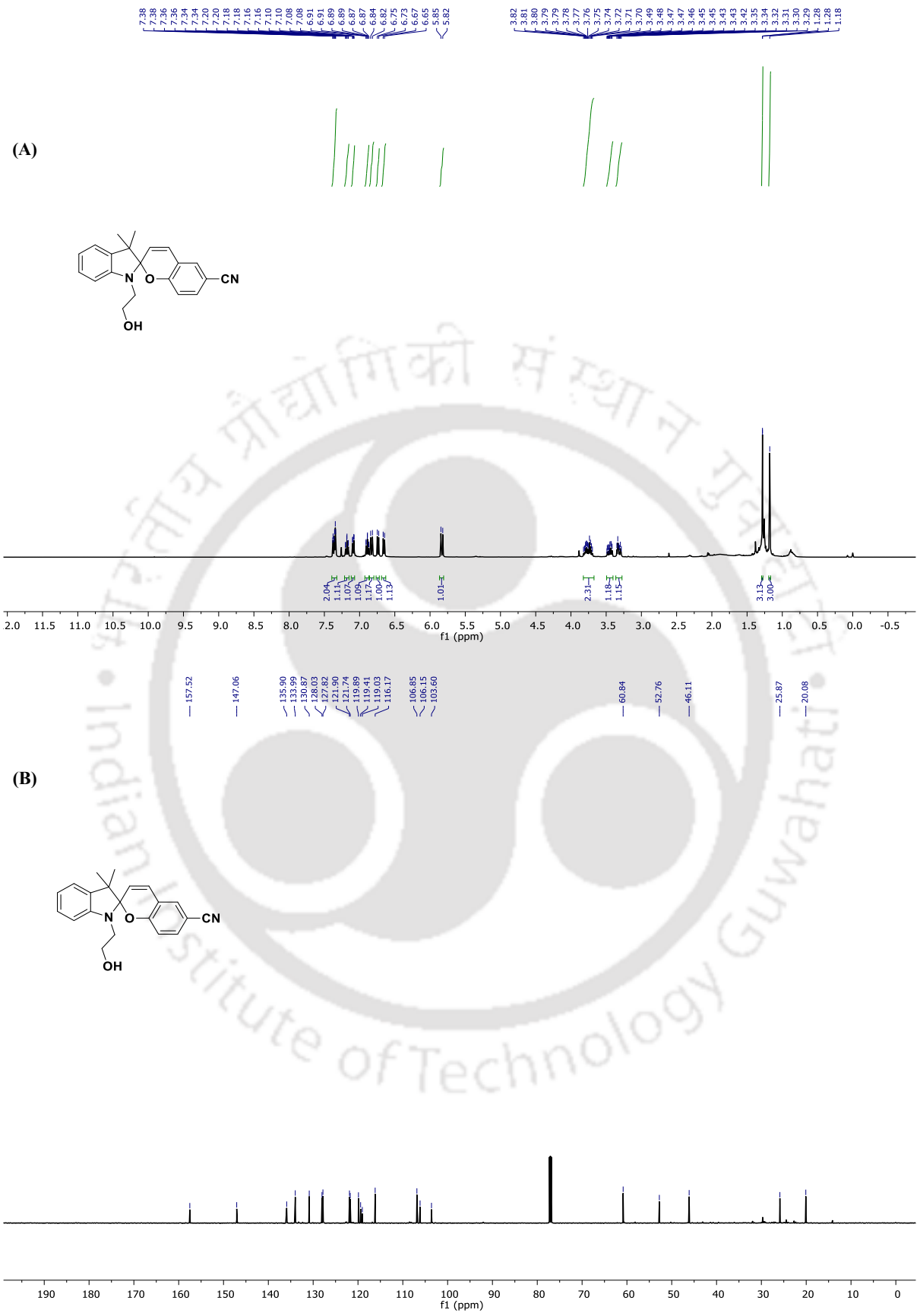

Fig. 4.30. ^{1}H NMR (A) and ^{13}C NMR (B) spectra of compound **2b.**

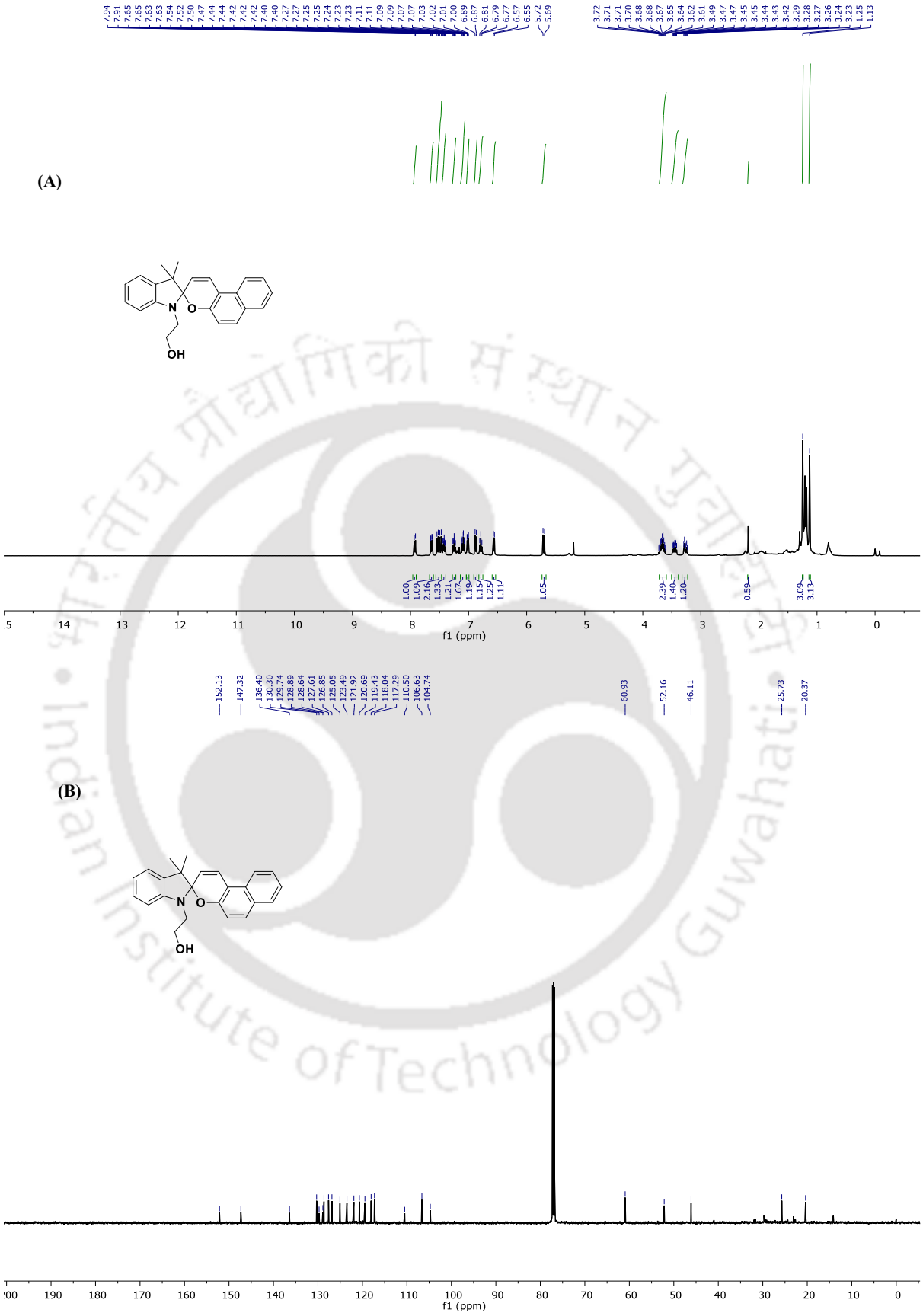

Fig. 4.31. ^{1}H NMR (A) and ^{13}C NMR (B) spectra of compound **2c.**

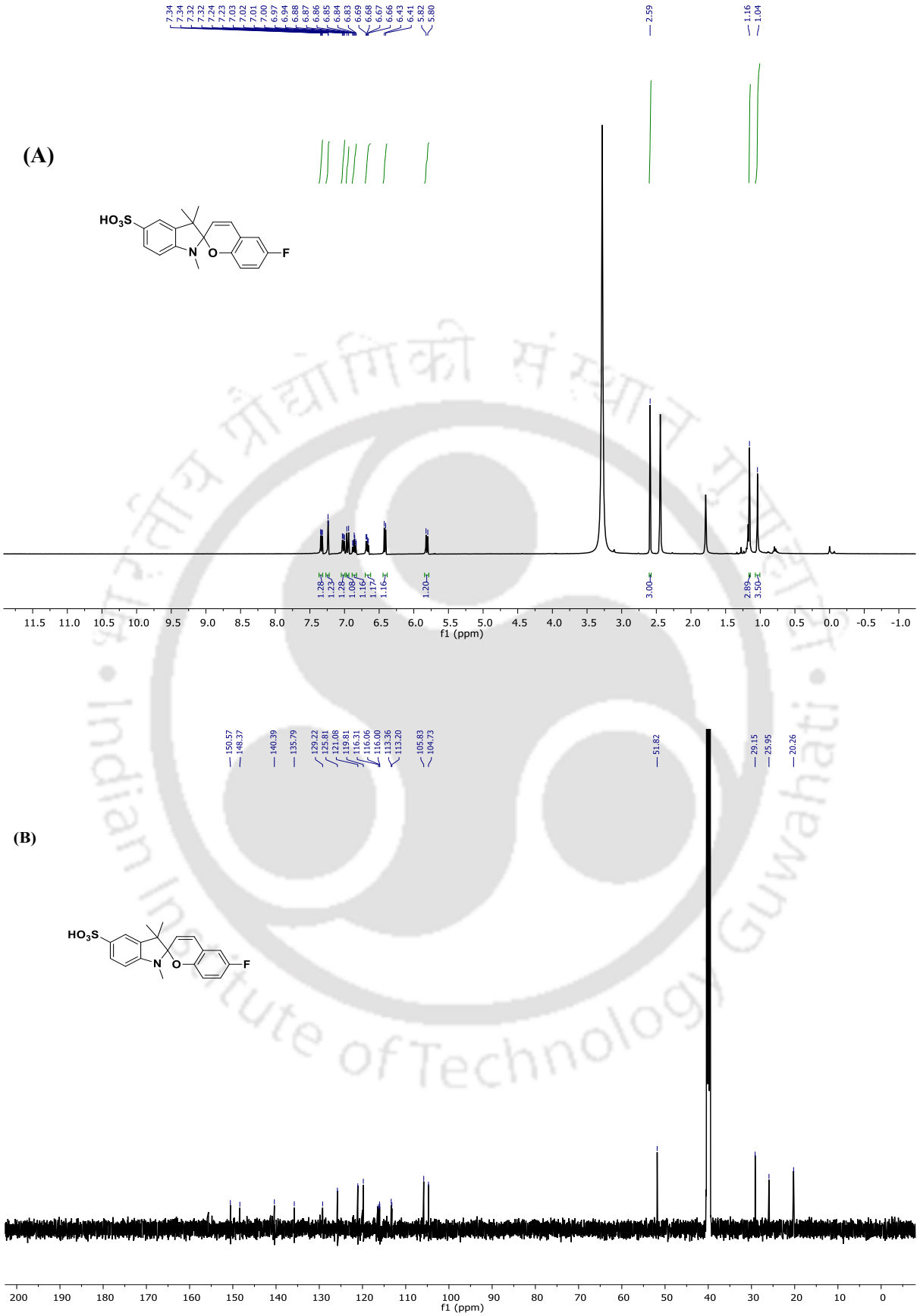

Fig. 4.32. ^{1}H NMR (A) and ^{13}C NMR (B) spectra of compound **3a.**

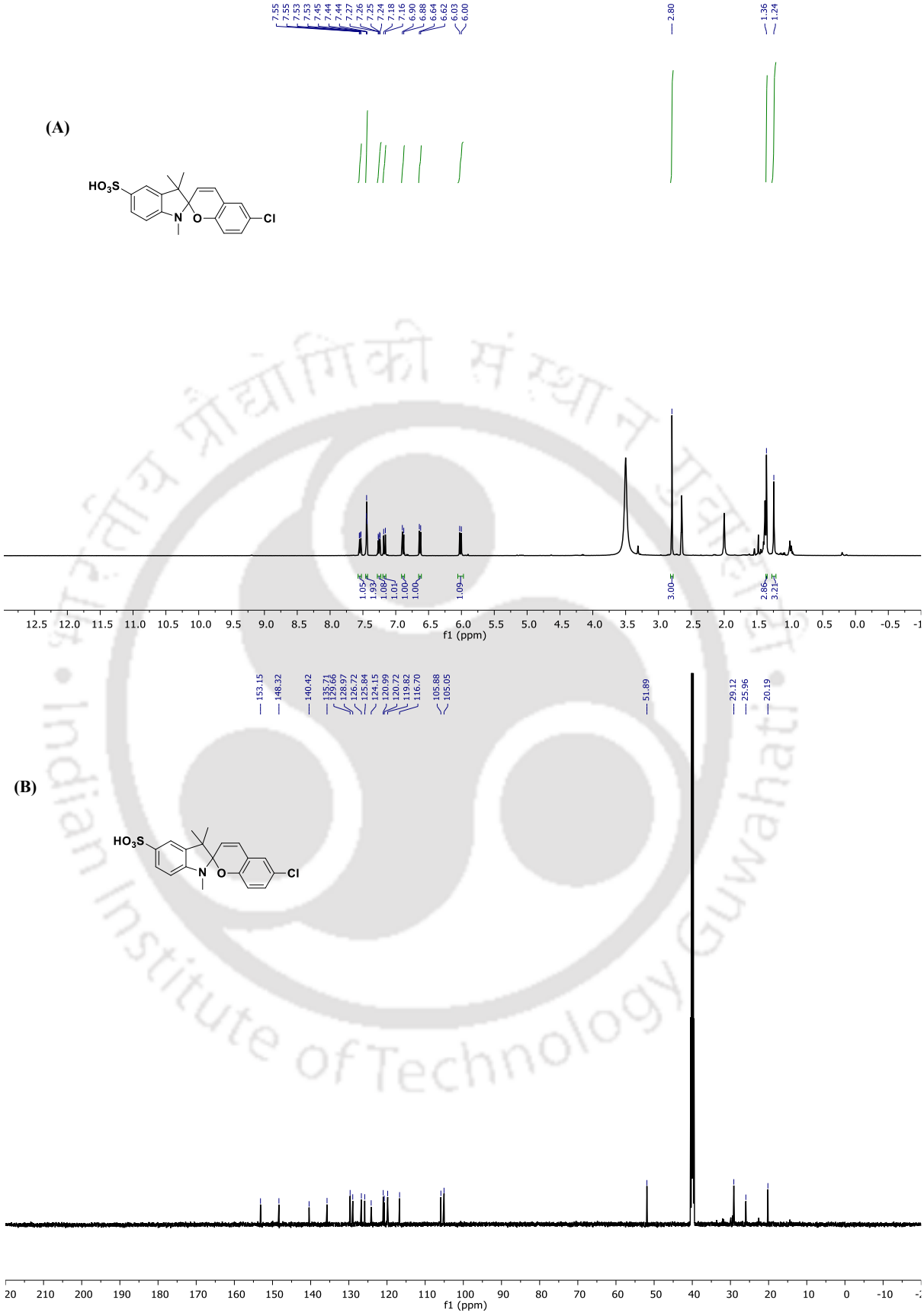

Fig. 4.33. ^{1}H NMR (A) and ^{13}C NMR (B) spectra of compound **3b.**

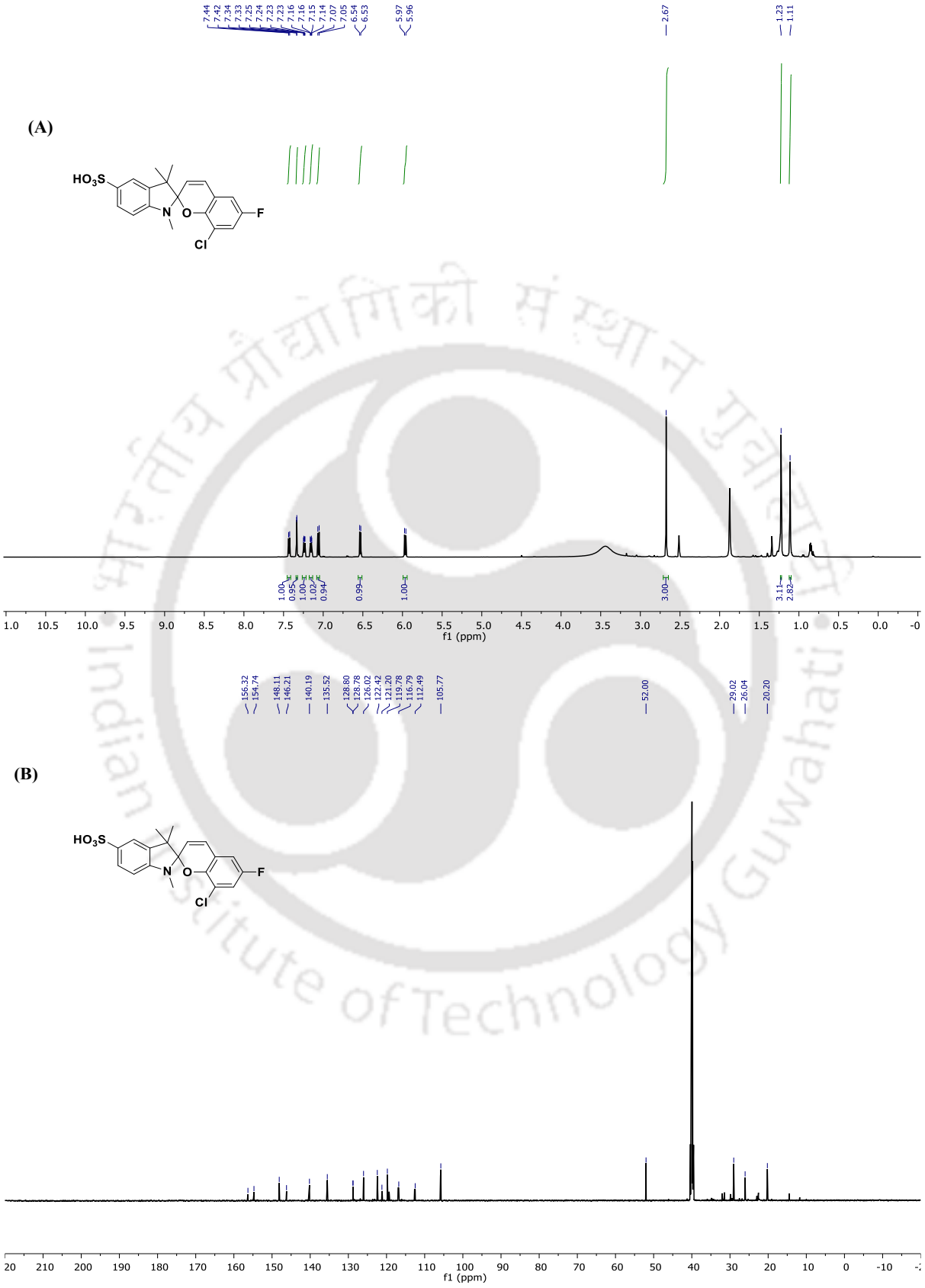

Fig. 4.34. ^{1}H NMR (A) and ^{13}C NMR (B) spectra of compound **3c.**

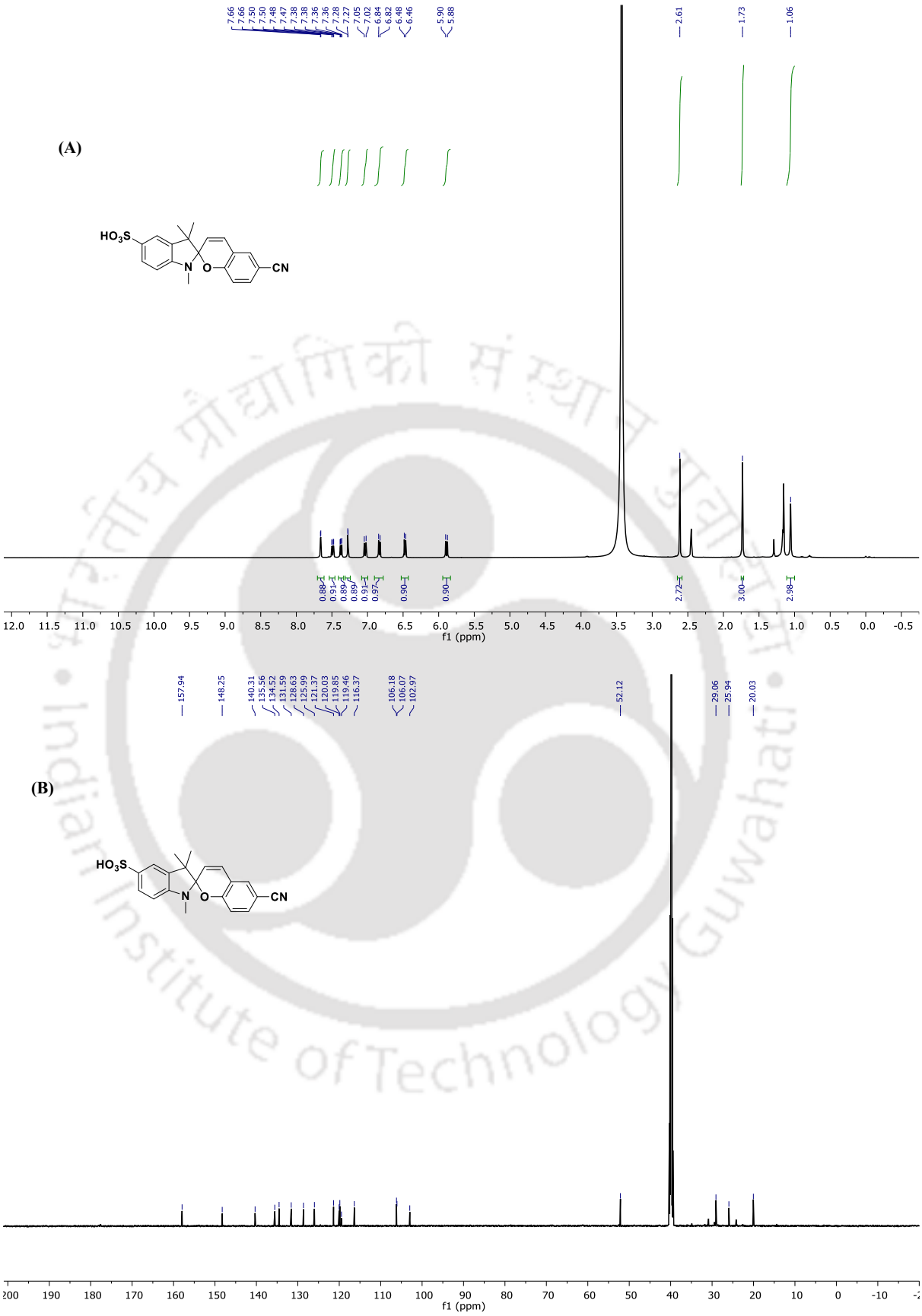

Fig. 4.35. ^{1}H NMR (A) and ^{13}C NMR (B) spectra of compound **3d.**

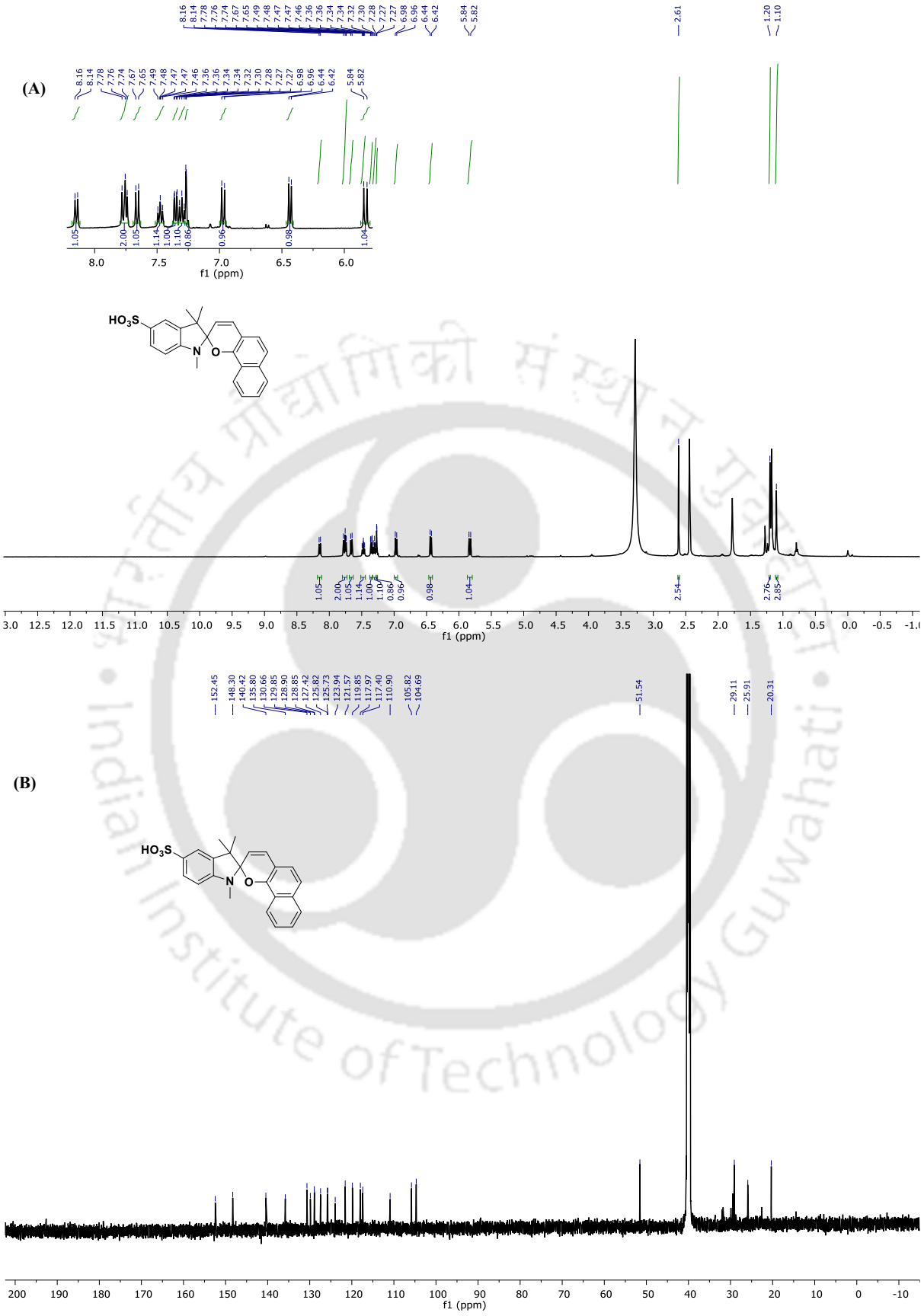

Fig. 4.36. ^{1}H NMR (A) and ^{13}C NMR (B) spectra of compound **4.3e.**

4.5.20. HPLC traces:

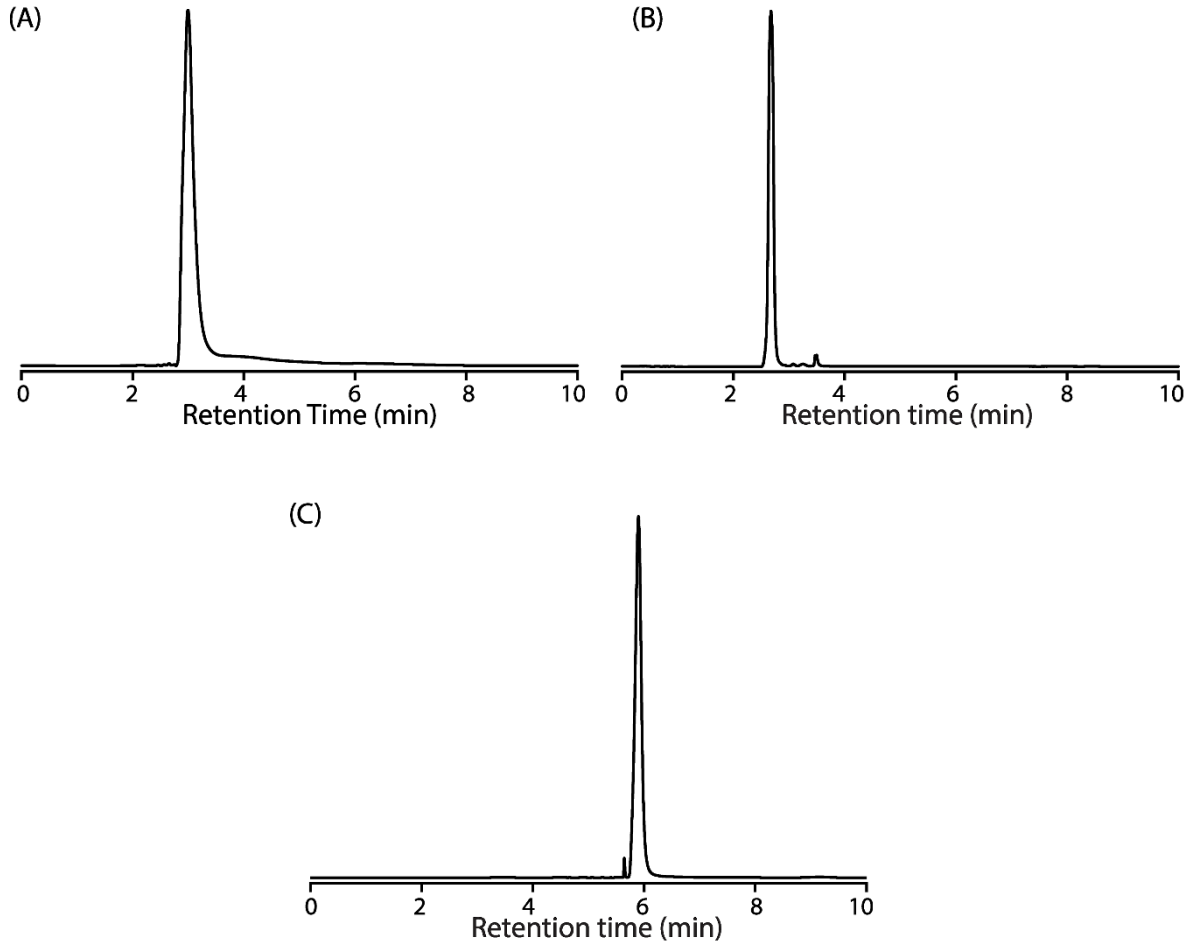

Fig. 4.37. HPLC traces of **3a** (A), **3d** (B), **4.3e** (C).

In this Chapter, the molecules synthesized has two isomers (spiropyran and merocyanine). The spiropyran isomer is in racemic mixture but the active form, which is merocyanine form, is planar and does not have a chiral centre. So, the potent isomer is a single product with no racemic mixture.

4.6. References

1. Jiang, K.; Wang, Q.; Chen, X.-L.; Wang, X.; Gu, X.; Feng, S.; Wu, J.; Shang, H.; Ba, X.; Zhang, Y., Nanodelivery optimization of IDO1 inhibitors in tumor immunotherapy: challenges and strategies. *Int. J. Nanomed.* **2024**, 8847-8882.

2. Das, N. M.; Prusty, B. M.; Sahoo, A.; Mazumder, P.; Chauhan, S.; Hazarika, G.; Kumar, S.; Dhabal, D.; Manna, D., Photoresponsive prodrug for regulated inhibition of indoleamine 2, 3-dioxygenase 1 enzyme activity. *RSC Med. Chem.* **2025**, *16*, 3240-3250.

3. Röhrig, U. F.; Michielin, O.; Zoete, V., Structure and plasticity of indoleamine 2, 3-dioxygenase 1 (IDO1). *J. Med. Chem.* **2021,** *64* (24), 17690-17705.

4. Günther, J.; Däbritz, J.; Wirthgen, E., Limitations and off-target effects of tryptophan-related IDO inhibitors in cancer treatment. *Front. Immunol.* **2019,** *10*, 1801.

5. Panfili, E.; Rezzi, S. J.; Adamo, A.; Mazzoletti, D.; Massarotti, A.; Miggiano, R.; Fallarini, S.; Ambrosino, S.; Coletti, A.; Molinaro, P., Identification of a compound inhibiting both the enzymatic and nonenzymatic functions of indoleamine 2, 3-dioxygenase 1. *ACS Pharmacol. Transl. Sci.* **2024,** *7* (10), 3056-3070.

6. Rad, J. K.; Balzade, Z.; Mahdavian, A. R., Spiropyran-based advanced photoswitchable materials: A fascinating pathway to the future stimuli-responsive devices. *J. Photochem. Photobiol. C.* **2022,** *51*, 100487.

7. Fleming, C. L.; Li, S.; Grøtli, M.; Andréasson, J., Shining new light on the spiropyran photoswitch: a photocage decides between cis–trans or spiro-merocyanine isomerization. *J. Am. Chem. Soc.* **2018,** *140* (43), 14069-14072.

8. Li, L.; Yang, W.-W.; Xu, D.-G., Stimuli-responsive nanoscale drug delivery systems for cancer therapy. *J. Drug Target.* **2019,** *27* (4), 423-433.

9. Reifarth, M.; Bekir, M.; Bapolisi, A. M.; Titov, E.; Nußhardt, F.; Nowaczyk, J.; Grigoriev, D.; Sharma, A.; Saalfrank, P.; Santer, S., A dual pH-and light-responsive spiropyran-based surfactant: Investigations on its switching behavior and remote control over emulsion stability. *Angew. Chem., Int. Ed.* **2022,** *61* (21), e202114687.

10. Fuchter, M. J., On the promise of photopharmacology using photoswitches: a medicinal chemist's perspective. *J. Med. Chem.* **2020,** *63* (20), 11436-11447.

11. Liu, Y.; Wang, T.; Wang, W., Photopharmacology and photoresponsive drug delivery. *Chem. Soc. Rev.* **2025**.

12. Pradhan, N.; Akhtar, N.; Nath, B.; Peña-García, J.; Gupta, A.; Pérez-Sánchez, H.; Kumar, S.; Manna, D., Inhibition of immunosuppressive indoleamine 2, 3-dioxygenase by targeting the heme and apo-form. *Chem Commun* **2021,** *57* (3), 395-398.

13. Das, N. M.; Prusty, B. M.; Pradhan, N.; Gupta, A.; Carmena-Bargueño, M.; Karn, R.; Pérez-Sánchez, H.; Kumar, S.; Manna, D., Evaluation of mode of indoleamine 2, 3-dioxygenase 1 inhibition by 4, 7-dichloroquinolines. *Eur. J. Med. Chem. Rep.* **2023,** *9*, 100110.

14. Cheow, L. F.; Viswanathan, R.; Chin, C.-S.; Jennifer, N.; Jones, R. C.; Guccione, E.; Quake, S. R.; Burkholder, W. F., Multiplexed analysis of protein–ligand interactions

by fluorescence anisotropy in a microfluidic platform. *Anal. Chem.* **2014,** *86* (19), 9901-9908.

15. Yamamoto, S.; Nishimura, K.; Morita, K.; Kanemitsu, S.; Nishida, Y.; Morimoto, T.; Aoi, T.; Tamura, A.; Maruyama, T., Microenvironment pH-induced selective cell death for potential cancer therapy using nanofibrous self-assembly of a peptide amphiphile. *Biomacromolecules* **2021,** *22* (6), 2524-2531.

16. Shamsipur, M.; Ghavidast, A.; Pashabadi, A., Phototriggered structures: Latest advances in biomedical applications. *Acta Pharm. Sin. B.* **2023,** *13* (7), 2844-2876.

17. Barman, S.; Das, J.; Biswas, S.; Maiti, T.; Singh, N. P., A spiropyran–coumarin platform: an environment sensitive photoresponsive drug delivery system for efficient cancer therapy. *J. Mater. Chem. B.* **2017,** *5* (21), 3940-3944.

18. You, Q.-H.; Fan, L.; Chan, W.-H.; Lee, A. W.; Shuang, S., Ratiometric spiropyran-based fluorescent pH probe. *RSC Adv.* **2013,** *3* (36), 15762-15768.

19. Malachowski, W. P.; Winters, M.; DuHadaway, J. B.; Lewis-Ballester, A.; Badir, S.; Wai, J.; Rahman, M.; Sheikh, E.; LaLonde, J. M.; Yeh, S.-R., O-alkylhydroxylamines as rationally-designed mechanism-based inhibitors of indoleamine 2, 3-dioxygenase-1. *Eur. J. Med. Chem.* **2016,** *108*, 564-576.

20. Scolaro, L. M.; Castriciano, M.; Romeo, A.; Patane, S.; Cefalì, E.; Allegrini, M., Aggregation behavior of protoporphyrin IX in aqueous solutions: clear evidence of vesicle formation. *J. Phys. Chem. B* **2002,** *106* (10), 2453-2459.

21. Micali, N.; Villari, V.; Romeo, A.; Castriciano, M. A.; Scolaro, L. M., Evidence of the early stage of porphyrin aggregation by enhanced Raman scattering and fluorescence spectroscopy. *Phys. Review. E* **2007,** *76* (1), 011404.

22. Panda, S.; Roy, A.; Deka, S. J.; Trivedi, V.; Manna, D., Fused heterocyclic compounds as potent indoleamine-2, 3-dioxygenase 1 inhibitors. *ACS Med. Chem. Lett.* **2016,** *7* (12), 1167-1172.

23. Paul, S.; Roy, A.; Deka, S. J.; Panda, S.; Trivedi, V.; Manna, D., Nitrobenzofurazan derivatives of N′-hydroxyamidines as potent inhibitors of indoleamine-2, 3-dioxygenase 1. *Eur. J. Med. Chem.* **2016,** *121*, 364-375.

24. Borah, R.; Mamidi, N.; Panda, S.; Gorai, S.; Pathak, S. K.; Manna, D., Elucidating the interaction of γ-hydroxymethyl-γ-butyrolactone substituents with model membranes and protein kinase C–C1 domains. *Mol. Biosyst.* **2015,** *11* (5), 1389-1399.

25. Yang, W.; Du, D.-M., Highly enantioselective Michael addition of nitroalkanes to chalcones using chiral squaramides as hydrogen bonding organocatalysts. *Org. Lett.* **2010,** *12* (23), 5450-5453.

26. Takikawa, O.; Kuroiwa, T.; Yamazaki, F.; Kido, R., Mechanism of interferon-gamma action. Characterization of indoleamine 2, 3-dioxygenase in cultured human cells induced by interferon-gamma and evaluation of the enzyme-mediated tryptophan degradation in its anticellular activity. *J Biol Chem* **1988,** *263* (4), 2041-2048.

27. Nelp, M. T.; Kates, P. A.; Hunt, J. T.; Newitt, J. A.; Balog, A.; Maley, D.; Zhu, X.; Abell, L.; Allentoff, A.; Borzilleri, R., Immune-modulating enzyme indoleamine 2, 3-dioxygenase is effectively inhibited by targeting its apo-form. *Proc Natl Acad Sci U S A* **2018,** *115* (13), 3249-3254

.

5. Conclusion

In this thesis, we have successfully described the role of IDO1 in the immunosuppression process associated with various life-threatening diseases. **Chapter 1** elaborates the role of IDO1 and the importance of IDO1 inhibition. In **Chapter 2** we describe the development dichloroquinoline derivatives, mimicking linrodostat, which show moderate apo-IDO1 inhibitory activity by releasing the heme from the holo-IDO1 pocket and also binding with the free heme, preventing it from reinserting inside the apo-IDO1 pocket. Though dichloroquinoline showed moderate inhibition of apo-IDO1 and also binds to heme, it lacks target-specific drug release, hence, in **Chapter 3**, photopharmacology was introduced, where the tryptamine-based azole derivatives linked to a photo-sensitive linker act as a prodrug, and when 400 nm light is applied. They release the tryptamine-based azole derivative, exhibiting decent IDO1 inhibition. In **Chapter 4**, the spiropyran derivatives were developed that act as apo IDO1 inhibitors when converted to merocyanine derivatives in the presence of light or pH, act as an apo-IDO1 inhibitor by releasing heme and binding to the apo-IDO1 pocket. The spiropyran derivatives also bind to the free heme in its merocyanine form. These photoswitch derivatives enable us to explore a dual-stimuli-responsive IDO1 inhibitor, demonstrating temporal and target-specific drug release.

6. Future prospects

In future research prospects, the non-enzymatic pathways for IDO1 inhibition can be explored and this may lead to a promising yet under-investigated area. Though most current studies primarily focus on inhibiting the enzymatic catalytic activity of IDO1 but the emerging evidence highlights the significance of targeting the apo form of IDO1, which is an inactive form of IDO1 lacking the heme cofactor. This form exhibits non-catalytic signaling functions that contribute to immune regulation in the tumor microenvironment, and selective inhibitors that bind to this apo form could offer a novel approach for modulating both enzymatic and non-enzymatic activities of IDO1 for enhancement of therapeutic benefit. Moreover, developing IDO1 inhibitors with covalent linkers can offer a potential for irreversible inhibition, which in turn may lead to more sustained and effective suppression of IDO1 activity. Such covalent inhibitors can form stable, irreversible bonds with the enzyme, leading to potentially overcome the limitations associated with reversible binding and enzyme turnover. Additionally, incorporating fluorescent tagging with IDO1 inhibition strategies opens exciting breakthrough for dual-function therapeutic and diagnostic tools. Fluorescent labeling could enable real-time

visualization as well as tracking of IDO1 inhibitor localization and dynamics within biological systems and facilitate mechanistic studies and aiding in precision delivery. The combination of fluorescence with potent inhibition could enhance understanding of the role of IDO1 and improve the design of targeted therapies.

In summary, future research should focus on the targeting both enzymatic and non-enzymatic pathways of IDO1. Researcher should emphasize on developing irreversible covalent inhibitors as well as the fluorescent markers to advance both the therapeutic efficacy and mechanistic understanding of IDO1 inhibition in disease contexts such as cancer immunotherapy.

AMERICAN CHEMICAL SOCIETY LICENSE
TERMS AND CONDITIONS

Nov 23, 2025

This Agreement between Niku Moni Das ("You") and American Chemical Society ("American Chemical Society") consists of your license details and the terms and conditions provided by American Chemical Society and Copyright Clearance Center.

License Number	6154780279445
License date	Nov 23, 2025
Licensed Content Publisher	American Chemical Society
Licensed Content Publication	Journal of Medicinal Chemistry
Licensed Content Title	Inhibition Mechanisms of Indoleamine 2,3-Dioxygenase 1 (IDO1)
Licensed Content Author	Ute F. Röhrig, Aline Reynaud, Somi Reddy Majjigapu, et al
Licensed Content Date	Oct 1, 2019
Licensed Content Volume	62
Licensed Content Issue	19
Volume number	62
Issue number	19
Type of Use	Thesis/Dissertation
Requestor type	Non-profit

Format	Print
Portion	Table/Figure/Micrograph
Number of Table/Figure/Micrographs	1
Title of new work	Development of Inhibitors for Immunosuppressive Indolamine 2,3 Dioxygenase 1 Enzyme
Institution name	Indian Institute of Technology, Guwahati
Expected presentation date	Jan 2026
Portions	Scheme 1
The Requesting Person / Organization to Appear on the License	Niku Moni Das
Requestor Location	CF-26, Dhansiri Hostel, IIT Guwahati Guwahati, 781039 India
Payment Type	Invoice
Email Address	d.niku@iitg.ac.in
Billing Address	Indian Institute of Technology, Guwahati CF 26, Dhansiri Hostel, IIT Guwahati Guwahati, India 781039
Total	0.00 USD
Terms and Conditions	

American Chemical Society's Policy on Thesis and Dissertations

If your university requires you to obtain permission, you must use the RightsLink permission system.

See RightsLink instructions at
http://pubs.acs.org/page/copyright/permissions.html.

This is regarding request for permission to include **your** paper(s) or portions of text from **your** paper(s) in your thesis.
Permission is now automatically granted; please pay special attention to the **implications** paragraph below. The Copyright Subcommittee of the Joint Board/Council Committees on Publications approved the following:

> Copyright permission for published and submitted material from thesis and dissertations
> ACS extends blanket permission to students to include in their thesis and dissertations their own articles, or portions thereof, that have been published in ACS journals or submitted to ACS journals for publication, provided that the ACS copyright credit line is noted on the appropriate page(s).
>
> Publishing implications of electronic publication of thesis and dissertation material
> Students and their mentors should be aware that posting of thesis and dissertation material on the Web prior to submission of material from that thesis or dissertation to an ACS journal may affect publication in that journal. Whether Web posting is considered prior publication may be evaluated on a case-by-case basis by the journal's editor. If an ACS journal editor considers Web posting to be "prior publication", the paper will not be accepted for publication in that journal. If you intend to submit your unpublished paper to ACS for publication, check with the appropriate editor prior to posting your manuscript electronically.

Reuse/Republication of the Entire Work in Thesis or Collections: Authors may reuse all or part of the Submitted, Accepted or Published Work in a thesis or dissertation that the author writes and is required to submit to satisfy the criteria of degree-granting institutions. Such reuse is permitted subject to the ACS' "Ethical Guidelines to Publication of Chemical Research" (http://pubs.acs.org/page/policy/ethics/index.htmlb); the author should secure written confirmation (via letter or email) from the respective ACS journal editor(s) to avoid potential conflicts with journal prior publication*/embargo policies. Appropriate citation of the Published Work must be made. If the thesis or dissertation to be published is in electronic format, a direct link to the Published Work must also be included using the ACS Articles on Request author-directed link - see http://pubs.acs.org/page/policy/articlesonrequest/index.html

* Prior publication policies of ACS journals are posted on the ACS website at http://pubs.acs.org/page/policy/prior/index.html

If your paper has not yet been published by ACS, please print the following credit line on the first page of your article: "Reproduced (or 'Reproduced in part') with permission from [JOURNAL NAME], in press (or 'submitted for publication'). Unpublished work copyright [CURRENT YEAR] American Chemical Society." Include appropriate information.

If your paper has already been published by ACS and you want to include the text or portions of the text in your thesis/dissertation, please print the ACS copyright credit line on the first page of your article: "Reproduced (or 'Reproduced in part') with permission from [FULL REFERENCE CITATION.] Copyright [YEAR] American Chemical Society." Include appropriate information.

Submission to a Dissertation Distributor: If you plan to submit your thesis to UMI or to another dissertation distributor, you should not include the unpublished ACS paper in your thesis if the thesis will be disseminated electronically, until ACS has published your paper. After publication of the paper by ACS, you may release the entire thesis (**not the**

individual ACS article by itself) for electronic dissemination through the distributor; ACS's copyright credit line should be printed on the first page of the ACS paper.

v1.4

Questions? customercare@copyright.com.

RightsLink

Evaluation of mode of indoleamine 2,3-dioxygenase 1 inhibition by 4,7-dichloroquinolines

Author:
Niku Moni Das,Biswa Mohan Prusty,Nirmalya Pradhan,Anjali Gupta,Miguel Carmena-Bargueño,Rama Karn,Horacio Pérez-Sánchez,Sachin Kumar,Debasis Manna

Publication: European Journal of Medicinal Chemistry Reports

Publisher: Elsevier

Date: December 2023

© 2023 The Authors. Published by Elsevier Masson SAS.

Content Excluded

This content has been excluded from the RightsLink's service. Please contact Elsevier directly with your request.

Photoresponsive prodrug for regulated inhibition of indoleamine 2,3-dioxygenase 1 enzyme activity

N. M. Das, B. M. Prusty, A. Sahoo, P. Mazumder, S. Chauhan, G. Hazarika, S. Kumar, D. Dhabal and D. Manna, *RSC Med. Chem.*, 2025, **16**, 3240 **DOI:** 10.1039/D5MD00061K

Photoswitchable Inhibitors: Temporally Regulated Inhibition of IDO1 Enzyme Using Photoactive Merocyanine Derivatives

N. M. Das, S. BISWAS, S. Chauhan, A. Sahoo, D. Dhabal and D. Manna, *Chem. Commun.*, 2025, Accepted Manuscript , **DOI:** 10.1039/D5CC05796E

Publications

1. Das, N. M.; Prusty, B. M.; Pradhan, N.; Gupta, A.; Carmena-Bargueño, M.; Karn, R.; Pérez-Sánchez, H.; Kumar, S.; Manna, D., Evaluation of mode of indoleamine 2, 3-dioxygenase 1 inhibition by 4, 7-dichloroquinolines. *Eur. J. Med. Chem. Rep.* **2023,** *9*, 100110.

2. Hazarika, G.; Das, S.; **Das, N. M**.; Manna, D., A pH-responsive covalent organic network: Morphology change leads to capture and removal of phosphate ions from water. *J. Mater. Chem. A* **2024,** *12* (30), 19559-19566.

3. Das, N. M.; Prusty, B. M.; Sahoo, A.; Mazumder, P.; Chauhan, S.; Hazarika, G.; Kumar, S.; Dhabal, D.; Manna, D., Photoresponsive prodrug for regulated inhibition of indoleamine 2, 3-dioxygenase 1 enzyme activity. *RSC Med. Chem.* **2025**, *16*, 3240-3250.

4. Das, N. M.; BISWAS, S.; Chauhan, S.; Sahoo, A.; Dhabal, D.; Manna, Photoswitchable Inhibitors: Temporally Regulated Inhibition of IDO1 Enzyme Using Photoactive Merocyanine Derivatives. *Chem. Commun.* **2025**.